THE TRANSLATIONAL MOTION OF PARTICLES IN A VISCOELASTIC LIQUID

Thesis by

Grant F. Tiefenbruck

In Partial Fulfillment of the Requirements

for the Degree of

Doctor of Philosophy

California Institute of Technology
Pasadena, California
1980
(Submitted November 16, 1979)

Acknowledgments

I wish to thank my advisor L. Gary Leal for suggesting this thesis project and for his many suggestions which added greatly to the technical merit of this work.

I would also like to thank the competent technicians George Griffith, Chic Nakawatase, Mike Nagy and John Yehle for their assistance in designing the experiments and for their friendship during coffee breaks.

While at Caltech, I enjoyed the company and friendships of many past and present graduate students. I would like to extend a special thanks to Clarke Berdan, Paul Chan, Mark Cronshaw, Seong Lee, Bill Moonan, Grant Robertson, Art Stelson, Dave Strand, Ted Watson and Gary Whatley.

I would also like to thank the people at First Congregational Church in Pasadena for their concern and interest in my family and our life in Pasadena.

I wish also to thank my parents for their faith in me and their words of encouragement.

Finally, I wish to thank my wife, Brenda, and my daughter, Laura, whose love and understanding make it possible to be happy anywhere.

Abstract

The translational motion of two different particles at low Reynolds number in a viscoelastic liquid is studied. The first study is an experimental investigation of the motion of a slender rod near a vertical wall. When the rod is not too near the wall, its motion is found to be in qualitative agreement with theoretical solutions for the motion of a rod in an unbounded second-order fluid. When the rod is nearer to the wall, its motion is shown to correspond qualitatively to a simple superposition of the motion in an unbounded second-order fluid and the motion in a Newtonian fluid near a vertical wall. The second study is a numerical solution of the equations governing the motion of a solid sphere and a spherical bubble in a viscoelastic fluid of infinite extent. The computed solutions are compared with analytic solutions obtained by asymptotic methods. It is found that many quantities are described quite well by the asymptotic theory considerably beyond the expected range of validity. Many features of the flow can be described by the model fluid behavior in shear and extensional flows.

Table of Contents

CHAPTER I. Introduction

I. INTRODUCTION

The use of polymers and polymer solutions in the chemical processing industry has led to an intense interest in the rheological behavior of these materials. One of the many areas where this information is useful is in describing the motion of small particles or gas bubbles in a non-Newtonian fluid, and a special case of this class of flows is the simple translational motion of the particle through an otherwise quiescent fluid. Two examples of translational particle motions which are of technological significance are the motion and dissolution of gas bubbles in common fermentation liquors and the sedimentation of solid particles in a non-Newtonian suspension.

The flow properties of most polymer solutions or melts are known as viscoelastic, by which we mean that the fluid demonstrates dynamical effects which reflect a finite memory for past deformations; i.e. shows a dependence of the dynamical properties at the present instant on the material configuration at earlier times. Some polymer solutions also fall into a class of materials which are often called purely-viscous. In a linear shear flow, such fluids exhibit only a shear stress which depends in a nonlinear fashion on the instantaneous velocity gradient. While the literature of non-Newtonian fluid mechanics contains widespread use of such specific-sounding terms as *viscoelastic*, *purely-viscous* and *pseudo-plastic* to describe various liquids, very little is known about the detailed dynamical behavior of these fluids either for general flows or, specifically, for the translational particle motions to be discussed in this thesis. The voluminous literature which has accumulated over the last thirty years is primarily concerned with the applicability of

various phenomenological constitutive relationships in a very special class of flows, known as viscometric, where the fluid locally undergoes a simple shearing motion. The main result is that there are now several constitutive relationships which, at least qualitatively, are known to describe most viscometric flow phenomena. Unfortunately, none of these relationships is known to be applicable to non-viscometric flows. In fact, it is conceivable for two liquids to behave identically in a viscometric flow, and yet behave quite differently in a non-viscometric flow. With the exception of rectilinear motion through a straight circular tube, nearly all flows of technological importance are non-viscometric. Thus, the lack of knowledge concerning the applicability of the proposed constitutive equations to non-viscometric flows represents an extremely important deficiency in our ability to handle non-Newtonian flow problems of technological importance.

One possible approach to the resolution of this problem is to attempt to develop constitutive equations which are known "à priori" to be applicable for non-viscometric, as well as viscometric, flows. Such an attempt would be made, in principle, from a deductive analysis of material behavior at some suitable microscale. If the material is structurally simple and dilute, this analysis can, and has been, carried out (e.g. Goddard and Miller, 1967). The resulting constitutive equation is valid for any linear velocity field, but is not directly useful for technological problems since it is only applicable to the simple material analyzed. While the constitutive equations for these simple models have sometimes provided a framework for the correlation of experimental data and may

serve as inspiration for phenomenological equations of the classical continuum-mechanical approach, the class of materials represented is rather narrow unless new, untested hypotheses are introduced.

The obvious complement (alternative?) to this deductive development of constitutive models is a direct comparison of experimental observation for non-viscometric motions and theoretical prediction for the same flows using specific phenomenological models. Such studies should initially focus only on fluid motions which exhibit a major change in behavior when compared with that of a Newtonian fluid. Such problems can provide a reasonable basis for comparison between theory and experiment. Two outstanding examples of such motions are the translation of a spherical particle and the translation of a slender rod-like particle, both at low particle Reynolds number. In this thesis, we shall treat theoretically the translational motion of a solid sphere and a spherical bubble in an infinite expanse of a viscoelastic liquid. We also experimentally study the motion of a slender rod-like particle in a viscoelastic liquid near a vertical wall.

II. Experimental Behavior of Non-Newtonian Liquids

The behavior of macromolecular solutions and melts is known to differ qualitatively in many ways from Newtonian fluids. Some known experimental phenomena which are characteristic of such materials include:

1. Shear-rate-dependent viscosity. For over fifty years it has been known that polymeric fluids are shear thinning. As the shear rate increases, the viscosity, defined as the ratio of the shear stress divided by the shear rate, drops dramatically to a limiting value which may be a factor of 10^{-2} to 10^{-4} smaller than the same ratio at zero-shear-rate

(see Bird, Armstrong and Hassager, 1977). For problems such as tube flow, this is the most important property of a macromolecular solution.

2. Normal stress effects in steady shear flows. A surprising property of macromolecular fluids is the existence of normal stresses in a simple shear flow. Since these normal stresses are unequal, some spectacular differences from Newtonian fluid behavior are observed. One of these is the so-called Weissenberg effect in which the polymer solution is observed to climb a rotating rod (Lodge, 1964). Another example is the slight upward bulging of the surface of a liquid as it flows down a tilted trough (Tanner, 1970).

3. Dynamic response in unsteady shear flows. If a steady shear flow is abruptly halted, it takes a finite amount of time for the stress components to return to their hydrostatic value (Huppler, Macdonald, Ashare, Spriggs, Bird and Holmes, 1967). Another example of time dependent response of a viscoelastic fluid is the recoil or recovery of deformation exhibited when a driving force (e.g. pressure gradient) is suddenly removed (Fredrickson, 1964). An effect of potential technological significance is the substantially increased mean flow rate which occurs when a small amplitude time dependent oscillation of the pressure gradient is superposed on a constant pressure gradient along the axis of a tube (Barnes, Townsend and Walters, 1969).

4. Other pheonomena. The examples given above all involve shearing flows ($u_x = \dot{\gamma} y$). In non-shearing flows there are additional phenomena. One example is die swell in which a stream of liquid emerging from a die may increase in diameter to several times the diameter of the die (Graessly,

Glassock and Crawley, 1970). Another interesting example is the tubeless siphon effect in which a siphon continues to operate even though the upstream end has been withdrawn from the fluid (James, 1966). A last example of macromolecular fluid behavior is the independence of the Nusselt number on Reynolds number beyond a "critical" value for flow past a heated cylindrical wire. This effect renders the hot wire anemometer inaccurate for polymer solutions (James and Acosta, 1970).

This list of phenomena is by no means exhaustive, but it is sufficient to demonstrate that macromolecular fluids do behave in a different and more complicated way than Newtonian fluids under similar conditions.

III. Rheological Models of Non-Newtonian Fluids

It is clear that no minor correction to the constitutive equation for a Newtonian fluid will account for all of the phenomena listed above. Indeed, no available constitutive equation has been shown to quantitatively account for all of these phenomena. Below, we shall discuss some of the more useful equations which have been employed by engineers and rheologists.

In the past, engineers have been primarily concerned with describing the shear thinning viscosity of polymer solutions and melts. To that end they have used a generalized Newtonian fluid model given by

$$\underline{\underline{\tau}} = 2\eta(\dot{\gamma})\underline{\underline{e}} \tag{1}$$

in which $\underline{\underline{\tau}}$ is the extra stress tensor, $\underline{\underline{e}}$ is the rate of strain tensor given by

$$\underline{\underline{e}} = \frac{1}{2}\left(\nabla\underline{u} + \nabla\underline{u}^{T}\right) \tag{2}$$

and $\dot{\gamma}$ is a scalar given by

$$\dot{\gamma} = \left[2(\underline{\underline{e}}:\underline{\underline{e}})\right]^{\frac{1}{2}} \tag{3}$$

The factor of two inside the square bracket is chosen so that in a simple shear flow where the velocity field is given by $u_x = \dot{\gamma} y$, $\tau_{xy} = \eta(\dot{\gamma})\dot{\gamma}$. The most widely used form for $\eta(\dot{\gamma})$ is

$$\eta = m\dot{\gamma}^{n-1} \tag{4}$$

which defines the power-law model in which m and n are constants that are characteristic of the fluid. The power-law form is motivated, in part, by the fact that the viscosity versus shear-rate curves for many polymer solutions are approximately linear on a log-log plot over a wide range of shear rates. One obvious deficiency of the power-law model, even for simple shear flows, is that it does not exhibit constant limiting values for the viscosity at high and low shear rates, but rather yields an unrealistic continuous decrease of the viscosity to zero as $\dot{\gamma} \to \infty$ and an increase to ∞ as $\dot{\gamma} \to 0$. A somewhat more complicated empirical model which does not have these drawbacks is the so-called Carreau Model (Bird et al., 1977), which is given by

$$\frac{\eta - \eta_\infty}{\eta_0 - \eta_\infty} = \left[1 + (\lambda\dot{\gamma})^2\right]^{\left(\frac{n-1}{2}\right)}$$

in which λ is a time constant characteristic of the fluid, η_0 is the zero-shear-rate viscosity, η_∞ is the limiting viscosity for large shear rates, and n has the same meaning as above in the power-law region. The Carreau equation is known to fit experimental shear viscosity data very well. Of course, the generalized Newtonian fluid model cannot represent any of the normal stress effects, transient responses, or other "elastic" phenomena associated with most polymer solutions and melts, and is thus mainly useful for steady, uni-directional shear flows in confined domains.

One of the most successful theories for describing the motion of a viscoelastic fluid evolved from the concept of a "simple material" due to Noll (1958). A "simple material" is described as one whose response to any deformation history is determined by its responses to pure stretch histories. Noll (1958) proved that an incompressible "simple fluid" may be characterized by a constitutive relation of the form

$$\underline{\underline{T}} = - p \underline{\underline{I}} + \underline{\underline{F}}(\underline{\underline{U}}_t^t)$$

where $\underline{\underline{U}}_t^t$ represents the history up to the time t of the relative stretch tensor $\underline{\underline{U}}_t(\tau)$ which is calculated by comparing the material configuration at the past time τ with that at the present time t. Thus, although the fluid may have a definite memory of all its past configurations, it reacts only by comparing the past configurations to the present one. Now, clearly one cannot solve too many fluid mechanics problems if it is assumed that the instantaneous stress on a fluid element depends upon the entire strain history of that fluid element. The only tractable problems are those in which the flow leaves the fluid very little to remember, so that the subtleties of extended memory are minimized. The flows in which the fluid locally undergoes a simple shearing motion, which we call viscometric flows, are of this type. For viscometric flows, Coleman and Noll (1959) were able to show that the response of any "simple fluid" can be determined completely in terms of three scalar functions of the shear rate alone. To demonstrate the nature of viscometric flows, we shall consider the case of simple steady shear flow where the velocity field is given by

$$u_1 = \dot{\gamma} x_2 \qquad u_2 = 0 \qquad u_3 = 0 \qquad \dot{\gamma} = \text{constant} .$$

In this case, the stress components become

$$T_{12} = \dot{\gamma}\eta(\dot{\gamma}) \ , \qquad T_{23} = T_{13} = 0$$
$$T_{11} - T_{33} = \sigma_1(\dot{\gamma})$$
$$T_{22} - T_{33} = \sigma_2(\dot{\gamma})$$

where η, σ_1 and σ_2 are shear rate dependent scalar functions which completely characterize the simple fluid in <u>any</u> viscometric flow. The first and second normal stress differences, N_1 and N_2, whch are frequently used by rheologists are related, to σ_1 and σ_2 in the form

$$N_1 = \sigma_1 - \sigma_2 \qquad N_2 = \sigma_2$$

The theory of simple fluids places no restriction on η, σ_1 and σ_2 other than requiring that they be single valued even functions of $\dot{\gamma}$.

Later, Coleman and Noll (1961) developed the concept of a simple fluid with a fading memory for past configurations and used it to show that the Newtonian fluid constitutes the proper first approximation to this class of simple fluids for a sufficiently slow flow. The "small" parameter in this development is the ratio of the largest intrinsic relaxation time scale of the fluid to the time scale of the motion. At the second approximation, the simple fluid with fading memory reduces to the familiar second-order fluid form originally investigated by Rivlin and Ericksen (1955), among others, namely;

$$\underline{\underline{T}} = - p \, \underline{\underline{I}} + 2\eta_0 \underline{\underline{e}} + 2\alpha_1 \frac{\delta \underline{\underline{e}}}{\delta t} + 4\alpha_2 \underline{\underline{e}}^2 \qquad (6)$$

In equation (6), α_1 and α_2 must be much smaller than η_0. The symbol $\delta/\delta t$ is the properly invariant co-deformational time derivative which is defined for an arbitrary tensor $\underline{\underline{B}}$ as

$$\frac{\delta \underline{\underline{B}}}{\delta t} = \frac{\partial \underline{\underline{B}}}{\partial t} + \underline{u}\cdot\nabla\underline{\underline{B}} + (\nabla\underline{u})\cdot\underline{\underline{B}} + \underline{\underline{B}}\cdot(\nabla\underline{u})^T$$

We note here that any properly invariant time derivative could be used in equation (6) without changing the qualitative predictions of a fluid described by this equation. For a simple shear flow, the second-order fluid approximation for the viscometric functions η, σ_1 and σ_2 is given by

$$\eta = \eta_o \qquad \sigma_1 = \alpha_2\dot{\gamma}^2 \qquad \sigma_2 = (2\alpha_1 + \alpha_2)\dot{\gamma}^2 \tag{7}$$

It is obvious from equation (7) that all of the second-order fluid constants can, in principle, be evaluated from viscometric data. The second-order fluid has been employed by many workers to determine the first effects of memory for non-viscometric flows.

The method of approximation used by Coleman and Noll can be carried to any order desired. When the expansion is truncated after terms of $O\left((\nabla u)^n\right)$, the resulting model is called an n^{th}-order fluid. The primary problem with the n^{th}-order fluid model is that it has a finite radius of convergence beyond which the full nonlinear "parent" constitutive model would presumably be needed. In addition, since n^{th}-order fluids are based upon a Taylor series expansion of the stress functional, they cannot represent rapidly varying or discontinuous flows. For example, the relaxation of stress following the cessation of steady shear flow cannot be described by an n^{th}-order fluid model.

To qualitatively describe the stress in abruptly changing flows, we can employ the sub-class of simple fluids which are known as differential models. A widely used differential model is that which was introduced

and thoroughly studied nearly twenty years ago by Oldroyd (1958). The basic six constant Oldroyd model, in its most general form, may be written as

$$\underline{\underline{\tau}} + \lambda_1 \frac{\mathcal{D}\underline{\underline{\tau}}}{\mathcal{D}t} - \mu_1(\underline{\underline{e}}\cdot\underline{\underline{\tau}} + \underline{\underline{\tau}}\cdot\underline{\underline{e}}) + \mu_o(\underline{\underline{\tau}}:\underline{\underline{I}})\underline{\underline{e}}$$

$$= 2\eta_o\underline{\underline{e}} + 2\eta_o\lambda_2 \frac{\mathcal{D}\underline{\underline{e}}}{\mathcal{D}t} - 4\eta_o\mu_2(\underline{\underline{e}}\cdot\underline{\underline{e}}) \tag{8}$$

where λ_1, μ_1, μ_o, η_o, λ_2 and μ_2 are constants characteristic of the material and $\mathcal{D}/\mathcal{D}t$ represents the Jaumann or corotational derivative of a tensor. For an arbitrary tensor $\underline{\underline{B}}$, this derivative is defined by

$$\frac{\mathcal{D}\underline{\underline{B}}}{\mathcal{D}t} = \frac{\partial\underline{\underline{B}}}{\partial t} + \underline{u}\cdot\nabla\underline{\underline{B}} + \underline{\underline{w}}\cdot\underline{\underline{B}} - \underline{\underline{B}}\cdot\underline{\underline{w}} \tag{9}$$

where $\underline{\underline{w}}$ is the vorticity tensor

$$\underline{\underline{w}} = \frac{1}{2}\left(\nabla\underline{u} - (\nabla\underline{u})^T\right) \tag{10}$$

The corotational derivative describes the time rate of change relative to a reference frame which rotates and translates with the material element.

With $\mu_1 = \mu_2 = \mu_o = 0$, the model reduces to the so-called corotational Jefferey's model which has been recommended by Bird et al. (1974) as a useful model for studying polymer behavior in complex flow problems. Another useful derivative of the full Oldroyd equation is the four constant co-deformational Oldroyd model which has been used extensively by Walters and co-workers. For this model $\mu_1 = \lambda_1$, $\mu_2 = \lambda_2$ and $\mu_o \neq 0$. When $\mu_1 = \lambda_1$ and $\mu_2 = \lambda_2$, the terms $(\underline{\underline{e}}\cdot\underline{\underline{\tau}} + \underline{\underline{\tau}}\cdot\underline{\underline{e}})$ and $(\underline{\underline{e}}\cdot\underline{\underline{e}})$ are conveniently consolidated with the corotational derivative, giving the Oldroyd or co-deformational derivative

$$\frac{\delta\underline{\underline{B}}}{\delta t} = \frac{\partial\underline{\underline{B}}}{\partial t} + \underline{u}\cdot\nabla\underline{\underline{B}} - \left[(\nabla\underline{u})^T\cdot\underline{\underline{B}} + \underline{\underline{B}}\cdot\nabla\underline{u}\right] \tag{11}$$

The co-deformational derivative describes the rate of change relative to a frame of reference which not only translates and rotates with a fluid element, but also deforms with it. From a purely continuum mechanical viewpoint, there is no reason to prefer one of the two-time derivatives described above over the other, or indeed over any other time derivative which is properly invariant to a change of reference frame. In fact, the two sets of terms involving λ_1 and μ_1, and λ_2 and μ_2 can be thought of as defining a general tensorially invariant time derivative which will be intermediate to the two derivatives listed above, provided $0 \leq \mu_1 \leq \lambda_1$ and $0 \leq \mu_2 \leq \lambda_2$. The only constraint is that one would expect, from a physical point of view, to have the same time derivative appear on both sides of the constitutive equation.

In the present work, we will therefore utilize the Oldroyd model with

$$\mu_1 = \alpha\lambda_1 \qquad \text{and} \qquad \mu_2 = \alpha\lambda_2 \qquad \text{where} \qquad 0 \leq \alpha \leq 1$$

thus reducing the number of material parameters by one, while simultaneously building the concept of an intermediate, but equal, time derivative into the general Oldroyd model. In the co-deformational limit ($\alpha = 1$) used by Walters, the primary role of the term involving μ_0 is to allow for shear thinning of the viscosity, which is generally accepted as one of the most important qualitative characteristics of a polymeric fluid. If $\alpha \neq 1$, on the other hand, we will show that shear thinning is predicted by the model without the μ_0 term. Since the μ_0 term is <u>not</u> known to provide any other essential contribution to the qualitative response of the material, we shall choose $\mu_0 = 0$ in the present work. The final form of the Oldroyd model to be used in this thesis is thus

$$\underline{\underline{\tau}} + \lambda_1 \left\{ \frac{\mathcal{D}\underline{\underline{\tau}}}{\mathcal{D}t} - \alpha(\underline{\underline{e}}\cdot\underline{\underline{\tau}} + \underline{\underline{\tau}}\cdot\underline{\underline{e}}) \right\} = 2\eta_0\underline{\underline{e}} + 2\eta_0\lambda_2 \left\{ \frac{\mathcal{D}\underline{\underline{e}}}{\mathcal{D}t} - 2\alpha(\underline{\underline{e}}\cdot\underline{\underline{e}}) \right\} \qquad (12)$$

We shall show later that this model qualitatively predicts many of the known phenomena of viscoelastic fluid flows. We note here, however, that there is strong precedent for the choice $0 < \alpha < 1$ in the many model studies of solutions and suspensions where deductive theoretical analysis has shown this restriction to be satisfied in every case known to this investigator (e.g. Phan Tien and Tanner, 1977; Lumley, 1971; Hinch and Leal, 1972).

We assume that any model chosen for initial studies of non-viscometric flow (such as the present investigation) should produce at least qualitatively correct response in viscometric flows, as well as any other well-documented non-viscometric flow. It should be remarked, however, that the main motivation for this assumption is the fact that shear flow behavior is so heavily documented (indeed, very little information about flow behavior in other geometries is even available), rather than the fact that correct behavior in shear flow is known to be important for correct behavior in other non-viscometric flows.

Indeed, there is considerable evidence in the suspension rheology literature that shear flow is "special" in the sense that it is always a weak flow (see Tanner and Huilgol, 1975), whereas most flows of technological interest can be strong if the velocity gradients are sufficiently large, and thus shear flow would be expected to be a rather poor "test case" for rheological equations of state. Nevertheless, at the present time we are forced by lack of other data to accept shear flow behavior as a dominant criterion for acceptability of a constitutive model for initial studies

of non-viscometric flows. Let us then consider the behavior of the model given by equation (12) in several simple flows, starting with a steady linear shearing flow. The velocity field in this case is given by

$$u_x = \dot{\gamma} y \qquad u_y = u_z = 0$$

and the resulting stress components calculated from (12) are

$$\tau_{yx} = \eta_o \dot{\gamma} \left[\frac{1 + \lambda_1 \lambda_2 (1 - \alpha^2) \dot{\gamma}^2}{1 + \lambda_1^2 (1 - \alpha^2) \dot{\gamma}^2} \right] \tag{13}$$

$$N_1 = \tau_{xx} - \tau_{yy} = \frac{2\eta_o \dot{\gamma}^2 (\lambda_1 - \lambda_2)}{1 + \lambda_1^2 (1 - \alpha^2) \dot{\gamma}^2} \tag{14}$$

$$N_2 = \tau_{yy} - \tau_{zz} = \frac{-\eta_o \dot{\gamma}^2 (1 - \alpha)(\lambda_1 - \lambda_2)}{1 + \lambda_1^2 (1 - \alpha^2) \dot{\gamma}^2} \tag{15}$$

For $\lambda_1 > \lambda_2 > 0$, we see that the non-Newtonian viscosity ($\equiv \tau_{yx}/\dot{\gamma}$) decreases from η_o to $\eta_\infty = \eta_o(\lambda_2/\lambda_1)$ as $\dot{\gamma}$ goes from 0 to ∞ for $\alpha \neq 1$. The primary normal stress difference, N_1, which is indicative of an extra tension, as compared to a Newtonian fluid, in the x-direction, increases quadratically with $\dot{\gamma}$ for small $\dot{\gamma}$. As $\dot{\gamma}$ increases, N_1 increases monotonically until it reaches a limiting value as $\dot{\gamma} \to \infty$. The fact that N_2, the second normal stress difference, is negative means that there is also a tension in the z-direction in qualitative agreement with the observation of an upward bulge in the free surface of a polymeric liquid in the tilted trough experiment cited earlier. A negative value of N_2 is also in agreement with refractive index measurements of Wales and Philippoff (1973) and direct measurement by Olabisi and Williams (1972) in a cone

and plate rheometer. In addition, Leal (1975) has shown that the qualitative observation that slender rod-like particles in simple shear flow drift through Jefferey orbits until the particle rotates about its axis of revolution is also consistent with a negative value of N_2. We also note that the ratio of the second normal stress difference to the first can be adjusted in the range $0 \geq N_2/N_1 \geq -\frac{1}{2}$ by a suitable choice of α. Experimentally, this ratio is found to be about - 0.1 (e.g. see Christiansen and Leppard, 1974). We should also mention two unrealistic features of the model in shear flow. First is the fact that for $\alpha \neq 1$, λ_2/λ_1 must be greater than or equal to 1/9. This restriction is required in order that the shear stress be a monotonically increasing function of shear rate in a simple shear flow as required by simple thermodynamic considerations. Since $\eta_\infty/\eta_o = \lambda_2/\lambda_1$, however, this constraint severely limits the degree of shear thinning relative to the two to four orders of magnitude which is often observed in polymer solutions and melts. While quantitative agreement with such liquids is thus out of the question for a wide range of shear rates, an appreciable degree of shear thinning can be made to occur over a restricted range of shear rates and it thus remains to be seen how severe a restriction this may be in realistic, non-viscometric flows. The second unrealistic feature of the model involves the first normal stress difference. If we examine equation (14) for small $\dot{\gamma}$, we see that as λ_1 increases, N_1 increases which is consistent with other indications of <u>stronger</u> viscoelastic behavior with increasing λ_1. However, if we examine the expression for N_1 for large $\dot{\gamma}$ we see

$$N_1(\infty) = \frac{2\eta_0(\lambda_1 - \lambda_2)}{\lambda_1^2(1 - \alpha^2)}$$

Thus for large $\dot{\gamma}$, N_1 decreases for increasing λ_1. We therefore find the unrealistic combination of increased normal stress effects at small $\dot{\gamma}$ and decreased normal stress effects at large $\dot{\gamma}$ both arising from an increase in λ_1. This decrease in N_1 for increasing λ_1 at large $\dot{\gamma}$ is a basic fault of all Oldroyd models, not just the form examined here.

Another flow which can be used to examine the qualitative acceptability of the constitutive equation (12) is the sudden start up of a shear flow $u_x = \dot{\gamma}y$ when the fluid has been at rest for $t < 0$. The transient expressions for the various stress components are

$$\tau_{yx} = \eta_0\dot{\gamma}\left[\frac{1 + \lambda_1\lambda_2(1 - \alpha^2)\dot{\gamma}^2}{1 + \lambda_1^2(1 - \alpha^2)\dot{\gamma}^2} + \frac{1 - \lambda_2/\lambda_1}{1 + \lambda_1^2(1 - \alpha^2)\dot{\gamma}^2}\right.$$
$$\left. \cdot \left(\lambda_1\dot{\gamma}(1 - \alpha^2)^{\frac{1}{2}} \sin\left[(1 - \alpha^2)^{\frac{1}{2}}\dot{\gamma}t\right] - \cos\left[(1 - \alpha^2)^{\frac{1}{2}}\dot{\gamma}t\right]\right) e^{-t/\lambda_1}\right] \tag{16}$$

$$N_1 = \frac{2\eta_0\dot{\gamma}^2(\lambda_1 - \lambda_2)}{1 + \lambda_1^2(1 - \alpha^2)\dot{\gamma}^2}\left[1 - \frac{e^{-t/\lambda_1}}{\lambda_1\dot{\gamma}(1 - \alpha^2)^{\frac{1}{2}}} \sin\left[(1 - \alpha^2)^{\frac{1}{2}}\dot{\gamma}t\right]\right.$$
$$\left. - e^{-t/\lambda_1}\cos\left[(1 - \alpha^2)^{\frac{1}{2}}\dot{\gamma}t\right]\right] \tag{17}$$

From equation (16), we see that τ_{yx} always rises to its maximum value at $(1 - \alpha^2)^{\frac{1}{2}}\dot{\gamma}t = \pi/2$ and then undergoes damped oscillations about its steady state value. Similarly, the expression for N_1 rises to its maximum at $(1 - \alpha^2)^{\frac{1}{2}}\dot{\gamma}t = \pi$ and then also undergoes damped oscillations about its steady state value. Experimentally it is found that the maximum in N_1 occurs after the maximum in τ_{yx}, in accord with the above results

(Meissner, 1972). However, in most experiments the curves simply rise to a maximum and then settle monotonically to their steady state values. We thus conclude that the model gives qualitatively correct predictions, although the details are not quite correct.

We next explore the relaxation of the stresses after an abrupt cessation of a steady linear shear flow $u_x = \dot{\gamma}y$ at $t = 0$. The expressions for the shear stress and first normal stress difference in this case are

$$\tau_{yx} = \frac{\eta_0\dot{\gamma}(1 - \lambda_2/\lambda_1)}{1 + \lambda_1^2(1 - \alpha^2)\dot{\gamma}^2} e^{-t/\lambda_1} \tag{18}$$

$$N_1 = \frac{2\eta_0\dot{\gamma}^2(\lambda_1 - \lambda_2)}{1 + \lambda_1^2(1 - \alpha^2)\dot{\gamma}^2} e^{-t/\lambda_1} \tag{19}$$

If we compare the steady state shear stress with equation (18) evaluated at $t = 0$, we observe that there is a discontinuity at $t = 0$, whereas the expression for N_1 is continuous at $t = 0$. If we divide equations (18) and (19) by the steady state values ($t < 0$), we obtain the following ratios:

$$\frac{\tau_{yx}(t > 0)}{\tau_{yx}(t < 0)} = \frac{(1 - \lambda_2/\lambda_1)e^{-t/\lambda_1}}{1 + \lambda_1\lambda_2(1 - \alpha^2)\dot{\gamma}^2} \tag{20}$$

$$\frac{N_1(t > 0)}{N_1(t < 0)} = e^{-t/\lambda_1} \tag{21}$$

Examination of these "normalized" ratios shows that the shear stress relaxation trajectory will lie below the corresponding normal stress relaxation trajectory. This is in agreement with experimental observation (Huppler et al, 1967). The experiments also show that both of the above

relax faster with increasing $\dot{\gamma}$. This phenomenon is correctly predicted by the model for the shear stress ratio in the sense that the initial jump is larger for larger values of $\dot{\gamma}$, but the predicted normal stress ratio shows no such effect.

Uniaxial extensional motion is the one non-viscometric flow where a reasonable quantity of experimental data is available. While there is some controversy as to whether a steady elongational flow exists, it is generally believed that the elongational viscosity of a macromolecular fluid increases above the Newtonian value ($\bar{\eta} = 3\eta_o$). This increase in elongational viscosity is consistent with the tubeless siphon effect described earlier. The velocity field for this irrotational flow is

$$u_x = Ex \qquad u_y = -Ey/2 \qquad u_z = -Ez/2$$

For steady uniaxial extension, the elongational viscosity $\left(\bar{\eta} \equiv (\tau_{xx} - \tau_{zz})/E\right)$ is thus predicted via equation (12) to be

$$\bar{\eta} = 3\eta_o \left(\frac{1 - \alpha\lambda_2 E(1 + 2\alpha\lambda_1 E)}{(1 - 2\alpha\lambda_1 E)(1 + \alpha\lambda_1 E)} \right) \tag{22}$$

Of particular interest here is the prediction of a "critical" extension rate at which the elongational viscosity becomes unbounded, namely

$$E = 1/2\alpha\lambda_1$$

The increase in elongational viscosity from the Newtonian value of $3\eta_o$ is in agreement with experiments such as those of Metzner and Metzner (1970) in which $\bar{\eta}/\eta_o$ was conservatively estimated to be 1700 in one instance. The validity of the inference of a limit in attainable extension rates, E, to values less than $1/2\alpha\lambda_1$ is best discussed in the context of the transient start-up of uniaxial extensional flow from a state of rest. The transient elongational viscosity for this case is predicted to be

$$\frac{\bar{\eta}}{\eta_o} = 3\left(\frac{1 - \alpha\lambda_2 E(1 + 2\alpha\lambda_1 E)}{(1 - 2\alpha\lambda_1 E)(1 + \alpha\lambda_1 E)}\right) - \left(1 - \frac{\lambda_2}{\lambda_1}\right)$$
$$\cdot \left(\frac{2\exp\left[-(1 - 2\alpha\lambda_1 E)\frac{t}{\lambda_1}\right]}{1 - 2\alpha\lambda_1 E} + \frac{\exp\left[-(1 + \alpha\lambda_1 E)\frac{t}{\lambda_1}\right]}{1 + \alpha\lambda_1 E}\right) \qquad (23)$$

First, we note that this expression predicts a monotonic increase to steady state provided that $1 - 2\alpha\lambda_1 E > 0$. This is in agreement with the data of Laun and Munstedt (1978) for low density polyethylene. In addition, we see that the "critical" extension rate $E = 1/2\alpha\lambda_1$ is really a demarcation between bounded stress values at large times, which occur for $E < 1/2\alpha\lambda_1$, and unbounded exponential growth with time which occurs for $E > 1/2\alpha\lambda_1$. For $E = 1/2\alpha\lambda_1$ the expression for $\bar{\eta}$ becomes

$$\bar{\eta}/\eta_o = 2\left(1 - \frac{\lambda_2}{\lambda_1}\right)\frac{t}{\lambda_1} + \frac{2}{3}\left(1 + \frac{\lambda_2}{2\lambda_1}\right)\left(1 - e^{-3t/2\lambda_1}\right) + \frac{\lambda_2}{\lambda_1}\left(2 + e^{-3t/2\lambda_1}\right)$$

This expression reduces to that derived by Denn and Marucci (1971) for the case $\lambda_2 = 0$. Note that the elongational viscosity does not even reach the Newtonian value until slightly more than one relaxation time has passed, thus showing that extremely large tensile stresses are not experienced at all instants of time at the "critical" extension rate. Thus, unbounded stresses would not be expected to occur in real flows since the local value of E may be changed through global changes in the flow type.

Equation (23) is in agreement with the expression obtained by Bird et al. (1974) for a corotational Jefferey's model (i.e. $\alpha = 0$) but

disagrees with the expression obtained by Zana (1975) for the case of $\alpha = 1$. Zana's expression for $\bar{\eta}$ is continuous at $t = 0$, whereas the expression obtained here is not. We believe this reflects an error in Zana's solution. However, the only qualitative conclusion that would be changed from Zana (1975) is that $\lambda_2 = \lambda_1$ gives the Newtonian value $\bar{\eta} = 3\eta_o$ for all times, not just as $t \to \infty$. Since it is generally accepted that $\bar{\eta}$ is larger than the Newtonian value, $3\eta_o$, we conclude that α must be greater than zero.

In summary, then, the proposed model for the extra stress tensor given by equation (12) exhibits a shear thinning viscosity, normal stresses in steady shear flow, and reasonable transients in start-up and cessation of shear flow. In addition, the elongational viscosity is found to increase with extension rate in uniaxial extensional flows, again in qualitative agreement with available experimental information. Based upon these results, we conclude that the model is a good candidate for initial studies of non-viscometric flows.

4. Existing Theoretical Analyses of Translational Particle Motions in Non-Newtonian Fluids

Theoretical studies of the translational motion of particles in viscoelastic fluids at low Reynolds number have been pursued actively for almost twenty years. Due to the nonlinearities in the governing equations, which are associated with the more commonly proposed constitutive relationships for the fluid, the resulting analytical solutions have been limited almost exclusively to cases where the fluid exhibits only a small departure from Newtonian behavior. The only exception to this is for the motion of particles in generalized Newtonian fluids. For such fluids, Bird (1960) and Johnson (1960) have derived variational principles for the associated boundary value problems which allow approximate determination of drag coefficients and velocity fields. These "solutions" to the variational equations must satisfy the boundary conditions of the problem and the equation of continuity. The only constraints on the use of these variational principles are that the convective acceleration terms must be zero or negligible, and the flow must be steady. Slattery (1962) and Wasserman and Slattery (1964) used them to compute upper and lower bounds on the drag coefficient for a sphere moving at zero Reynolds number in a power law fluid of infinite extent. The two bounds do not coincide for $n < 0.9$, leading to some uncertainty in predicting the terminal velocity. Recent improvements by Yoshioka and Adachi (1973) and Mohan and Venkateswarlu (1976a) have narrowed the gap between the two bounds significantly. The first attempt to use the variational principle for the creeping flow of a power law fluid past a Newtonian fluid sphere was made by Nakano and Tien (1968). A slight improvement on their solution was reported by Mohan

(1974) who included the dissipation of energy in the drop. Mohan and Venkateswarlu (1976a) obtained the corresponding lower bound on the drag coefficient for this problem.

Perturbation solutions can also be obtained for the power law fluid if we restrict n so that $|n - 1| \ll 1$. Hirose and Moo-Young (1969) were the first to carry out this type of an analysis for a spherical gas bubble in a power law fluid. Their result for the drag force on the bubble is

$$\text{Drag} = 4\pi(3)^{\frac{n-1}{2}} \left(\frac{13 + 4n - 8n^2}{(2n + 1)(n + 2)}\right) m \left(\frac{U_\infty}{a}\right)^n a^2 \qquad (24)$$

where m and n are the material constants which characterize the fluid [see equation (4)], U_∞ is the velocity of the bubble, and a is the bubble radius. Another solution to the same problem, employing an improved method of analysis, has recently been obtained by Bhavaraju, Mashelkar and Blanch (1978). Their result for the drag force on the bubble is

$$\text{Drag} = 4\pi(3)^{\frac{n-1}{2}} \left(1 - 7.66 \left(\frac{n - 1}{2}\right)\right) m \left(\frac{U_\infty}{a}\right)^n a^2 \qquad (25)$$

Acharya, Mashelkar and Ulbrecht (1976) have published a solution for the flow of a power law fluid past a solid sphere under the same restrictions. Their solution is unacceptable, however, since the drag coefficient does not lie between the upper and lower bounds of Wasserman and Slattery in the region $0.8 < n < 1.0$. All of the solutions mentioned above show an increase in the drag coefficient with decreasing n if the values of U_∞, a and m are held constant.

Other investigations for generalized Newtonian fluids include Adachi, Yoshioka and Yamamoto (1973) who used an extended method of moments to obtain an approximate solution to the flow of a power law fluid past a sphere at Reynolds number of 60. A numerical solution for a Carreau viscosity generalized Newtonian fluid at Reynolds numbers ranging from 0.1 to 60 was later reported by Adachi, Yoshioka and Sakai (1977). The Ellis fluid model, a generalized Newtonian fluid in which $\eta = \eta(\tau)$ [see Bird, Armstrong and Hassager (1977)], has been treated by Hopke and Slattery (1970) who found variational principles for this fluid and used them to calculate upper and lower bounds on the drag coefficient for the low Reynolds number flow past a solid sphere. Mohan and Venkateswarlu (1976b) studied the corresponding problem for a spherical fluid drop.

Up to this point, we have only discussed theoretical solutions for purely viscous fluids. The first solution for low Reynolds number motion of a viscoelastic fluid past a solid sphere in an unbounded domain was Leslie's (1961) small Wi ($= \frac{U_\infty \lambda_1}{a}$) solution for the Oldroyd (1958) model. The result for the drag on the sphere for the four constant model used extensively by Walters and co-workers is

$$\text{Drag} = 6\pi\eta_0 U_\infty a \left\{1 - \left(\frac{U_\infty \lambda_1}{a}\right)^2 \left[\frac{401 - 143\lambda_2/\lambda_1}{25025} + \frac{471\mu_0/\lambda_1}{2275}\right]\left(1 - \frac{\lambda_2}{\lambda_1}\right)\right\} \quad (26)$$

We see that the presence of elasticity reduces the drag on the sphere. If $(\mu_0/\lambda_1) \simeq 1$, we see that the term involving this quantity which is associated with shear thinning of the viscosity is more than ten times larger than the remaining term involving λ_2/λ_1 which is associated with "elasticity" of the fluid. Caswell and Schwarz (1962) and Giesekus (1963) studied the translational motion of a sphere in a third-order fluid, also for small Wi. Giesekus made

use of the known relationships between the Oldroyd fluid parameters and the third-order fluid parameters for small Wi to show that his solution is identical to Leslie's solution. Since the Caswell and Schwarz solution does not agree with these two solutions, it is believed to be in error. Mena and Caswell (1974) later included the inertia terms for an Oldroyd fluid in a formal matched asymptotic expansion for small, but non-zero Reynolds number.

Wagner and Slattery (1971) were the first to study the motion of drops in a viscoelastic liquid. They assumed that both the inner and the outer fluids could be represented by a third-order fluid model and solved the resulting problem for Wi << 1. The principal results of their analysis were an expression for the drag (reduced relative to the Newtonian value) and an expression for the drop shape (prolate spheroidal). There are several algebraic or printing errors in the work, which casts some doubt upon the results. Moo-Young and Hirose (1972) used the same six constant Oldroyd model used by Leslie in the solid sphere problem to analyze the motion of a gas bubble in a viscoelastic liquid. Subsequent analysis by me (as part of the present study) and Shirotsuka and Kawase (1974), using the same fluid model to study the motion of non-Newtonian drop, showed errors in the Moo-Young and Hirose work. Our result for the drag on a spherical gas bubble for the four constant Oldroyd model used by Walters is

$$\text{Drag} = 4\pi\eta_o U_\infty a \left(1 - \left(\frac{U_\infty \lambda_1}{a}\right)^2 \left(1 - \frac{\lambda_2}{\lambda_1}\right)\left[\frac{9\mu_o/\lambda_1}{25} - \frac{7}{75} - \frac{2\lambda_2/\lambda_1}{75}\right]\right) \qquad (27)$$

This result is identical to that of Shirotsuka and Kawase. Of particular interest here is the observation that if μ_o is small enough, the drag on the bubble will actually be greater than in a Newtonian fluid with the same viscosity as the zero-shear-rate viscosity, η_o. Due to the complexity

of the solutions, no one has determined whether the solutions of Wagner and Slattery and Shirotsuka and Kawase can be reduced to the same form if the relationships between the various material parameters are employed.

Ajayi (1975) also used the six constant Oldroyd model to analyze the flow of a viscoelastic liquid past a drop. He stopped after obtaining the first correction to the stresses. Using this information he showed that the drop shape would change to prolate spheroidal as a first approximation. Hassager (1977) presented similar findings for the motion of a gas bubble in a second-order fluid.

The only attempt to analyze the motions of a viscoelastic fluid past a particle, outside the domain of near-Newtonian behavior (Wi << 1), is the study of Ultman and Denn (1971). These authors used an Oseen-type linearization to solve for the motion of a Maxwell fluid at finite Wi past a sphere and an infinite circular cylinder for low Reynolds number. Due to the importance given this particular work by other investigators, we will defer discussion of it until later.

The above studies represent the extent of analytical investigation of the flow of non-Newtonian liquids past a spherical object. Due to the nonlinearity of the constitutive equations employed, it will be necessary to employ numerical techniques to push our knowledge of non-Newtonian flow behavior beyond the small Wi level for this problem.

The only theoretical investigation of the effect of finite container walls on the translational motion of particles in a viscoelastic fluid is by Caswell (1970). Caswell used the n^{th}-order fluid model to represent the fluid (thus again restricting the study to near-Newtonian behavior) and derived an expression for the effect of the wall which corresponds to the

usual Faxén correction in Newtonian fluids. He later extended these results (1972) by examining the effect of terms which are ordinarily suppressed by symmetry. He found that spheres sedimenting in a non-Newtonian fluid in a circular cylinder were much more likely to migrate radially than spheres sedimenting in a Newtonian liquid.

Theoretical studies of non-spherical particles in non-Newtonian fluids have received much less attention than the study of spheres. The first author to analyze the translational motion of a non-spherical particle was Leal (1975) who studied slender rod-like particles in a second-order fluid. He found that a slender rod would sediment with the same velocity as in a Newtonian fluid which had the same zero-shear-rate viscosity. The significant difference between Newtonian and second-order fluid behavior was that the particle was predicted to rotate toward the vertical so that it eventually fell with its long axis parallel to the gravitational acceleration vector. More recently, Brunn (1977) developed the framework for analyzing the sedimentation of a general transversely isotropic particle in a second-order fluid. Using symmetry arguments alone, he was able to show that the particle must rotate toward either the vertical or the horizontal. Unfortunately, however, he did not carry out the detailed calculations which are necessary to predict which of these orientations would be stable for a given particle.

All of the solutions listed above are strictly valid only for fluids whose behavior is very nearly Newtonian. Whether they provide correct qualitative predictions outside this domain can only be judged by comparison with solutions (presumably numerical) of the complete equations of motion for

a fully nonlinear constitutive equation, or preferably by comparison with experimental data.

Among the small Wi solutions for a rigid sphere, only the result for the drag given by Giesekus is easily adapted for comparison with the numerical solutions which we have obtained using the fluid model given by equation (12). Similar small Wi results for a bubble should be obtainable from the third-order fluid solution of Wagner and Slattery, but their results are believed to contain some errors. Since the small Wi motion of a bubble in the viscoelastic fluid described by equation (12) is an important theoretical result for comparison with subsequent numerical solutions. we have carried out the pertinent analysis which is described below. The results which we obtain can be compared with equation (27) of Shirotsuka and Kawase (1974) for the case of $\alpha = 1$.

We shall consider the case of a Newtonian gas bubble rising in an infinite expanse of the viscoelastic fluid described by equation (12). Since this problem is axisymmetric, we can satisfy the continuity equation by introducing the streamfunction ψ. All of the kinematic variables are then expressed in terms of derivatives of ψ. The velocities are nondimensionalized by the velocity far from the sphere U_∞, the radial coordinate is scaled by the sphere radius a, and the stresses are nondimensionalized by $\eta_0 U_\infty/a$. The surface boundary conditions for this problem are $u_r = 0$ and $\tau_{r\theta} = 0$ at $r = 1$. The pertinent governing equations are written out in Chapter III, and will not be repeated here. In order to obtain a solution valid for small $Wi\left(= \frac{U_\infty \lambda_1}{a}\right)$ we assume asymptotic expansions of the form $\psi = \psi_0 + Wi\psi_1 + Wi^2\psi_2 + \ldots$ for all of the dependent variables of the problem. Substituting into the governing equations and collecting all

terms which are independent of Wi we obtain

$$(\tau_{rr})_o = 2(e_{rr})_o;\ (\tau_{\theta\theta})_o = 2(e_{\theta\theta})_o;(\tau_{\phi\phi}) = 2(e_{\phi\phi})_o;(\tau_{r\theta})_o = 2(e_{r\theta})_o \tag{28}$$

Thus, substituting (28) into the equations of motion and eliminating p_o we obtain

$$E^4\psi_o = 0 \tag{29}$$

where

$$E^2 = \frac{\partial^2}{\partial r^2} + \frac{\sin\theta}{r^2}\frac{\partial}{\partial\theta}\left(\frac{1}{\sin\theta}\frac{\partial}{\partial\theta}\right) \tag{30}$$

The solution to (29) is, of course, the standard Hadamard-Rybczynski result

$$\psi_o = \left(\frac{1}{2}r^2 - \frac{1}{2}r\right)\sin^2\theta \tag{31}$$

The terms of the constitutive equations which are first order in Wi, may now be obtained in the form

$$\begin{aligned}
(\tau_{rr})_1 &= 2(e_{rr})_1 + (1-\varepsilon)\left\{\cos^2\theta\left(\frac{6}{r^3} - \frac{5}{r^4} + \frac{4\alpha}{r^4}\right) - \frac{2}{r^3} + \frac{1}{r^4}\right\} \\
(\tau_{\theta\theta})_1 &= 2(e_{\theta\theta})_1 - (1-\varepsilon)\left\{\cos^2\theta\left(\frac{3}{r^3} - \frac{5}{2r^4} - \frac{\alpha}{r^4}\right) - \frac{1}{r^3} + \frac{1}{2r^4}\right\} \\
(\tau_{\phi\phi})_1 &= 2(e_{\phi\phi})_1 - (1-\varepsilon)\left\{\cos^2\theta\left(\frac{3}{r^3} - \frac{5}{2r^4} - \frac{\alpha}{r^4}\right) - \frac{1}{r^3} + \frac{1}{2r^4}\right\} \\
(\tau_{r\theta})_1 &= 2(e_{r\theta})_1 + (1-\varepsilon)\sin\theta\cos\theta\left(\frac{3}{r^3} - \frac{3}{r^4}\right)
\end{aligned} \tag{32}$$

where $\varepsilon = \lambda_2/\lambda_1$

Substituting these expressions into the equations of motion at O(Wi), we obtain

$$\frac{\partial p_1}{\partial r} = \frac{1}{r^2 \sin\theta}\frac{\partial}{\partial\theta}(E^2\psi_1) + (1-\varepsilon)\left\{\cos^2\theta\left(\frac{9}{r^4} - \frac{4}{r^5} - \frac{10\alpha}{r^5}\right) - \frac{3}{r^4} + \frac{2}{r^5}\right\} \tag{33a}$$

$$\frac{1}{r}\frac{\partial p_1}{\partial\theta} = \frac{-1}{r\sin\theta}\frac{\partial}{\partial r}(E^2\psi_1) + (1-\varepsilon)\sin\theta\cos\theta\left(\frac{6}{r^4} - \frac{2}{r^5} - \frac{2\alpha}{r^5}\right) \tag{33b}$$

and the pressure p_1 may be eliminated from these expressions to obtain the governing differential equation for ψ_1, namely

$$E^4\psi_1 = -\frac{12(1-\varepsilon)\alpha\sin^2\theta\cos\theta}{r^5} \tag{34}$$

Solving equation (34) subject to the appropriate boundary conditions, we obtain

$$\psi_1 = \frac{\alpha(1-\varepsilon)}{10}\left(-3 + \frac{5}{r} - \frac{2}{r^2}\right)\sin^2\theta\cos\theta \tag{35}$$

Finally, repeating the above process, we calculate all of the terms in the constitutive model which are of order Wi^2.

$$\begin{aligned}(\tau_{rr})_2 = {} & 2(e_{rr})_2 - \frac{\alpha(1-\varepsilon)^2}{10}\cos\theta\left(\frac{144}{r^4} - \frac{520}{r^5} + \frac{560}{r^6} - \frac{192}{r^7}\right) \\ & + \frac{\alpha(1-\varepsilon)^2}{10}\cos^3\theta\left(\frac{216}{r^4} - \frac{856}{r^5} + \frac{1000}{r^6} - \frac{368}{r^7}\right) - (1-\varepsilon)\cos\theta\left(\frac{24}{r^4} - \frac{38}{r^5} + \frac{15}{r^6}\right) \\ & + (1-\varepsilon)\cos^3\theta\left(\frac{36}{r^4} - \frac{66}{r^5} + \frac{31}{r^6}\right) - \alpha(1-\varepsilon)\cos\theta\left(\frac{12}{r^5} - \frac{6}{r^6}\right) \\ & + \alpha(1-\varepsilon)\cos^3\theta\left(\frac{36}{r^5} - \frac{30}{r^6}\right) + \alpha^2(1-\varepsilon)\cos^3\theta\,\frac{8}{r^6} \\ & - \frac{\alpha^2(1-\varepsilon)^2}{10}\cos\theta\left(\frac{48}{r^5} - \frac{120}{r^6} + \frac{64}{r^7}\right) + \frac{\alpha^2(1-\varepsilon)^2}{10}\cos^3\theta\left(\frac{144}{r^5} - \frac{360}{r^6} + \frac{192}{r^7}\right)\end{aligned} \tag{36a}$$

$$(\tau_{\theta\theta})_2 = 2(e_{\theta\theta})_2 + \frac{\alpha(1-\varepsilon)^2}{10}\cos\theta\left(\frac{90}{r^4} - \frac{358}{r^5} + \frac{415}{r^6} - \frac{152}{r^7}\right)$$

$$- \frac{\alpha(1-\varepsilon)^2}{10}\cos^3\theta\left(\frac{126}{r^4} - \frac{526}{r^5} + \frac{635}{r^6} - \frac{240}{r^7}\right) + (1-\varepsilon)\cos\theta\left(\frac{15}{r^4} - \frac{25}{r^5} + \frac{21}{2r^6}\right)$$

$$- (1-\varepsilon)\cos^3\theta\left(\frac{21}{r^4} - \frac{39}{r^5} + \frac{37}{2r^6}\right) - \alpha(1-\varepsilon)\cos\theta\left(\frac{3}{r^5} - \frac{3}{2r^6}\right)$$

$$+ \alpha(1-\varepsilon)\cos^3\theta\left(\frac{9}{r^5} - \frac{15}{2r^6}\right) - \frac{\alpha^2(1-\varepsilon)\cos^3\theta}{r^6}$$

$$- \frac{\alpha^2(1-\varepsilon)^2}{10}\cos\theta\left(\frac{12}{r^5} - \frac{40}{r^6} + \frac{24}{r^7}\right) + \frac{\alpha^2(1-\varepsilon)^2}{10}\cos^3\theta\left(\frac{36}{r^5} - \frac{100}{r^6} + \frac{56}{r^7}\right) \tag{36b}$$

$$(\tau_{\phi\phi})_2 = 2(e_{\phi\phi})_2 + \frac{\alpha(1-\varepsilon)^2}{10}\cos\theta\left(\frac{54}{r^4} - \frac{162}{r^5} + \frac{145}{r^6} - \frac{40}{r^7}\right)$$

$$- \frac{\alpha(1-\varepsilon)^2}{10}\cos^3\theta\left(\frac{90}{r^4} - \frac{330}{r^5} + \frac{365}{r^6} - \frac{128}{r^7}\right) + (1-\varepsilon)\cos\theta\left(\frac{9}{r^4} - \frac{13}{r^5} + \frac{9}{2r^6}\right)$$

$$- (1-\varepsilon)\cos^3\theta\left(\frac{15}{r^4} - \frac{27}{r^5} + \frac{25}{2r^6}\right) - \alpha(1-\varepsilon)\cos\theta\left(\frac{3}{r^5} - \frac{3}{2r^6}\right)$$

$$+ \alpha(1-\varepsilon)\cos^3\theta\left(\frac{9}{r^5} - \frac{15}{2r^6}\right) - \frac{\alpha^2(1-\varepsilon)\cos^3\theta}{r^6}$$

$$- \frac{\alpha^2(1-\varepsilon)^2}{10}\cos\theta\left(\frac{12}{r^5} - \frac{20}{r^6} + \frac{8}{r^7}\right) + \frac{\alpha^2(1-\varepsilon)^2}{10}\cos^3\theta\left(\frac{36}{r^5} - \frac{80}{r^6} + \frac{40}{r^7}\right) \tag{36c}$$

$$(\tau_{r\theta})_2 = 2(e_{r\theta})_2 + \frac{\alpha(1-\varepsilon)^2}{10}\sin\theta\cos^2\theta\left(\frac{144}{r^4} - \frac{593}{r^5} + \frac{705}{r^6} - \frac{256}{r^7}\right)$$

$$+ (1-\varepsilon)\sin\theta\cos^2\theta\left(\frac{24}{r^4} - \frac{93}{2r^5} + \frac{45}{2r^6}\right) - \frac{\alpha(1-\varepsilon)^2}{10}\sin\theta\left(\frac{36}{r^4} - \frac{127}{r^5} + \frac{135}{r^6} - \frac{44}{r^7}\right)$$

$$- (1-\varepsilon)\sin\theta\left(\frac{6}{r^4} - \frac{9}{r^5} + \frac{3}{r^6}\right) + \alpha(1-\varepsilon)\sin\theta\cos^2\theta\left(\frac{9}{2r^5} - \frac{9}{2r^6}\right)$$

$$+ \frac{\alpha^2(1-\varepsilon)^2}{10}\sin\theta\cos^2\theta\left(\frac{18}{r^5} - \frac{50}{r^6} + \frac{32}{r^7}\right) \tag{36d}$$

Thus, the equations of motion at $O(Wi^2)$ become

$$\frac{\partial p_2}{\partial r} = \frac{1}{r^2 \sin\theta}\frac{\partial}{\partial\theta}(E^2\psi_2) - \frac{\alpha(1-\varepsilon)^2}{10}\cos\theta\left(\frac{216}{r^5} - \frac{400}{r^6} + \frac{168}{r^8}\right)$$
$$+ \frac{\alpha(1-\varepsilon)^2}{10}\cos^3\theta\left(\frac{360}{r^5} - \frac{660}{r^6} - \frac{180}{r^7} + \frac{448}{r^8}\right) - (1-\varepsilon)\cos\theta\left(\frac{36}{r^5} - \frac{35}{r^6} + \frac{6}{r^7}\right)$$
$$+ (1-\varepsilon)\cos^3\theta\left(\frac{60}{r^5} - \frac{54}{r^6} - \frac{3}{r^7}\right) + \alpha(1-\varepsilon)\cos\theta\left(\frac{33}{r^6} - \frac{18}{r^7}\right)$$
$$- \alpha(1-\varepsilon)\cos^3\theta\left(\frac{108}{r^6} - \frac{117}{r^7}\right) - \alpha^2(1-\varepsilon)\cos^3\theta\,\frac{30}{r^7}$$
$$+ \frac{\alpha^2(1-\varepsilon)^2}{10}\cos\theta\left(\frac{132}{r^6} - \frac{440}{r^7} + \frac{288}{r^8}\right)$$
$$- \frac{\alpha^2(1-\varepsilon)^2}{10}\cos^3\theta\left(\frac{432}{r^6} - \frac{1420}{r^7} + \frac{928}{r^8}\right) \qquad (37a)$$

and

$$\frac{1}{r}\frac{\partial p_2}{\partial\theta} = \frac{-1}{r\sin\theta}\frac{\partial}{\partial r}(E^2\psi_2) + \frac{\alpha(1-\varepsilon)^2}{10}\sin\theta\cos^2\theta\left(\frac{270}{r^5} - \frac{588}{r^6} + \frac{60}{r^7} + \frac{192}{r^8}\right)$$
$$- \frac{\alpha(1-\varepsilon)^2}{10}\sin\theta\left(\frac{54}{r^5} - \frac{104}{r^6} + \frac{10}{r^7} + \frac{24}{r^8}\right) + (1-\varepsilon)\sin\theta\cos^2\theta\left(\frac{45}{r^5} - \frac{36}{r^6} - \frac{6}{r^7}\right)$$
$$- (1-\varepsilon)\sin\theta\left(\frac{9}{r^5} - \frac{7}{r^6} + \frac{3}{2r^7}\right) - \alpha(1-\varepsilon)\sin\theta\cos^2\theta\left(\frac{36}{r^6} - \frac{36}{r^7}\right)$$
$$+ \alpha(1-\varepsilon)\sin\theta\left(\frac{3}{r^6} - \frac{3}{2r^7}\right) + \alpha^2(1-\varepsilon)\sin\theta\cos^2\theta\,\frac{3}{r^7}$$
$$- \frac{\alpha^2(1-\varepsilon)^2}{10}\sin\theta\cos^2\theta\left(\frac{144}{r^6} - \frac{470}{r^7} + \frac{312}{r^8}\right)$$
$$+ \frac{\alpha^2(1-\varepsilon)^2}{10}\sin\theta\left(\frac{12}{r^6} - \frac{40}{r^7} + \frac{24}{r^8}\right) \qquad (37b)$$

Eliminating p_2, we thus obtain

$$E^4\psi_2 = -\frac{\alpha(1-\varepsilon)^2}{10}\sin^2\theta\left(\frac{120}{r^6}-\frac{60}{r^7}\right)+\frac{\alpha^2(1-\varepsilon)^2}{10}\sin^2\theta\left(\frac{72}{r^6}-\frac{200}{r^7}+\frac{120}{r^8}\right)$$
$$+\frac{\alpha(1-\varepsilon)^2}{10}\sin^2\theta\cos^2\theta\left(\frac{960}{r^6}-\frac{900}{r^7}\right)$$
$$-\frac{\alpha^2(1-\varepsilon)^2}{10}\sin^2\theta\cos^2\theta\left(\frac{576}{r^6}-\frac{1440}{r^7}+\frac{600}{r^8}\right)+(1-\varepsilon)\sin^2\theta\ \frac{3}{r^7}$$
$$+\alpha(1-\varepsilon)\sin^2\theta\left(\frac{18}{r^6}-\frac{9}{r^7}\right)+(1-\varepsilon)\sin^2\theta\cos^2\theta\left(\frac{18}{r^6}+\frac{27}{r^7}\right)$$
$$-\alpha(1-\varepsilon)\sin^2\theta\cos^2\theta\left(\frac{144}{r^6}-\frac{135}{r^7}\right)-\frac{\alpha^2(1-\varepsilon)\sin^2\theta\cos^2\theta\ 108}{r^7} \qquad (38)$$

The solution of (38) is conveniently expressed in terms of

$$Q_1(\eta) = 1-\eta^2 = \sin^2\theta$$

and

$$Q_3(\eta) = -1+6\eta^2-5\eta^4 .$$

Noting that

$$\sin^2\theta\cos^2\theta = \eta^2(1-\eta^2) = \frac{1}{5}(Q_1+Q_3)$$

this solution is

$$\psi_2 = -\frac{\alpha(1-\varepsilon)^2}{10}Q_1\left(\frac{4}{7r}-\frac{1}{r^2}+\frac{3}{7r^3}\right)+\frac{\alpha^2(1-\varepsilon)^2}{50}Q_1\left(\frac{2}{3}r+\frac{16}{21r}-\frac{3}{r^2}+\frac{11}{7r^3}\right)$$
$$+\frac{(1-\varepsilon)}{5}Q_1\left(\frac{3}{5}r-\frac{1}{r}+\frac{1}{4r^2}+\frac{3}{20r^3}\right)+\frac{\alpha(1-\varepsilon)}{5}Q_1\left(\frac{3}{7r}-\frac{3}{4r^2}+\frac{9}{28r^3}\right)$$
$$-\frac{\alpha^2(1-\varepsilon)}{5}Q_1\left(\frac{9}{10}r-\frac{9}{7r}+\frac{27}{70r^3}\right)+\frac{\alpha(1-\varepsilon)^2Q_3}{50}\left(\frac{335}{49r}+\frac{645}{49r^3}-\frac{20}{r^2}+\frac{50\ell n\ r}{7r^3}\right)$$
$$-\frac{\alpha^2(1-\varepsilon)^2}{50}Q_3\left(\frac{127}{98r}+\frac{402}{49r^3}-\frac{12}{r^2}+\frac{80\ell n\ r}{7r^3}+\frac{5}{2r^4}\right)$$
$$-\frac{\alpha^2(1-\varepsilon)}{5}Q_3\left(\frac{27}{49r}-\frac{27}{49r^3}-\frac{6\ell n\ r}{7r^3}\right)+$$

$$+\frac{(1-\varepsilon)Q_3}{5}\left(\frac{69}{196r}+\frac{9}{392r^3}-\frac{3}{8r^2}-\frac{3\ell n\ r}{14r^3}\right)$$

$$-\frac{\alpha(1-\varepsilon)}{5}Q_3\left(\frac{201}{196r}+\frac{387}{196r^3}-\frac{3}{r^2}+\frac{15\ell n\ r}{14r^3}\right) \qquad (39)$$

Although higher-order terms could, in principle, be calculated, we terminate our efforts here, and turn to the use of the solutions (31), (35) and (39) for determination of the drag on the bubble. For this problem, the drag is given by

$$\text{Drag} = 2\pi\eta_o U_\infty a \int_0^\pi (\tau_{rr} - p)_{r=1} \sin\theta\cos\theta\, d\theta$$

Thus, utilizing the expressions for τ_{rr} and p obtained above, the result is

$$\text{Drag} = 4\pi\eta_o U_\infty a \left[1 - \frac{Wi^2}{75}(18 - 25\alpha^2 - 2\alpha^2\varepsilon)(1-\varepsilon)\right] \qquad (40)$$

For the case of $\alpha = 1$, the above result is identical to equation (28) Shirotsuka and Kawase (1974) for $\mu_o = 0$, and this provides some confidence in the solution. We note that the drag on the bubble is predicted to be larger than in a Newtonian fluid for $\alpha > \left(18/(25+2\varepsilon)\right)^{\frac{1}{2}}$. A possible rationalization may be that as α increases, the effects of increasing elongational viscosity eventually overtake the effects of shear thinning to produce a larger drag.

One use of the equations obtained above, in addition to using them for a comparison with numerical solutions in Chapter III, is to determine the influence of viscoelasticity on mass transfer at large Peclet number. Zana and Leal (1978) have shown that for large $Pe(\equiv \frac{U_\infty a}{D})$ the velocity field is dominated by the free streaming motion due to the buoyancy

induced bubble rise. Specifically, in this regime, the velocity due to bubble collapse is asymptotically small, and the solutions obtained above for the velocity fields near a rising bubble of constant volume may be used to evaluate the convection terms in the convective-diffusion equation. A general equation for large Pe mass transfer from a fluid sphere, given by Baird and Hamielec (1962), is

$$Sh = \sqrt{\frac{2}{\pi}} \left[\int_0^{\pi} - (U_\theta)_{r=1} \sin^2\theta \, d\theta \right]^{\frac{1}{2}} Pe^{\frac{1}{2}} \tag{41}$$

With a few simple manipulations, it is easily shown that the only terms of U_θ which contribute to the above expression for the Sherwood number are those involving $Q_1(n)$. For a Newtonian fluid in creeping flow, Levich (1962) found that

$$Sh = 0.65 \, Pe^{\frac{1}{2}} \tag{42}$$

When we substitute the expression for U_θ from our present <u>non</u>-Newtonian solution into equation (41), we obtain

$$Sh = 0.65 \, Pe^{\frac{1}{2}} \left[1 + Wi^2(1 - \varepsilon) \left(\frac{13}{50} + \frac{3\alpha}{70} + \frac{\alpha^2(1 - \varepsilon)}{21} - \frac{\alpha(1 - \varepsilon)}{35} - \frac{72\alpha^2}{175} \right) \right]^{\frac{1}{2}} \tag{43}$$

Since the Weissenberg number is small, we may approximate (43) by

$$Sh = 0.65 \, Pe^{\frac{1}{2}} \left(1 + Wi^2(1 - \varepsilon) \left(\frac{13}{100} + \frac{3\alpha}{140} + \frac{\alpha^2(1 - \varepsilon)}{42} - \frac{\alpha(1 - \varepsilon)}{70} - \frac{36\alpha^2}{175} \right) \right) \tag{44}$$

In Figure 1, we plot equation (44) in the modified form of $\left(\frac{Sh}{0.65 \, Pe^{\frac{1}{2}}} - 1 \right) \frac{1}{Wi^2}$ as a function of α. From the figure, it is obvious that the presence of viscoelasticity can either help or hinder mass transfer

in this particular case depending upon the value of α. Although Wi was too large for the present analysis to apply, the experiments of Zana and Leal (1978) suggest that mass transfer is enhanced in a viscoelastic fluid. This suggests in turn that α should be restricted to values $0 < \alpha < 0.8$ so that the rate of mass transfer is increased.

In obtaining the small Wi solution for the bubble, we assumed that the shape was spherical instead of calculating it from the normal stress balance as is strictly required. The normal stress condition can be written in the dimensionless form

$$\frac{1}{R_1} + \frac{1}{R_2} = \left(\frac{\eta_o U_\infty}{\sigma}\right) (\tau_{rr} - p)_{r=1} \tag{45}$$

where R_1 and R_2 are the radii of curvature of the bubble and σ is the surface tension. It is known that (45) is satisfied exactly by the spherical shape for a Newtonian fluid at zero Reynolds number. Thus, the assumption of a spherical shape provides a valid first approximation provided $\left(\frac{\eta_o U_\infty^2 \lambda_1}{\sigma a}\right) << 1$, and we can use the solution we have obtained to calculate the first corrections to the bubble shape. We assume that the bubble will be axisymmetric. Thus, the surface is defined by $r_s = 1 + f(\eta)$ where $\eta = \cos\theta$. For small deformations $f(\eta)$, Landau and Lifschitz (1959) have shown that

$$\frac{1}{R_1} + \frac{1}{R_2} = 2 - 2f - \frac{d}{d\eta}\left((1 - \eta^2)\frac{df}{d\eta}\right) \tag{46}$$

For the bubble, the normal stress balance now becomes

$$2 - 2f - \frac{d}{d\eta}\left((1 - \eta^2)\frac{df}{d\eta}\right) = \left(\frac{\eta_o U_\infty}{a}\right)(\tau_{rr} - p)_{r=1} \tag{47}$$

The condition of constant volume implies

$$\int_{-1}^{1} f \, d\eta = 0 \tag{48}$$

If we specify that the origin of the coordinate system be at the centroid of the bubble, we obtain the following additional condition

$$\int_{-1}^{1} \eta f \, d\eta = 0 \tag{49}$$

From the form of the streamfunction (35) and (39), plus the equations (48) and (49), we can guess that the deformation, f, will be given by a series of Legendre polynomials starting with $P_2(\eta)$. If $(\tau_{rr} - p)_{r=1}$ has a term represented by $a_n P_n(\eta), n \geq 2$, the corresponding value of f is $\frac{a_n}{(n+2)(n-1)} P_n(\eta)$. When we carry out all of the necessary calculations using the solution just obtained for the velocity field, we find that f is given by

$$f = \left(\frac{\eta_0 U_\infty}{\sigma}\right) \left\{ Wi\left[(1-\varepsilon)\left(\frac{\alpha}{5} + \frac{1}{2}\right) P_2(\eta) + 0\left(\frac{\eta_0 U_\infty}{\sigma}\right)\right] + Wi^2(1-\varepsilon)\left(\frac{96 + 74\alpha + 50\alpha^2}{490} - \frac{(1-\varepsilon)}{7350}\left[446\alpha + 153\alpha^2\right]\right) P_3(\eta)\right\} \tag{50}$$

Equation (50) is strictly valid only if $\left(\frac{\eta_0 U_\infty}{\sigma}\right) << Wi$ since otherwise we would need to apply a shape correction to the velocity field at $O\left(Wi \cdot \frac{U_\infty}{\sigma}\right)$ prior to the velocity field correction at $O(Wi^2)$. The O(Wi) term in equation (50) matches the expression given by Ajayi (1975) for $\alpha = 1$. With suitable parameter identification between the second-order fluid and our model, this term also matches the expression given by Hassager (1977). Neither of these two authors have included the P_3 term found here because they stopped their analysis at a lower approximation in Wi. The important thing to notice about equation (5) is the positive coefficient of the P_2

and P_3 terms. The P_2 term causes the bubble to become a prolate spheroid. The P_3 term causes the front end of the bubble to flatten and the back end of the bubble to be drawn out even further. The effect of these terms on the bubble shape is depicted in Figure 2. For positive coefficients of P_2 and P_3 this means that the drop is being deformed into a "teardrop" shape as is also observed experimentally. The effect of increasing α in equation (50) is to make the coefficients of P_2 and P_3 more positive. Thus in contrast to the drag or effect on mass transfer, this comparison with experiment provides no useful estimate of α since the shape is a "teardrop" for all α in the allowable range $0 \leq \alpha \leq 1$.

As we have already noted, the above solutions for particle motion in a viscoelastic liquid have all been based upon the implicit assumption of small deviations from Newtonian behavior. The only work which purports to provide an approximate representation of the flow in the domain of strong elasticity is the analysis of Ultman and Denn (1971) for a generalized Maxwell constitutive model. Ultman and Denn applied an Oseen-like linearization both to the constitutive equation and to the dynamic inertia terms in the equations of motion, and then used these linearized equations to develop analytical solutions along the classical lines of Lamb (1945). An approximate numerical method was used to "satisfy" the appropriate boundary conditions at the body surface. This analysis, which was represented as being valid for finite values of Wi [i.e. O(1)], led to predictions of a drag coefficient which decreased only slightly, but with streamlines which showed an enormous upstream shift for relatively small values of Wi (for example, Wi < 0.5). In addition, the calculated results showed an apparent separation phenomena for Wi = 5/12. While such startling changes in flow structure with very small changes in fluid elasticity (Wi) are not impossible, it appeared to us that they should be viewed with some skepticism. Consequently, we carried out a brief

theoretical investigation of the analysis of Ultman and Denn.

The dimensionless linearized equations of motion for creeping flow, used by Ultman and Denn, are

$$Re \frac{\partial \underline{u}}{\partial x} = - \nabla p + \nabla \cdot \underline{\underline{\tau}} \tag{51}$$

$$\underline{\underline{\tau}} + Wi \frac{\partial \underline{\underline{\tau}}}{\partial x} = 2\underline{\underline{e}} \tag{52}$$

$$\nabla \cdot \underline{u} = 0 \tag{53}$$

in which $Re = \rho U_\infty a/\eta_0$ is the Reynolds number based on the zero shear rate viscosity and $Wi = U_\infty \lambda/a$ is the Weissenberg number which is a ratio of the characteristic relaxation time of the fluid to the convective time scale of the motion. Combining equations (51) and (52), we obtain

$$Re\left(1 + Wi \frac{\partial}{\partial x}\right) \frac{\partial \underline{u}}{\partial x} = - \left(1 + Wi \frac{\partial}{\partial x}\right) \nabla p + \nabla^2 \underline{u} \tag{54}$$

Our discussion will be confined to $Re << 1$, since it is the dependence on Wi which is of primary concern here. For $Re \to 0$, it is known that the right-hand side of equation (54) will provide an adequate representation of the fluid motion near the body. We now define $\hat{p}$ as

$$\hat{p} = \left(1 + Wi \frac{\partial}{\partial x}\right) p \tag{55}$$

Then, incorporating (55) and letting $Re \to 0$, the equation (54) becomes simply

$$\nabla \hat{p} = \nabla^2 \underline{u} \tag{56}$$

Since we are not concerned with the effects of fluid inertia, we may use the boundary conditions of uniform translation at large distances and zero velocity on the sphere surface. The solution of (56) with these

boundary conditions is nothing more than Stokes solution with $\hat{p}$ replacing p. In order to calculate the drag on the sphere, we need to be able to invert equations (52) and (55) for the stress tensor, $\underline{\underline{\tau}}$, and the pressure, p, respectively, using the known kinematics and $\hat{p}$. In principle, this inversion can be done, but the resulting expressions are too unwieldy to use. Therefore, we opt for an asymptotic solution of equations (52) and (55). Thus, we seek solutions for p and $\underline{\underline{\tau}}$ in the asymptotic form

$$p = p_o + Wi\ p_1 + Wi^2 p_2 + \ldots$$

$$\underline{\underline{\tau}} = \underline{\underline{\tau}}_o + Wi\ \underline{\underline{\tau}}_1 + Wi^2 \underline{\underline{\tau}}_2 + \ldots$$

The solution for p is easily shown to be

$$p = -\frac{3\cos\theta}{2r^2} - \frac{3Wi}{2r^3}(3\cos^2\theta - 1) - \frac{9Wi^2}{2r^4}(5\cos^3\theta - 3\cos\theta) + O(Wi^3) \quad (57)$$

Similarly τ_{rr} and $\tau_{r\theta}$ are found to be

$$\tau_{rr} = 3\cos\theta\left(\frac{1}{r^2} - \frac{1}{r^4}\right) + Wi\left(3\cos^2\theta - 1\right)\left(\frac{3}{r^3} - \frac{6}{r^5}\right)$$

$$+ Wi^2\left[\cos^3\theta\left(\frac{54}{r^4} - \frac{150}{r^6}\right) - \cos\theta\left(\frac{36}{r^4} - \frac{90}{r^6}\right)\right] + O(Wi^3) \quad (58)$$

$$\tau_{r\theta} = -\frac{3\sin\theta}{2r^4} + Wi\sin\theta\cos\theta\left(\frac{9}{2r^3} - \frac{12}{r^5}\right)$$

$$+ Wi^2\left[\sin\theta\left(\frac{27}{r^4} - \frac{90}{r^6}\right) - \sin^3\theta\left(\frac{36}{r^4} - \frac{225}{2r^6}\right)\right] + O(Wi^3) \quad (59)$$

Now, the drag on the sphere is given by

$$\text{Drag} = 2\pi\eta_o U_\infty a \int_o^\pi \left[(\tau_{rr} - p)\cos\theta - \tau_{r\theta}\sin\theta\right]_{r=1} \sin\theta\, d\theta \quad (60)$$

Substituting equations (57), (58) and (59) into equation (60) and carrying out the integration we obtain

$$\text{Drag} = 6\pi\eta_0 U_\infty a\,(1 + O(Wi^3)) \tag{61}$$

The results of the above analysis are in striking contrast to the results obtained by Ultman and Denn. We find that the streamlines are symmetric for small Wi, and, indeed, that the velocity field is identical to the velocity field for creeping flow of a Newtonian fluid past a sphere. We see no evidence for any separation phenomena at any value of Wi if the Re is much smaller than one. Finally, the drag on the sphere remains unchanged from the Stokes' result for a Newtonian fluid, at least through terms of $O(Wi^2)$. It should be emphasized that the differences between the present results and those of Ultman and Denn is not due to the restriction that $Re \ll 1$. Indeed, equation (54) can be solved in its entirety for the conditions $Re \sim Wi \ll 1$ by using methods similar to those used to solve the Oseen equations for a Newtonian liquid. This is done in Appendix B. The above results concerning the drag on the sphere and the detailed flow structure are unchanged by the addition of small inertial effects.

An examination of the reasons for the failure of Ultman and Denn's linearized theory is presented in Appendix A.

5. Experimental Studies of the Translational Motion of Particles in Non-Newtonian Fluids

We now turn our attention to previous experimental investigations of particle motions in non-Newtonian, and especially viscoelastic fluids which arethe topic of this thesis. We shall compare the experimental findings with the limited theoretical investigations just discussed.

Apparently, the first serious experimental investigation of the translational motion of particles in a viscoelastic fluid was that of Tanner (1961), who studied the gravitationally induced settling of a sphere at low Reynolds number in a solution of polyisobutylene in carbon tetrachloride. The usual Faxen correction was employed to account for the influence of the walls. The major result of this work was the observation that the drag on the sphere decreased relative to Stokes law at a rate which was proportional to $(U_\infty/a)^2$ for 'small' U_∞/a, where U_∞ is the terminal velocity of the sphere in an unbounded fluid and a is the sphere radius. This is in obvious qualitative agreement with the small Wi solutions of Leslie and Giesekus. These qualitative findings were confirmed by the more recent experiments of Broadbent and Mena (1974) who measured the drag force on a sphere in polyacrylamide (PAA) at low Reynolds number using a leaf spring and air bearing balance. They showed that the "time constant" found from a plot of the drag data versus $(U_\infty/a)^2$ was in agreement with a third-order fluid description of the shear thinning viscosity for shear rates less than 1. Also included in this work were photographs of a single streamline for the flow past a sphere which showed no appreciable change from the streamlines for a Newtonian fluid.

In a somewhat earlier study, Subbaraman, Mashelkar and Ulbrecht (1971) measured the terminal velocity of several different sized spheres in solutions of CMC, PAA and polydimethylsiloxane with the intention of inferring the zero-shear-rate viscosity. When the influence of the wall was accounted for by using Caswell's correction, they found that their data for solutions of PAA and CMC demonstrated a departure of the drag from the Stokes value which was again proportional to $(U_\infty/a)^2$. They also found that the extrapolated value of the zero-shear-rate viscosity agreed with a determination of that value from a cone and plate viscometer. In 1975, Zana, Tiefenbruck and Leal (see Appendix A) published detailed streamline photographs for the motion of a sphere in PAA and water and in PAA, glycerine and water. For small Reynolds number and small Weissenberg number, no difference could be detected between Newtonian and viscoelastic streamlines. As the Weissenberg number increased, however, a small but noticeable upstream shift of the streamlines was noted. The magnitude of the streamline shift increases up to approximately Wi = 10 where the rate of increase with Wi decreases sharply. This upstream shifting of the streamlines is not predicted by any of the theories discussed in the previous section and thus remains a theoretical challenge.

Finally, Sigli and Coutanceau (1977) have studied the motion of spheres in a circular cylinder where the ratio of sphere diameter to cylinder diameter is greater than 0.25.

They found that the presence of the wall increased the effects of fluid elasticity. They showed photographs taken in a laboratory reference frame which indicated a region behind the sphere in which the fluid moved in the opposite direction to the sphere.

The majority of earlier studies were carried out using purely-viscous fluids (or at least ignored any elasticity in the test fluids). Among these investigations was that of Slattery and Bird (1961) who reported drag coefficients for spheres moving through five aqueous solutions of carboxymethylcellulose (CMC) with concentrations ranging from 0.6 to 5.3% by weight. The Reynolds numbers for these experiments ranged from 10^{-4} to 10^{3}. The data were presented in the form of empirical correlations for the drag coefficient using the purely-viscous, Ellis model to represent the fluid rheology. The model parameters were determined from tube flow experiments. However, as indicated above, no attempt was made to determine the elastic nature of these liquids, in spite of the fact that CMC is known to display measurable normal stresses once the concentration reaches 1.2% [Subbaraman et al. (1971)].

Later, Turian (1967) studied the motion of falling spheres near the zero shear stress limit in two solutions of hydroxyethylcellulose (HEC) and two solutions of polyethylene oxide (PEO) at 20°C and 30°C. Both of these polymers form aqueous solutions which demonstrate appreciable elastic effects [Acharya et al. (1976)]. Special emphasis was placed on determining the effect of the wall on the sphere motion. This was accomplished by using seven cylinders with different inside diameters and several sizes of ruby and steel spheres. Turian's data indicated that the effect of the wall is smaller for the non-Newtonian liquids than it is for Newtonian liquids when the ratio of sphere diameter to cylinder diameter are the same, but is nevertheless significant (16% of the Stokes drag for diameter ratios as small as 0.1). Turian presented his own correlation for the drag coefficient at low Reynolds number in which he

used the Faxén correction to reflect the influence of the wall and the Ellis model to represent the fluid rheology. The model parameters in Turian's study were fit to shear viscosity data in a cone and plate viscometer, with the zero shear-rate value determined by extrapolation of the sphere velocity data. As in the earlier study of Slattery and Bird (1961), no attempt was made to evaluate the influence of elastic effects.

When the results of the above two experimental studies are compared with the theoretical predictions for purely-viscous fluids by Wasserman and Slattery (1964) and Hopke and Slattery (1970), it is evident that neither of the theories does particularly well. Both of these theories consistently underpredict the drag coefficient. The average of Wasserman and Slattery's upper and lower bounds was found to predict the drag coefficient for the experimental conditions of Slattery and Bird with an average error of 18%. However, when the same expression is used for Turian's data, the error is 58%. On the other hand, the average of Hopke and Slattery's upper and lower bounds predicts Turian's data with an error of 16% while the error for the Slattery and Bird experiments is 29%. Thus, solutions based upon the generalized Newtonian fluid are seen to be of limited value for prediction of the motion of a sphere, even when the fluids are purposely chosen to minimize elastic effects relative to the purely-viscous characteristic of a shear thinning viscosity.

The most exhaustive experimental work for the motion of a sphere in a non-Newtonian liquid is the study of Acharya, Mashelkar and Ulbrecht (1976). They measured drag coefficients for several sizes of steel, glass, red acrylic and black phenolic spheres in solutions of CMC, PAA, PEO, HEC and

and Carbopol. Data were correlated over a wide range of Reynolds number (10^{-4} to 10^{4}) using power law relationships to represent both the viscosity and the first normal stress difference. The rheological data used in the correlations were measured using a Weissenberg Rheogoniometer. For Reynolds number less than one, Acharya et al. (1976) found that all of the data could be correlated in terms of the shear thinning viscosity alone. However, the drag coefficient was still larger than the value predicted by Wasserman and Slattery. While there is thus no theoretical justification for the low Reynolds number correlation presented by Acharya et al., it does accurately describe the results of their experiment. Perhaps the reason that the correlation appears to work is that Acharya et al. (1976) have avoided strongly elastic fluids.

A few summarizing comments are in order on these experimental observations for translational motion of rigid spherical particles in non-Newtonian fluids. First, the initial decrease of the drag from the Stokes law value for "strongly" viscoelastic liquids depends quadratically upon U_∞/a in qualitative agreement with the small Wi theories. If independent values of λ_1 were available, it is possible that the theories might be shown to be in quantitative agreement, at least for small values of U_∞/a. The inferred values of λ_1 from the measured dependence of drag on $(U_\infty/a)^2$ range from .2 sec to 2 sec, which is quite reasonable for a "normal" viscoelastic fluid. Second, although the data for 'weakly' elastic fluids appear to correlate well with the parameters of a purely-viscous fluid model, there is a considerable numerical discrepancy between the predicted terminal velocities for such a model and the actual data. An obvious

inference is that the fluid's elastic behavior, while weaker than for the 'strongly' viscoelastic fluids described above, is still significant for the particle drag. The apparent correlation with purely viscous fluid parameters may be due to the fact that the parameters characteristic of elasticity were not varied significantly in these studies of weaker elastic fluids. Further, the wall effect on the drag on the sphere appears to be adequately described, for small Wi, by Caswell's analysis which employs the results of Giesekus for the motions of a sphere in an unbounded fluid. Caswell has shown that Turian's data can be described quite well using these results. For larger Wi, the effect of elasticity on the drag coefficient is not known experimentally. Also unexplained is the upstream shift of the streamlines for the flow past an isolated sphere. It seems highly probable that this is a manifestation of the elastic nature of these fluids. Finally, the 'reverse flow' behavior described by Sigli and Coutanceau would also appear to be elastic in origin, but as yet remains unexplained.

After the translational motion of a rigid sphere, perhaps the next most studied translational motion of a particle in a non-Newtonian fluid is the buoyancy induced rise of a gas bubble. Among the first authors to consider this problem were Astarita and Apuzzo (1965). For weakly elastic polymer solutions such as Carbopol or low concentrations of CMC, they found that the terminal velocity-bubble volume relationship for small bubbles (i.e. small Reynolds numbers) was of the form suggested by Stokes law with the definition of Reynolds number modified to a form compatible with the power-law model. The terminal velocity curve in these fluids varied smoothly with increasing volume from this behavior to the well-known

Davies-Taylor relationship for large bubbles. The corresponding bubble shapes were the usual Newtonian type which pass from spherical to oblate spheroidal to spheroidal cap. However, the results were quite different for polymer solutions which demonstrate appreciable normal stresses at shear rates of O(1). For small bubbles, the terminal velocity-bubble volume relationship was again found to define a curve which appears to depend only upon the power law index n. However, at a critical volume which was slightly different for each of the four elastic liquids used (the critical radius was on the order of 0.28 cm), the terminal velocity exhibited an abrupt rise, by as much as a factor of six, with only an infinitesimal increase in volume. The terminal velocity-bubble volume curve then proceeded smoothly to the Davies-Taylor expression for large bubbles. The bubble shapes were also unusual. For extremely small bubbles, both the Reynolds number and the Weissenberg number are small and the shape is thus spherical. However, as the volume of the bubble increases, the bubble shape first changes to prolate spheroidal then becomes teardrop shaped, followed by oblate spheroidal with a cusp and, finally, by a spherical cap shape which still retains a cusp on its lower surface.

Other workers who reported similar observations include Calderbank, Johnson and Loudon (1970) who studied carbon dioxide bubbles in a constant volume tank in PEO, and Leal, Skoog and Acrivos (1971) who studied air bubbles in PAA. Leal et al. also measured the terminal velocity of glass spheres in the same PAA solutions. They found that the terminal velocity of the glass spheres was the same, when small corrections were employed

for the density difference, as the velocity of the air bubbles in the volume range prior to the terminal velocity discontinuity. In addition, the glass spheres showed no discontinuity in terminal velocity. These two observations when combined with the observation that the change in bubble shape is very slight at transition, provide strong indirect evidence that it is a change in surface boundary conditions which is responsible for the observed velocity transition for the bubbles.

Acharya, Mashelkar and Ulbrecht (1977) studied the motion of bubbles in CMC, PAA and PEO for both high and low Reynolds number. In the low Reynolds number regime they observed a velocity jump even for CMC, which had not been discerned by Astarita and Apuzzo, who also studied CMC solutions. According to Acharya et al. (1977), the magnitude of the jump in this case (less than a factor of 2) is quantitatively accounted for by by employing the empirical correlation for the velocity of a sphere with a no-slip surface and the solution of Hirose and Moo-Young (1969) for a freely circulating spherical bubble, both in a power law fluid. This result for purely viscous fluids is thus seen to support the hypothesis that the velocity transition is caused by an abrupt change in surface boundary conditions. When Acharya et al. attempted to apply these purely-viscous fluid arguments to a viscoelastic fluid, however, they found that the agreement became worse as the fluid became more elastic. The rise velocity for large bubbles (high Reynolds number) was found to agree with predictions based upon an inviscid wave analogy.

Zana and Leal (1978) studied the motion of air and carbon dioxide bubbles in four solutions of PAA with the objective of examining the

differences (if any) between dissolving and non-dissolving bubbles. For non-dissolving air bubbles, the data essentially reproduced the earlier results of Leal, Skoog and Acrivos (1971). For dissolving carbon dioxide bubbles, on the other hand, Zana and Leal found that there was only a rapid variation in terminal velocity with instantaneous volume, but no discontinuity in terminal velocity. Perhaps more important, however, they showed that the magnitude of both the velocity transition and the bubble eccentricity correlated with the Weissenberg number, in addition to the power law index n for these strongly viscoelastic liquids. In this regard, Zana and Leal's (1978) investigation is seen to complement the work of Acharya et al. (1977), which showed a correlation only with n and to suggest that those authors were operating primarily in the "purely-viscous" regime where elastic effects are only weakly manifested in the bubble's motion.

There have also been a few studies of the motion of liquid drops in non-Newtonian fluids. The early work on this problem was done by Mhatre and Kintner (1959). They observed drop shapes in viscoelastic fluids which were similar to those described above for gas bubbles. In addition, and perhaps more importantly, they also observed a steep increase in terminal velocity when the drop reached a critical volume. Similar work with the same results was reported by Warshay, Bogusz, Johnson and Kintner (1959) and by Fararoui and Kintner (1961).

More recently, Acharya, Mashelkar and Ulbrecht (1978) studied the motion of drops in dilute solutions of CMC, PAA and PEO. All of the drops studied here were in the "post transition regime". Considering the weak

elasticity of the fluids studied, it is not surprising that for low Reynolds number (Re < 1) they were able to show agreement with the theoretical solution for a Newtonian drop in a power-law fluid due to Mohan (1974). For Reynolds numbers larger than one, they found that the drag coefficient in viscoelastic liquids was higher than the drag coefficient in purely-viscous liquids with similar viscosity curves. This may be due to the observed differences in the size of the wake for the two fluids. Finally, at large Reynolds numbers, they found that the terminal velocity of the drops was independent of the suspending fluid rheology and was accurately described by an extended wave analogy developed by Marucci, Apuzzo and Astarita (1970).

The conclusions that we can draw from these studies are somewhat different from those we made for the solid sphere. First, we note that the terminal velocity of bubbles and drops in purely-viscous fluids appears to be adequately described by theoretical analysis using a power-law fluid, whereas this is not true for a sphere. Second, the effect of elasticity is clearly present in the shapes reported for bubbles and drops in viscoelastic liquids. These shapes are at least in qualitative accord with the predictions of the small Wi solutions cited earlier. Third, we conclude that the magnitude of the velocity transition is likely to be associated with elastic effects since the argument of Acharya et al. (1977) using generalized Newtonian fluids is able to account for a jump of only a factor of 2 as compared with the Newtonian value of 3/2. No adequate explanation for the abruptness of the jump has yet been found.

All of the above studies have been concerned with spherical or nominally spherical particles. Many naturally occurring particles are nonspherical, and the experimental investigation of nonspherical particles

is thus also extremely important. However, the only study of the translational motion of nonspherical particles in a non-Newtonian fluid of which we are aware is the brief investigation of Zana and Leal [see Leal (1975)]. These authors showed that a slender rod sedimenting in a viscoelastic liquid would rotate toward the vertical, as predicted earlier in the same work, but did not carry out any more detailed studies.

The dearth of experimental data for translational motions of nonspherical particles motivated the study of the motion of a slender rod presented in Chapter II. This particular problem was chosen since it is the only one where there exists a complete theoretical analysis. The motion of a slender rod near a wall is also of interest because of the change in particle orientation which occurs for a Newtonian fluid. This easily detectable effect should allow us to assess the effect of the wall on a slender rod in a non-Newtonian fluid.

In Chapter III, we shall study the low Reynolds number translational motion of a spherical particle in a viscoelastic liquid using the Oldroyd-type constitutive equation which was detailed earlier. The method of investigation will be via numerical solution of the governing partial differential equations and associated boundary conditions. This method of attack is necessary since we want the results to be valid for non-trivial values of the Weissenberg number. Since linearization of the constitutive equation is not possible in these circumstances, numerical solution is our only recourse. We examine the influence of slip (freely circulating) and no slip boundary conditions in the motion of spherical particles. Thus, not only do we obtain results for the drag on a rigid sphere which we can compare with data, but we also hope to shed some light on the velocity transition phenomenon. The numerical results may also help to assess the range of validity of the small Weissenberg number solutions.

References

Acharya, Mashelkar and Ulbrecht, Rheol. Acta 15, 19 (1976).

Acharya, Mashelkar and Ulbrecht, Chem. Eng. Sci. 32, 863 (1977).

Acharya, Mashelkar and Ulbrecht, Can. J. Chem. Eng. 56, 19 (1978).

Adachi, Yoshioka and Sakai, J. Non-Newtonian Fluid Mech. 3, 107 (1977).

Adachi, Yoshioka and Yamamoto, Chem. Eng. Sci. 28, 2033 (1973).

Ajayi, J. Eng. Math. 9, 273 (1975).

Astarita and Apuzzo, AIChE J. 11, 815 (1965).

Baird and Hamielec, Can. J. Chem. Eng. 40, 119 (1962).

Barnes, Townsend and Walters, Nature 224, 585 (1969).

Bhavaraju, Mashelkar and Blanch, AIChE J. 24, 1063 (1978).

Bird, Physics of Fluids 3, 539 (1960).

Bird, Hassager and Abdel-Khalik, AIChE J. 20, 1041 (1974).

Bird, Armstrong and Hassager, "Dynamics of Polymeric Liquids: Vol. 1 Fluid Mechanics", John Wiley and Sons, New York, N.Y. (1977).

Broadbent and Mena, Chem. Eng. J. 8, 11 (1974).

Brunn, J. Fluid Mech. 82, 529 (1977).

Calderbank, Johnson and Loudon, Chem. Eng. Sci. 25, 235 (1970).

Caswell, Chem. Eng. Sci. 25, 1167 (1970).

Caswell, Chem. Eng. Sci. 27, 373 (1972).

Caswell and Schwarz, J. Fluid Mech. 13, 417 (1962).

Christiansen and Leppard, Trans. Soc. Rheol. 18, 65 (1974).

Coleman and Noll, Arch. Rat. Mech. Anal. 3, 289 (1959).

Coleman and Noll, Ann. N.Y. Acad. Sci. 89, 672 (1961).

Denn and Marucci, AIChE J. 17, 101 (1971).

Fararoui and Kintner, Trans. Soc. Rheol. 5, 369 (1961).

Fredrickson, A. G., "Principles and Applications of Rheology", Prentice-Hall, Englewood Cliffs, N.J. (1964).

Giesekus, Rheol. Acta 3, 59 (1963).

Goddard and Miller, J. Fluid Mech. 28, 657 (1967).

Graessly, Glassock and Crawley, Trans. Soc. Rheol. 14, 519 (1970).

Hassager, "Chemical Engineering with Per Søltoft" (ed. K. Østergaard and Aa. Fredenslund) Teknisk Forlag, Copenhagen, Denmark (1977).

Hinch and Leal, J. Fluid Mech. 52, 683 (1972).

Hirose and Moo-Young, Can. J. Chem. Eng. 47, 265 (1969).

Hopke and Slattery, AIChE J. 16, 224 (1970).

Huppler, Macdonald, Ashare, Spriggs, Bird and Holmes, Trans. Soc. Reol. 11, 181 (1967).

James, Nature 212, 754 (1966).

James and Acosta, J. Fluid Mech. 42, 269 (1970).

Johnson, Physics of Fluids 3, 871 (1960).

Lamb, "Hydrodynamics", Dover Publications, New York, N.Y. (1945).

Landau and Lifschitz, "Fluid Mechanics", Addison-Wesley, Reading, Mass. (1959).

Laun and Munstedt, Rheol. Acta (1978).

Leal, Skoog and Acrivos, Can. J. Chem. Eng. 49, 569 (1971).

Leslie, Quart. J. Mech. and Appl. Math. 14, 36 (1961).

Levich, "Physiochemical Hydrodynamics", Prentice-Hall, Englewood Cliffs, N.J. (1962).

Lodge, "Elastic Liquids", Academic Press, New York (1964).

Lumley, Phys. of Fluids 14, 2282 (1971).

Marucci, Apuzzo and Astarita, AIChE J. 16, 538 (1970).

Meissner, J. Appl. Polymer Sci. 16, 2877 (1972).

Mena and Caswell, Chem. Eng. J. 8, 125 (1974).

Metzner and Metzner, Rheol. Acta 9, 174 (1970).

Mhatre and Kintner, Ind. Eng. Chem. 51, 865 (1959).

Mohan, AIChE J. 20, 180 (1974).

Mohan and Venkateswarlu, Int. J. Multiphase Flow 2, 563 (1976a).

Mohan and Venkateswarlu, Int. J. Multiphase Flow 2, 571 (1976b).

Moo-Young and Hirose, Can. J. Chem. Eng. 50, 128 (1972).

Nakano and Tien, AIChE J. 14, 145 (1968).

Noll, Arch. Rat. Mech. Anal. 2, 197 (1958).

Olabisi and Williams, Trans. Soc. Rheol. 16, 727 (1972).

Oldroyd, Proc. Roy. Soc. A245, 278 (1958).

Phan Tien and Tanner, J. Non-Newtonian Fluid Mech. 2, 353 (1977).

Rivlin and Ericksen, J. Rat. Mech. Anal. 4, 350 (1955).

Shirotsuka and Kawase, Kagaku Kogaku 38, 797 (1974).

Sigli and Coutanceau, J. Non-Newtonian Fluid Mech. 2, 1 (1977).

Slattery, AIChE J. 8, 663 (1962).

Slattery and Bird, Chem. Eng. Sci. 16, 231 (1961).

Subbaraman, Mashelkar and Ulbrecht, Rheol. Acta 10, 429 (1971).

Tanner, Quart. J. Mech. and Appl. Math. 14, 47 (1961).

Tanner, Trans. Soc. Rheol. 14, 483 (1970).

Tanner and Huilgol, Rheol. Acta 14, 959 (1975).

Turian, AIChE J. 13, 999 (1967).

Ultman and Denn, Chem. Eng. J. 2, 81 (1971).

Wagner and Slattery, AIChE J. 17, 1198 (1971).

Wales and Phillippoff, Rheol. Acta 12, 25 (1973).

Warshay, Bogusz, Johnson and Kintner, Can. J. Chem. Eng. 37, 29 (1959).

Wasserman and Slattery, AIChE J. 10, 383 (1964).

Yoshioka and Adachi, J. Chem. Eng. Jap. 6, 134 (1973).

Zana, PhD Thesis, California Inst. of Technology (1975).

Zana and Leal, Int. J. Multiphase Flow 4, 237 (1978).

Zana, Tiefenbruck and Leal, Rheol. Acta 14, 891 (1975).

Figure Captions

Figure 1. $Y = \left(\frac{Sh}{0.65\ Pe^{\frac{1}{2}}} - 1 \right) \frac{1}{Wi^2}$ versus the rheological parameter α.

Figure 2. Some "typical" bubble shapes

A. $r = 1 + 0.2\ P_2(\cos\theta)$

B. $r = 1 + 0.2\ P_2(\cos\theta) + 0.2\ P_3(\cos\theta)$

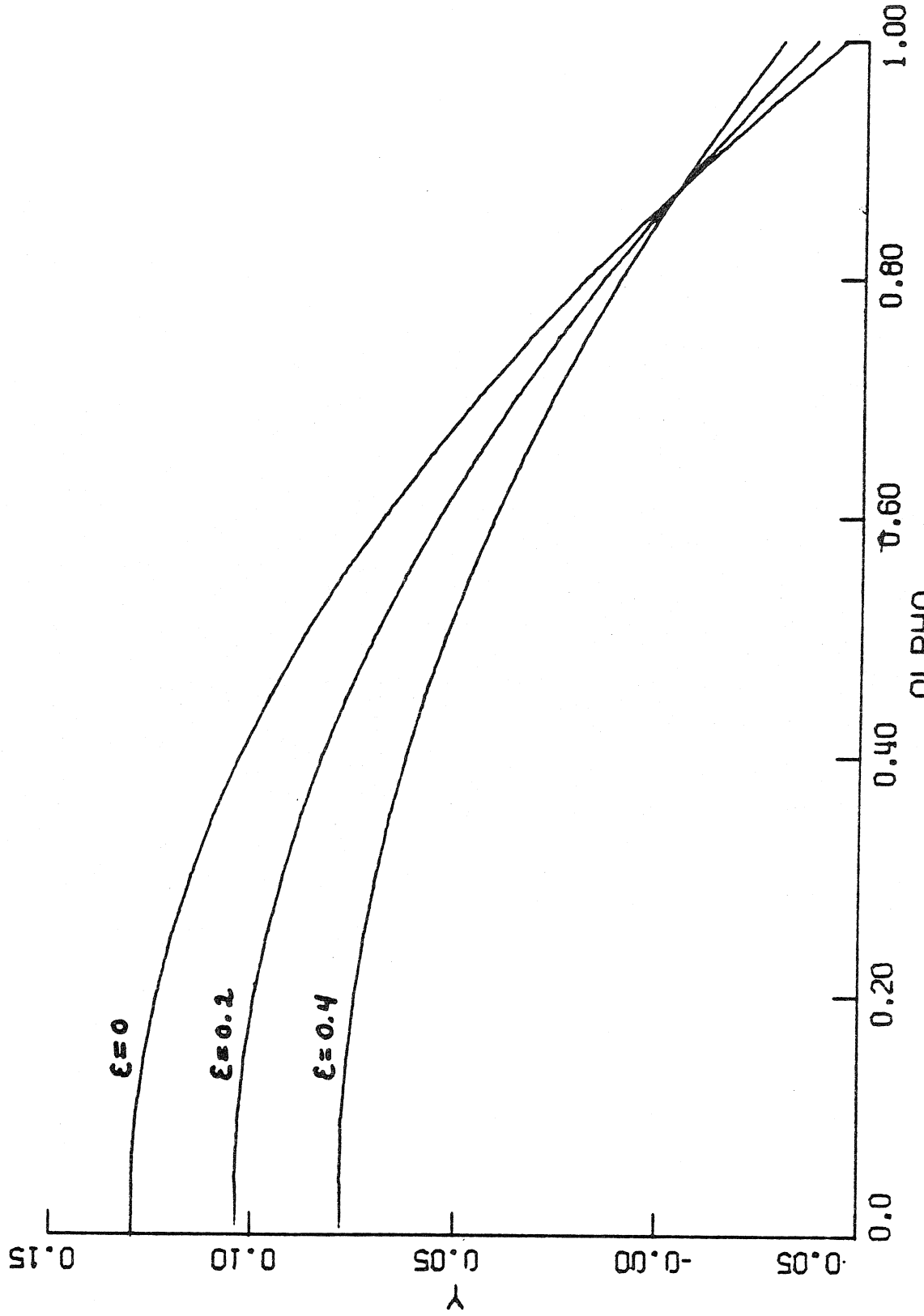

Figure 1

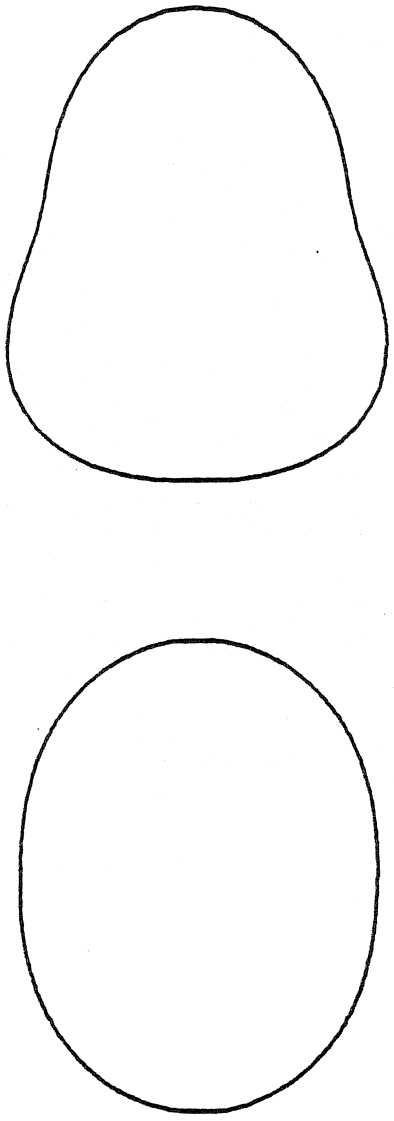

Figure 2

APPENDIX A. A Note on the Creeping Motion of a Viscoelastic Fluid Past a Sphere

(This paper was published in Rheologica Acta, V. 14.)

A NOTE ON THE CREEPING MOTION OF A VISCOELASTIC FLUID PAST A SPHERE

E. Zana, G. Tiefenbruck and L. G. Leal

Chemical Engineering
California Institute of Technology
Pasadena, California 91125

INTRODUCTION

Among the general class of nonviscometric flows of a viscoelastic liquid, one of the most important is the uniform translation past a submerged object, such as a cylinder or sphere. In spite of this, relatively little progress has been made in the theoretical description of such flows since the governing equations are nonlinear not only in the convective acceleration (or inertia) terms, but also in the constitutive model for the fluid. Indeed, with one exception which we shall discuss below, all theoretical studies to date have been restricted to the limit of "slow" flow in which the nonlinear contributions are either neglected altogether, or at least are embedded within the framework of a small parameter perturbation expansion about the linear, Newtonian creeping flow state. The conditions required for validity of such an analysis are $Re \ll 1$, $We \ll 1$, where $Re(\equiv ud/\nu)$ is the Reynolds number and $We(\equiv \lambda u/d)$ is the Weissenberg number which is a ratio of the largest characteristic relaxation or retardation time for the fluid, λ, and the convective time scale d/u of the fluid motion. The Weissenberg number thus provides a measure of the relative importance of the fluid's elasticity. The best known example of an analysis of this type is the creeping ($Re \equiv 0$) flow solution for the rheologically slow ($We \ll 1$) flow of a viscoelastic fluid past a sphere, which was obtained (independently) by Leslie (1961), Caswell and Schwarz (1962) and Giesekus (1963). The solution shows a small downstream shift in the streamlines at $O(We)$, and a decrease in the drag at $O(We^2)$. More recently, Mena and Caswell (1974) have carried the small We analysis one step further for both a cylinder and a sphere by including inertia terms in formal matched asymptotic expansions for small, but nonzero Reynolds number.

The only investigation which purports to provide an approximate representation of the flow for strong elasticity (i.e. moderate to large We) is the analysis of Ultman and Denn (1971), which is based upon an Oseen-like linearization of the dynamic inertia terms, as in the usual Newtonian case, and also of the nonlinearities in the generalized Maxwell constitutive model which was adopted for the work. An approximate numerical method was used to "satisfy" the appropriate boundary conditions at the body surface. Both in the original analysis and in subsequent discussions of the work (cf. Astarita and Marrucci, 1974) it has been implicitly assumed that the Oseen linearization provides a uniformly valid first approximation to both the convective and constitutive nonlinearities provided only that $Re << 1$, without any fundamental restriction on We. Indeed, realistic solutions were claimed by Ultman and Denn (1970) for $Re \lesssim 1$, provided only that We satisfied the additional condition $ReWe \leq .05$, which was obtained by requiring the mean square error in satisfying boundary conditions at the body surface to be no greater than that obtained in the Newtonian case for $Re = 1$. It is important to emphasize that the condition on We was intended as a restriction on the accuracy of the approximation involved in solving the governing linearized equations of motion, rather than an inherent restriction on the validity of the linearization itself. One feature of the governing equations, which seems to support their validity for $Re << 1$, but Weissenberg number essentially unrestricted, is the fact that they change type from elliptic to hyperbolic at $ReWe = 1$. As Ultman and Denn (1970) and a number of subsequent investigators have pointed out, this change in type seems to correlate reasonably well with (and even explain in a qualitative sense) a

variety of experimental observations which are otherwise difficult to comprehend (cf. James and Acosta 1970, Ultman and Denn, 1970). In spite of such apparent successes of the theory, however, certain of its other features are difficult to accept. For example, Ultman and Denn's (1971) calculations for ReWe as small as .05 (where the small We solutions might be expected to be relevant) show an enormous upstream shift of the streamlines--assumed by Ultman and Denn to be a physically realistic consequence of nonzero, if weak fluid elasticity. In addition, the calculated flow structure near the body surface in some cases shows streamlines actually crossing the body boundary. Finally, the calculated results show an apparent separation phenomenon which occurs for very small values of Re provided that We is larger than 5/12. While clearly not impossible, such fundamental changes in flow structure with very small changes in ReWe or We from the Newtonian value (zero) must be viewed with some skepticism and we believe subjected to further study.

Unfortunately, there have been very few attempts to actually observe the streamlines experimentally for the motion of a viscoelastic fluid past either a solid sphere or cylinder. The only studies of which we are aware are those of Ultman (1970)--reported in Ultman and Denn (1971)--and of Broadbent and Mena (1974). The values of Re and We for these two experiments are given in Table 1.† In both cases, Re << 1 and We << 1. However, the results obtained were very different. Ultman and Denn (1971) published a single die-streak photograph for the motion of 1.7% aqueous solution of

†In the case of Broadbent and Mena (1974), We was calculated from the coefficient of the quadratic term in the expression for the drag in flow past a solid sphere which was measured in the same work. The value of We for Ultman and Denn (1971) was apparently mis-printed as 3.2. However, simple calculation using Ultman and Denn's stated values for λ of :04 sec, velocity u = .077 cm/sec, and cylinder diameter, 2R = 3/8 inch leads to the value quoted here of 3.2×10^{-3}.

CMC-7H past a cylinder which showed the apparent existence of a large upstream shift in streamlines, as predicted by their theory. On the other hand, similar photographs for a cylinder and a sphere obtained by Broadbent and Mena showed essentially no shift in the streamlines either upstream or downstream. The latter result would appear to be in accord with the small Re, small We theories listed at the beginning of this section which predict only a very slight and likely imperceptible downstream shift but is clearly contradictory both to the experiment and theory of Ultman and Denn (1971). However, both Broadbent and Mena's and Ultman and Denn's flow visualization experiments were restricted to a single value of Re and We, and the data consist of one (U. - D.) or two (B. - M.) die-streaks at a moderate distance from the body.

Motivated by the restricted amount of available data, and by the apparent contradictions between the existing experimental and theoretical studies, the present work was undertaken to obtain detailed visualization of the motion of a viscoelastic fluid past a solid sphere for $Re \ll 1$ but with We varied over a wide range. This work has led us to a re-examination of the theoretical analysis of Ultman and Denn (1971), which we describe briefly in the last section of the present communication.

EXPERIMENTAL RESULTS

The experiments were conducted in a vertical tank with dimensions 6" x 6" x 7'. The sphere was supported in the liquid by a thin but stiff horizontal wire which was attached several diameters from the sphere to lightweight vertical strings as shown in Figure 1. Preliminary experiments showed that this configuration for the sphere produced little, if any,

disturbance of the flow in the meridional symmetry plane, where observations were made. The relative motion between the sphere and surrounding fluid was produced by simply pulling the sphere vertically upward at a known rate through the otherwise quiescent fluid. Flow visualization was accomplished using micron size polyethylene particles as tracer material. These particles were found to be nearly neutrally buoyant and, in fact, would neither float to the surface nor sink to the bottom of the tank on a time scale of several weeks. The field of view was illuminated through two very narrow slits (4" in length and .15 mm in width) which were placed on either side of the column at a position which bisected the sphere as it moved through the field of view. Photographs were obtained using a Graflex single lens reflex camera, which was mounted on a movable platform. The film used was type 57, high speed (ASA 3000) Polaroid, and exposure times of several seconds were typical. A more detailed description of the apparatus and experimental methods may be found in Zana (1975).

The experiments were designed to yield small values of the Re (maximum 0.1), but a wide range of We. This was accomplished by using two different solutions of the commercial polymer Separan AP30, several different size spheres, and a relatively wide range of translational velocities. The basic conditions of the experiments are summarized in Table 2.

The key data from the present experimental study are the streakline flow visualization photographs. Several representative examples covering the range $Re < 0.12$ and $10^{-2} \leqslant We \leqslant 22$ are reproduced in Figure 2. Included is the case $Re = 10^{-4}$, $We = 10^{-2}$ (Figure 2a) which corresponds approximately to the prior experiments cited in Table 1, and a case $Re = .08$, $We = .62$ (Figure 2c) corresponding to the value $ReWe = .05$ for which the Ultman and

Denn calculations show strong upstream shifting of the streamlines.

At the smallest values of We, the streamlines at all radial positions are perfectly symmetric fore and aft, with no discernible shift in either the upstream or downstream directions. This behavior is clearly at odds with the experimental observation of Ultman and Denn (1971), but consistent with the more recent photograph of Broadbent and Mena (1974). For larger values of We, however, there is a definite upstream shift in the streamlines, which increases in degree with increase of We, but at a decreasing rate for the larger values of We. Two streamlines, which terminate at the same downstream points (0.1 and 0.6 sphere diameters from the axis of symmetry) were traced from Figures 2a and 2e in order to illustrate more clearly the magnitude of the upstream shift. These are reproduced in Figure 3a. Clearly, even for We = 10 where elastic effects would be expected to be large, the magnitude of the upstream shift is relatively small and primarily limited to the region nearest to the sphere. Nowhere in the flow is the shift anywhere near the magnitude suggested by Ultman and Denn's study. A more direct comparison is provided in Figure 3b where we have traced two streamlines from Figure 2c, for ReWe = .05, together with several of Ultman and Denn's calculated streamlines for the same value of ReWe (Figure 5 of their paper). Again it is evident that the magnitude of the experimentally observed shift is extremely small compared to that predicted by their theory.

In order to provide at least a qualitative measure of the dependence of the upstream shift on We, three streamlines starting downstream at 0.1, 0.2 and 0.4 sphere radii from the symmetry axis were traced out from the experimental pictures for several different values of We, and the difference

in the area bounded by these streamlines between the upstream and downstream half of the flow field was measured. This difference, normalized with respect to the total area under the same streamline, is listed in Table 3 for eight different values of We, with Re < 0.12. In a Newtonian fluid in this Reynolds number range, no inertia-induced shifting can be detected. Although the actual numbers $\Delta A/A_{total}$ are somewhat arbitrary, we believe that they nevertheless provide a useful relative measure of skewness for different values of We and different distances from the body. For the smallest values of We, no shift could be detected, as we have suggested above. However, with increase of We (and also of ReWe), the magnitude of the streamline shift increases up to approximately We ≈ 10 (ReWe ∿ 1) where the rate of increase with We appears to decline fairly rapidly. This later result is similar to James and Acosta's (1970) heat transfer measurements from a cylinder in which Nu number was found to become independent of the uniform stream velocity at velocities greater than the shear wave velocity (i.e. ReWe ≥ 1). One final point is to note that the region of flow influenced by the presence of sphere increases with increasing elasticity. This can be seen by comparing the streamlines 0.6 diameters away from the symmetry line in Figures 3a, and 3b. For We = 0.6, no shift can be detected at this distance from the sphere. For We = 10, however, there is a definite upstream shift, though it is greatly reduced in magnitude compared to that for the streamlines which are closer to the body (cf. Table 3).

DISCUSSION

The experimental results of the preceding section have shown conclusively that the theory of Ultman and Denn greatly exaggerates the degree of upstream skewing of the streamlines. In view of this, plus the physical significance which has been associated with the change in type of Ultman and Denn's model at ReWe = 1, we have undertaken to re-examine the validity of its basic assumptions. Among these, the most fundamental is the linearization of the constitutive model and equations of motion using an Oseen-type approximation. As we have noted previously, both Ultman and Denn (1971) and subsequent investigators have assumed that this linearization is valid for Re << 1 only, with any restriction on We being a result of subsequent approximations which are required to solve the linearized equations and boundary conditions.

We contend, however, that the linearized equations themselves do not provide a uniformly valid approximation to the elastic flow contributions for the type of problem considered, even if Re and We are both vanishingly small. In order to clearly illustrate this point, it is useful to briefly consider the equations of motion, and an Oldroyd rate-type constitutive equation of the same general form as that adopted by Ultman and Denn. In dimensional form, these are

$$\rho\left(\frac{\partial u_i}{\partial t} + u_k \frac{\partial u_i}{\partial x_k}\right) = -\frac{\partial p}{\partial x_i} + \frac{\partial}{\partial x_k}\tau_{ik} \tag{1}$$

and

$$\tau_{ik} + \lambda_1 \frac{D\tau_{ik}}{Dt} + \mu_o \tau_{jj} e_{ik} - \mu_1(\tau_{ij}e_{jk} + \tau_{jk}e_{ij}) \tag{2}$$

$$+ \nu_1 \tau_{j\ell} e_{j\ell} \delta_{ik} = 2\mu\left[e_{ik} + \lambda_2 \frac{De_{ik}}{Dt} - 2\mu_2 e_{ij}e_{jk} + \nu_2 e_j\, e_{j\ell}\delta_{ik}\right]$$

where D/Dt is the generalized Oldroyd time derivative, and λ_i, μ_i and ν_i are all material coefficients. For slow flows, these equations may be non-dimensionalized with respect to the free stream velocity U, the body diameter ℓ, and the characteristic viscous stress, $\mu U/\ell$. Denoting the non-dimensionalized quantities with overbars, we thus substitute

$$u_i = U\bar{u}_i \ , \quad x_i = \ell\bar{x}_i \ , \quad p = \left(\frac{\mu U}{\ell}\right)\bar{p} \ , \quad \tau_{ik} = \left(\frac{\mu U}{\ell}\right)\bar{\tau}_{ik}$$

and

$$t = \left(\frac{\ell}{U}\right)\bar{t}$$

into the equations (1) and (2) to obtain

$$\frac{\partial \bar{u}_i}{\partial \bar{t}} + \bar{u}_k \frac{\partial \bar{u}_i}{\partial \bar{x}_k} = \frac{1}{Re}\left(- \frac{\partial \bar{p}}{\partial \bar{x}_i} + \frac{\partial}{\partial \bar{x}_k}\bar{\tau}_{ik}\right) \tag{3}$$

with

$$\bar{\tau}_{ik} + We\left[\frac{D\bar{\tau}_{ik}}{D\bar{t}} + \frac{\mu_o}{\lambda_1}\bar{\tau}_{jj}\bar{e}_{ik} - \frac{\mu_1}{\lambda_1}(\bar{\tau}_{ij}\bar{e}_{jk} + \bar{\tau}_{jk}\bar{e}_{ij}) + \frac{\nu_1}{\lambda_1}(\bar{\tau}_{j\ell}\bar{e}_{j\ell}\delta_{ik})\right] = 2\bar{e}_{ik} + 2We\left[\frac{\lambda_2}{\lambda_1}\frac{D\bar{e}_{ik}}{D\bar{t}} - 2\frac{\mu_2}{\lambda_1}\bar{e}_{ij}\bar{e}_{jk} + \frac{\nu_2}{\lambda_1}\bar{e}_{j\ell}\bar{e}_{j\ell}\delta_{ik}\right] \tag{4}$$

The quantities (μ_o/λ_1), (μ_1/λ_1), (ν_1/λ_1), λ_2/λ_1, μ_2/λ_1, and ν_2/λ_1 are all dimensionless ratios of intrinsic time constants for the constitutive model and are generally of order unity.

The Oseen-type linearization may now be formally invoked to simplify the exact equations (3) and (4), i.e. we assume

$$\bar{u}_i = \delta_{i1} + u_i' \ ; \quad \bar{e}_{ik} = e_{ik}' \ ; \quad \bar{\tau}_{ik} = \tau_{ik}' \ ; \quad p = p'$$

and neglect all terms which are quadratic in any of the primed variables.

With $\lambda_2 \equiv 0$, the resulting equations are those which were obtained by Ultman and Denn (1971). The key question is whether the linearized equations provide a uniformly valid approximation to the exact equations (3) and (4) in some appropriate limit. In the special case We ≡ 0, corresponding to a Newtonian fluid, it is by now well-known that the Oseen linearization does provide such an approximation for the nonlinear inertia terms provided only that Re << 1. Far from the body (i.e. $\bar{r} = O(Re^{-1})$), where the convective term is the same order of magnitude as the pressure and viscous terms, the Oseen linearization is a good first approximation since $|u_i'| << 1$. Near to the body where the linearization is poor, the convective terms are asymptotically small compared to the pressure and viscous terms (provided Re << 1), and the linearized equation of motion still provides a valid first approximation to the exact equation (3).

When the Oseen linearization is applied to (4), the only terms surviving (for a steady flow) are

$$\tau'_{ik} + We \frac{\partial \tau'_{ik}}{\partial \bar{x}} = 2e'_{ik} + 2We \frac{\lambda_2}{\lambda_1} \frac{\partial e'_{ik}}{\partial \bar{x}} \qquad (5)$$

Clearly, the equation (5) will provide a good approximation to (4) at large distances from the body. However, near to the body for arbitrary We, it will not. At first, it may seem that a similar argument could be applied to the neglected nonlinear terms in the constitutive model for We << 1, as was just used in discussing the nonlinear term in (3) for Re << 1. Indeed, near to the body where the linearization is inaccurate, all of the nonlinear terms are dominated by the Newtonian terms provided We << 1, as before. The difference is that far out, where the linearization is accurate, the correctly modelled term which is left is still small compared to the dominant Newtonian terms if We << 1, as required in the region near to the

body. Thus, unlike the linear approximation of the inertia terms which is of greatest relative significance in the region where it is also most accurately modelled, the elastic contribution is restricted by the requirement We << 1 to be of second order significance compared to the dominant Newtonian terms everywhere in the flow domain. Furthermore, in view of inaccuracy of the Oseen linearization near to the body, it is clear that the linearized equation (5) does not even provide a uniformly valid first approximation to the small elastic corrections. One consequence is that the asymptotic solution for small but nonzero We using (5) does not agree even qualitatively with the corresponding limiting solutions of Leslie (1961) and others which are based on the full constitutive model (4). Most evident is the difference in streamline displacement which is downstream in the solutions of Leslie (1961) and others, but completely unchanged through $O(We^2)$ using (5). Furthermore, the drag coefficient is predicted to decrease at $O(We^2)$ according to Leslie, but again to remain unchanged when the linearized model is used.

Our conclusion, then, is that the Oseen-linearized theory of Ultman and Denn (1971) for the motion of a viscoelastic fluid past a submerged body is not a uniformly valid approximation of the elastic contributions to the fluid behavior for <u>any</u> value of We.[†] Thus, though the calculations of Ultman and Denn did show an upstream shift of the streamlines, as also observed experimentally (but with much smaller magnitude), the theoretical result must be considered as completely without substance since it was based on a model which is incapable of correctly modelling the physics. A

[†] A similar conclusion is also inherent in the independent work of Mena and Caswell (1974). These authors show that the Oseen equations may be utilized in the outer region of a matched asymptotic expansion for small Re (and We), but do not consider the apparent alternative which one is led to from the Newtonian case (We ≡ 0) of using the Oseen equations to provide a uniformly valid first approximation.

similar remark must also be made with regard to the apparent correlation between the change in type of Ultman and Denn's equations at ReWe = 1, and the occurrence of experimentally observed discontinuities in certain features of the flow at a similar value of ReWe (cf. Ultman and Denn (1970)). A clear understanding of the physics responsible for these and other equally important features of the motion of a viscoelastic fluid past a submerged body must await further investigation.

ACKNOWLEDGEMENTS

This work was supported, in part, by the National Science Foundation through grants GK35468 and ENG74-17590.

REFERENCES

1. Astarita,G., and Marucci,G., Principles of Non-Newtonian Fluid Mechanics, McGraw-Hill Co. (UK) Limited,Berkshire,England (1974)
2. Broadbent,J.M.,and Mena,B.,Chem.Eng. J.,8,11 (1974)
3. Caswell,B., and Schwarz,W. H., J. Fluid Mech., 13, 417 (1962)
4. Giesekus,H., Rheol. Acta,3, 59 (1963)
5. James, D. F., and Acosta,A. J., J. Fluid Mech.,42, 269 (1970)
6. Lamb, H., Hydrodynamics, Cambridge University Press, Cambridge (1932)
7. Leslie, F. M., Quart. J. Appl. Math., 14, 36 (1961)
8. Mena,B., and Caswell, B., Chem. Eng. J., 8, 125 (1974)
9. Oseen, C. W., Hydrodynamik, Akademische Verlagsgesellschaft Leipzig (1927)
10. Proudman,I., and Pearson, J. R. A., J. Fluid Mech., 2,237 (1957)
11. Ultman, J. S., Ph.D. Thesis, U. of Delaware, Newark, Del. (1970)
12. Ultman, J. S., and Denn, M. M.,Trans. Soc. Rheol., 14, 307 (1970)
13. Ultman, J. S., and Denn, M. M., Chem Eng. J., 2,81 (1971)
14. Zana, E., Ph.D. Thesis, California Institute of Technology, Pasadena, California (1975)

TABLE CAPTIONS

Table 1: Re and We Numbers for the Experiments of Ultman and Denn, and Broadbent and Mena.

Table 2: Values of λ, d and u for the Experiments in Two Viscoelastic Liquids.

Table 3: Difference in Area Bounded by Streamlines Between Upstream and Downstream Half of the Flow Field.

FIGURE CAPTIONS

Figure 1: The Experimental Configuration

Figure 2: Experimental Streamlines (Flow from Left to Right)

Figure 2a: $Re = 10^{-4}$, $We = 10^{-2}$

Figure 2b: $Re = 1.5 \times 10^{-3}$, $We = 0.17$

Figure 2c: $Re = 0.08$, $We = 0.62$

Figure 2d: $Re = 0.05$, $We = 1.00$

Figure 2e: $Re = 0.10$, $We = 10.0$

Figure 2f: $Re = 0.12$, $We = 22.0$

Figure 3a: A Comparison of Experimental Streamlines

—— $Re = 10^{-4}$, $We = 10^{-2}$

—·— $Re = 0.1$, $We = 10.0$

Point A: 0.1 diameter away from symmetry axis.

Point B: 0.6 diameter away from symmetry axis.

Figure 3b: A Comparison of Experimental and Theoretical Streamlines

——— $Re = 10^{-4}$, $We = 10^{-2}$ (Experimental, this work)

_·_·_ $Re = 0.08$, $We = 0.62$ (Experimental, this work)

– – – $Re = 0.10$, $We = 0.50$ (Theoretical, Ultman and Denn, 1971, RE Solution, N = 2)

— — — Re = 0.10, We = 0.50 (Theoretical, Ultman and Denn, 1971, MSE Solution, N = 4)

Point A: 0.16 diameter away from symmetry axis

Point B: 0.60 diameter away from symmetry axis

Table 1

Investigators	Re	We
Ultman & Denn (1971)	2×10^{-4}	3.2×10^{-3}
Broadbent & Mena (1974)	2×10^{-2}	1.0×10^{-2}

Table 2

Solution	λ(sec)	d(cm)	u(cm/sec)
1% AP30-Water by weight	3.8	1.56	0.05
		2.56	0.68 - 2.34
		0.64	1.60 - 7.40
		0.34	1.80
0.523% AP30 -	15.0	0.95	1.28 - 1.45
45.6% Water -		1.90	0.005 - 0.38
53.9% Glycerine by weight		1.75	1.04 - 1.52

Table 3

Re	We	ReWe	$\Delta A/A_{total}$ 0.1 Radius Away	$\Delta A/A_{total}$ 0.2 Radius Away	$\Delta A/A_{total}$ 0.42 Radius Away
10^{-4}	10^{-2}	10^{-6}	--[†]	--	--
1.5×10^{-3}	0.17	2.5×10^{-4}	--	--	--
0.08	0.62	0.05*	0.039	0.0213	--
0.08	9.25	0.74	0.1468	0.1275	0.0700
0.09	9.70	0.87	0.1798	0.1475	0.0873
0.10	10.00	1.00	0.1894	0.1539	0.0915
0.12	22.2	2.66	0.1960	0.1540	0.1033

[†] No measurable difference

* Same case as Ultman and Denn's theoretical streamline pictures.

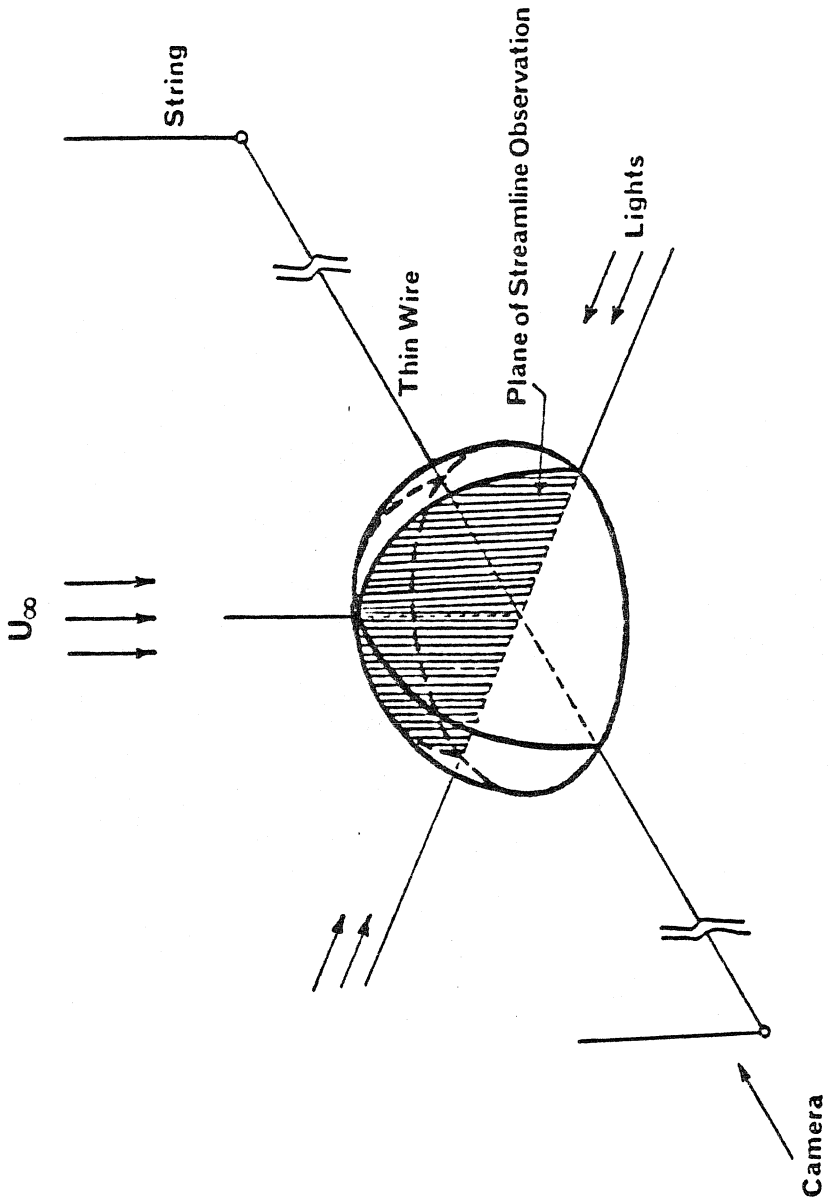
String
Thin Wire
Plane of Streamline Observation
Lights
U_∞
Camera

Figure 1

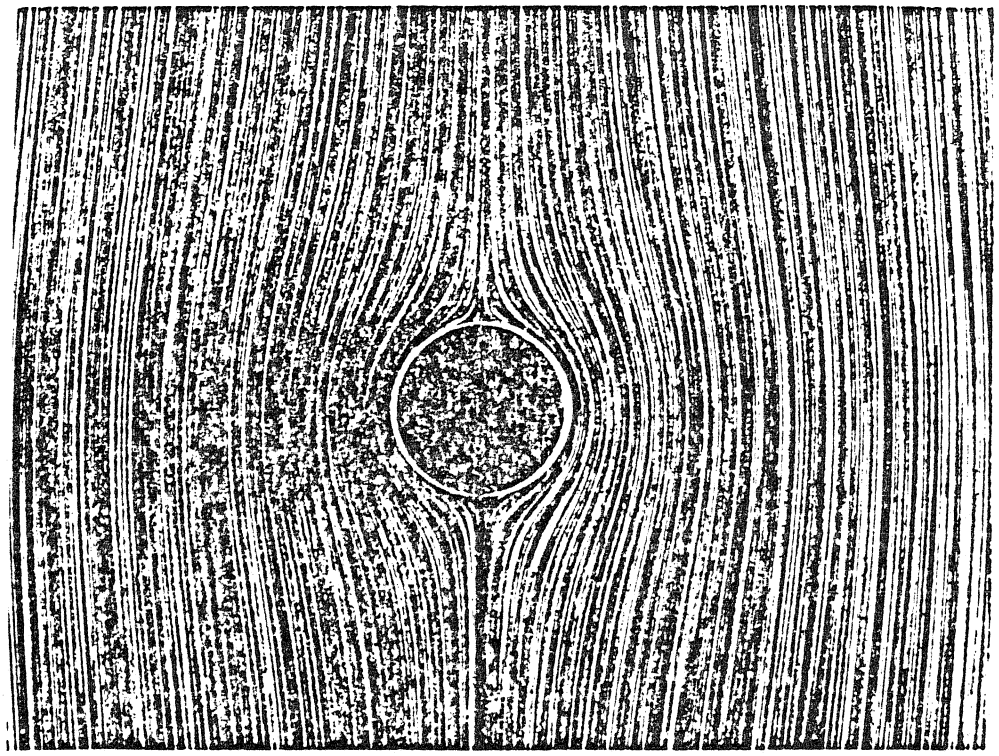

FIGURE 2b Re = $1.5X10^{-3}$, We = 0.17

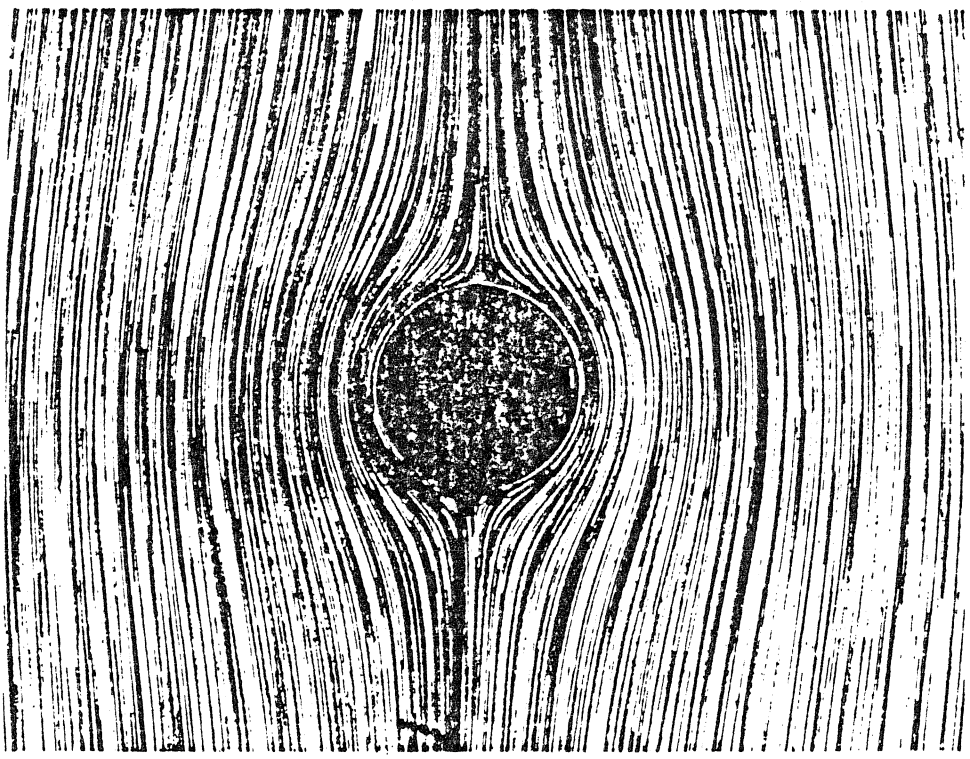

FIGURE 2a Re = 10^{-4}, We = 10^{-2}

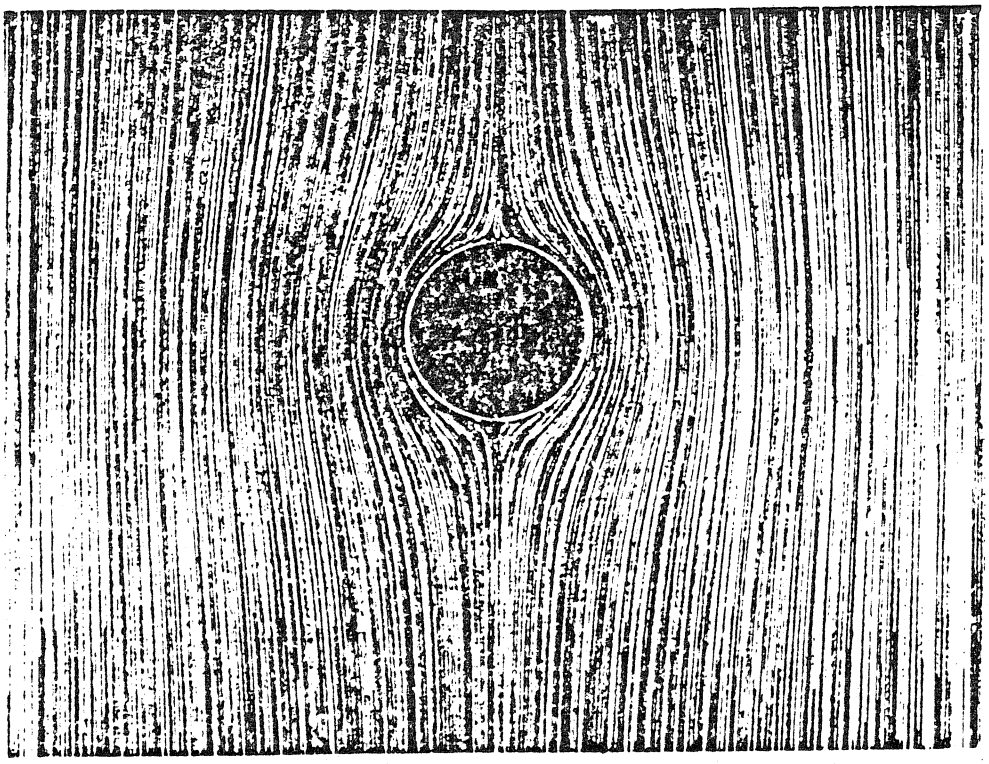

FIGURE 2d Re = 0.05, We = 1.0

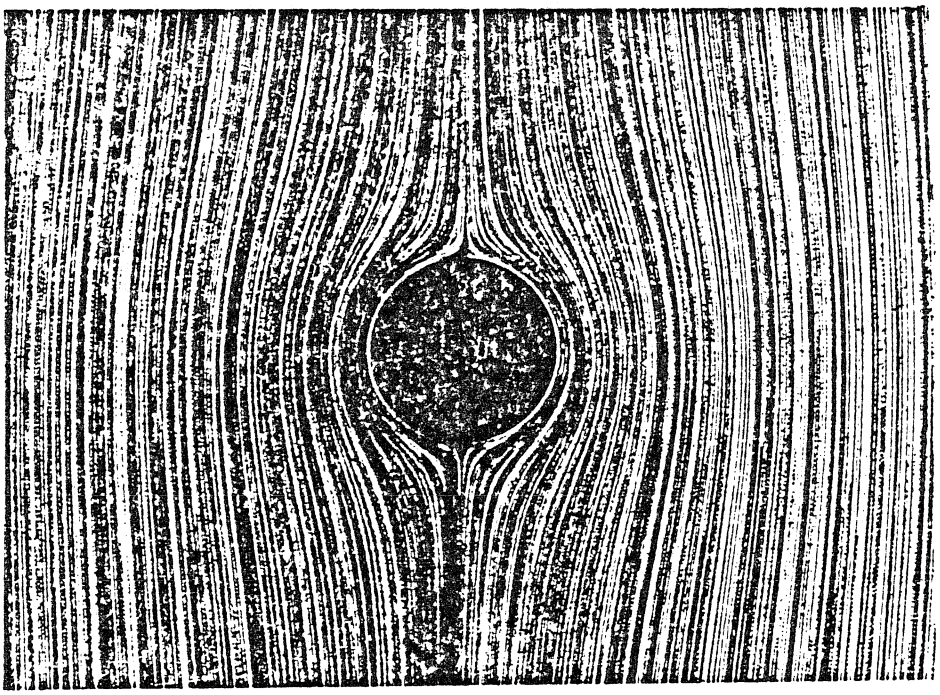

FIGURE 2c Re = 0.08, We = 0.62

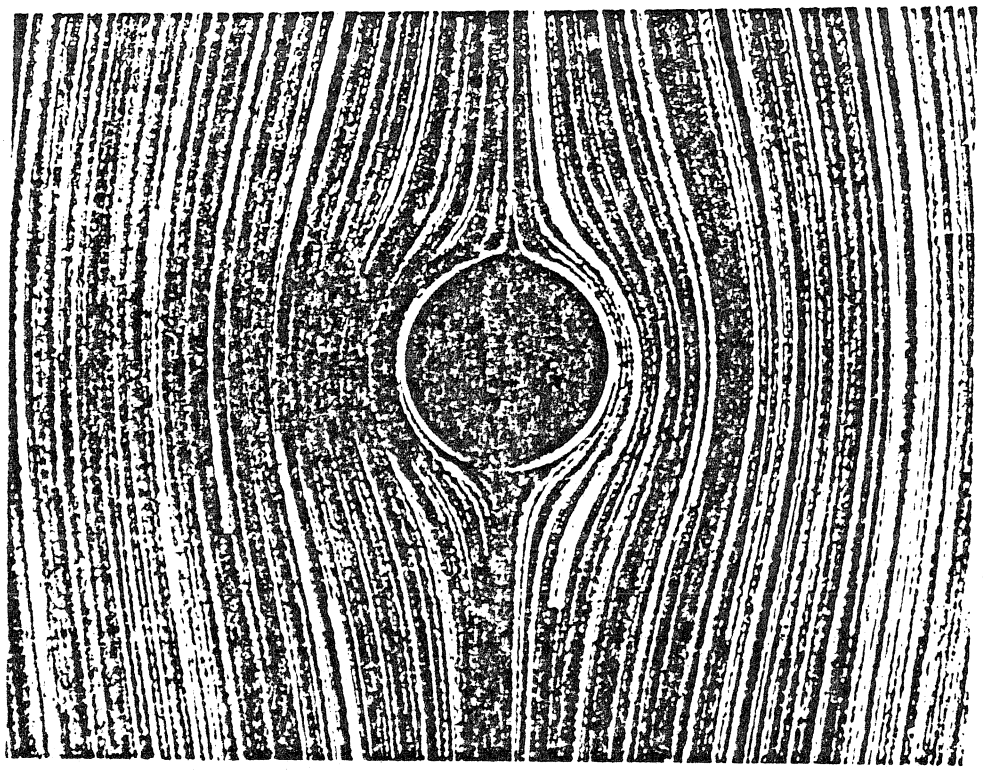

FIGURE 2f Re = 0.12, We = 22.0

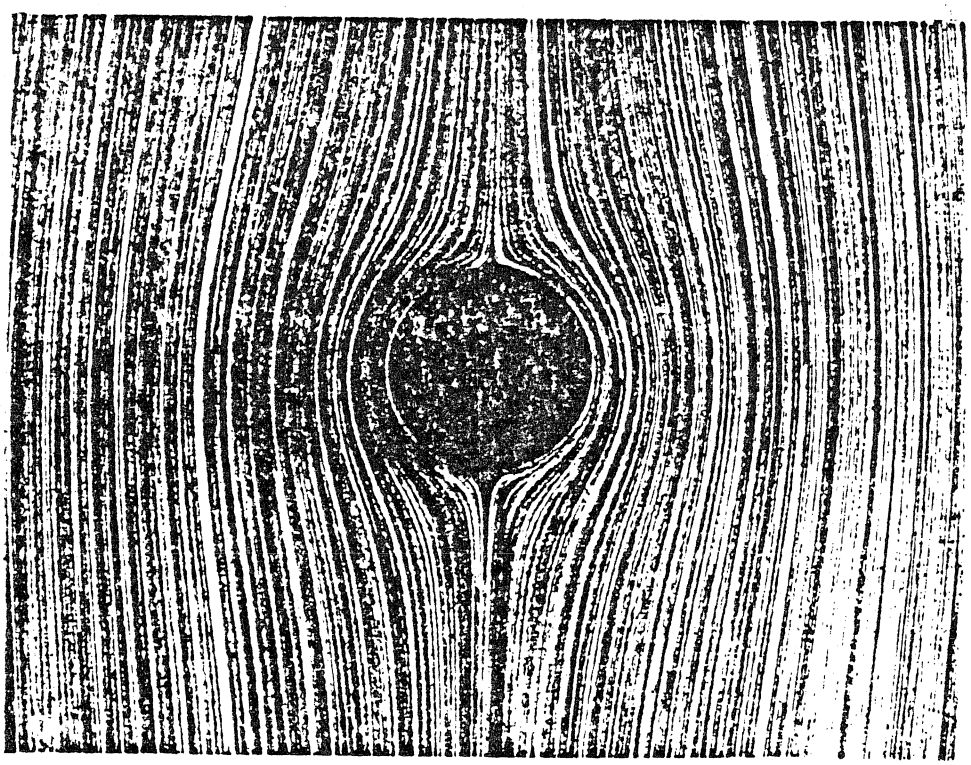

FIGURE 2e Re = 0.1, We = 10.0

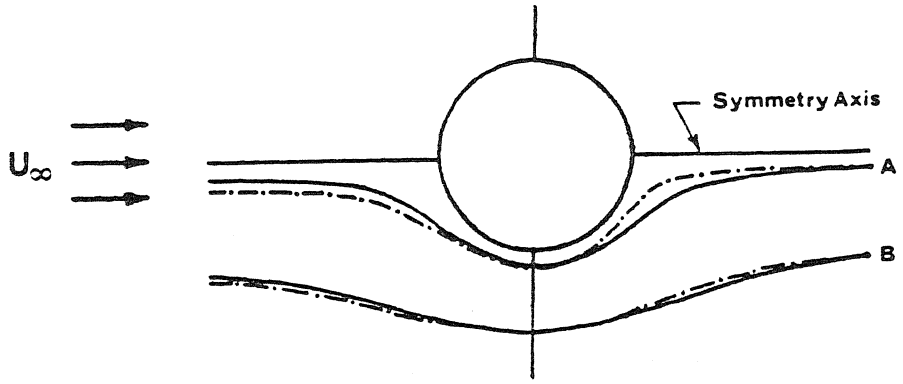

Figure 3a

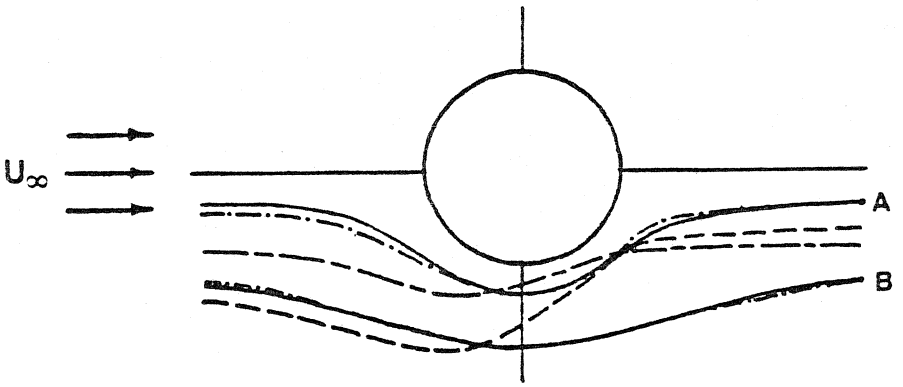

Figure 3b

APPENDIX B: Solution to the Full Equations Used by Ultman and Denn

In the main text it was implied that the effects of inertia were small if Re << 1. However, it might be argued that a combination of inertia and elastic effects could produce a noticeable difference. Therefore, it is useful to examine the solution to the full equations derived by Ultman and Denn.

The dimensionless equations they used to describe the motion of a Maxwell fluid past a sphere are

$$\mathrm{Re}\left(1 + \mathrm{Wi}\,\frac{\partial}{\partial x}\right)\frac{\partial \underline{u}}{\partial x} = -\left(1 + \mathrm{Wi}\,\frac{\partial}{\partial x}\right)\nabla p + \nabla^2 \underline{u} \qquad (B.1)$$

$$\nabla\cdot\underline{u} = 0 \qquad (B.2)$$

Following Ultman and Denn's 1971 paper we write

$$\underline{u} = \underline{i} - \nabla\phi + \underline{q} \qquad (B.3)$$

where the velocity is written as the sum of a constant (the uniform stream at large r), a rotational part $\underline{q}$ and an irrotational part denoted by the gradient of a scalar potential ϕ. Equations (1) and (2) are satisfied by

$$p = \mathrm{Re}\,\frac{\partial\phi}{\partial x} \qquad (B.4)$$

$$\underline{q} = \frac{1}{\mathrm{Re}}\left(\nabla - \mathrm{ReWi}\,\frac{\partial}{\partial x} - \mathrm{Re}\,\underline{i}\right)\chi \qquad (B.5)$$

where the scalar functions ϕ and χ satisfy

$$\nabla^2\phi = 0 \qquad (B.6)$$

$$\left(\bar{\nabla}^2 - 2\alpha\,\frac{\partial}{\partial \bar{x}}\right)\chi = 0 \qquad (B.7)$$

and $\alpha = \dfrac{\mathrm{Re}}{2\omega}$ $\qquad \omega^2 = 1 - \mathrm{ReWi}$

$$\bar{x} = x/\omega \qquad \bar{y} = y \qquad \bar{z} = z \qquad \bar{r} = (x^2/\omega^2 + y^2 + z^2)^{1/2}$$

The solutions to (6) and (7) which behave properly at large r are given by

$$\phi = \frac{A_o}{r} + \frac{A_1 x}{r^3} + A_2\left(\frac{3x^2}{r^5} - \frac{1}{r^3}\right) + A_3\left(\frac{5x^3}{r^7} - \frac{3x}{r^5}\right) + \ldots \tag{B.8}$$

$$\chi = \frac{B_o e^{-\alpha(\bar{r}-\bar{x})}}{\bar{r}} + B_1 e^{-\alpha(\bar{r}-\bar{x})}\left(\frac{\alpha\bar{x}}{\bar{r}^2} + \frac{\bar{x}}{\bar{r}^3}\right) + B_2 e^{-\alpha(\bar{r}-\bar{x})}\left(\frac{3\bar{x}^2}{\bar{r}^2} - 1\right)\left(\frac{\alpha^2}{\bar{r}^2} + \frac{3\alpha}{\bar{r}^2} + \frac{3}{\bar{r}^3}\right) \tag{B.9}$$

The solution for χ represents the first difference between this work and that of Ultman and Denn. They assumed that a meaningful solution could be obtained by retaining just the B_o term.

In order to obtain the unknown constants, we must apply the no-slip condition at the body. To facilitate the determination of constants, we expand χ for small values of $\alpha\bar{r}$, ignoring terms of order α^2. This represents an assumption that both Re and ReWi will be much smaller than one. Therefore χ becomes

$$\chi \simeq B_o\left[\frac{1}{\bar{r}} - \alpha + \frac{\alpha x}{\omega\bar{r}}\right] + B_1\left[\frac{x}{\omega\bar{r}^3} + \frac{\alpha x^2}{\omega^2\bar{r}^3}\right] + B_2\left[\frac{9x^2}{\omega^2\bar{r}^5} + \frac{9\alpha x^3}{\omega^3\bar{r}^5} - \frac{3}{\bar{r}^3} - \frac{3x}{\omega\bar{r}^3}\right] \tag{B.10}$$

The expressions for the velocities become

$$U_x = 1 + \frac{A_o x}{r^3} + A_1\left(\frac{3x^2}{r^5} - \frac{1}{r^3}\right) + A_2\left(\frac{15x^3}{r^7} - \frac{9x}{r^5}\right) + A_3\left(\frac{35x^4}{r^9} - \frac{30x^2}{r^7} + \frac{3}{r^5}\right)$$
$$- B_o\left[\frac{1}{2\bar{r}} + \frac{x}{Re\,\bar{r}^3} + \frac{x^2}{2\omega^2\bar{r}^3}\right] + B_1\left[\frac{\omega}{Re\,\bar{r}^3} - \frac{3x^2}{\omega Re\,\bar{r}^5} - \frac{3x^3}{2\omega^3\bar{r}^5}\right]$$
$$+ B_2\left[\frac{3}{2\bar{r}^3} + \frac{27x}{Re\,\bar{r}^5} + \frac{9x^2}{\omega^2\bar{r}^5} - \frac{45x^3}{Re\omega^2\bar{r}^7} - \frac{45x^4}{2\omega^4\bar{r}^7}\right] \qquad (B.11)$$

$$U_y = \frac{A_o y}{r^3} + A_1\,\frac{3xy}{r^5} + A_2\left(\frac{15x^2y}{r^7} - \frac{3y}{r^5}\right) + A_3\left(\frac{35x^3y}{r^9} - \frac{15xy}{r^7}\right)$$
$$- B_o\left(\frac{y}{Re\,\bar{r}^3} + \frac{xy}{2\omega^2\bar{r}^3}\right) - B_1\left(\frac{3xy}{\omega Re\,\bar{r}^5} + \frac{3x^2y}{2\omega^3\bar{r}^5}\right)$$
$$+ B_2\left(\frac{9y}{Re\,\bar{r}^5} + \frac{9xy}{2\omega^2\bar{r}^5} - \frac{45x^2y}{Re\,\omega^2\bar{r}^7} - \frac{45x^3y}{2\omega^4\bar{r}^7}\right) \qquad (B.12)$$

The only difficulty remaining is that the boundary condition must be applied at $r = 1$ not at $\bar{r} = 1$. Examining the equation for $\bar{r}$

$$\bar{r} = (x^2/\omega^2 + y^2 + z^2)^{1/2} = \left(r^2 + \left(\frac{1 - \omega^2}{\omega^2}\right)\,x^2\right)^{1/2} = \left(r^2 + \frac{ReWi}{1 - ReWi}\,x^2\right)^{1/2}$$

$$\bar{r} \simeq (r^2 + ReWi\;x^2)^{1/2} \simeq r\left(1 + \frac{ReWi\;x^2}{2r^2}\right) \qquad (B.13)$$

In arriving at equation (13), we have made use of the previous assumption that $ReWi \ll 1$. Using equation (13) in equations (11) and (12), and dropping terms of the order ReWi, we obtain the following

$$U_x = 1 + \frac{A_o x}{r^3} + A_1\left(\frac{3x^2}{r^5} - \frac{1}{r^3}\right) + A_2\left(\frac{15x^3}{r^7} - \frac{9x}{r^5}\right) + A_3\left(\frac{35x^4}{r^9} - \frac{30x^2}{r^7} + \frac{3}{r^5}\right)$$

$$- B_o\left(\frac{1}{2r} + \frac{x}{Re\ r^3} + \frac{x^2}{2r^3} - \frac{3Wi\ x^3}{2r^5}\right)$$

$$+ B_1\left(\left(\frac{1}{Re} - \frac{Wi}{2}\right)\frac{1}{r^3} - \left(\frac{1}{Re} + Wi\right)\frac{3x^2}{r^5} - \frac{3x^3}{2r^5} + \frac{15Wi\ x^4}{2r^7}\right)$$

$$+ B_2\left(\frac{3}{2r^3} + \frac{27x}{Re\ r^5} + \frac{9x^2}{r^5} - \left(\frac{1}{Re} + \frac{5Wi}{2}\right)\frac{45x^3}{r^7} - \frac{45x^4}{2r^7} + \frac{315Wi\ x^5}{2r^9}\right) \qquad (B.14)$$

$$U_y = \frac{A_o y}{r^3} + A_1\frac{3xy}{r^5} + A_2\left(\frac{15x^2y}{r^7} - \frac{3y}{r^5}\right) + A_3\left(\frac{35x^3y}{r^9} - \frac{15xy}{r^7}\right)$$

$$- B_o\left(\frac{y}{Re\ r^3} + \frac{xy}{2r^3} - \frac{3Wi\ x^2y}{2r^5}\right)$$

$$- B_1\left(\left(\frac{1}{Re} + \frac{Wi}{2}\right)\frac{3xy}{r^5} + \frac{3x^2y}{2r^5} - \frac{15Wi\ x^3y}{2r^7}\right)$$

$$+ B_2\left(\frac{9y}{Re\ r^5} + \frac{9xy}{2r^5} - \left(\frac{1}{Re} + \frac{3Wi}{2}\right)\frac{45x^2y}{r^7} - \frac{45x^2y}{2r^7} + \frac{315x^4y\ Wi}{2r^9}\right) \qquad (B.15)$$

Now the equations are of the form where the no-slip conditions at the surface of the sphere can be applied. In order for the velocities to be zero on the surface of the sphere, each coefficient of every power of x and y should be equal to zero. The resulting equations for the unknown constants are

$$A_1 - 3A_3 + \frac{B_o}{2} - B_1\left(\frac{1}{Re} - \frac{Wi}{2}\right) - \frac{3B_2}{2} = 1 \qquad (B.16)$$

$$A_o - 9A_2 - B_o/Re + 27B_2/Re = 0 \qquad (B.17)$$

$$3A_1 - 30A_3 - \frac{B_o}{2} - 3B_1\left(\frac{1}{Re} + Wi\right) + 9B_2 = 0 \qquad (B.18)$$

$$15A_2 + \frac{3B_oWi}{2} - \frac{3B_1}{2} - 45B_2\left(\frac{1}{Re} + \frac{5Wi}{2}\right) = 0 \qquad (B.19)$$

$$35A_3 + \frac{15B_1Wi}{2} - \frac{45B_2}{2} = 0 \qquad (B.20)$$

$$\frac{315WiB_2}{2} = 0 \qquad (B.21)$$

$$A_o - 3A_2 - \frac{B_o}{Re} + \frac{9B_2}{Re} = 0 \qquad (B.22)$$

$$3A_1 - 15A_3 - \frac{B_o}{2} - 3B_1\left(\frac{1}{Re} + \frac{Wi}{2}\right) + \frac{9B_2}{2} \qquad (B.23)$$

$$15\ A_2 + \frac{3B_oWi}{2} - \frac{3B_1}{2} - 45B_2\left(\frac{1}{Re} + \frac{3Wi}{2}\right) = 0 \qquad (B.24)$$

$$35A_3 + \frac{15B_1Wi}{2} - \frac{45B_2}{2} = 0 \qquad (B.25)$$

$$\frac{315WiB_2}{2} = 0 \qquad (B.26)$$

Thus we have nine independent equations for the seven unknown constants since equation (20) is the same as equation (25) and equation (21) is the same as equation (26). This brings us to our final assumption. In order to make this system of equations have a unique solution, we have to make an assumption regarding the magnitude of B_2. If we assume that B_2 is of $O(Wi^2)$, and then ignore all terms of $O(Wi^3)$, equation (21) becomes an identity and equation (24) and equation (19) then become the same. The solution of the resulting system of equations is

$$A_o = \frac{3}{2Re} \qquad A_1 = \frac{1}{4} + \frac{3Wi}{2Re} \qquad A_2 = \frac{3Wi^2}{2Re} \qquad A_3 = 0 \qquad B_o = \frac{3}{2} \qquad B_1 = \frac{3Wi}{2} \qquad B_2 = \frac{Wi^2}{2}$$

We observe that B_2 is indeed of $O(Wi^2)$, hence we know that the error in the solution of the flow problem is $O(Re,Wi^3)$. If we insert the constants determined above into the velocity field expressions given by equations (14) and (15), we obtain

$$U_x = 1 - \frac{3}{4r} - \frac{1}{4r^3} + \frac{3x^2}{4}\left(\frac{1}{r^5} - \frac{1}{r^3}\right)$$

$$U_y = \frac{3xy}{4}\left(\frac{1}{r^5} - \frac{1}{r^3}\right)$$

which is easily recognized as Stokes solution for the velocity field of a Newtonian fluid moving past a sphere of zero Reynolds number. The pressure, p, is determined from equation (4). The result for the pressure is

$$p = -\frac{3x}{2r^3} - \frac{3Wi}{2}\left(\frac{3x^2}{r^5} - \frac{1}{r^3}\right) - \frac{9Wi^2}{2}\left(\frac{5x^3}{r^7} - \frac{3x}{r^5}\right) + \ldots$$

When we make the substitution of $\cos\theta = x/r$, we find that the above result for the pressure agrees with the result obtained in equation (57) of Chapter I. Ultman has shown that the drag coefficient depends only upon A_0 for this method of solution, ($C_D = 8A_0$). Thus we see that the drag remains unchanged from the Stokes value at this level of approximation. The difference between this solution and the one published by Ultman and Denn lies in the manner of satisfying the boundary conditions. We conclude that the method used by them to satisfy the no-slip condition was faulty, and thus led to the unusual behavior of the solution which they reported.

CHAPTER II. A Note on Rods Falling Near a Vertical Wall in a Viscoelastic Liquid

(This paper is to be published in the Journal of non-Newtonian Fluid Mechanics.)

A Note on Rods Falling Near a Vertical Wall in a Viscoelastic Liquid

by

G. Tiefenbruck and L. G. Leal
Department of Chemical Engineering
California Institute of Technology
Pasadena, California 91125

Summary

The motion of a slender rod near a vertical wall in a viscoelastic liquid is investigated experimentally. When the particle is not too near the wall, its motion is compared to existing theoretical solutions for the motion of a slender rod in an unbounded second-order fluid. In this case, it is found that the theory and experiment are in qualitative agreement provided the particle is at least two half-lengths from the wall. When the particle is nearer to the wall, its motion is shown to correspond qualitatively to a simple superposition of the motion in a second-order fluid of infinite extent and the motion in a Newtonian fluid near a vertical wall.

Introduction

Problems involving the motion of small particles in a viscoelastic suspending fluid have received considerable attention in recent years. Interest in these problems is due, in part, to their importance in such diverse technological applications as the processing of fiber or particle loaded polymers, and the mass transfer from gas bubbles in common fermentation liquors. At the other end of the spectrum, however, experimental and theoretical studies of particle motion provide a fertile ground for the development of badly needed physical understanding of viscoelastic fluid motion outside the class of viscometric flow which has been studied almost exclusively by rheologists.

The motion of particles in non-Newtonian, and especially viscoelastic, fluids can be considerably different from their motion in a Newtonian fluid. When the particle Reynolds number is sufficiently small, these differences can be conveniently categorized into two distinct classes: one, in which the instantaneous fluid and particle motion differs little from the Newtonian case, but in which there is a gradual "drift" of the particle/fluid configuration to a new state which differs from the initial state by a large amount; and the second, in which the instantaneous fluid/particle motion differs by a large amount from the corresponding Newtonian problem. An example of the latter type would be the velocity field and particle motion for buoyancy-driven translation of a moderate sized gas bubble through a quiescent viscoelastic fluid (cf. Zana and Leal [1]). Examples of the former type include the drift of axisymmetric particles toward a preferred equilibrium orbit in simple shear flow (Gauthier, Goldsmith and Mason [2]; also Leal [3], and the cross-stream migration of

rigid spheres in unidirectional shear flows (Ho and Leal [4], Chan and Leal [5]).

The present paper is concerned with the sedimentation of slender rod-like particles in a quiescent suspending fluid. In an unbounded fluid domain, this problem is one of the class which can exhibit strong accumulative effects of weak, instantaneous non-Newtonian contribution to the particle's motion. Specifically, in a Newtonian fluid the orientation of the particle at zero Reynolds number is "indeterminate", in the sense that there is no preferred equilibrium orientation. Indeed, in the absence of disturbance effects such as Brownian rotation or particle interactions, the particle orientation in this case does not change from its value at some initial instant.

The addition of a viscoelastic contribution to the angular velocity of the particle can then yield a gradual drift toward a preferred equilibrium orientation even if the viscoelastic effect is very weak. Indeed, a rod-like particle in an unbounded viscoelastic fluid has been shown theoretically and experimentally to rotate to an equilibrium orientation in which the axis is vertical (Leal [3]).

A recent extension of the theory of creeping motion for slender bodies in a Newtonian fluid has been the development of methods to include hydrodynamic interactions with container walls. Russel, Hinch, Leal and Tiefenbruck [6], have presented both experimental and theoretical results for the motion of a slender rod near a single vertical wall. In this case the particle rotates in a deterministic fashion as it approaches the wall, though of course, the statistical distribution of orientations in a suspension of sedimenting particles nevertheless remains indeterminate as a

result of the indeterminacy in "initial" orientation for a single particle at large distances from the wall. In the present paper, we present some experimental observations for the motion of rod-like particles near a vertical wall when the suspending fluid is viscoelastic. In this case, there is a preferred steady state orientation (vertical) in the absence of any wall, and the particle motion thus consists qualitatively of a superposition of "viscoelastic rotation" toward the vertical and "wall-induced rotation" which, if it resembled the wall-induced rotation in a Newtonian fluid, would correspond to rotation toward either the vertical or horizontal depending upon the initial orientation of the particle (cf. Russel et al. [6]).

One motivation for the present study is simply that one would like to understand the effects of container walls on sedimentation of non-spherical particles in a viscoelastic suspension. However, the results of the investigation also add to our general knowledge of the behavior of viscoelastic liquids. Specifically, comparison of experimental and theoretical results for lateral migration in shear flow (cf. Chan and Leal 1978 [5]) seems to suggest that weak viscoelastic behavior influences particle/wall interactions relatively less than it influences particle motions in an unbounded fluid. On the other hand, Sigli and Coutanceau's [7] study of inertial effects in the movement of large particles through a tube filled with a polymeric liquid suggests the opposite effect in a strongly viscoelastic flow. The present investigation provides a further qualitative indication of the nature of particle/wall interactions when the viscoelastic contributions to particle motion are weak.

Apparatus and Procedure

The method of investigation here, as in our previous Newtonian experiments, was to obtain a continuous photographic record of the particle motion. The position of the center of the particle and the orientation of the particle with respect to the horizontal was then determined from these pictures as a function of time.

The experiments were conducted in a plexiglass tank with a 15" by 15" cross-section and a height of 36". The tank was placed on a stand which was adjusted so that the walls of the tank were vertical. On the back wall of the tank, horizontal and vertical reference lines were marked at regular intervals, to assist in the determination of particle position and orientation.

The viscoelastic fluid used in this study was a 1% by weight solution of the commercial coagulation polymer Separan AP-30 in distilled water. This solution has a shear thinning viscosity and appreciable normal stresses in a linear shear flow. The detailed rheological properties of 1% Separan in water have been reported elsewhere (Leal, Skoog and Acrivos [8], Bruce and Schwarz [9]), and will not be repeated here. For our purposes we need only the value of the zero shear rate viscosity which is 120 poise, the value of the density which is 1.0 g/cm^3, and the value of the principal relaxation time of the fluid, as deduced from the primary normal stress difference in linear shear flow, which is 3.8 seconds. Separan AP-30 in water is colorless and clear, making it ideally suited for the present photographic study.

The particles used in this work were cut from a copper wire and then rolled to a nominal diameter of 0.033 cm. The rolling, which was done between two smooth, flat stainless steel plates, also had the beneficial effect of straightening the particles and the more important effect of work hardening the soft copper wire, leading to a particle which is effectively rigid under conditions of the present experiments. The particles were 2.54 cm long. Thus the aspect ratio (particle diameter/particle length) of the rods was 0.013 A check of the particles under a microscope verified that they were straight and had a constant radius except for a small region near the ends which was slightly tapered. The measured density of the rolled copper wire was 8.32 g/cm^3.

The motion of the particles was recorded on high speed (ASA 400) 16 mm movie film with a Bolex camera, operated in a frame by frame mode. The camera was mounted on a counterweighted platform which could be moved up or down at a variable, but controlled speed. Thus we were able to track the particle during its entire fall, generating a record of the particle trajectory. Lighting for the pictures was provided by a spotlight mounted on the same platform as the camera. The light was only turned on at the instant of exposing each frame, and then it was immediately switched off, so as to minimize possible natural convection effects in the tank. Quantitative measurements of particle position and orientation were made from the film using a microfilm reader and the reference lines on the back

of the tank. Parallax errors were accounted for by using the known geometry of the experiment to calculate a correction. The system of reference lines on the back of the tank showed no distortion in the pictures, therefore we believe there is minimal error due to refraction effects. A typical run would take as long as thirty minutes, during which as many as sixty frames would be shot at constant intervals.

Results

a) Particle Motion Far from the Wall

When the particles are sufficiently far from a wall, they are expected to sediment as if they were in an unbounded fluid. This case is of some interest in itself, and has been studied theoretically by Leal [3] and Brunn [10]. Both of these authors considered the motion of slender rod-like particles in a second-order fluid, this representing the first non-Newtonian term in a general "retarded motion" expansion. At this level of approximation, it was shown that there is no non-Newtonian contribution to the hydrodynamic drag for a slender, axi-symmetric particle with fore-aft symmetry. On the other hand, the angular rotation of the particle, which is zero for a Newtonian fluid at zero Reynolds number, was found to be nonzero at the second-order fluid level, with a stable equilibrium orientation occurring only when the particle is vertical. The rate of rotation toward this equilibrium position was predicted to depend on the magnitude of the non-Newtonian contributions to the fluid's rheology, as well as the particle geometry and initial orientation. The only prior experimental work on this problem of sedimentation

in a viscoelastic fluid, Leal [3], was restricted to demonstrating that the particle actually rotates toward the vertical, as predicted. No detailed comparison was made between the experimentally observed or theoretically predicted rates of rotation, nor were other details of the particle's motion studied. Thus, it is of interest to compare the current results for particles which are far from the wall, with the second-order fluid theories.

As a preliminary, it is useful to recall the basic results and restrictions which are inherent in the theories. Foremost among these is the fact that the second-order fluid model is strictly applicable only when the intrinsic relaxation time scale of the fluid, τ, is much smaller than the convective time scale of the motion ℓ/u^*, where ℓ is an appropriate characteristic length scale of the particle and u^* an appropriate characteristic velocity scale. In the present problem, ℓ is conveniently chosen as the particle half-length. An appropriate characteristic velocity is the actual translational velocity of the particle. Since this is unknown, but predicted not to change at the second-order fluid level (Leal [3]), it is convenient to use the predicted "slender body" value for a rod of infinite axis ratio at zero Reynolds number in a Newtonian fluid. Apart from an O(1) correction factor to account for particle orientation, this is

$$u^* = \frac{\Delta\rho g\, r_o^2\, \ell n(2\ell/r_o)}{2\eta}$$

where $\Delta\rho$ is the density difference between the particle and the fluid, g is the gravitational acceleration constant, and r_o is the radius of the cylindrical particle. The viscosity of the fluid, η, is taken here to be the

zero shear rate limiting value for the Separan/water solution. Let us denote u* for $\eta = \eta_o$ as u^*_o. With these quantities used to evaluate u^*_o for the conditions of our experiments, we obtain

$$u^*_o \sim 0.041 \text{ cm/sec} .$$

The principle relaxation time of the fluid, τ, was estimated earlier to be 3.8 seconds and thus we can calculate the ratio, λ, of time scales for the fluid and the fluid's motion,

$$\lambda = \frac{u^*_o \dot{\tau}}{\ell} \sim 0.12$$

The magnitude of λ, which is sometimes called the Deborah number, is indicative of the importance of elastic effects on the motion of the particle. We see that λ is small, but not negligible in the present experiments. The retarded motion results for a second-order fluid, on the other hand, are strictly valid in the asymptotic limit $\lambda \to 0$. An obvious and important question is whether $\lambda \sim 0.12$ is sufficiently small for the asymptotic theory to provide quantitative or even qualitatively correct results. This question is particularly significant since other problems involving particle motions in an unbounded, viscoelastic fluid (cf. Leal [3], Ho and Leal [4], and Tiefenbruck and Leal [11]) have led to the rather surprising conclusion that the second-order fluid theory will yield reasonably accurate results for λ as large as 1.

For convenience in the present discussion, as well as in the analysis of experimental data which follows, we adopt the coordinate system shown in Figure 1. Assuming the analysis of particle motion in a second-order fluid to be applicable under conditions of our experiment, as indicated above, it is expected that the translational velocity components will be

given by the results relevant to motion in an unbounded, Newtonian fluid [recall, there is no $O(\lambda)$ contribution to the drag for a slender, axisymmetric particle with fore-aft symmetry in an unbounded fluid], i.e.

$$u_x = \frac{dx}{dt} = -0.64 \frac{u_o^*}{2} \sin\theta\cos\theta \tag{1}$$

$$u_y = \frac{dy}{dt} = \frac{u_o^*}{2} (1 + 0.64 \sin^2\theta) \tag{2}$$

The number 0.64 in the above expressions is the correction to the classical slender body results which is necessary due to the finite axis ratio of the particles (see Russel et al. [6]). Integrating equations (1) and (2) and dividing by ℓ, we obtain the following dimensionless trajectory equations

$$\frac{x_o - x}{\ell} = 0.64 \frac{u_o^*}{2\ell} \int_0^t \sin\theta\cos\theta dt \tag{3}$$

$$\frac{y - y_o}{\ell} = \frac{u_o^*}{2\ell} \left[t + 0.64 \int_0^t \sin^2\theta dt \right] \tag{4}$$

which depend on the instantaneous orientation of the particles, $\theta(t)$. For a second-order fluid, the theories of Leal [3] and Brunn [10] show

$$\ell n(\tan\theta/\tan\theta_o) = At \tag{5}$$

in which θ_o is the initial orientation and A is a constant which depends upon the rheological parameters of the fluid and the detailed variation of the particle cross-sectional area with position along its major axis. It is of interest to test both the predicted independence of translational velocities on the change from a Newtonian to a second-order fluid, and the predicted dependence of particle orientation on time as given by equation (5).

Let us first consider the orientation of the particle as a function of time. The experimental results are shown in Figure 2, where we have plotted $\ell n(\tan\theta/\tan\theta_o)$ versus the time t for four different values of θ_o. For values of time less than 500 sec, equation (5) appears to describe the data quite well with a value of A equal to 0.0021 sec^{-1}. For a circular cylinder with an axis ratio equal to that of the experimental particles, and estimates of material constants in the second-order fluid model, Leal's asymptotic slender body theory gives $A \sim 0.0028\ sec^{-1}$. This degree of agreement between theory and experiment is well within expectations since the theory is first-order in $[\ell n(2\ell/r_o)]^{-1}$ and thus pertains strictly to particles which are more slender than those used here. The fact that the predicted value of A is larger than the experimental value is qualitatively consistent with theoretical corrections for finite aspect ratio in Newtonian fluids (cf. Figure 3, Russel et al. [6]). The more important linearity between $\ell n(\tan\theta/\tan\theta_o)$ and t is clearly confirmed by our present experimental results. It should be noted in this regard that the deviation of the data from a straight line at larger times is due primarily to the presence of the wall. We will discuss the interactions with the wall in detail in the next section.

Let us now turn to the predicted trajectories, (3) and (4). In order to provide a valid test of the independence of drag on deviations from Newtonian rheology in the second-order fluid regime, we must use the experimentally determined value of $A = 0.0021\ sec^{-1}$ in equation (5) to evaluate the right hand sides of equations (3) and (4). The integrals in these expressions were calculated numerically using a trapezoidal rule.

Our objective is to compare the experimentally measured trajectories with the calculated results. For this purpose, we plot experimental values of the horizontal and vertical displacements at various points in time, i.e. $(x_o - x)/\ell$ and $(y - y_o)/\ell$, versus the theoretical values of the same quantities calculated as explained above. These plots are presented in Figures 3 and 4, respectively. If the theory and experiments were in perfect agreement, the points would of course, fall along the 45° trajectories which are shown as solid lines in these figures. We see that the measured and predicted values are, in fact, in reasonable qualitative agreement. Nevertheless, quantitative discrepancies are clearly evident. In particular, there is more spread in the data than might be expected, especially for small times when the particle is far from the wall.

This difference between experiment and theory appears to be due primarily to the idealization which is inherent in the use of a second-order fluid model for the description of the Separan AP30 solution at small but finite Deborah numbers. In particular, the second-order fluid model allows for normal stress effects in simple shear flow, but no shear-thinning of the apparent viscosity. The Separan AP30 solution, on the other hand, exhibits a small but significant degree of shear thinning even in the low shear-rate range of the present experiments. A particle will sediment, all else being equal, more rapidly for larger values of θ. Thus the mean shear rate in the suspending fluid will also increase with an increase in θ.

This increase in mean shear-rate has no consequence for creeping flows if the fluid is Newtonian. However, the same is not the case for a

shear thinning liquid such as Separan AP30 in water. In equations (3) and (4) it was assumed that u_o^* was independent of time (or equivalently that the viscosity η was independent of the changes in shear rate which are caused by changes in the particle orientation). Since this is not precisely true, the comparison between experiment and theory in Figures 3 and 4 will be affected. Specifically, since the particle has a different initial orientation in each of the experimental runs, the data will reflect a different mean viscosity history for each run. When plotted in the fashion of Figures 3 and 4, this will lead to an apparent scatter when the data from the different runs are compared. The importance of this effect may be tested by replotting the data in a manner which reflects the fact that the viscosity is expected to vary with the particle orientation. This is accomplished by shifting the data for the three runs with the largest initial orientation angles, θ_i^*, so that the first data point in each case matches the values of $(x_o - x)/\ell$ and t from the fourth run at the same angle $\theta = \theta_i^*$. A similar shifting was also applied to the vertical displacement data for the particle. The resulting plots are shown in Figures 5 and 6, respectively. In effect, this method of shifting assumes that there is a unique value of particle velocity (and thus fluid viscosity) for each orientation, θ. If this assumption is correct, when incremental displacements are compared for the same orientation angles, they should be identical from run to run. The collapse of the data in Figures 5 and 6 to a single universal curve therefore suggests strongly that it was the shear dependence (and thus the orientation dependence) of viscosity which was responsible for the data spread in Figures 3 and 4. Figures 5 and 6 also

allow a comparison of the experimental results with the results predicted on the basis of (3) and (4) with $\eta = \eta_0 = \text{const.}$ The predicted trajectories are plotted in figures 5 and 6. The experimental results for horizontal displacement, in figure 5, are, in fact, in quite good agreement with the simple theory ($\eta = \eta_0$). The results for vertical displacement, in figure 6, show a larger deviation between theory and experiment, and the data indicate smaller vertical velocities than predicted by equation (4). We have not been able to trace the source of this difference.

We may summarize the results of this section by saying that the second-order fluid theory for an unbounded fluid provides a qualitatively correct description of the particle motion when the particle is more than approximately two half-lengths from the wall. However, in contrast to earlier results on particle migration (Ho and Leal [4]) and orbit drift in shear flow, (Leal [3]), the weak shear thinning which exists for small but non-zero λ is seen to play a non-negligible role in the present results. For this reason, significant deviations between theory and experiment occur for somewhat smaller values of λ than would have been expected on the basis of our earlier studies. Let us now turn to the interactions between the particle and the wall.

b) Particle Interactions with the Wall

Before describing the interactions of a particle with the wall in Separan/water, it is useful to recall the most important results from the previous Newtonian fluid experiments. Specifically, it was found that there were two distinct modes of wall induced particle rotation, the so-called 'glancing' and 'reversing' turns. In the 'glancing' turn, the end

of the particle nearest the wall moves in such a manner that the angle of the particle with respect to the horizontal increases. In the 'reversing' turn, on the other hand, the particle appears to pivot about the end nearest the wall, finally moving away from the wall with the opposite end leading. Particles which approached the wall with orientation angles, θ, greater than a "critical" value were found to undergo the glancing turn, while those with smaller angles θ underwent the reversing turn.

In figure 7, we have plotted our results for the present experiments in Separan AP30/water. This plot shows the distance between the particle center and the wall as a function of the orientation of the particle with respect to the horizontal. The solid line at the bottom of the figure delineates a "forbidden region" in which some portion of the rod would be required to penetrate the wall. As in the preceeding Newtonian study, the particle trajectories show both "glancing" and "reversing" turns due to interaction with the wall. Specifically, runs (b) and (c) demonstrate the 'glancing' turn, while run (f) is an example of a reversing turn. In contrast to the Newtonian problem, however, the tendancy to rotate toward the vertical in an <u>unbounded</u> viscoelastic fluid means that a particle can only exhibit a 'reversing' turn if it starts sufficiently near the wall, in addition to being sufficiently near the horizontal in its initial orientation. Extrapolation of the curve (f) to $\theta = 0$ suggests, in fact, that <u>no</u> reversing turn could occur for a particle which was initially more than 6.5 particle half-lengths from the wall. Although the value 6.5 is obviously specific to the particular particle geometry and viscoelastic fluid of the present experiments (i.e. 1% Separan AP30 in water), the general conclusion that 'reversing' turns are limited, not only to initial orientations sufficiently

near horizontal (as is also true in a Newtonian fluid), but also to particles which are simultaneously close to the wall, is expected to be true for the general class of viscoelastic suspending fluids. It may be noted that a particle which is sedimenting in a container with vertical side-walls will generally be restricted to a single reversing or glancing turn since it will rotate to the vertical and thus fall parallel to the walls prior to travelling across the container for a second wall encounter.

Although a theory of particle motion in a viscoelastic fluid near a wall could, in principle, be constructed for a second-order fluid along the lines outlined by Leal [3], using the solution of Russell et al. [6] for the motion of a slender rod-like particle near a wall in a Newtonian solution, the magnitude of the necessary algebraic manipulations is so formidable that the analysis is impractical. An admittedly "ad hoc" alternative is to simply superpose the wall interactions for motion in a Newtonian fluid, as calculated by Russel et al. [6], with the non-Newtonian contribution of (3) - (5) for particle motion in an unbounded second-order fluid. The results from this simple approach, plotted in a manner similar to the experimental data in figure 7, are shown in figure 8. Comparison of figures 7 and 8 shows that the "ad hoc" theory is in reasonable qualitative agreement with the experimental observations — thus suggesting that the simple superposition described above is a reasonable approximation to the dominant physics of the particle's motion. This is not altogether unexpected since it is only the non-Newtonian "corrections" to the particle-wall interaction which are missed out in the approximate theory, and these are expected to be small relative to the dominant Newtonian fluid contributions for small λ.

A more detailed comparison of figures 7 and 8 shows that the theory underestimates the maximum distance which a particle can be from the wall, and still undergo a 'reversing' turn. This is not too surprising since the distance for significant interaction between the particle and wall in a Newtonian fluid was also underestimated by the slender-body theory of Russel et al. [6] for small values of θ. Indeed, if we had estimated the particle-wall interaction from the experimental data of our earlier study, rather than from the theory, the agreement between "theory" and experiment in the present work (i.e. figures 7 and 8) would have been much better. This suggests that any non-Newtonian contribution to the particle-wall interactions must be relatively unimportant.

The simple theory of figure 8 reveals an additional, more subtle feature of the particle-wall interaction process which, due to the limited depth of the experimental tank, is less obvious in the experimental data of figure 7. This is the fact that a particle which undergoes a 'glancing' turn without passing too close to the wall actually overshoots the vertical orientation, and continues to rotate while simultaneously moving away from the wall. Furthermore, the results plotted in figure 8 suggest that all trajectories approach the value $\theta = \pi/2$ for large x along a common asymptote. The reason that the particle continues to rotate past $\theta = \pi/2$ when it is near the wall is simply that the wall interactions continue to generate a torque even though the viscoelastic contribution to particle rotation has momentarily vanished. We shall discuss the asymptotic behavior as the orientation re-approaches $\pi/2$ for larger x at a later point in this section. First, let us consider the experimental results in greater detail.

Examining the experimental data in figure 7, we see that the trajectory (c) is indeed smooth and continuous through $\theta = \pi/2$ as predicted. Run (b) also exhibits a smooth curve through $\pi/2$, but the effect of the wall appears to be smaller than expected on the basis of figure 8. Run (a) shows no discernible effect of the wall at all. Unfortunately, the available experimental tank was too short to allow a more definitive study of this aspect of particle-wall interactions. Part of the difficulty, as we shall see, is that the particle only re-approaches the vertical in the asymptotic limit, $t \to \infty$. Further, we found it impossible to achieve reproducible results unless the particle was initially started at four or five half-lengths from the wall. In spite of these limitations, however, the available data suggest that the wall-particle interaction is over-estimated for the larger values of x and $\theta \sim \pi/2$ by the "ad hoc" second-order fluid theory. In this sense, the present experimental results are consistent with the earlier investigation of the lateral drift problem by Chan and Leal [5] which also seemed to support the conclusion that the magnitude of wall effects on particle motion was over-estimated by a second-order fluid theory.

Runs (d) and (e) warrant special attention since the approximate theory of figure 8 is not capable of providing any insight as to the expected behavior once the minimum separation distance between the particle and wall is small (of the order of the particle radius). The experimental trajectories appear to suggest that the particle makes contact with the wall. After this happens, the leading end continues to slide down the wall, and the orientation approaches $\pi/2$. Once this happens, the

particle ceases to rotate and appears simply to slide very slowly down the wall until it reaches the bottom of the tank. This behavior is, of course, different from the 'glancing' turns which occur when the separation between the particle and wall is larger, and cannot be explained by the slender-body theory which is inherent in figure 8. The fact that the particle slides down the wall suggests that it does not actually hit the wall, but only comes close to it. This finding agrees with a similar conclusion from our previous Newtonian fluid investigation.

The only example of a 'reversing' turn in the experimental data of figure 7 is run (f). As indicated above, this particular form of wall-particle interaction is not very common due to the influence of fluid elasticity which tends to cause the particles to turn toward the vertical before they encounter the wall. In the region prior to reaching $\theta = 0°$, run (f) reflects the competing effects of contributions to the particle rotation due to fluid viscoelasticity and to hydrodynamic interactions with the wall which are in the opposite sense! After the particle has passed through the horizontal, on the other hand, the two contributions add so that the particle approaches the vertical more rapidly than it would in an unbounded fluid. This is most easily seen by choosing a value of x (say 2), and then noting the angles at which it intercepts the trajectory (f) (26.5 and -36°). As the particle moves away from the wall, we see that the slope of the trajectory approaches the far-field value. As θ approaches $-\pi/2$, we anticipate an asymptotic approach to vertical in a manner similar to the 'glancing' turns as depicted in the left most trajectory of figure 8.

The most important practical implication of the particle-wall interactions which we have described is their effect on the concentration distribution for a dilute suspension of sedimenting, rod-like particles in a viscoelastic fluid. In order to determine what this effect may be, it is necessary to consider the asymptotic behavior of the trajectories of Figure 8 which overshoot $\theta = \pi/2$. This may be discussed quite simply in terms of the governing equations for the "ad hoc" theory, approximated for $|\theta'| << 1$ where $\theta' \equiv (\theta - \pi/2)$.

$$\frac{\partial y}{\partial t} = \frac{1}{f(\varepsilon)} \tag{6}$$

$$\frac{\partial x}{\partial t} = \frac{\theta'}{2f(\varepsilon)} \tag{7}$$

$$\frac{\partial \theta'}{\partial t} = \frac{3\varepsilon}{2f(\varepsilon)} x^2 \left[\frac{1 + \frac{1}{2x^2}}{\left(1 + \frac{1}{x^2}\right)^{1/2}} - 1 \right] - \left(\frac{A\ell}{u_o^*}\right)\theta' \tag{8}$$

where

$$\varepsilon \equiv [\ell n(2\ell/r_o)]^{-1}$$

and

$f(\varepsilon)$ = correction to the drag for motion parallel to the particle axis, due to the finite axis ratio of the particle (see Figure 3 of Russell et al. [6]).

The quantities A, ℓ, u_o^* and r_o which are inherent in the scaling factors ℓ and u_o^* of equations (6) - (8) were defined earlier.

The two terms on the right hand side of equation (8), for the time-evolution of θ', represent the interaction induced rotation due to the wall and rotation induced by the non-Newtonian properties of the bulk fluid, respectively.

It is the balance between these two effects which produces the characteristic over-shoot and return behavior which is demonstrated in Figure 8. An approximate theory for the "common" trajectory at large x and small θ' may be obtained from (6) - (8) by assuming $\partial\theta'/\partial t \approx 0$, so that

$$\theta' = \frac{3\varepsilon U_o^*}{2A\ell f(\varepsilon)} x^2 \left[\frac{1 + \frac{1}{2x^2}}{\left(1 + \frac{1}{x^2}\right)^{\frac{1}{2}}} - 1 \right] \tag{9}$$

Equation (9) with the constants evaluated for the conditions of the present experiments is reproduced as the solid line in Figure 9. Substituting θ' from equation (9) into (7) then gives the following equation for x

$$\frac{dx}{dt} = \beta x^2 \left[\frac{1 + \frac{1}{2x^2}}{\left(1 + \frac{1}{x^2}\right)^{\frac{1}{2}}} - 1 \right] \tag{10}$$

where

$$\beta = \frac{3\varepsilon U_o^*}{4A\ell f^2(\varepsilon)}$$

The above equation for x cannot be integrated analytically as written. To proceed further we thus approximate the right-hand side of equation (10) as a power series in x^{-1}. Upon integrating the resulting expression, we obtain

$$\frac{8x^3}{3} + 8x - 4 \log\left(\frac{x + 1}{x - 1}\right) = \beta t + c \tag{11}$$

where c is a constant of integration. If we evaluate β using the values of the constants from the present experiments, $\beta = 1.59$. Thus, for example, if the particle was at $x = 2$ for $t = 0$, then at $t = 240$, $x = 5.20$. The real time for the particle to travel the horizontal distance of 4.06 cm in this example will be over 2 hours! During that same period of time, the

particle would have fallen vertically over 254 cm! The values of y corresponding to four values of x at equal increments of time are shown in Figure 9, to give some perspective of the relative magnitudes of the horizontal and vertical velocity components. The points in Figure 9 represent numerical results from the full "ad hoc" theory which show the degree of approach to the asymptotic behavior for various values of x and θ'. The key feature of the solution (11) is that it shows that

$$x \to \infty \qquad \text{as} \qquad \theta' \to 0.$$

for an infinitely deep and wide tank. For an infinitely deep tank of finite width, a particle which undergoes a 'glancing' turn would thus be expected to move to the center where, for reasons of symmetry, it would stop moving normal to the wall. We note here that a similar theory may be developed for θ approaching $-\pi/2$ which is the case for the 'reversing' turn. The ultimate position of the rods in this case is also "far" from the wall. Thus, a dilute suspension of rods sedimenting in a finite tank should exhibit a "particle free" zone near the wall which increases in width with depth in the tank. As a consequence, the particle concentration at the center of the tank must also increase with increasing depth. The eventual development of an "equilibrium" concentration distribution in which almost all of the particles are near the center of the tank, at least in principle, is in contrast to the case of a Newtonian suspending fluid where the distribution of particles would be expected to remain more nearly uniform. It should be noted in the non-Newtonian case that the results of Figure 7, runs (d) and (e), suggest a second concentration peak, albeit with relatively few particles, which would be located right at the wall. In this region, particles which approach near enough to the

wall with $\theta > \sim 60°$ appear to be "trapped" and remain very close to the wall for subsequent times.

In summary then, the particle interaction with the wall appears to agree reasonably well with predictions based upon a simple "ad hoc" superposition of wall induced rotation in a Newtonian fluid, and rheologically induced rotation in a viscoelastic liquid. Both 'glancing' and 'reversing' turns are evident, but the latter are limited to a relatively small range of initial orientations and positions relative to the wall. The effect of the wall on the concentration distribution for a dilute suspension of sedimenting rods is predicted to be much different for a viscoelastic liquid than for a Newtonian suspending fluid.

Acknowledgment

The authors wish to thank the National Science Foundation for the grant which made this work possible.

References

1. Zana, E. and Leal, L. G. 1978 Int. J. of Multiphase Flow 4, 237.
2. Gauthier, F., Goldsmith, H. L. and Mason, S. G. 1971 Rheol. Acta 10, 344.
3. Leal, L. G. 1975 J. Fluid Mechanics 69, 305.
4. Ho, B. P. and Leal, L. G. 1976 J. Fluid Mechanics 76, 783.
5. Chan, P. and Leal, L. G. 1978 J. Fluid Mechanics, to appear.
6. Russel, W. B., Hinch, E. J., Leal, L. G. and Tiefenbruck, G. 1977 J. Fluid Mechanics 83, 273.
7. Sigli, D. and Coutanceau, M. 1977 J. Non-Newtonian Fluid Mechanics 2, 1.
8. Leal, L. G., Skoog, J. and Acrivos, A. 1971 Can J. Chem. Eng. 49, 569.
9. Bruce, C. and Schwarz, W. H. 1969 J. Pol Sci. A-2 7, 909.
10. Brunn, P. 1977 J. Fluid Mechanics 82, 529.
11. Tiefenbruck, G. and Leal, L. G. "Numerical Solutions for Flow of an Oldroyd Fluid Past Solid Spheres and Spherical Bubbles," 1979, in preparation.

Figure Captions

Figure 1. The coordinate system.

Figure 2. Variation of $\ell n(\tan\theta/\tan\theta_0)$ versus time. ■ $\theta_0 = 42.5°$, ● $\theta_0 = 32°$, ▲ $\theta_0 = 20.5°$, ◆ $\theta_0 = 48°$. The open markers represent points where the particle is within 2ℓ of the wall.

Figure 3. Experimental horizontal particle displacement versus predicted horizontal displacement. ■ Run (b) $x_0 = 6.55$, ● Run (c) $x_0 = 6.37$, ▲ Run (d) $x_0 = 6.48$, ◆ Run (a) $x_0 = 6.53$. The open markers represent points where the particle is within 2ℓ of the wall.

Figure 4. Experimental vertical particle displacement versus predicted horizontal displacement. ■ Run (b), ● Run (c), ▲ Run (d), ◆ Run (a). The open markers represent points where the particle is within 2ℓ of the wall.

Figure 5. Horizontal displacement of particle center as a function of time. Points are plotted in a manner such that the orientation is the same for all of the runs at each point in time. ■ Run (b), ● Run (c), ▲ Run (d), ◆ Run (a).

Figure 6. Vertical displacement of particle center as a function of time. Points are plotted in a manner such that the orientation is the same for all runs at each point in time. ■ Run (b), ● Run (c), ▲ Run (d), ◆ Run (a).

Figure 7. The variation of the distance of the particle center from the wall and the orientation of the rods as they turn. + Run (a), □ Run (b), ⬡ Run (c), △ Run (d), X Run (e), ◇ Run (f).

Figure 8. Particle trajectories calculated by superposition of Newtonian hydrodynamic interaction with the wall and visco-elastic fluid induced rotation.

Figure 9. Asymptotic solution for the particle trajectory after 'glancing' turn.

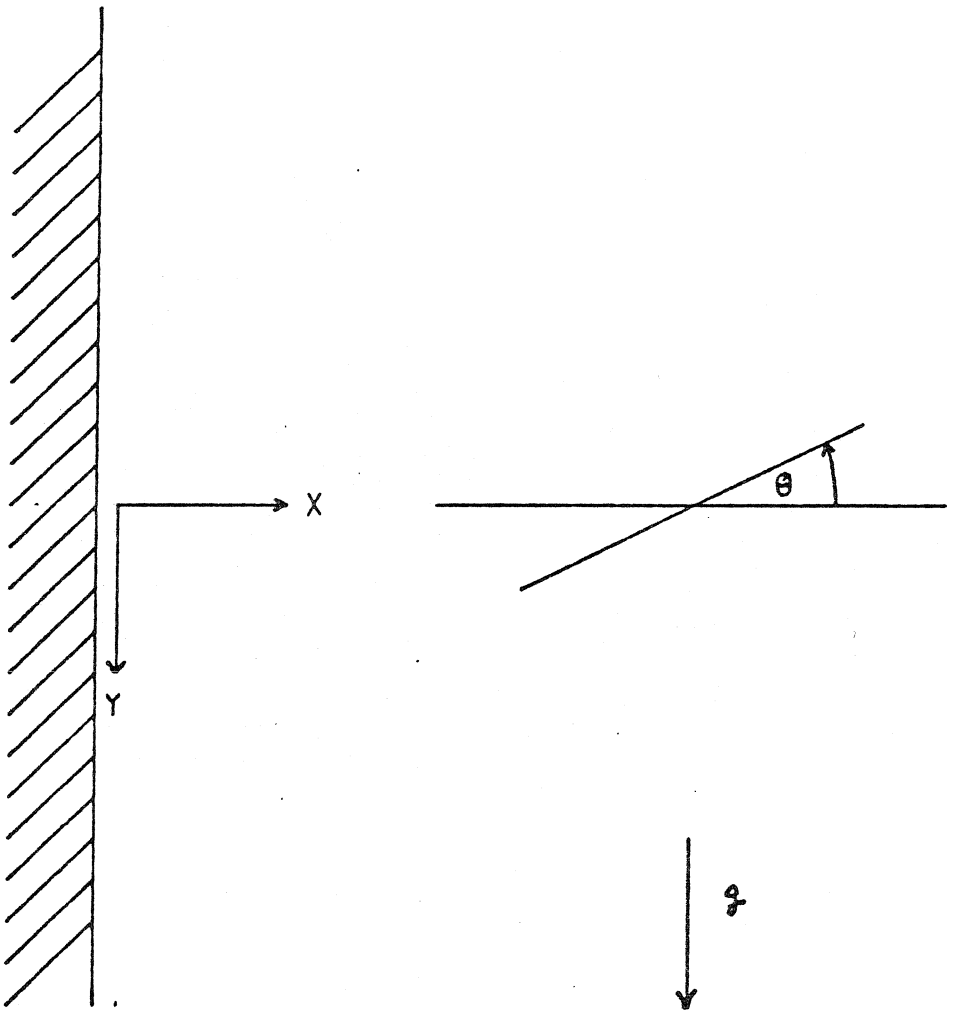

Figure 1.

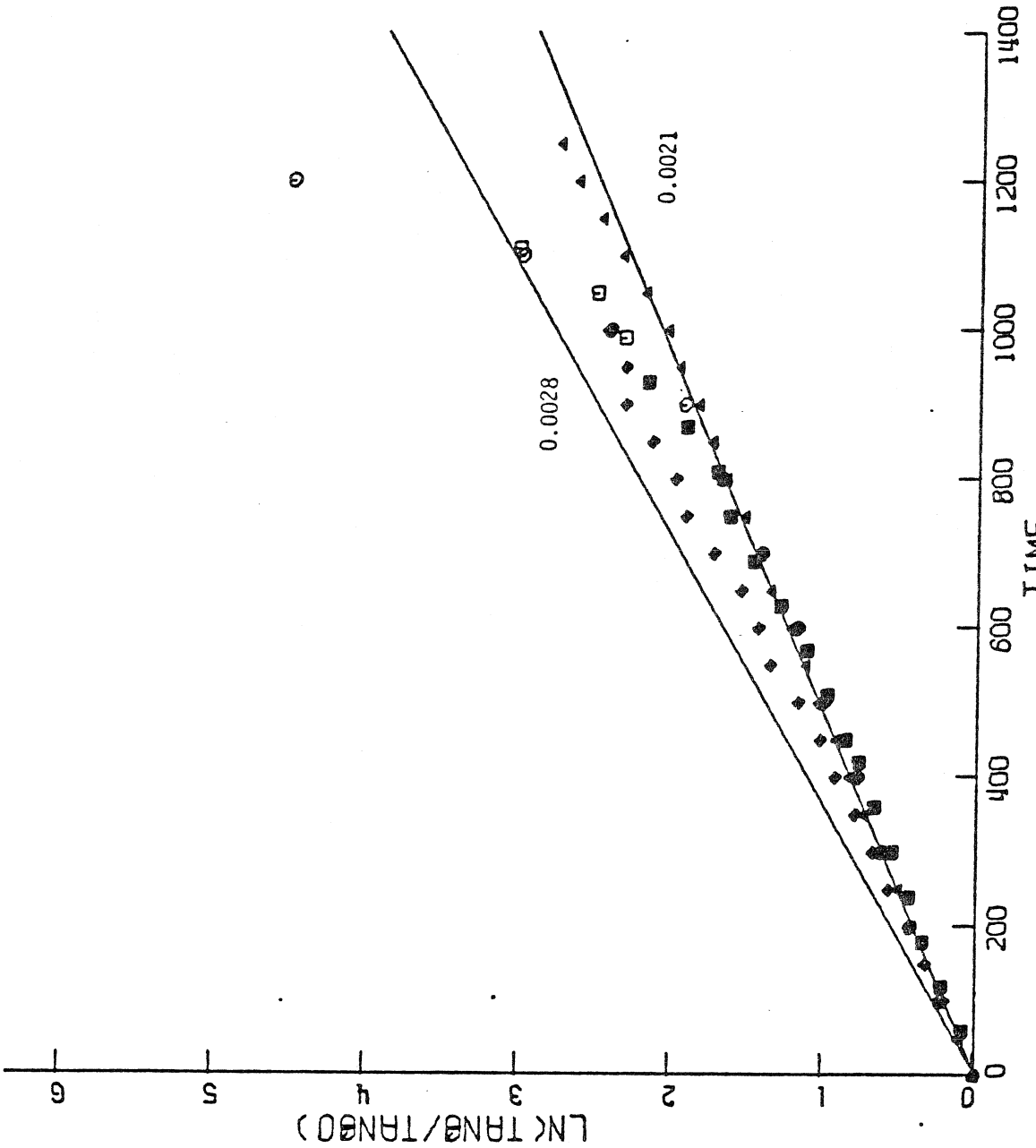
LN(TANθ/TANθ0)
0
1
2
3
4
5
6
0
200
400
600
800
1000
1200
1400
TIME
0.0028
0.0021

Figure 2.

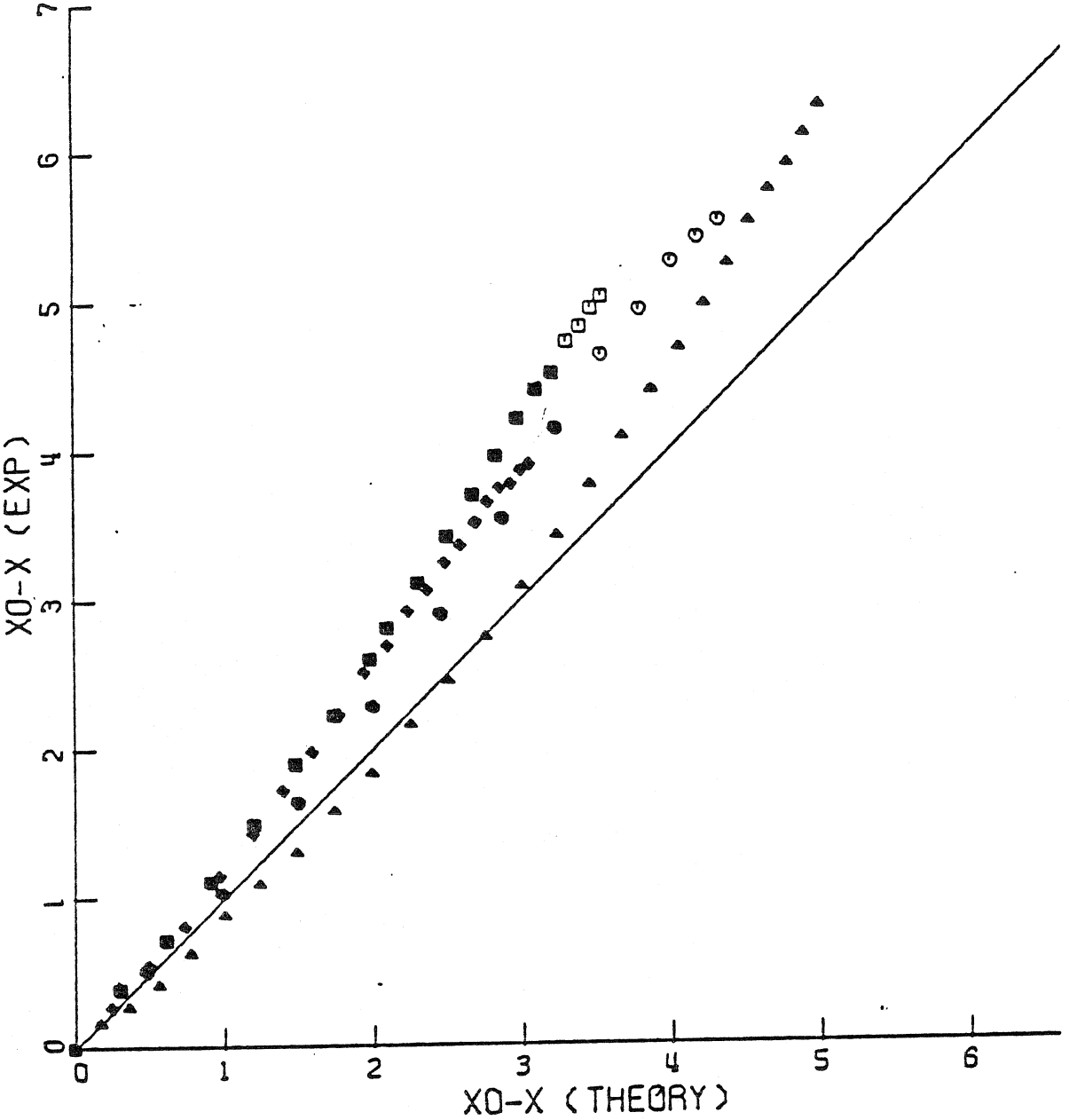

Figure 3.

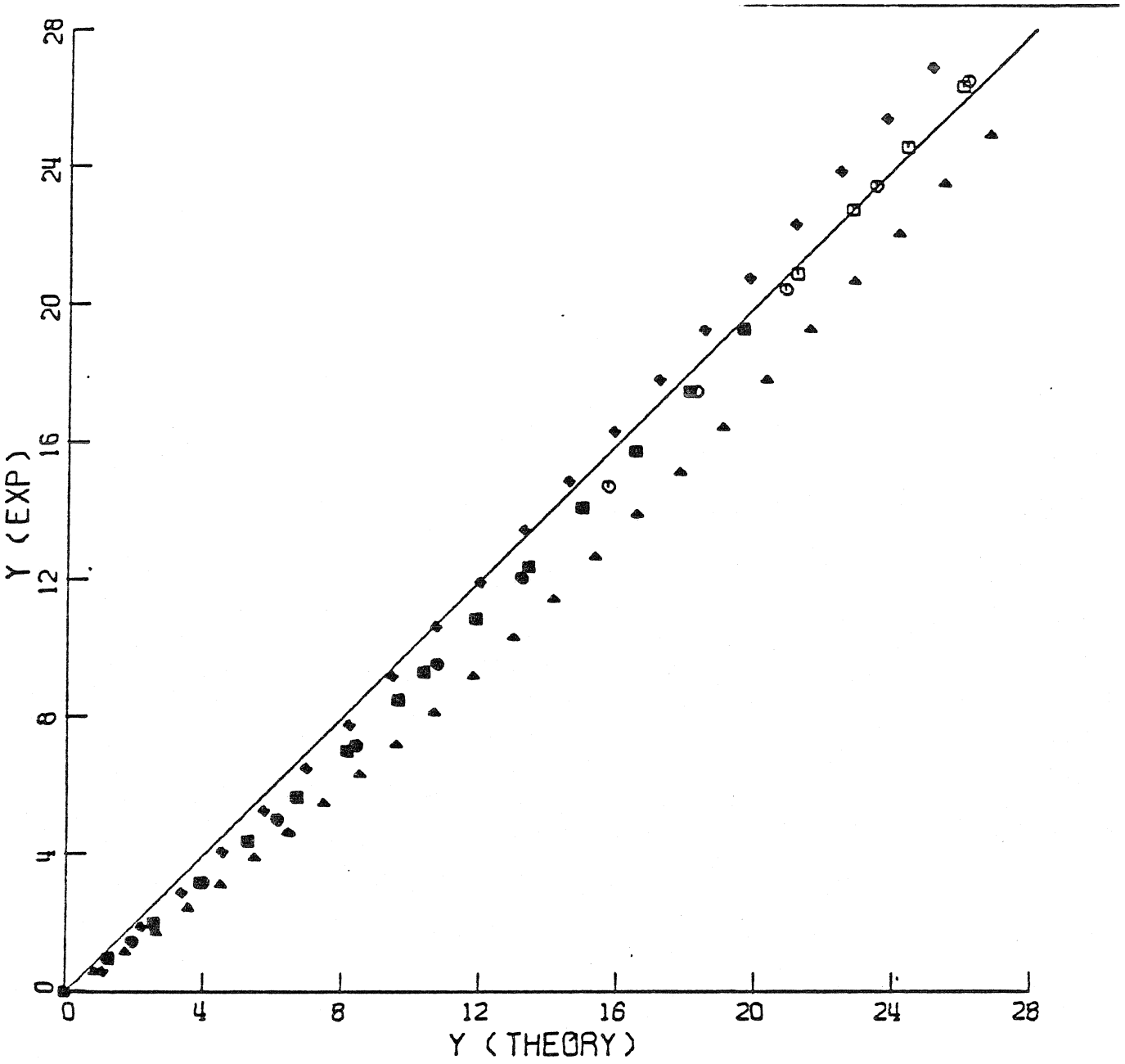

Figure 4.

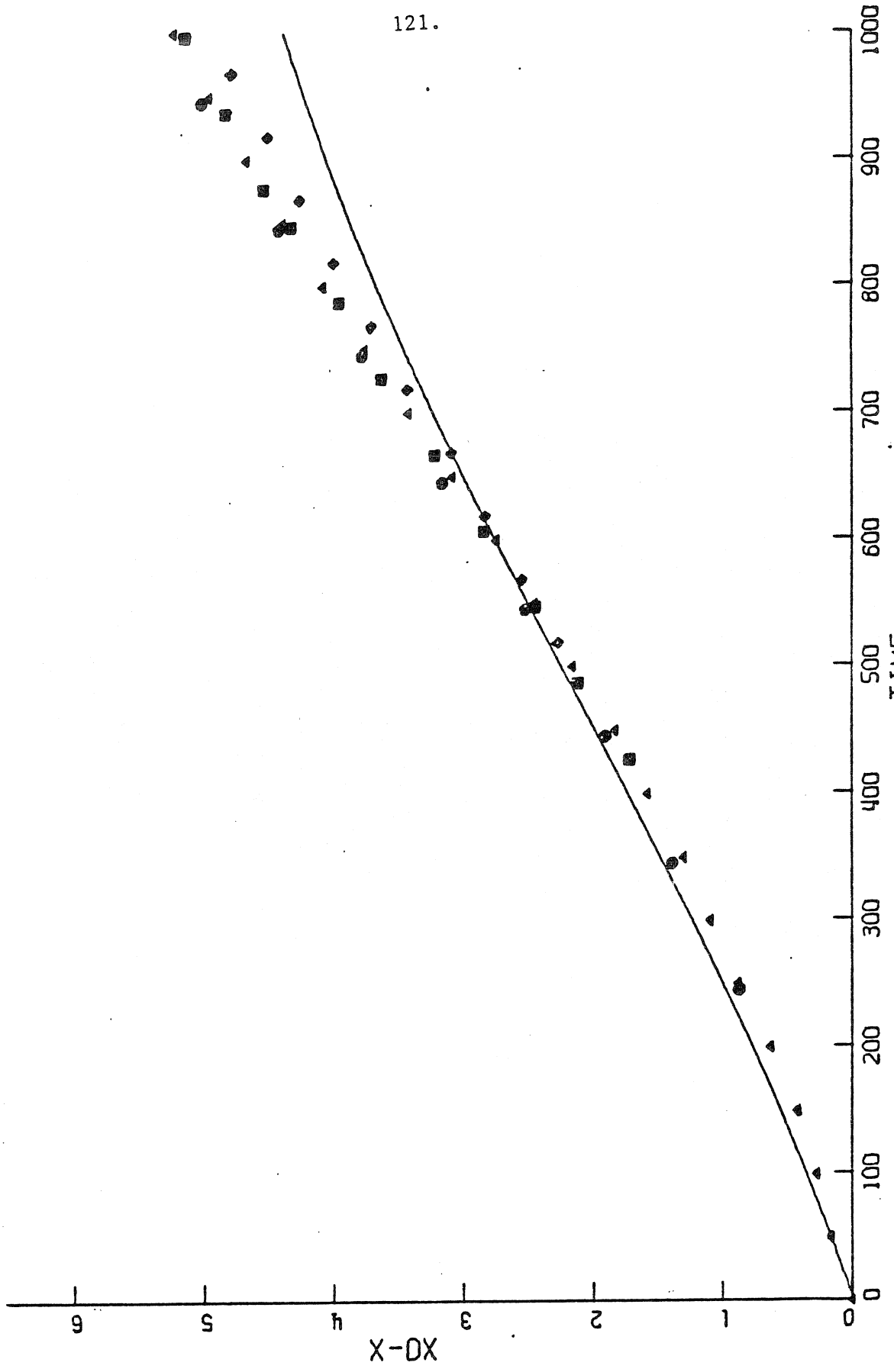

Figure 5.

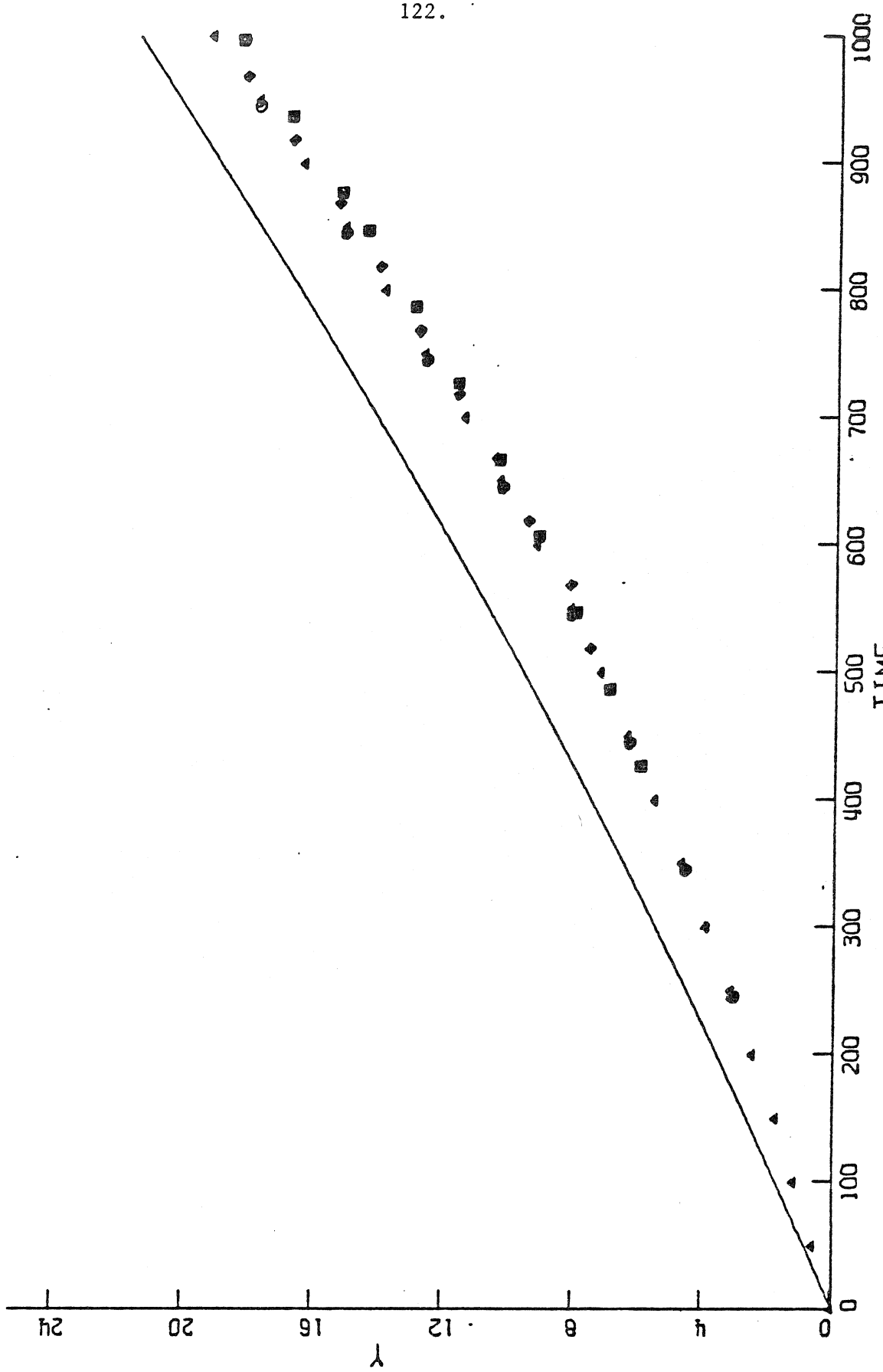

Figure 6.

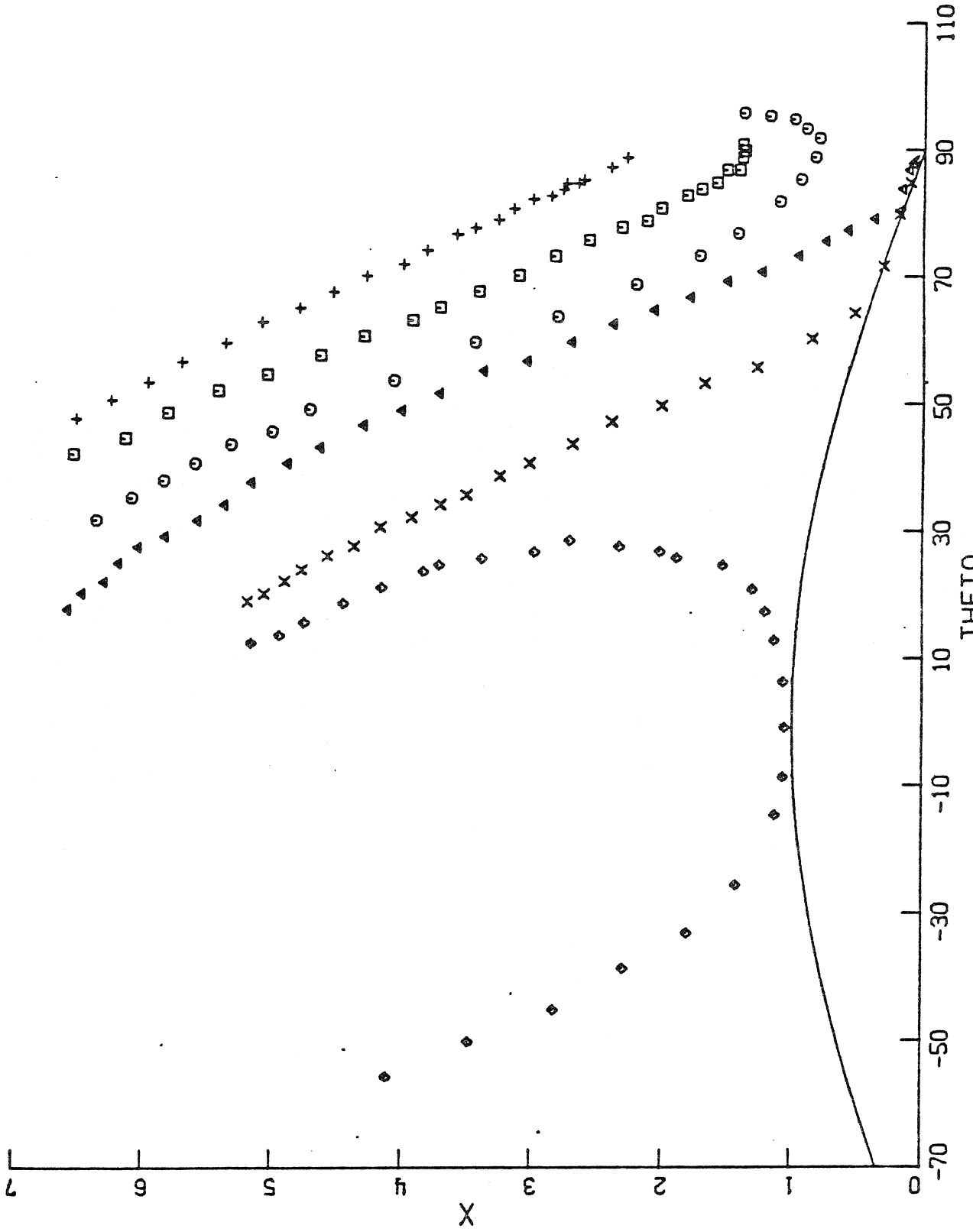

Figure 7.

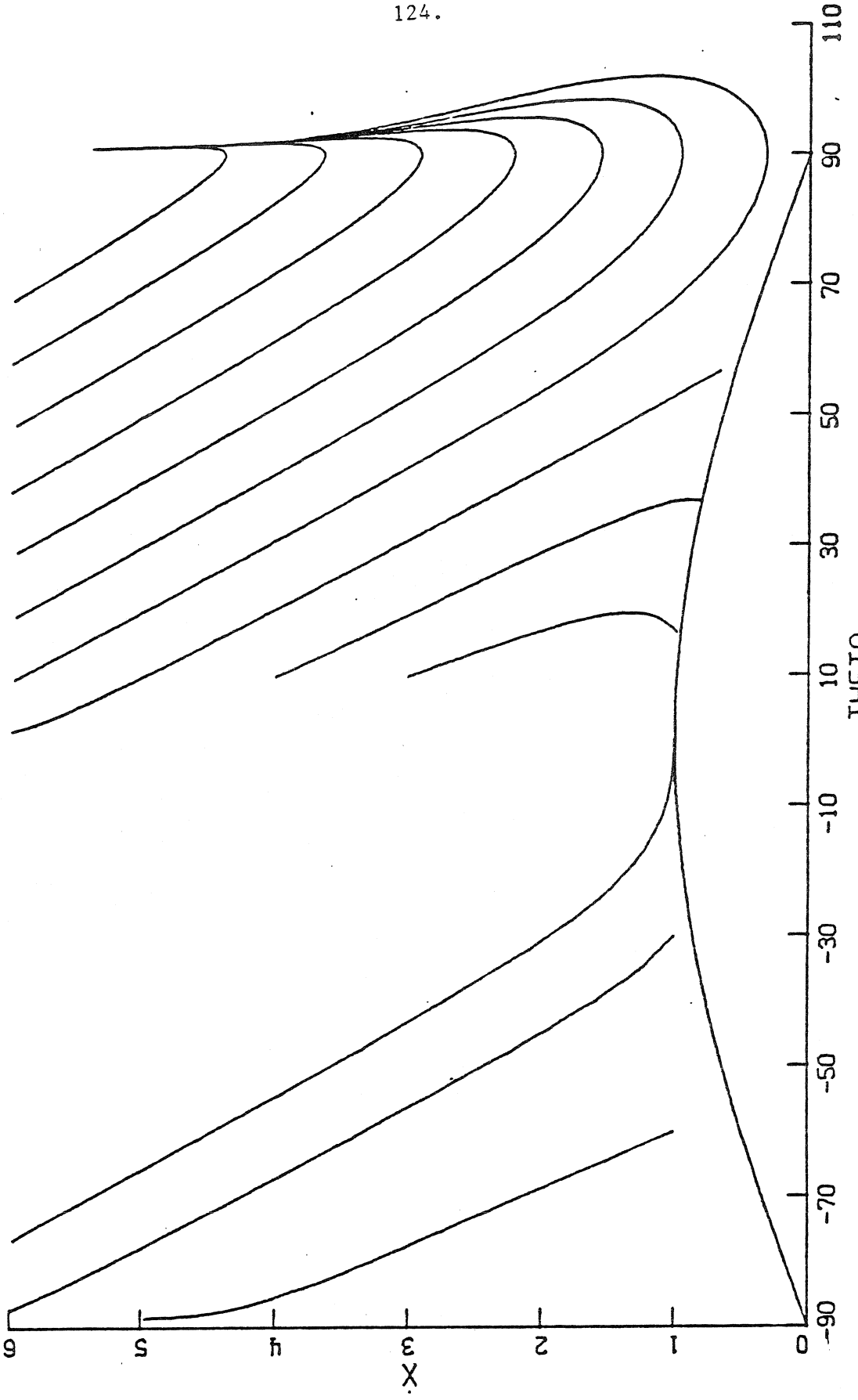

Figure 8.

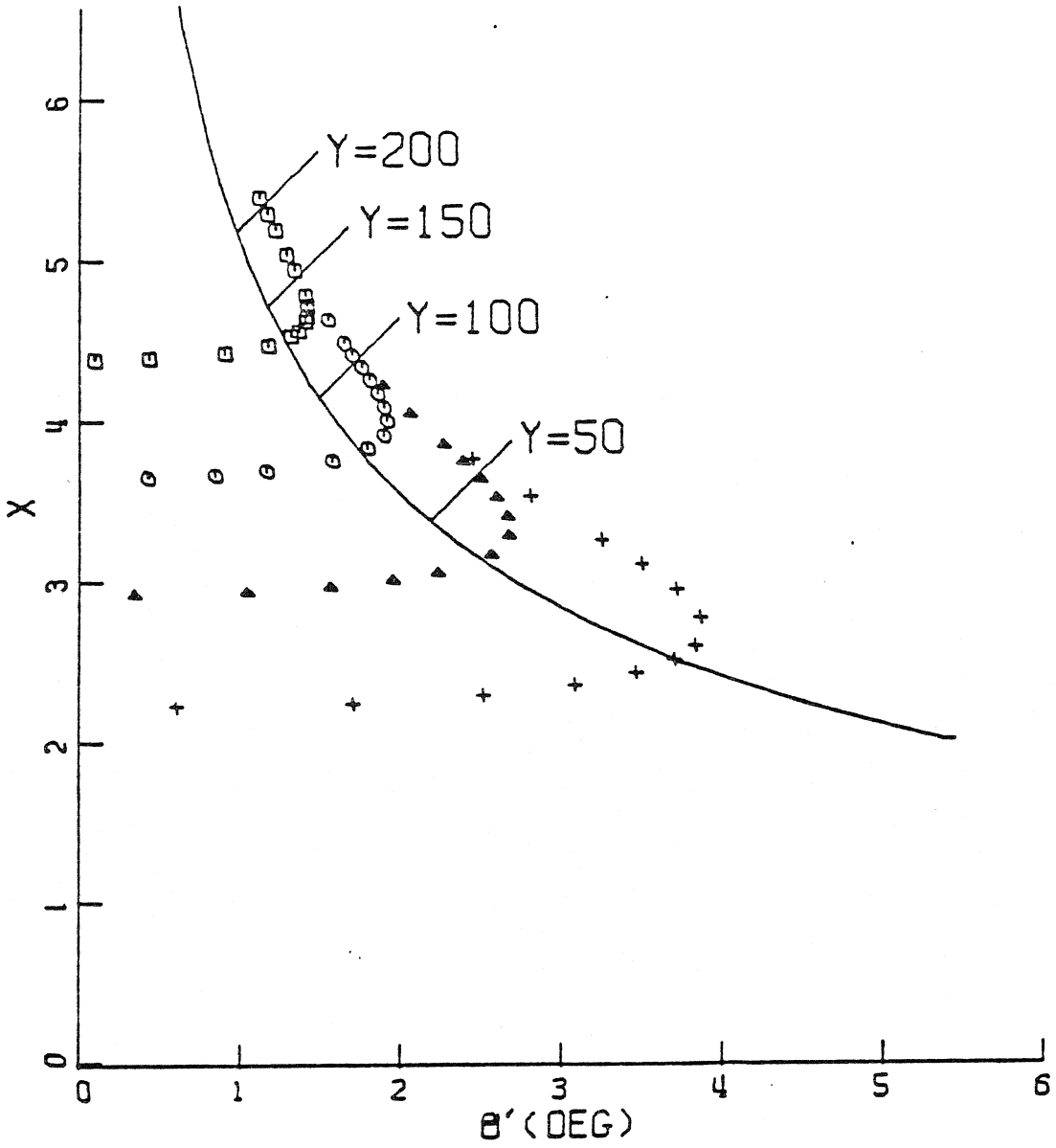

Figure 9.

This appendix consists of a paper that appeared in the Journal of Fluid Mechanics (1977).

J. Fluid Mech. (1977), *vol.* 83, *part* 2, *pp.* 273–287
Printed in Great Britain

Rods falling near a vertical wall

By W. B. RUSSEL,
Department of Chemical Engineering, Princeton University, Princeton, New Jersey 08540

E. J. HINCH,
Department of Applied Mathematics and Theoretical Physics, University of Cambridge

L. G. LEAL AND G. TIEFFENBRUCK
Chemical Engineering, California Institute of Technology, Pasadena

(Received 1 November 1976 and in revised form 3 May 1977)

As an inclined rod sediments in an unbounded viscous fluid it will drift horizontally but will not rotate. When it approaches a vertical wall, the rod rotates and so turns away from the wall. Illustrative experiments and a slender-body theory of this phenomenon are presented. In an incidental study the friction coefficients for an isolated rod are found by numerical solution of the slender-body integral equation. These friction coefficients are compared with the asymptotic results of Batchelor (1970) and the numerical results of Youngren & Acrivos (1975), who did not make a slender-body approximation.

1. Introduction

Sedimentation of a sphere through a Newtonian liquid in the absence of inertia is straightforward. In an unbounded fluid the sphere does not rotate and falls in the direction of gravity. The proximity of a vertical wall induces rotation about a horizontal axis parallel to the surface but causes no drift. This well-known behaviour follows from the linearity of the Stokes equations and the symmetry of the geometry.

With rodlike particles a more interesting behaviour can be observed. Taylor(1969) and others have demonstrated that the sedimentation rate of a rod depends on its orientation: a slender cylinder falls approximately twice as fast when it is vertical as it does when it is horizontal. Consequently a rod will drift laterally at intermediate orientations. The absence of rotation, however, again follows from reversibility.

In a tall container the horizontal drift must eventually bring the particle close to a side boundary. Since Batchelor (1970) has demonstrated that the far-field disturbance generated by a rod resembles that of the sphere which encloses it, one might expect interaction with a side to induce rotation. Indeed, this can be observed and is predicted by the far-field analysis of Caswell (1970). Unlike the case of a sphere, however, both the magnitude and the sign of the angular velocity depend on the orientation. According to Caswell's analysis, approach normal to the wall at an inclination of less than 45° to the vertical initially induces a negative angular velocity, i.e. the leading end rotates away from the wall, while at larger angles a positive rotation results. Thus two modes of interaction are suggested (figure 1). A rod approaching at a small angle turns

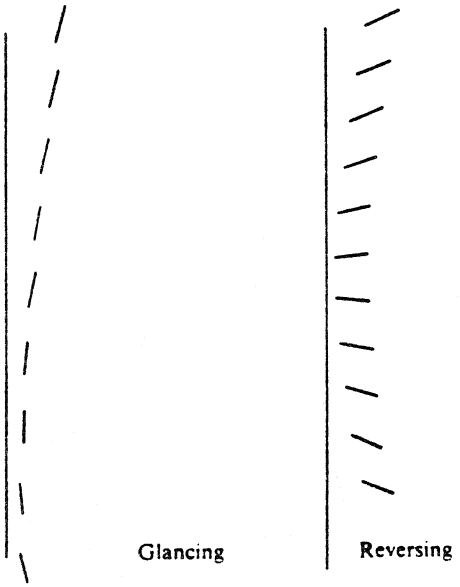

FIGURE 1. Glancing and reversing turns of a sedimenting rod, as predicted by the asymptotic theory of §2, with $\kappa = \frac{1}{60}$. The glancing turn starts from $\theta = 20°$ when $X = 3$ and the reversing turn starts from $\theta = 70°$ when $X = 3$. The rods are shown at time intervals of $4\pi\mu l^3/F_0$.

smoothly through the vertical and drifts away with the same end leading, a 'glancing' turn. At orientations closer to the horizontal the wall primarily retards the near end of the rod, causing it to pivot and then move away with the opposite end leading, a 'reversing' turn. While the far-field analysis indicates the orientation of approach separating the two modes to be 45°, we shall see that terms which have been neglected decrease the critical orientation.

In a tall container there is the possibility of a small rod repeatedly being turned away from the sides before it reaches the bottom. In the case of two vertical sides, symmetry requires the rod to oscillate periodically and not to approach a terminal position or orientation. This effect would lead to a fairly uniform distribution of the rods in the interior of the container, so long as interactions between the rods can be neglected.

The following sections contain an analysis of the interaction between a slender circular cylinder and a single plane wall. We first formulate the problem in terms of slender-body theory and present an asymptotic solution for the instantaneous motion. Then an independent, and more accurate, numerical solution of the integral equations is discussed and the trajectories calculated by the two different approaches are compared. As an aside, numerical results for the friction coefficients of a slender particle in an infinite fluid are compared with the third-order asymptotic solutions of Batchelor (1970) and the non-slender-body results of Youngren & Acrivos (1975). Finally we describe some simple experiments which verify the main theoretical predictions.

2. Theory

Slender-body analysis

Within the past decade slender-body theory, originally proposed for potential flows, has been extensively developed to describe the translation and rotation of rodlike

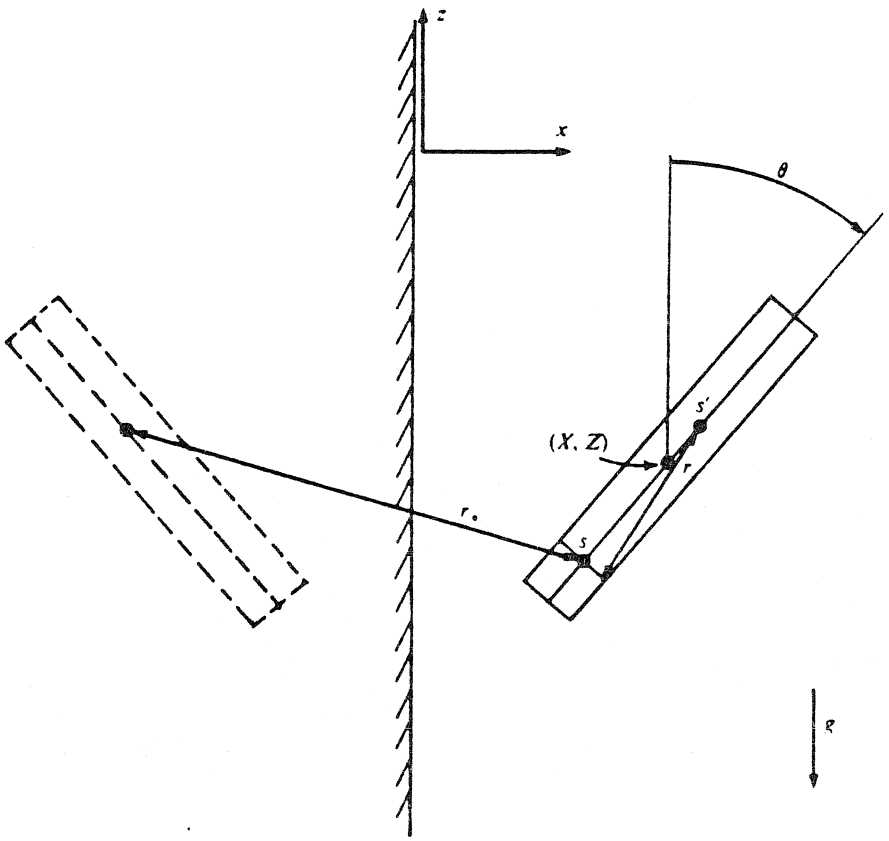

FIGURE 2. The co-ordinate system.

particles at low (zero) Reynolds number. The basic theory has been extended to include the effects of (i) blunt ends (Tuck 1964), (ii) centre-line curvature (Cox 1970), (iii) non-Newtonian suspending fluids (Leal 1975) and (iv) interactions with walls (Blake 1971). Here we use the last development to analyse the motion of a straight slender circular cylinder of radius R_0 and length $2l$ which is sedimenting through a viscous fluid in the vicinity of a plane wall. We assume that the plane of motion of the particle is perpendicular to the wall. Furthermore, end effects are ignored and attention is restricted to situations in which the cylinder is separated from the wall by a distance much greater than R_0. These simplifications retain most of the interesting physics governing the particle trajectory while making the analysis tractable.

The essence of slender-body theory lies in an approximate representation of the body's effect on the fluid by a distribution of singularities (i.e. point forces, force doublets and source doublets) along its axis. The nature and strength of these singularities are adjusted so that the disturbance flow cancels the applied flow at the particle surface, i.e. there is no slip. If a plane wall is present, an additional set of singularities must be distributed along the axis of the body's image in order to achieve no slip on the wall. The image system for a point force near a plane wall was obtained by Blake (1971). He found it to be a point force of equal magnitude but opposite sign plus a force doublet and a source doublet. These results suffice for our problem.

The co-ordinate system used is illustrated in figure 2, which also serves to define

certain other variables that appear in the theory. The midpoint of the particle is denoted by (X, Z) and its angle of inclination to the vertical by θ. The variables s and s' both specify the position of points on the particle axis relative to its midpoint. The distance between s' and a point on the particle surface at s is denoted by r, while the distance between s and the *image* of s' is denoted by r_*. For convenience, we scale all position and distance variables with respect to l. With these conventions, the two significant disturbance velocities at the cylinder surface are

$$u_x(s) = \frac{1}{8\pi\mu}\int_{-1}^{1}\left\{F_x(s')\left[\frac{1}{r}+\frac{(s-s')^2\sin^2\theta+\frac{1}{2}\kappa^2\cos^2\theta}{r^3}-\frac{1}{r_*}-\frac{r_*^2(x^2+x'^2)+6xx'(x+x')^2}{r_*^5}\right]\right.$$
$$\left.+F_z(s')\cos\theta\left[\sin\theta\,\frac{(s-s')^2-\frac{1}{2}\kappa^2}{r^3}-(s-s')\frac{r_*^2(s+s')\sin\theta-6xx'(x+x')}{r_*^5}\right]\right\}ds', \quad (1a)$$

$$u_z(s) = \frac{1}{8\pi\mu}\int_{-1}^{1}\left\{F_x(s')\cos\theta\left[\sin\theta\,\frac{(s-s')^2-\frac{1}{2}\kappa^2}{r^3}+(s-s')\frac{r_*^2(x-x')-6xx'(x+x')}{r_*^5}\right]\right.$$
$$\left.+F_z(s')\left[\frac{1}{r}+\frac{(s-s')^2\cos^2\theta+\frac{1}{2}\kappa^2\sin^2\theta}{r^3}-\frac{1}{r_*}-\frac{(s-s')^2(r_*^2-6xx')\cos^2\theta+2r_*^2xx'}{r_5^*}\right]\right\}ds', \quad (1b)$$

where $\kappa = R_0/l$ is the aspect ratio and

$$x = X+s\sin\theta, \quad x' = X+s'\sin\theta,$$
$$r^2 = (s-s')^2+\kappa^2, \quad r_*^2 = (s-s')^2+4X^2+4\sin\theta(sX+s'x).$$

The fluid motion normal to the plane of figure 2 is $O(\kappa)$ and therefore negligible. The appropriate image singularities have been included in (1), so that the boundary condition on the wall is automatically satisfied.

The integral equations (1) are solved by choosing the force distributions $F_x(s)$ and $F_z(s)$ in such a way that the disturbance velocities are of the form of a rigid-body motion:

$$u_x(s) = U_x+\Omega ls\cos\theta, \quad u_z(s) = U_z-\Omega ls\sin\theta. \quad (2)$$

The translational velocity of the rod (U_x, U_z) and its angular velocity Ω are determined by the conditions of constant force and zero couple on the particle:

$$\left.\begin{aligned}\int_{-1}^{1}F_x(s)\,ds = 0, \quad \int_{-1}^{1}F_z(s)\,ds = -F_0/l\\ \text{and}\qquad \int_{-1}^{1}[F_x(s)\cos\theta-F_z(s)\sin\theta]\,s\,ds = 0.\end{aligned}\right\} \quad (3)$$

In the following section, numerical solutions will be presented for the integral equations (1) subject to the side conditions (2) and (3); here we develop an asymptotic solution for the limit $\epsilon = 1/\ln(2/\kappa) \ll 1$.

The asymptotic analysis capitalizes on the quasi-local nature of the slender-body theory; i.e. the fact that the induced velocity at the cylinder's surface primarily depends on the force density at the nearest axial point, as long as the force density varies on a length scale of 1 and not κ. From (1) we have (Batchelor 1970)

$$\left.\begin{aligned}u_x(s) &= (4\pi\mu\epsilon)^{-1}[(1+\sin^2\theta)\,F_x(s)+\sin\theta\cos\theta\,F_z(s)]+\epsilon r_x,\\ u_z(s) &= (4\pi\mu\epsilon)^{-1}[\sin\theta\cos\theta\,F_x(s)+(1+\cos^2\theta)\,F_z(s)]+\epsilon r_z,\end{aligned}\right\} \quad (4)$$

where the correction terms v_x and v_z vary with s and are not local. Even when the rod is very near to the wall, i.e. $\theta \sim 0$, $X \ll 1$ and $X/\kappa \gg 1$, de Mestre & Russel (1975) showed that the local nature is preserved with $\epsilon = 1/\ln(2/\kappa)$ in (4) being replaced by $1/\ln(2X/\kappa)$, but for simplicity we suppress this extension by assuming that κ is very much smaller than X. In order to make the disturbance velocities in (4) vary linearly with s as required by (2), we must clearly choose, at lowest order, force distributions which vary linearly with s. The only such force distribution consistent with (3) is

$$F_x = O(\epsilon F_0/l), \quad F_z = -\tfrac{1}{2}F_0/l, \tag{5}$$

which results in

$$U_x \sim -\frac{\sin\theta\cos\theta}{8\pi\mu l\epsilon}F_0, \quad U_z \sim \frac{1+\sin^2\theta}{8\pi\mu l\epsilon}F_0, \quad \Omega = O\left(\frac{F_0}{\mu l^2}\right). \tag{6}$$

Substituting the first approximation to the force distribution (5) into the integral equation (1) yields the correction terms v_x and v_z in (4). The force distributions are then adjusted locally to cancel these corrections. The constraints (3), however, do not permit these adjustments to the force distributions to contain a part which varies linearly with s. The parts of v_x and v_z which vary linearly with s are balanced by adjustments to the translational and rotational velocities U_x, U_z and Ω. Thus we find

$$U_x = -\frac{\sin\theta\cos\theta}{8\pi\mu l\epsilon}F_0 + \frac{\epsilon}{2}\int_{-1}^{1} v_x(s)\,ds, \tag{7a}$$

$$U_z = -\frac{1+\sin^2\theta}{8\pi\mu l\epsilon}F_0 + \frac{\epsilon}{2}\int_{-1}^{1} v_z(s)\,ds \tag{7b}$$

and

$$\Omega = \frac{3\epsilon}{2l}\int_{-1}^{1}[v_x\cos\theta - v_z\sin\theta]\,s\,ds. \tag{7c}$$

After much algebra, evaluating v_x and v_z in (4) and substituting into (7), we find the analytic expression for the angular velocity:

$$\Omega = \frac{3F_0}{32\pi\mu l^2}\left\{2XI_0S^2 + I_1S(1+4S^2) + 2X(2+3S^2-4S^4)\frac{(X^2+C^2)^{\frac{1}{2}}-X}{C^2} - 2S^2(1+4S^2)\right.$$
$$\left. - \frac{2X}{(X^2+C^2)^{\frac{1}{2}}} + L_1S[X^2(1+4S^2) - S^2(3-4S^2)] - L_2XS^2(1-4S^2)\right\}[1+O(\epsilon)], \tag{8}$$

where

$$S = \sin\theta, \quad C = \cos\theta, \quad I_n = \int_{-1}^{1} s^n \ln(R_+/R_-)\,ds, \quad L_1 = \ln\frac{1+S^2}{A_+ - A_-}, \quad L_2 = \frac{A_+}{A_-},$$

$$R_\pm = \{s^2 + 2[2XSF(1-2S^2)]s + 1 + 4X^2 \pm 4XS\}^{\frac{1}{2}} \pm 1 + 2XS - s(1-2S^2),$$

$$A_\pm = [(X^2+C^2)^{\frac{1}{2}} + XS \pm C^2]/(XFS).$$

Corresponding equations for the translational velocity components can also be obtained. However, the resultant expressions have not been integrated analytically because of their complexity. Instead, for trajectory calculations, we have used the velocities (6*a*, *b*) without wall effects. As illustrated by the numerical computations which follow, the dominant error in these approximations lies in the $O(\epsilon)$ and higher corrections to the resistance coefficient rather than the $O(\epsilon/\ln X)$ wall effect. We note that the shape of the slender body does not enter the asymptotic theory at the level of approximation in (8). Thus, although we have worked with a circular cylinder for

simplicity, (8) is applicable to any slender body. In view of its algebraic complexity, we have checked (8) against the theory of de Mestre & Russel (1975) for $\theta = 0$ and $\frac{1}{2}\pi$ and against numerical evaluations of (6*a*). Furthermore, we have confirmed that $\Omega \to 0$ as $X \to \infty$ as expected.

Numerical solution of the integral equation

Slender bodies can be easily constructed with κ sufficiently small for little error to be expected in the predictions of the integral equations resulting from (1). The asymptotic solution (6*a*, *b*) and (8) of the integral equations, however, has a more limited application because particles rarely have $\epsilon = 1/\ln(2/\kappa)$ small. For example, in the experiment described in §3 the particles have $\kappa = \frac{1}{60}$ and $\epsilon = 0{\cdot}209$. A numerical solution of the integral equations was therefore sought to make reasonable predictions for these particles.

The integral equations from the slender-body theory were discretized by dividing the rod into N segments of equal length. Within each segment the Stokeslet force distribution was assumed to have a constant value, introducing $2N$ unknowns, and the integral was evaluated at the centre of each segment, providing $2N$ equations. Care is needed in integrating the kernel function. While the part of the kernel arising from the images in the wall is adequately treated by the trapezoidal rule using the two end points of the segment, such a treatment of the remaining, non-image part of the kernel would result in large, $O(1/\ln N)$ truncation errors. This part was integrated analytically and the resulting analytic expressions rearranged to avoid the numerical subtraction of nearly equal large numbers. The discrete form of the integral equation was thus $2N$ linear equations for the velocity distribution in terms of the $2N$ values of the Stokeslet distribution. While no elements of the coupling matrix vanish, the diagonal is fairly strong, reflecting the singular nature of the integral equation at small κ. A Gauss–Seidel iterative procedure was therefore adopted to solve for the Stokeslet distribution. The iteration was started from the lowest-order asymptotic result and usually converged to an r.m.s. error of 10^{-4} in less than seven iterations. When time stepping the configuration, the iteration was started with the converged result from the previous time step and often required only a single iteration. To avoid systematic errors, the iterative sweep was started from alternate ends at each time step.

To determine the motion of the rod near the wall, three integral equations were solved for each configuration, corresponding to the three velocity distributions for translation of the rod at unit velocity parallel and perpendicular to the wall and for rotation at unit angular velocity. For each velocity distribution, the net force and couple acting on the rod were evaluated from the Stokeslet distributions and the correct linear combination chosen so that the couple vanished and the net force was unity parallel to the wall. This translation and rotation were finally used in a fourth-order Runge–Kutta time-stepping procedure to calculate the next configuration. A step size for which the rod fell through its own length in two time increments generally produced an accuracy of better than 10^{-3}. Smaller time steps are necessary very near the wall, so automatic interval halving was used.

To assess the accuracy of the numerical solution of the integral equation, several studies were performed without the images in the wall. The motion of a rod in an unbounded fluid has received considerable attention and Batchelor's (1970) third-order asymptotic theory is available for comparison. First the effect of increasing N on

the numerical representation of the Stokeslet distribution was studied for perpendicular translation and $\kappa = \frac{1}{60}$. The general shape of the distribution does not change for $N = 3, 7, 15$ and 31 (at which the centre of the end segment is within one radius of the end). Except for the end segments, where the distribution sharply rose by 60%, the predicted values of the force distribution differed by less than $\frac{1}{2}$%. Varying the length of the numerical segment or subtracting a special analytic end correction might have improved the representation.

The main side study evaluated the various friction coefficients for a free circular cylinder as predicted by the slender-body integral equation. The net forces $\mathscr{F}_1$ and $\mathscr{F}_2$ on a rod translating parallel and perpendicular to itself, respectively, were calculated together with the couple $\mathscr{L}_2$ on a rod rotating about an axis perpendicular to itself and the stresslet $\mathscr{S}_{11}$ when the rod is placed in a pure axially symmetric straining motion. At fixed κ these friction coefficients varied little with N, and the error scaled on $\ln N/N$, as expected from the poor representation of the end regions. For the rotation, the most sensitive of the three coefficients involved in the wall interactions, the result at $\kappa = \frac{1}{60}$ for $N = 10$ had a 7% error and that for $N = 28$ a $3\frac{1}{2}$% error. The results for the friction coefficients extrapolated to $N = \infty$ are shown in figure 3, normalized by the first-order asymptotic prediction.

Also shown in figure 3 are Batchelor's (1970) third-order asymptotic results [his equations (8.11)–(8.14)]. At $\kappa = \frac{1}{60}$ the first-order asymptotic results are poor, with the stresslet out by a factor of two. The third-order theory narrows this gap to 13%.

In the case of $\mathscr{F}_1$ and $\mathscr{L}_2$ we have in addition been able to compare our results with those of Youngren & Acrivos (1975). They solved numerically the integral equation for Stokeslet singularities distributed on the surface of the rod including the ends, and thereby made no slender-body approximation. Our slender-body numerical results for $\mathscr{F}_1$ tend quickly to the full numerical results, with an error of $0{\cdot}4\kappa$ coming from the ends. The agreement for $\mathscr{L}_2$ is not so good, with a 5% difference between the two results at $\kappa = \frac{1}{20}$. (Note that in their table 4 Youngren & Acrivos give the couples multiplied by a factor of 8.) It is not clear whether the discrepancy is due to the slender-body approximation or whether the numerical results are inaccurate at large aspect ratio.

Results

The equations of motion for a rod moving near a wall have been integrated numerically as outlined in the previous subsection. Figure 1 shows the two possible ways in which the rod can turn. Those rods which start far from the wall at an initial inclination to the vertical greater than 67° turn such that they are horizontal at closest approach, while those starting with an initial inclination less than 27° are vertical at their nearest point. Each of the two turns is symmetric under time reversals, so that after the turn the particles tend to the initial inclination to the horizontal but with the opposite sign. Between 27° and 67° the slender-body theory predicts a collision with the wall, although the analysis breaks down for separations less than a diameter. The neglected end effects then become very large and stop the rod from touching the wall. Simple lubrication considerations presented in the appendix suggest that these effects will immobilize the end, causing the rod to pivot through a horizontal position, although this behaviour is not entirely confirmed by the experiments. A detailed analysis of such collisions is complicated by their sensitivity to the precise shape of the end of the rod, with a possibility that the symmetry of the turn would be lost for imperfect ends.

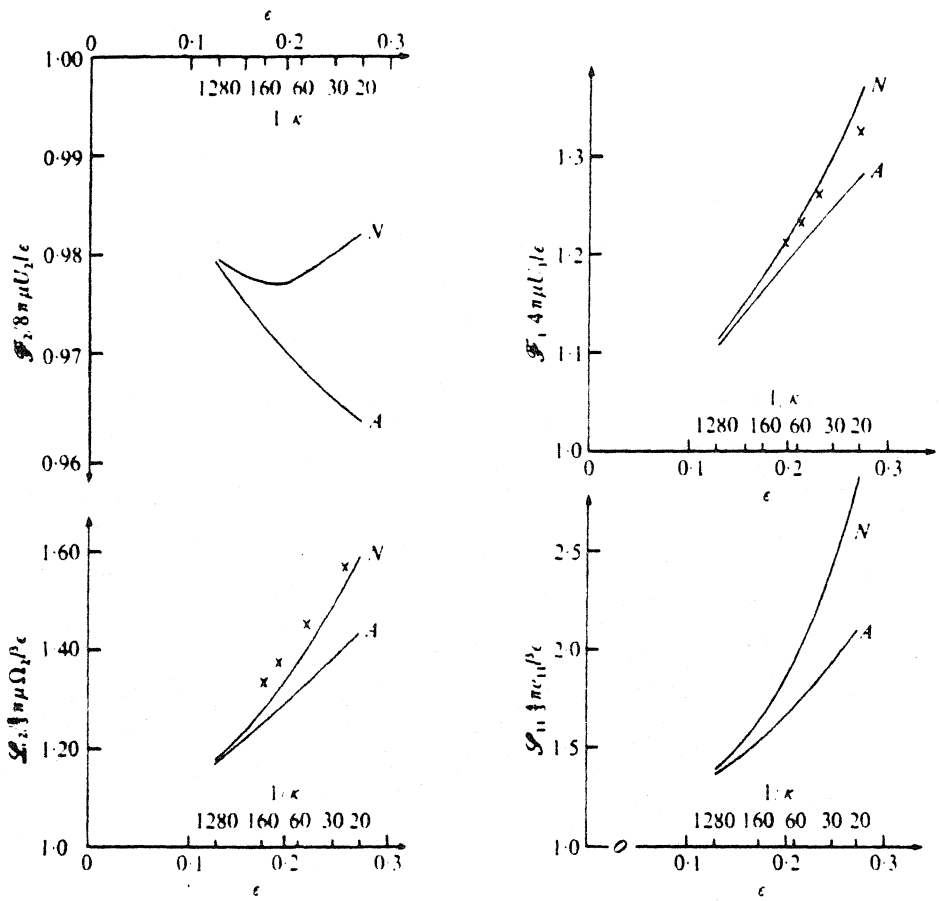

FIGURE 3. The friction coefficients for slender circular cylinders for perpendicular ($\mathscr{F}_2$) and parallel ($\mathscr{F}_1$) translation, for rotation about an axis perpendicular to the cylinder ($\mathscr{L}_2$) and for pure straining motion in the direction of the cylinder ($\mathscr{S}_{11}$). Our numerical results (N) are compared with Batchelor's third-order asymptotic results (A) and the full numerical results of Youngren & Acrivos (crosses).

In figure 1 the vertical length scale is seen to be large: the rod falls much faster than it moves sideways or rotates. This is particularly evident for the near-vertical glancing turns. An alternative presentation of the results is given in figure 4, where the trajectory is plotted as the inclination from the vertical θ *vs.* the distance X from the wall to the centre of the rod. Markers at equal time separations ($8\pi\mu l^2/F_0$) are placed along the trajectories. The shaded region denotes the forbidden configurations in which some part of the rod lies within the wall. The trajectories terminating in this region indicate collisions with the wall at finite orientations, even with very fine numerical resolution. Most trajectories show little rotation one particle length from the wall. Rods approaching at 45°, for which the angular velocity vanishes in the far-field analysis of Caswell (1970), rotate through less than 1° before approaching within one quarter of their length from the wall and rotate through only 5° before colliding with the wall. The exceptions are particles which turn at a large distance from the wall. These start near the horizontal or vertical and turn slowly, therefore falling through a large vertical distance before completing the turn.

The full curves in figure 4 are based on the numerical solution of the integral equa-

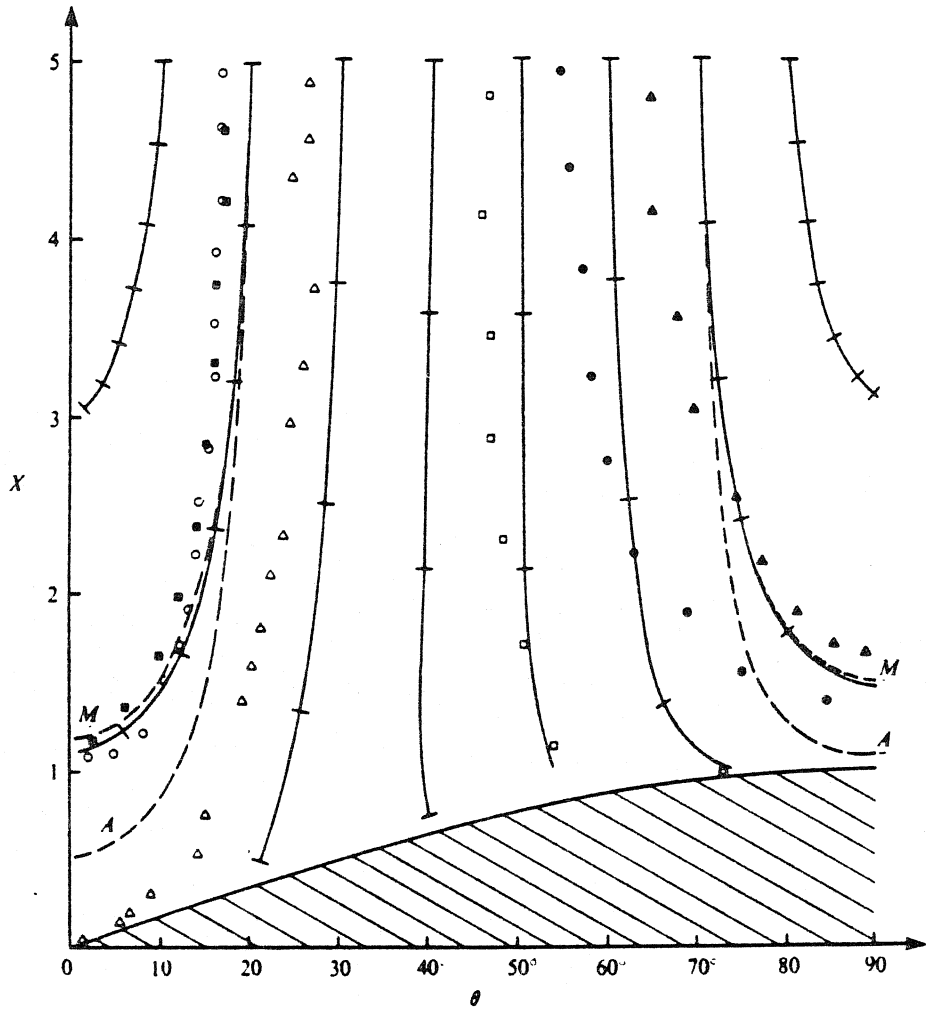

FIGURE 4. The variation of the distance from the wall and the orientation of the rods as they turn. Numerical solution of the integral equation yields the solid curves, which are marked at time intervals of $8\pi\mu l^3/F_0$. The dashed curves labelled A are trajectories for 20° and 70° obtained from (6*a*, *b*) and (8). The dashed curves labelled M use the modified friction coefficients of figure 3. Experimental data points: ▲, θ_∞ = 65°; ●, θ_∞ = 54°; □, θ_∞ = 47°; △, θ_∞ = 27°; ○, θ_∞ = 17° (run 1); ■, θ_∞ = 17° (run 2).

tions. The results from the first-order asymptotic solution of the integral equations are also plotted as dashed curves labelled A for the 20° and 70° trajectories. This asymptotic theory underestimates the drag on the rods, allowing them to come much closer to the wall; indeed, the band of initial angles leading to collisions widens to 23°-69°. Because most of the error in the asymptotic theory comes from the poor friction coefficients for translation, a modified theory was developed in which the numerically evaluated friction coefficients replace the asymptotic ones but the angular velocity remains that of the first-order asymptotic theory. The resulting trajectories for this modified theory, plotted as dashed curves labelled M, lie very near the full numerical curves and demand somewhat less computer time. The success of the modified theory indicates that the wall has little effect on the translational velocity of the rods.

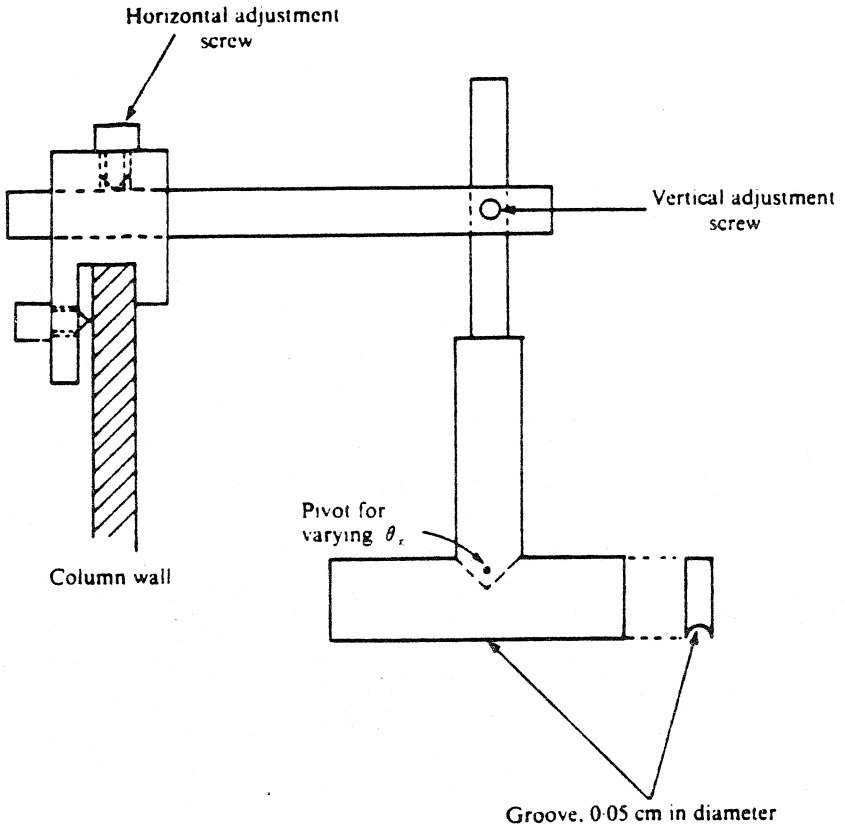

FIGURE 5. The particle release mechanism. Not drawn to scale.

3. Experiment

Apparatus and procedure

The experiments were conducted in a Plexiglas tank with a 2 ft by 2 ft cross-section and a height of 5 ft. The tank was placed on a stand which was adjusted so that the walls were vertical.

The particles were made from aluminium screen wires. These wires were placed between two smooth flat stainless-steel plates and then rolled to a nominal diameter of 0·0254 cm. The aspect ratio $1/\kappa = l/R_0$ of the particles ranged from 59 to 69. A qualitative check with a microscope showed the particles to be straight and of constant radius. The particles were in addition shiny, which made them well suited for photographic study, and light, with a measured density of 2·36 g/cm^3.

The liquid used was a white mineral oil supplied by Standard Oil Co. of California. This liquid is colourless and clear, ideally suited for a photographic study. At 22·2 °C, the density of the liquid is 0·88 g/cm^3 and its viscosity is 170 cP.

In order that the experiment can be compared with the theory it is important to release the particle in a way which does not cause it to turn out of the plane perpendicular to the wall, or cause a significant disturbance in the surrounding fluid. The release mechanism which we used is shown in figure 5. Its significant feature is the thin metal plate with a groove 0·05 cm in diameter in the bottom edge. Just prior to starting the experiment, the groove is wetted with the liquid being used. The slender

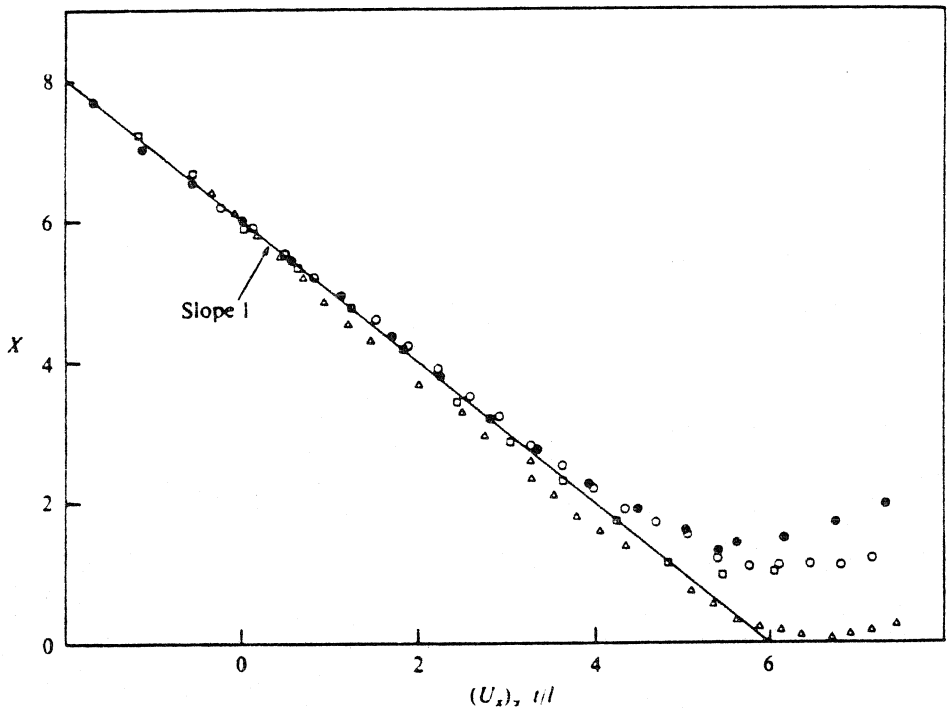

FIGURE 6. Distance between the particle centre and the wall as a function of time. ●, $\theta_z = 54°$; □, $\theta_z = 47°$; △, $\theta_z = 27°$; ○, $\theta_z = 17°$.

body is then carefully placed in the groove. When the plate is submerged in the liquid, the slender body slowly slides out of the groove. The plate can be adjusted such that the particle is released in the proper plane. We found that this system successfully launched about 80% of the particles.

The motion of the particles was recorded on 16 mm cine film with a Bolex camera. The camera was mounted on a counterweighted platform which could be moved up or down at a variable, but controlled speed. The particle was thus tracked during its entire fall, and a continuous film obtained of its trajectory. Quantitative measurements were made from the film using a microfilm reader. Vertical position was measured from image lines on the back of the tank. Horizontal position was determined using a photograph of a ruler taken prior to the experiments. A typical run lasted 5 min, during which thirty frames would be taken at constant intervals.

Results

The purpose of the experiments was to verify, at least qualitatively, the theory described in §2. Thus measurements were made of the position of the particle centre and the particle orientation as functions of time for various initial inclinations ranging from 17° to 65°. We present data here for the five representative cases $\theta_z = 17°$ (two sets), 27°, 47°, 54° and 65°, which include one 'glancing' turn (17°), two 'reversing' turns (54° and 65°), one 'colliding' turn (47°), and one turn just on the border between 'glancing' and 'colliding' (27°). Plots showing horizontal and vertical position as a function of time for initial inclinations of 17°, 27°, 47° and 54° are given in figures 6

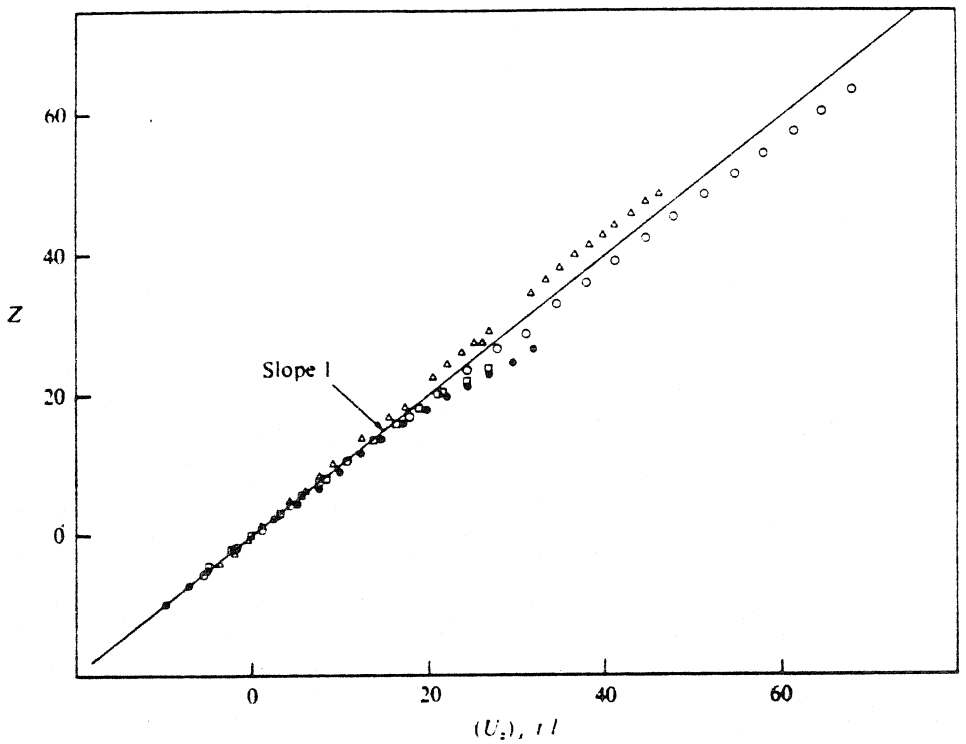

FIGURE 7. Vertical displacement of the particle centre as a function of time. ●, $\theta_\infty = 54°$; □, $\theta_\infty = 47°$; △, $\theta_\infty = 27°$; ○, $\theta_\infty = 17°$.

and 7. The measured angle of inclination as a function of horizontal position for all five initial angles has been superimposed on figure 4, where it may be directly compared with the theoretical results. An indication of the degree of reproducibility of the data is provided by the two independent sets of data for $\theta_\infty = 17°$ in figure 4. We shall discuss figures 4, 6 and 7 in detail shortly.

First, it is useful to consider the motion of the particle when it is far from the wall. All of the experiments were started with the separation between the particle and the wall sufficiently large that the sedimentation rate was constant and the particle rotation nil. The existence of such a regime suggests strongly that both inertia and end effects of the top and bottom of the tank have a negligible influence on the particle motion. For, if inertia or end effects were significant, the particle would rotate and translate with a velocity which varies with time. The absence of a measureable inertia effect is important since the Reynolds numbers based on the observed velocities show values as large as 0·1. A further check on the importance of inertia or end effects is provided by a comparison between the measured velocities and theoretical values corresponding to the drag coefficients of figure 3. The horizontal and vertical velocity components are listed in table 1. The two sets of values are in good agreement, thus confirming the lack of significant inertia or end effects. A final demonstration, which also illustrates a degree of self-consistency in the data, is the fact that the vertical and horizontal positions, plotted *vs.* time in the manner of figures 6 and 7, collapse onto universal curves when the particles are far from the wall.

Turning to the regime of wall interactions, it is clear from figure 4 that the observa

	Experimental		Theoretical	
θ_∞	U_z	U_x	U_z	U_x
56	0·206	0·0495	0·209	0·048
47	0·210	0·051	0·221	0·050
27	0·265	0·044	0·254	0·041
17	0·255	0·0275	0·265	0·028

TABLE 1. Particle velocities (cm/s).

tions and predictions are at least in qualitative accord. In particular, the 'glancing' and 'reversing' modes of interaction are both evident, the former for $\theta_\infty = 17°$ and the latter for $\theta_\infty = 54°$ and 65°. In addition, at intermediate angles, e.g. $\theta_\infty = 47°$, the particle appears, with the resolution available, to hit the boundary and then complete its rotation.† Even from a quantitative point of view, the two cases $\theta_\infty = 17°$ and $\theta_\infty = 27°$ are in excellent agreement with theory, certainly well within expectations given the approximations of the theory and uncertainties in the experimental data. The case $\theta_\infty = 27°$ appears to be close to the maximum angle for a 'glancing' turn, as the particle comes extremely close to touching the wall.

The three cases of larger initial inclination, $\theta_\infty = 47°$, 54° and 65°, in which the particle undergoes a 'reversing' turn, are in poorer agreement with the theory. In particular, the influence of the wall is felt at a much greater distance than that predicted. This is especially evident for $\theta_\infty = 54°$ and 65°, where the particle inclination is already changing when the centre is some 5 half-lengths from the wall. The horizontal velocity is less influenced, but it too begins to be affected by the wall at nearly 3 half-lengths separation distance. We may note that the end of the particle comes very close to touching the wall for $\theta_\infty = 47°$, as predicted by the slender-body theory, but apparently it does not make contact. The strongest evidence for no contact is that the particle continues to slide vertically down the wall, rather than pivoting about a fixed end.

Several other features of the observed particle motions are worth noting. First, the particle trajectories are reversible. We have only shown data corresponding to the approach to the boundary. However, complete symmetry was observed between the approach and retreat. This is true even for $\theta_\infty = 47°$, where the particle end is very close to the wall, thus providing further evidence that the particle and wall do not touch. Second, the angle of inclination appears more sensitive to the influence of the wall than any of the other variables. In particular, the plots of figures 6 and 7 show close agreement with predicted translational velocities in an infinite fluid, right down to one half-length separation between the wall and particle. Indeed, except for separations of one half-length or smaller, deviations from the infinite-fluid result are well within normal experimental error, and probably of little significance.

Clearly, most features of the motion of rod-like particles near a plane wall are correctly predicted by the slender-body analysis of §2. Some points of disagreement, for example the lack of contact between particle and wall for $\theta_\infty = 47°$, may result from end corrections neglected in the analysis. Other points of disagreement, however, are

† We shall discuss this last point in more detail later.

not so easily explained and thus require further study. Most important are the deviations between theory and experiment which are found at large distances when the initial inclination is large (i.e. $\theta_\infty = 54°$ and $65°$). At present, we see no obvious explanation for these differences either in the theory or in experiments.

L. G. Leal and G. Tieffenbruck wish to thank the National Science Foundation for its support of their participation in this work, through grant ENG 74-17590.

Appendix. A lubrication theory for a 'colliding' turn

The way in which lubrication forces acting on the end of the rod manage to stop it colliding with the wall makes an interesting study for the method of matched asymptotic expansions. Here we summarize the basic results. Time is non-dimensionalized by $4\pi\mu l/F_0$ and lengths remains non-dimensionalized by the half-length of the rod. For simplicity we assume that the rod has a spherical end of radius κR with R of order unity. Except for lubrication forces acting on the end, no interaction with the wall is included as appropriate at the lowest order of slender-body theory.

The standard expressions for the lubrication forces become applicable when the separation d between the rod and the wall is somewhat smaller than κ, i.e. the thickness of the rod. These lubrication forces do not affect the motion, however, until $d = O(\kappa^2 \ln \kappa)$, because the friction coefficient for the whole rod is $1/\kappa \ln \kappa$ larger than that for the small end. Initially only the normal lubrication force acts, and it dramatically slows down the horizontal motion towards the wall. The normal force also causes a negative angular velocity.

The tangential lubrication force becomes important after a short time $O(\kappa \ln \kappa)$, when

$$d = O(\kappa^2 \exp(5 \cos^2 \theta / R \kappa \ln \kappa)).$$

This occurs in spite of the fact that the friction coefficient associated with the tangential lubrication force is $O((d/\kappa) \ln (d/\kappa))$ smaller than that associated with the normal force, because the normal velocity drops more dramatically than the tangential velocity. The action of the tangential lubrication force is to decrease the tangential velocity of the end of the rod, and to make the rod rotate with a positive angular velocity.

There then follows a long phase in which the rod rotates virtually pivoting on a fixed end. The pivoting turn lasts for a period of time

$$\frac{3}{4} \frac{1}{\ln \kappa} \ln \left(\tan \frac{\theta_\infty}{2} \right).$$

During the turn the end of the rod slips vertically a distance $O(\kappa)$ while the minimum separation is predicted to be

$$d = \kappa^2 R^2 \exp(\tfrac{3}{4} \sin \theta_\infty / \kappa^2 \ln \kappa R^2).$$

This minimum separation is extremely small; indeed, so small that physical contact must be expected in practice, e.g. in the experiments of § 3 a separation smaller than 10^{-100} m is predicted. Physical contact, or any other breakdown of the lubrication theory, would of course destroy the symmetry of the turn. The reason for the smallness of the minimum separation is not difficult to see: the normal lubrication force

$$\tfrac{3}{2} \kappa^2 R^2 \dot{d}/d$$

remains $O(1)$ during the turn, which lasts for $1/\ln \kappa$, thus $\ln (d/d_0) = O(1/\kappa^2 \ln \kappa)$.

REFERENCES

BATCHELOR, G. K. 1970 *J. Fluid Mech.* **44**, 419.
BLAKE, J. R. 1971 *Proc. Camb. Phil. Soc.* **70**, 303.
CASWELL, B. 1970 *Chem. Engng Sci.* **27**, 373.
COX, R. G. 1970 *J. Fluid Mech.* **44**, 791.
LEAL, L. G. 1975 *J. Fluid Mech.* **69**, 305.
MESTRE, N. J. DE & RUSSEL, W. B. 1975 *J. Engng Math.* **9**, 81.
TAYLOR, G. I. 1969 In *Problems of Hydrodynamics and Continuum Mechanics*, p. 718. SIAM Publ.
TUCK, E. O. 1964 *J. Fluid Mech.* **18**, 619.
YOUNGREN, G. K. & ACRIVOS, A. 1975 *J. Fluid Mech.* **69**, 377.

CHAPTER III. Translational Motion of a Sphere in a Viscoelastic Liquid

1. Introduction

The mechanical behavior of macromolecular fluids in viscometric flows is now reasonably well understood. However, with the exception of tube flow, nearly all of the technologically important flows are associated with non-viscometric fluid motions. One interesting and important non-viscometric fluid motion is the flow around a submerged object. The only attempts to describe the motion of a viscoelastic fluid for this class of flows have employed the so-called "retarded motion" expansion which effectively reduces the constitutive behavior to that of the n^{th}-order fluid which is usually associated with the names of Rivlin and Ericksen. Such an expansion necessarily restricts viscoelastic effects to a secondary role. Nevertheless, for the class of particle motions which involve cumulative, weak viscoelastic contributions, the "retarded motion" expansion has been shown to yield qualitatively correct predictions of particle motions, both in uniform streaming flow and in shear flow [c.f. Tiefenbruck and Leal (1979) and Chan and Leal (1979)]. What is needed now is a description of particle motions when the effects of viscoelasticity are strong. Analytical description would be preferable, but such problems must await the development of new, hopefully more general, mathematical approximations. The only real hope for developing such approximations is to obtain a better understanding of the physics of viscoelastic fluid motion. Perhaps the best way to acquire this understanding is to compare experimental results with exact theoretical descriptions for the same problem. Due to the nonlinearity of the constitutive equations, such solutions must be obtained numerically. A specific problem, from the class of particle motions which will allow

comparison with experimental data, as well as being of direct technological interest is the streaming motion past a sphere.

The uniform translational motion of a Newtonian fluid past a sphere has been treated theoretically for a number of different cases. The solution for the motion of a sphere in a "perfect fluid" may be found in Lamb (1945). Stokes (1851) analytically investigated the motion of a sphere in a Newtonian fluid in the creeping flow or inertialess regime. Stokes' solution was later extended by Oseen (1910) to include weak inertial effects and still further extended by Proudman and Pearson (1957) by use of the method of matched asymptotic expansions. When the convective acceleration terms in the Navier-Stokes equations are not small, the resulting nonlinear problem must be treated numerically. Hand computations using finite difference techniques were carried out by Kawaguti (1950) and Jenson (1959). The methods of Jenson were extended to a finer grid by Hamielec, Hoffman and Ross (1967) who solved the equations on a digital computer. The motion of a sphere in a power law fluid in the creeping flow regime was studied by Wasserman and Slattery (1964). Using variational methods they were able to obtain upper and lower bounds for the drag coefficient. Yoshioka, Adachi and Ishimura (1971) studied the same problem for a Bingham fluid. The creeping flow of a micropolar fluid (a rather exotic fluid with a nonsymmetric stress tensor) past a sphere was analyzed by Rao and Rao (1970).

The study of the motion of a sphere in a viscoelastic fluid was begun by Leslie (1961) who carried out a "retarded motion" asymptotic analysis for an Oldroyd fluid. For weakly elastic liquids the problem is linearized about the Newtonian solution given by Stokes.

Similar solutions were obtained by Caswell and Schwarz (1962) and Giesekus (1963) for third-order fluids. Giesekus used the known relations between the third-order fluid and the Oldroyd model in the "slow flow" limit to show that his solution and Leslie's were in fact identical. Due to the nonlinearity of all realistic constitutive equations, this is as far as analytical investigation can take us. To proceed further, the problem must be attacked numerically. In this work, we shall obtain exact numerical solutions to the equations governing the flow of an incompressible viscoelastic fluid past a spherical obstacle.

One area for the application of the solutions for sphere motion is in describing bubble motion in gas-liquid contact mass transfer equipment. The analysis of such problems begins by considering an isolated bubble. For the motion of a single bubble in a viscoelastic liquid, it has been observed experimentally that the terminal velocity versus bubble volume curve has a discontinuity at a "critical" volume [$\simeq 0.1$ cm^3, see e.g. Zana and Leal (1978)]. It is generally believed that the cause of this discontinuity is an abrupt change of the surface conditions from solid-like behavior (no slip) to a freely circulating behavior (zero shear stress). Leal, Skoog and Acrivos (1971) have shown that the change in bubble shape is not very significant at the point of transition. Indeed, glass spheres were found to fall at the same velocity as the bubble rises if suitable corrections for the density difference are made. In the light of this observation, a spherical shape is used to represent the bubble in our present study. The actual shape for this problem would be slightly teardrop. Since the flow of a viscoelastic fluid past a sphere is already a difficult problem, we have chosen to forego the problems associated with

the nonspherical bubble shape and employ spherical coordinates centered in the bubble.

One of the problems associated with theoretical studies of particle motion in strongly elastic liquids is the choice of an appropriate constitutive equation to describe the fluid. Since none of the currently proposed constitutive equations can quantitatively describe all of the known viscoelastic phenomena, the most we can require from the constitutive model is that it qualitatively reproduce all of the known viscometric flow phenomena with a single set of thermodynamically acceptable values for the material coefficients, and that it not be qualitatively inconsistent with the limited non-viscometric flow data which presently exist. The model for the extra stress tensor, $\underline{\underline{\tau}}$, used in this work is a form of the model presented by Oldroyd (1958),

$$\underline{\underline{\tau}} + \lambda_1 \left\{ \frac{\mathcal{D}\underline{\underline{\tau}}}{\mathcal{D}t} - \alpha(\underline{\underline{e}}\cdot\underline{\underline{\tau}} + \underline{\underline{\tau}}\cdot\underline{\underline{e}}) \right\} = 2\eta_o \underline{\underline{e}} + 2\eta_o\lambda_2 \left\{ \frac{\mathcal{D}\underline{\underline{e}}}{\mathcal{D}t} - 2\alpha(\underline{\underline{e}}\cdot\underline{\underline{e}}) \right\} \qquad (1)$$

where η_o, λ_1, λ_2 and α are positive valued constants. $\frac{\mathcal{D}}{\mathcal{D}t}$ is the Jaumann or corotational derivative given for an arbitrary tensor $\underline{\underline{B}}$ as

$$\frac{\mathcal{D}\underline{\underline{B}}}{\mathcal{D}t} = \frac{\partial \underline{\underline{B}}}{\partial t} + \underline{u}\cdot\nabla\underline{\underline{B}} + \underline{\underline{w}}\cdot\underline{\underline{B}} - \underline{\underline{B}}\cdot\underline{\underline{w}} \qquad (2)$$

In equations (1) and (2), the rate of strain tensor, $\underline{\underline{e}}$, and the vorticity tensor, $\underline{\underline{w}}$, are given by

$$\underline{\underline{e}} = \frac{1}{2}\left(\nabla\underline{u} + (\nabla\underline{u})^T\right) \qquad \underline{\underline{w}} = \frac{1}{2}\left(\nabla\underline{u} - (\nabla\underline{u})^T\right)$$

The model represented by equation (1) is consistent with the forms

suggested by deductive studies of dilute suspensions where $0 \leq \alpha \leq 1$. The limit $\alpha = 0$ is obtained only for the special case of a suspension of spheres or near-spheres where the microstructure rotates exactly with the local vorticity. The limit $\alpha = 1$ corresponds to a suspension of rod-like particles with an infinite axis ratio. In order to elucidate the model behavior in viscometric flow, we may consider the model predictions from equation (1) for steady simple shear flow $u_x = \dot{\gamma} y$

$$\tau_{yx} = \eta_o \dot{\gamma} \left(\frac{1 + \lambda_1 \lambda_2 (1 - \alpha^2) \dot{\gamma}^2}{1 + \lambda_1^2 (1 - \alpha^2) \dot{\gamma}^2} \right)$$

$$N_1 = \tau_{xx} - \tau_{yy} = \frac{2\eta_o \dot{\gamma}^2 (\lambda_1 - \lambda_2)}{1 + \lambda_1^2 (1 - \alpha^2) \dot{\gamma}^2}$$

$$N_2/N_1 = -(1 - \alpha)/2$$

Thus we see that the model predicts shear thinning for $\lambda_2 < \lambda_1$, $\alpha \neq 1$. The model also predicts a positive first normal stress difference and a negative second normal stress difference in qualitative agreement with experimental observation for simple shear flow. It may be noted, however, that λ_2/λ_1 must be greater than 1/9 to insure that the shear stress is a monotonically increasing function of shear rate in a simple shear flow, and this restricts the maximum degree of shear-thinning to 1/9; which is less than is observed. For steady uniaxial extensional flow, the model gives the following result,

$$\tau_{xx} - \tau_{zz} = 3\eta_o E \left(\frac{1 - \alpha\lambda_2 E(1 + 2\alpha\lambda_1 E)}{(1 - 2\alpha\lambda_1 E)(1 + \alpha\lambda_1 E)} \right)$$

where E is the extension rate. We note that for non-zero α the model predicts an increasing elongational viscosity in uniaxial extensional flow. Thus we can see that as α increases from zero to one, the extensional viscosity increases, while the degree of shear thinning at a given shear rate decreases. For a more detailed discussion of the model behavior in these simple flows, the interested reader is referred to Tiefenbruck (1980).

The study of Leal et al., cited above, found that only 30% of the observed velocity jump could be accounted for using a purely viscous (shear thinning) fluid model. Therefore, it appears that the magnitude of the velocity jump in the bubble velocity transition phenomenon is a manifestation of fluid elasticity. For any meaningful comparisons between experimental observations and theoretical predictions, it is necessary to solve the relevant governing equations for non-trivial values of the Weissenberg number, $Wi = \frac{u_\infty \lambda_1}{a}$. This dimensionless parameter can be viewed as the ratio of the time scale of the fluid memory, λ_1, to the convective time scale of the fluid motion, a/u_∞. To obtain the necessary theoretical results, our only recourse is to employ numerical techniques. The first numerical solution for a viscoelastic liquid, of which we are aware, was obtained by Gilligan and Jones (1970) who studied the flow caused by an infinite circular cylinder impulsively started from rest in a second-order fluid. Due to the growth of errors from their method of calculation for long times, they did not continue the integration to steady state. In view of the unacceptability of the second-order fluid in transient situations, it is hard to assess the results of their computation. Crochet and Pilate (1975, 1976, 1977) have considered plane flow

in a square cavity, flow through a contraction, and flow around cylindrical bodies all for a second-order fluid. Tanner, Nickell and Bilger (1975) and Caswell and Tanner (1978) have developed a finite element algorithm to treat the flow of a second-order fluid in planar channels and in typical wire coating geometries. While their program is set up to accept shear rate dependent parameters, the only efforts in the area have been for a power-law fluid in the wire coating problem. With the possible exception of nearly viscometric flows where the second-order fluid with rate dependent parameters is exact, the second-order fluid model is strictly valid only for "retarded" motions, where the Weissenberg number is much smaller than one. Numerical solutions using the second-order fluid model for finite Wi are therefore of questionable value. Even solutions for the more general n^{th}-order fluid model are of limited value since the retarded motion expansion is generally believed to have a finite radius of convergence, Wi = 1, beyond which only an infinite number of terms would suffice.

A model for a viscoelastic fluid which does not suffer from these drawbacks is the differential model introduced by Oldroyd (1958). The first numerical investigation of the flow of an Oldroyd fluid was that of Townsend (1973), who studied the following transient pipe flow problems

(1) Impulsively imposed pressure gradient

(2) Fluctuating pressure gradient

(3) Vibrating motion of the pipe along its axis

using a four constant Oldroyd fluid $(\eta_0,\lambda_1,\lambda_2,\mu_0)$ with a codeformational ($\alpha = 1$) time derivative. More recently, Akay and Kaye (1976) studied unsteady flows of a three constant corotational ($\alpha = 0$) Oldroyd model in

a concentric annulus geometry. Perera and Walters (1977a,b) have investigated the steady flow of the four constant codeformational Oldroyd model in L and T shaped channels and in the expansion/contraction/expansion problem. Finally, Gatski and Lumley (1978) have studied the motion of a three constant (codeformational) Oldroyd model through a hyperbolic contraction. These studies are all different from the previously mentioned second-order fluid studies in that they all solve the full differential constitutive equations in parallel with the equations of motion. In addition, all of these studies have used finite difference methods for solution of the resulting system of differential equations. In both of these features, the algorithm used in this work resembles that of these earlier investigators.

The one study which we are aware of that employs a differential model and uses the finite element formulation to discretize the problem is due to Kawahara and Takeuchi (1977) who considered various planar channel flows for a Maxwellfluid with a codeformational time derivative. The study was, however, limited to small Wi ($0 < Wi < 10^{-1}$), and serves to point out some of the difficulties associated with finite element formulations. Perhaps the major drawback is the lack of resolution associated with the relatively large elements and rather simple interpolation formulae which they were forced to employ. The flow around a sphere is found, in the present study, to exhibit large variations of velocity and stress over short distances near the sphere. Thus we would need to employ a prohibitive number of elements to achieve reasonable results via the finite element technique. Furthermore, in the absence of a variational principle, we would be forced to employ a Galerkin technique like

that described by Taylor and Hood (1973) for a Newtonian fluid, and the implementation of a finite element algorithm is thus also an extremely complicated problem. Finally, although Kawahara and Takeuchi say their program takes only a "reasonable running time", they fail to give any figures which can be compared with the currently available finite difference calculations. In the light of these difficulties and uncertainties involving finite element technique, and the wealth of experience and information in using finite difference methods in Newtonian flow problems, we have used a finite difference approach in the present work, as indicated earlier.

In section 2, we formulate the equations and appropriate boundary conditions for the flow of a viscoelastic liquid past both a solid sphere and a spherical bubble. In section 3, we discretize the governing equations and discuss the method of solution. In section 4, we shall discuss the results of the computation.

2. Problem Statement

The problem which we consider is the uniform streaming motion of an unbounded viscoelastic fluid past a spherical particle. For formulation of this problem, we use spherical polar coordinates (r,θ,ϕ) with the origin located at the center of the sphere and $\theta = 0$ in the downstream direction. The equations governing the steady motion of an incompressible fluid are the equation of continuity

$$\nabla\cdot\underline{u} = 0 \tag{3}$$

and the so-called "stress" equations of motion

$$\rho(\underline{u}\cdot\nabla\underline{u}) = \nabla\cdot\underline{\underline{T}} \tag{4}$$

where ρ is the fluid density, $\underline{u}$ is the fluid velocity and $\underline{\underline{T}}$ is the stress tensor. The stress tensor is usually represented by two terms as

$$\underline{\underline{T}} = -p\,\underline{\underline{I}} + \underline{\underline{\tau}} \tag{5}$$

where $\underline{\underline{\tau}}$ is the extra stress tensor which is caused by the fluid motion. It is important to note that p is not the same pressure as is normally associated with a Newtonian fluid since $\underline{\underline{\tau}}$ is not traceless. Rather, in non-Newtonian fluid mechanics it has become conventional to split the stress tensor in such a way that p is simply an isotropic term which is necessary to satisfy the governing equations. In this work, $\underline{\underline{\tau}}$ is given by equation (1).

To completely specify the problem, we need to consider the boundary conditions. At large distances from the sphere, the fluid velocity is required to approach that of the uniform stream, u_∞. Along the axes of symmetry $u_\theta = 0$ and $\frac{\partial u_r}{\partial \theta} = 0$. The boundary conditions at the surface of the sphere depend upon the nature of the spherical particle. For a solid sphere, we have zero velocity at the sphere surface, while for a spherical gas bubble, the appropriate conditions at the surface are zero <u>normal</u> velocity and zero shear stress.

In order to make the equations and boundary conditions dimensionless, we utilize the free stream velocity, u_∞, the sphere radius a and the typical stress $\eta_0 u_\infty/a$. The rheological parameter α is already dimensionless. The governing equations nondimensionalized in this manner are

$$\tau_{rr} + Wi \left\{ u_r \frac{\partial \tau_{rr}}{\partial r} + \frac{u_\theta}{r} \frac{\partial \tau_{rr}}{\partial \theta} + 2\tau_{r\theta}\left(w_{r\theta} - \frac{u_\theta}{r} - \alpha e_{r\theta}\right) - 2\alpha e_{rr}\tau_{rr} \right\}$$

$$= 2e_{rr} + 2\varepsilon Wi \left\{ u_r \frac{\partial e_{rr}}{\partial r} + \frac{u_\theta}{r} \frac{\partial e_{rr}}{\partial \theta} + 2e_{r\theta}\left(w_{r\theta} - \frac{u_\theta}{r} - \alpha e_{r\theta}\right) - 2\alpha e_{rr}^2 \right\} \tag{6}$$

$$\tau_{\theta\theta} + Wi \left\{ u_r \frac{\partial \tau_{\theta\theta}}{\partial r} + \frac{u_\theta}{r} \frac{\partial \tau_{\theta\theta}}{\partial \theta} - 2\tau_{r\theta}\left(w_{r\theta} - \frac{u_\theta}{r} + \alpha e_{r\theta}\right) - 2\alpha e_{\theta\theta}\tau_{\theta\theta} \right\}$$

$$= 2e_{\theta\theta} + 2\varepsilon Wi \left\{ u_r \frac{\partial e_{\theta\theta}}{\partial r} + \frac{u_\theta}{r} \frac{\partial e_{\theta\theta}}{\partial \theta} - 2e_{r\theta}\left(w_{r\theta} - \frac{u_\theta}{r} + \alpha e_{r\theta}\right) - 2\alpha e_{\theta\theta}^2 \right\} \tag{7}$$

$$\tau_{\phi\phi} + Wi \left\{ u_r \frac{\partial \tau_{\phi\phi}}{\partial r} + \frac{u_\theta}{r} \frac{\partial \tau_{\phi\phi}}{\partial \theta} - 2\alpha e_{\phi\phi}\tau_{\phi\phi} \right\}$$

$$= 2e_{\phi\phi} + 2\varepsilon Wi \left\{ u_r \frac{\partial e_{\phi\phi}}{\partial r} + \frac{u_\theta}{r} \frac{\partial e_{\phi\phi}}{\partial \theta} - 2\alpha e_{\phi\phi}^2 \right\} \tag{8}$$

$$\tau_{r\theta} + Wi \left\{ u_r \frac{\partial \tau_{r\theta}}{\partial r} + \frac{u_\theta}{r} \frac{\partial \tau_{r\theta}}{\partial \theta} + \left(w_{r\theta} - \frac{u_\theta}{r}\right)(\tau_{\theta\theta} - \tau_{rr}) \right.$$

$$\left. - \alpha\left(e_{r\theta}(\tau_{rr} + \tau_{\theta\theta}) + \tau_{r\theta}(e_{rr} + e_{\theta\theta})\right) \right\} = 2e_{r\theta} + 2\varepsilon Wi \left\{ u_r \frac{\partial e_{r\theta}}{\partial r} \right.$$

$$\left. + \frac{u_\theta}{r} \frac{\partial e_{r\theta}}{\partial \theta} + \left(w_{r\theta} - \frac{u_\theta}{r}\right)(e_{\theta\theta} - e_{rr}) - 2\alpha e_{r\theta}(e_{rr} + e_{\theta\theta}) \right\} \tag{9}$$

$$\frac{\partial \tau_{rr}}{\partial r} + \frac{1}{r \sin\theta} \frac{\partial}{\partial \theta}(\tau_{r\theta} \sin\theta) + \frac{2\tau_{rr} - \tau_{\theta\theta} - \tau_{\phi\phi}}{r} - \frac{\partial p}{\partial r}$$

$$= Re \left(u_r \frac{\partial u_r}{\partial r} + \frac{u_\theta}{r} \frac{\partial u_r}{\partial \theta} - \frac{u_\theta^2}{r} \right) \tag{10}$$

$$\frac{\partial \tau_{r\theta}}{\partial r} + \frac{3\tau_{r\theta}}{r} + \frac{1}{r}\frac{\partial \tau_{\theta\theta}}{\partial \theta} + \frac{(\tau_{\theta\theta} - \tau_{\phi\phi})\cot\theta}{r} - \frac{1}{r}\frac{\partial p}{\partial \theta}$$

$$= \mathrm{Re}\left(u_r \frac{\partial u_\theta}{\partial r} + \frac{u_\theta}{r}\frac{\partial u_\theta}{\partial \theta} + \frac{u_r u_\theta}{r}\right) \qquad (11)$$

$$\frac{1}{r^2}\frac{\partial}{\partial r}(r^2 u_r) + \frac{1}{r\sin\theta}\frac{\partial}{\partial \theta}(u_\theta \sin\theta) = 0 \qquad (12)$$

where $\mathrm{Wi} = \frac{u_\infty \lambda_1}{a}$ $\qquad$ $\mathrm{Re} = \frac{\rho u_\infty a}{\eta_o}$ $\qquad$ $\varepsilon = \frac{\lambda_2}{\lambda_1}$

In this work, we shall assume that the Reynolds number, Re, is much smaller than one, and thus ignore the inertia terms on the right-hand side of equations (10) and (11). The magnitude of the Weissenberg number is indicative of the importance of elastic effects on the stress experienced by a fluid element and therefore of its importance on the fluid motion.

Since the uniform streaming motion past a sphere is an axisymmetric problem, we may introduce the streamfunction, ψ, to satisfy the continuity equation (12). The velocity components are given in terms of ψ by

$$u_r = \frac{1}{r^2 \sin\theta}\frac{\partial \psi}{\partial \theta} \qquad u_\theta = -\frac{1}{r\sin\theta}\frac{\partial \psi}{\partial r} \qquad (13)$$

The problem is thus to solve (6) - (11), expressed in terms of the streamfunction, subject to the appropriate boundary conditions. The usual procedure when working with the streamfunction is to eliminate the pressure by taking the curl of the equations of motion. For the system of equations

used here, the resulting equation is

$$\frac{\partial^2 \tau_{r\theta}}{\partial r^2} + \frac{4}{r}\frac{\partial \tau_{r\theta}}{\partial r} - \frac{1}{r^2}\frac{\partial}{\partial \theta}\left(\frac{1}{\sin\theta}\frac{\partial}{\partial \theta}(\tau_{r\theta}\sin\theta)\right) + \frac{1}{r}\frac{\partial^2}{\partial r \partial \theta}(\tau_{\theta\theta} - \tau_{rr})$$

$$+ \frac{\cot\theta}{r}\frac{\partial}{\partial r}(\tau_{\theta\theta} - \tau_{\phi\phi}) - \frac{1}{r^2}\frac{\partial}{\partial \theta}(2\tau_{rr} - \tau_{\theta\theta} - \tau_{\phi\phi}) = 0 \qquad (14)$$

When we substitute the Newtonian expressions for $\underline{\underline{\tau}}$ in terms of ψ into equation (14), we obtain

$$E^4\psi = 0 \qquad (15)$$

where $E^2 = \frac{\partial^2}{\partial r^2} + \frac{\sin\theta}{r}\frac{\partial}{\partial \theta}\left(\frac{1}{\sin\theta}\frac{\partial}{\partial \theta}\right)$

The usual manner of obtaining the numerical solution of equation (15) is to split it into two second-order equations

$$E^2\psi = -\omega r \sin\theta \qquad (16)$$

$$E^2(\omega r \sin\theta) = 0 \qquad (17)$$

but, in any event, the differential operator E^4 is elliptic and there is no difficulty in obtaining numerical solutions for either formulation. However, if we consider the system of constitutive equations separately from equation (15), we obtain only hyperbolic operators, in spite of the fact that the combined form is an elliptic equation.

The presence of hyperbolic operators might, at first, appear to be an advantage since direct methods are available for integration of hyperbolic equations along characteristics. However, no satisfactory

scheme could be found to solve even the Newtonian problem, much less a fully viscoelastic problem. There are two basic difficulties with such an approach. First, the problem to be solved is, in fact, elliptic, no matter how it may be formulated. Indeed, the boundary conditions are not of the proper form for use with any of the usual schemes for integration along characteristics starting with initial values at one end. Second, it is only the particular solution to the various hyperbolic operators which produces the proper solution to the problem. The homogeneous wave solutions are clearly spurious. Due to the presence of truncation errors, however, their presence is unavoidable in numerical calculations. In order to overcome these difficulties, we have developed an "indirect" scheme which is similar to the decomposition to second-order elliptic operators represented by equations (16) and (17). To accomplish this, we simply write the stress as the sum of a viscous term and a non-Newtonian contribution

$$\underline{\underline{\tau}} = 2\underline{\underline{e}} - \underline{\underline{P}} \tag{18}$$

When we substitute (18) into (14), we obtain

$$E^2(\omega r \sin\theta) = r\sin\theta \left\{ \frac{\partial^2 P_{rr}}{\partial r^2} + \frac{4}{r}\frac{\partial P_{r\theta}}{\partial r} - \frac{1}{r^2}\frac{\partial}{\partial\theta}\left(\frac{1}{\sin\theta}\frac{\partial}{\partial\theta}(P_{r\theta}\sin\theta)\right) \right.$$
$$+ \frac{1}{r}\frac{\partial^2}{\partial r\partial\theta}(P_{\theta\theta} - P_{rr}) + \frac{\cot\theta}{r}\frac{\partial}{\partial r}(P_{\theta\theta} - P_{\phi\phi})$$
$$\left. - \frac{1}{r^2}\frac{\partial}{\partial\theta}(2P_{rr} - P_{\theta\theta} - P_{\phi\phi}) \right\} \tag{19}$$

and

$$E^2\psi = -\omega r\sin\theta \tag{20}$$

We can obtain $\underline{\underline{P}}$ in either of two ways. Either we can calculate $\underline{\underline{e}}$ and $\underline{\underline{\tau}}$ and then solve (18) for $\underline{\underline{P}}$, or we can substitute (18) into (1) and obtain a differential equation for $\underline{\underline{P}}$ which is then solved directly. We have employed both methods in this work and we have found that there is no effect on the solution and only a minimal difference in computation time. We have also found it advantageous to work with the disturbance stream-function, $\hat{\psi}$, given by

$$\hat{\psi} = \psi - \frac{1}{2} r^2 \sin^2\theta \tag{21}$$

rather than ψ itself. The accuracy of the many kinematic variables is greatly improved with this substitution. In order to enhance the resolution near the surface of the sphere, we have introduced an expanding mesh by transforming from a normal spherical coordinate system (r,θ,ϕ) to the system (z,η,ϕ) where $z = \ln r$ and $\eta = \cos\theta$. Preliminary computations using a (z,θ,ϕ) coordinate system with the usual centered difference formulations on the axis of symmetry produced inaccurate values of the stress components and pressure along the upstream axis of symmetry. Numerical experimentation showed that the introduction of the η coordinate and the use of one-sided differences greatly improved the calculation of the stress components along this axis. The primary difficulty in using the η coordinate arises in connection with terms like $\tau_{r\theta}$ or ω which behave like $\sin\theta$ near $\theta = 0,\pi$. $\sin\theta$ is, of course, given by $\sqrt{1 - \eta^2}$. Since $\sqrt{1 - \eta^2}$ is not represented very well by a Taylor series expansion near $\theta = 0,\pi$, errors are introduced into the computations. The simplest way to handle these terms is to multiply them by $\sin\theta$ and then make the appropriate changes in the governing equations.

In order to employ the streamfunction it is necessary to reconsider the boundary conditions which are to be satisfied. For large r it is easily shown that $\psi \to \frac{1}{2} r^2 \sin^2\theta$ as anticipated in equation (21). Furthermore, at the surface of the sphere and along the axes of symmetry

$$\psi = 0 \quad \text{for} \quad r = 1 \quad \text{and} \quad \theta = 0, \tag{22}$$

The second condition at the sphere surface depends upon whether the sphere is a solid or a bubble. For the rigid sphere, the condition on the streamfunction is

$$\frac{\partial \psi}{\partial r} = 0 \qquad r = 1 \tag{23}$$

For the freely circulating surface, the correct condition is not quite as obvious. However, it can be shown that $\tau_{r\theta} = 0$ at $r = 1$ implies that $e_{r\theta} = 0$ at $r = 1$, even when $\underline{\underline{\tau}}$ and $\underline{\underline{e}}$ are related via the constitutive equation (1). This results in the conditions for the streamfunction

$$2 \frac{\partial \psi}{\partial r} - \frac{\partial^2 \psi}{\partial r^2} = 0 \qquad r = 1 \tag{24}$$

All of the above conditions can also be represented, in different form of course, for $\hat{\psi}$.

Since the equation for $\underline{\underline{\tau}}$ involves derivatives with respect to spatial coordinates, it would appear that we would need extra conditions to determine the stress components on the boundaries of the computational region. This is not the case as we shall see below. Far away from the sphere, it is clear that $\underline{\underline{e}} = 0$ and thus $\underline{\underline{\tau}}$ must also be zero. Along the axes of symmetry $u_\theta = 0$, and $\underline{\underline{\tau}}$ may be expressed as a system of <u>ordinary</u>

differential equations with r as the independent variable. At both the forward and rear stagnation points, the constitutive equation always reduced to a system of algebraic equations. Indeed, for the case of a rigid sphere, the stress components over the entire surface are given by a system of algebraic equations. When the sphere surface is freely circulating, on the other hand, the non-zero normal stress components are related by a system of ordinary differential equations with η as the independent variable. Thus, the values of all stress components can be determined via either algebraic or ordinary differential equations along all boundaries of the computational domain, knowing only the values of $\underline{\underline{\tau}}$ at infinity.

Clearly, one of the difficulties with a numerical solution of the problem just formulated is the application of the boundary conditions for $r \to \infty$. In principle, one method of handling this problem is to impose the known boundary conditions for $r \to \infty$ at some large but finite value of r. For the creeping flow of a Newtonian fluid past a sphere, however, we know that the disturbance velocity drops off like 1/r. Therefore, if we apply $\underline{u} = \underline{u}_\infty$ at any reasonable finite r, we obtain an overestimate for the drag. For example, if we impose $\underline{u} = \underline{u}_\infty$ at r = 10, the calculated drag is $7.31\pi\mu u_\infty a$, approximately 20% high. One of the ways of minimizing this difficulty is to determine additional terms in the asymptotic solution for large r and then use that asymptotic expression evaluated at finite r as the boundary conditions. Such a method has been used by Robertson, Seinfeld and Leal (1973) in analyzing the combined forced and free convection of a Newtonian fluid past a flat plate. The derivation of an asymptotic solution for large r in the present case is carried out in the

appendix. The results given below are the stresses and disturbance flow due to a point force in a liquid described by a linearized version of equation (1). The asymptotic results are

$$\hat{\psi} \simeq \beta_1[r - Wi(1 - \varepsilon)\cos\theta]\sin^2\theta + O(1/r) \tag{25}$$

$$\tau_{rr} \simeq - 4\beta_1 \cos\theta/r^2 + O(r^{-3}) \tag{26a}$$

$$\tau_{\theta\theta} \simeq 2\beta_1 \cos\theta/r^2 + O(r^{-3}) \tag{26b}$$

$$\tau_{\phi\phi} \simeq 2\beta_1 \cos\theta/r^2 + O(r^{-3}) \tag{26c}$$

$$\tau_{r\theta} \simeq 0 + O(r^{-3}) \tag{26d}$$

The constant β_1 represents the strength of the point force and is related to the drag on the sphere via the equation.

$$\beta_1 = - \frac{1}{4} \int_{-1}^{1} [(\tau_{rr} - p)\eta - (\tau_{r\theta} \sin\theta)]_{r=1} \, d\eta \tag{27}$$

Thus, the asymptotic correction to the free-stream boundary-values introduces a coupling between the solution at large r and the solution at the sphere surface. At each iteration in the numerical algorithm a new estimate is obtained for β_1 and this value is then used to determine the boundary conditions at large r from (25) and (26a - d). As a measure of the improvement this type of boundary condition affords, we consider the Newtonian problem (Wi = 0) with equation (25) imposed at r = 10. The drag on the sphere in this case is 5.9970 $\pi\mu u_\infty a$, an error of only 0.05%.

3. Finite Difference Equations

Now that we have the equations and boundary conditions in a form suitable for solution, we can turn to the problem of discretization. In equations (19) and (20) we used centered differences for all of the derivatives. Thus, equation (20) at (η_j, z_i) is

$$\hat{\psi}(j,i+1) - 2\hat{\psi}(j,i) + \hat{\psi}(j,i-1) - \frac{\Delta z}{2}\left(\hat{\psi}(j,i+1) - \hat{\psi}(j,i-1)\right)$$
$$+ k^2(1-\eta_j^2)\left(\hat{\psi}(j+1,i) - 2\hat{\psi}(j,i) + \hat{\psi}(j-1,i)\right) = -e^{2z_i}(\Delta z)^2\zeta(j,i) \qquad (28)$$

where $\zeta = \omega r \sin\theta$ and $k = \Delta z/\Delta\eta$. If we reorganize equation (28), we recognize a block structure which is typical of elliptic partial differential equations discretized in this manner. This structure is given by

$$\begin{bmatrix} A_1 C_1 & & & & \\ B_2 A_2 C_2 & & & & \\ & \ddots & & & \\ & & B_\ell A_\ell C_\ell & & \\ & & & \ddots & \\ & & & & B_m A_m \end{bmatrix}$$

$$C_\ell = \left(1 - \frac{\Delta z}{2}\right) I_{nxn} \qquad B_\ell = \left(1 + \frac{\Delta z}{2}\right) I_{nxn}$$

$$A_\ell = \begin{bmatrix} -2\left(1 + k^2(1 - \eta_1^2)\right) & k^2(1 - \eta_1^2) & & \\ k^2(1 - \eta_2^2) & -2\left(1 + k^2(1 - \eta_2^2)\right) & k^2(1 - \eta_2^2) & \\ & & & \\ & & & -2\left(1 + k^2(1 - \eta_n^2)\right) \end{bmatrix}_{nxn}$$

where I_{nxn} stands for a (nxn) identity matrix. In the notation used here, m+2 is the number of z coordinate lines including the boundaries and n+2 is the number of η coordinate lines also including the boundaries. In the computation described below, m=61, n=29, $\Delta\eta = \frac{1}{15} \simeq 0.0667$, and $\Delta z = \ln(20)/62 \simeq 0.0483$. This system of equations, represented by (28), is inverted by taking advantage of the sparse block structure to reduce the number of operations needed. The algorithm for this inversion may be found in Dorr (1970), or Isaacson and Keller (1966). The inversion of the system of equations took approximately one minute on the California Institute of Technology's IBM 370-158. The "inverse" which is then stored for future use required storage of 206 K of computer memory.

Since equation (19) is of the same form as equation (20), we can use the same matrix calculated above to solve for ζ. All that needs to be changed is the inhomogeneous term. The inhomogeneous term, f, for equation (19) is

$$
\begin{aligned}
f(j,i) = e^{z_i}\Big\{ & P^*_{r\theta}(j,i+1) - 2P^*_{r\theta}(j,i) + P^*_{r\theta}(j,i-1) + 1.5\Delta z\Big(P^*_{r\theta}(j,i+1) \\
& - P^*_{r\theta}(j,i-1)\Big) - k^2(1-\eta_j^2)\Big(P^*_{r\theta}(j+1,i) - 2P^*_{r\theta}(j,i) + P^*_{r\theta}(j-1,i)\Big) \\
& + k(1-\eta_j^2)\Big(P_{rr}(j+1,i+1) - P_{rr}(j-1,i+1) - P_{rr}(j+1,i-1) + P_{rr}(j-1,i-1) \\
& - P_{\theta\theta}(j+1,i+1) + P_{\theta\theta}(j-1,i+1) + P_{\theta\theta}(j+1,i-1) - P_{\theta\theta}(j-1,i-1)\Big)/4 \\
& + \eta_j\Delta z\Big(P_{\theta\theta}(j,i+1) - P_{\phi\phi}(j,i+1) - P_{\theta\theta}(j,i-1) + P_{\phi\phi}(j,i-1)\Big)/2 \\
& + k\Delta z(1-\eta_j^2)\Big(2P_{rr}(j+1,i) - P_{\theta\theta}(j+1,i) - P_{\phi\phi}(j+1,i) - 2P_{rr}(j-1,i) \\
& + P_{\theta\theta}(j-1,i) + P_{\phi\phi}(j-1,i)\Big)/2\Big\} \qquad (29)
\end{aligned}
$$

where $P^{*}_{r\theta} = P_{r\theta}\sin\theta$. At this point we need to formulate boundary conditions for ζ which may be used in conjunction with the discrete form of equation (19). At large distances from the sphere ζ can be calculated from equations (20) and (25). From the symmetry conditions it is known that $\zeta = 0$ at $\theta = 0$ and π. Thus, equations (23) and (24) must be used to generate an equation for the surface vorticity for the cases of a solid sphere and a spherical gas bubble, respectively. Let us first consider the solid sphere. In this case, we find from equation (20) that $\zeta = -\left(\frac{\partial^2\psi}{\partial z^2}\right)_{z=0}$. Then, using the fact that $\psi = \frac{\partial\psi}{\partial z} = 0$ at $z = 0$, we obtain the following approximation for ζ.

$$\zeta_s(j,1) = -2\left(\frac{\hat{\psi}(j,2) + e^{(2\Delta z)}(1-\eta_j^2)/2}{(\Delta z)^2}\right) \qquad (30)$$

The formal Taylor series representation of the error in equation (30) is $O(\Delta z)$. However, Orzag and Israeli (1974) have found for several model problems that a representation like (30) for surface vorticity gives second-order accurate results, thus indicating that the formal Taylor series expansion may be misleading. The calculation of the vorticity at the surface of the bubble is not as straightforward, but is still not difficult. First, we write down a centered difference representation of equation (24). Then we write the discrete form of equation (20), both at the bubble surface. By eliminating the value of the vorticity below the bubble surface, we obtain the following expression for the surface vorticty

$$\zeta_B(j,1) = -2\left(\frac{\psi(j,2) + e^{(2\Delta z)}(1-\eta_j^2)/2}{z(1+1.5\Delta z)}\right) \tag{31}$$

The equations (30) and (31) are the required expressions for the surface vorticity. In order to calculate the stresses, we must be able to compute all of the necessary kinematic quantities. Once again, we employ central differences for all derivatives. The relevant expressions are

$$e_{rr}(j,i) = e^{-3z_i}\left[2\left(\frac{\hat{\psi}(j+1,i) - \hat{\psi}(j-1,i)}{2\Delta\eta}\right)\right.$$

$$\left. - \left(\frac{\hat{\psi}(j+1,i+1) - \hat{\psi}(j-1,i+1) - \hat{\psi}(j+1,i-1) + \hat{\psi}(j-1,i-1)}{4\Delta z\zeta\Delta\eta}\right)\right] \tag{32}$$

$$e_{\theta\theta}(j,i) = e^{-3z_i}\left[\frac{\eta_j}{(i-\eta_j^2)}\left(\frac{\hat{\psi}(j,i+1) - \hat{\psi}(j,i-1)}{2\Delta z}\right)\right.$$

$$+ \left(\frac{\hat{\psi}(j+1,i+1) - \hat{\psi}(j-1,i+1) - \hat{\psi}(j+1,i-1) + \hat{\psi}(j-1,i-1)}{4\Delta z\Delta\eta}\right)$$

$$\left. - \left(\frac{\hat{\psi}(j+1,i) - \hat{\psi}(j-1,i)}{2\Delta\eta}\right)\right] \tag{33}$$

$$e_{\phi\phi}(j,i) = -e^{-3z_i}\left[\left(\frac{\hat{\psi}(j+1,i) - \hat{\psi}(j-1,i)}{2\Delta\eta}\right) + \frac{\eta_j}{(1-\eta_j^2)}\left(\frac{\hat{\psi}(j,i+1) - \hat{\psi}(j,i-1)}{2\Delta z}\right)\right] \tag{34}$$

$$e^*_{r\theta}(j,i) = e_{r\theta}\sin\theta = \frac{e^{-3z_i}}{2}\left[3\left(\frac{\hat{\psi}(j,i+1) - \hat{\psi}(j,i-1)}{2\Delta z}\right)\right.$$

$$- \left(\frac{\hat{\psi}(j,i+1) - 2\hat{\psi}(j,i) + \hat{\psi}(j,i-1)}{(\Delta z)^2}\right)$$

$$\left. + (1-\eta_j^2)\left(\frac{\hat{\psi}(j+1,i) - 2\hat{\psi}(j,i) + \hat{\psi}(j-1,i)}{(\Delta\eta)^2}\right)\right] \tag{35}$$

$$\left(\omega^{*}_{r\theta} - \frac{u^{*}_{\theta}}{r}\right)(j,i) = \left(\omega_{r\theta} - \frac{u_{\theta}}{r}\right)\sin\theta = e^{-z_i}(1-\eta_j^2)$$

$$- \frac{e^{-3z_i}}{2}\left[\left(\frac{\hat{\psi}(j,i+1) - 2\hat{\psi}(j,i) + \hat{\psi}(j,i-1)}{(\Delta z)^2}\right) - 3\left(\frac{\hat{\psi}(j,i+1) - \hat{\psi}(j,i-1)}{2\Delta z}\right)\right.$$

$$\left. + (1-\eta_j^2)\left(\frac{\hat{\psi}(j+1,i) - 2\hat{\psi}(j,i) + \hat{\psi}(j-1,i)}{(\Delta\eta)^2}\right)\right] \qquad (36)$$

These equations are applicable throughout the flow domain except at the axes of symmetry, the surface of the sphere, and the outer boundary. At the outer boundary there is no problem computing any of the kinematic quantities since we have an analytic expression for $\hat{\psi}$. On the axes of symmetry it is easily shown that

$$e_{\theta\theta} = e_{\phi\phi} = -e_{rr}/2 \qquad \text{and} \qquad \omega_{r\theta} = e_{r\theta} = 0$$

To evaluate the derivatives on the axis of symmetry it is necessary to employ one-sided differences since we have no information on $\frac{\partial\psi}{\partial\eta}$ or $\frac{\partial^2\psi}{\partial\eta^2}$ at $\eta = \pm 1$. Thus we find that at $\eta = -1$ (j=1), e_{rr} is given by

$$e_{rr}(1,i) = e^{-3z_i}\left[2\left(\frac{4\hat{\psi}(2,i) - \hat{\psi}(3,i)}{2\Delta\eta}\right)\right.$$

$$\left. - \left(\frac{4\hat{\psi}(2,i+1) - \hat{\psi}(3,i+1) - 4\hat{\psi}(2,i-1) + \hat{\psi}(3,i-1)}{4\Delta z\Delta\eta}\right)\right] \qquad (37)$$

Similar expressions are used at $\eta = 1$ (j=31) except, of course, backward differences are employed instead of the forward differences used in equation (37).

The kinematic variables at the surface of the sphere depend, not surprisingly, upon whether the sphere is rigid or freely circulating. For a rigid sphere, it is easily shown that $e_{rr} = e_{\theta\theta} = e_{\phi\phi} = 0$ and

$$e^*_{r\theta} = \omega^*_{r\theta} = -\frac{1}{2}\left.\frac{\partial^2\psi}{\partial z^2}\right|_{z=0} = (\zeta_s/2) \quad \text{at } z=0 \tag{38}$$

For a bubble, on the other hand, $\omega_{r\theta} - u_\theta = e_{r\theta} = 0$ at $z=0$. Using equation (31), we thus find that

$$u^*_\theta = \omega^*_{r\theta} = -\zeta_B/2 \quad \text{at } z=0 \tag{39}$$

Furthermore, the continuity equation gives

$$\frac{\partial u_r}{\partial r} = e_{rr} = \frac{1}{2}\frac{\partial \zeta_B}{\partial \eta} \quad \text{at} \quad z=0 \tag{40}$$

Finally, it may be shown that

$$e_{\phi\phi} = \frac{\eta\zeta_B}{2(1-\eta^2)} \quad \text{at } z=0 \tag{41}$$

and $e_{\theta\theta}$ can be calculated by difference

$$e_{\theta\theta} = -e_{rr} - e_{\phi\phi} \ . \tag{42}$$

Equations (39) - (42) specify all of the needed kinematic quantities in the constitutive equation at the surface of a spherical bubble.

The computation of the stress components is handled differently from all of the above equations. It is easily shown that equations (6) - (9) are a system of ordinary differential equations if we follow lines of constant ψ i.e., follow a fluid element as it travels through the flow domain. Thus, it is seen that for a steady flow with no regions of

recirculation, the stress can be calculated at all points in the flow field, if the stress is specified at the inflow boundary, by integrating forward along the streamlines. In the algorithm used in this work, the specified value of the stress at the inflow region (large $z, \eta < 0$) is taken from the point force solution given by equation (36). While we cannot directly take advantage of the fact that the equations are ordinary differential equations along streamlines, we have designed our algorithm so that we mimick the "natural" scheme of integrating along streamlines as closely as possible. To do this, we sweep through the field starting from $\eta = -1$ and proceeding to $\eta = 1$ while simultaneously moving inward toward the sphere on rays of constant η where $u_r < 0$ and outward from the sphere where $u_r > 0$. Fortunately, u_r never changes signs more than once on a given ray in the solutions which we have obtained and this simplifies the programming effort considerably. The derivative terms in the stress equations were discretized in a one-sided manner such that information flowed to the point where the stress was to be calculated.

We reproduce below the discretized form of the constitutive equation used when u_r (denoted below as u) > 0. We note here that $-u_\theta \sin\theta$ (denoted below as v) is always > 0.

$$\tau_{rr}(j,i) + Wi\left\{u(j,i)e^{-z_i}\left(\frac{\tau_{rr}(j,i) - \tau_{rr}(j,i-1)}{\Delta z}\right)\right.$$

$$+ v(j,i)e^{-z_i}\left(\frac{\tau_{rr}(j,i) - \tau_{rr}(j-1,i)}{\Delta\eta}\right) + \frac{2\tau^*_{r\theta}(j,i)}{(1-\eta_j^2)}\left(\left(\omega^*_{r\theta} - \frac{u^*_\theta}{r}\right)(j,i)\right.$$

$$\left.\left. - \alpha e^*_{r\theta}(j,i)\right) - 2\alpha e_{rr}(j,i)\tau_{rr}(j,i)\right\} = 2e_{rr}(j,i)$$

$$+ 2\varepsilon Wi\left\{u(j,i)e^{-z_i}\left(\frac{e_{rr}(j,i) - e_{rr}(j,i-1)}{\Delta z}\right)\right.$$

$$+ v(j,i)e^{-z_i}\left(\frac{e_{rr}(j,i) - e_{rr}(j-1,i)}{\Delta\eta}\right) + \frac{2e^*_{r\theta}(j,i)}{(1-\eta_j^2)}\left(\left(\omega^*_{r\theta} - \frac{u^*_\theta}{r}\right)(j,i)\right.$$

$$\left.\left. - \alpha e^*_{r\theta}(j,i)\right) - 2\alpha e_{rr}(j,i)^2\right\} \qquad (43)$$

$$\tau_{\theta\theta}(j,i) + Wi\left\{u(j,i)e^{-z_i}\left(\frac{\tau_{\theta\theta}(j,i) - \tau_{\theta\theta}(j,i-1)}{\Delta z}\right)\right.$$

$$+ v(j,i)e^{-z_i}\left(\frac{\tau_{\theta\theta}(j,i) - \tau_{\theta\theta}(j-1,i)}{\Delta\eta}\right) - \frac{2\tau^*_{r\theta}(j,i)}{(1-\eta_j^2)}$$

$$\cdot\left(\left(\omega^*_{r\theta} - \frac{u^*_\theta}{r}\right)(j,i) + \alpha e^*_{r\theta}(j,i)\right) - 2\alpha e_{\theta\theta}(j,i)\tau_{\theta\theta}(j,i)\Big\} = 2e_{\theta\theta}(j,i)$$

$$+ 2\varepsilon Wi\left\{u(j,i)e^{-z_i}\left(\frac{e_{\theta\theta}(j,i) - e_{\theta\theta}(j,i-1)}{\Delta z}\right)\right.$$

$$+ v(j,i)e^{-z_i}\left(\frac{e_{\theta\theta}(j,i) - e_{\theta\theta}(j-1,i)}{\Delta\eta}\right)$$

$$\left. - \frac{2e^*_{r\theta}(j,i)}{(1-\eta_j^2)}\left(\left(\omega^*_{r\theta} - \frac{u^*_\theta}{r}\right)(j,i) + \alpha e^*_{r\theta}(j,i)\right) - 2\alpha e_{\theta\theta}(j,i)^2\right\} \qquad (44)$$

$$\tau_{\phi\phi}(j,i) + Wi \left\{ u(j,i)e^{-z_i} \left(\frac{\tau_{\phi\phi}(j,i) - \tau_{\phi\phi}(j,i-1)}{\Delta z} \right) \right.$$

$$\left. + v(j,i)e^{-z_i} \left(\frac{\tau_{\phi\phi}(j,i) - \tau_{\phi\phi}(j-1,i)}{\Delta\eta} \right) - 2\alpha e_{\phi\phi}(j,i)\tau_{\phi\phi}(j,i) \right\}$$

$$= 2e_{\phi\phi}(j,i) + 2\varepsilon Wi \left\{ u(j,i)e^{-z_i} \left(\frac{e_{\phi\phi}(j,i) - e_{\phi\phi}(j,i-1)}{\Delta z} \right) \right.$$

$$\left. + v(j,i)e^{-z_i} \left(\frac{e_{\phi\phi}(j,i) - e_{\phi\phi}(j-1,i)}{\Delta\eta} \right) - 2\alpha e_{\phi\phi}(j,i)^2 \right\} \qquad (45)$$

$$\tau^*_{r\theta}(j,i) + Wi \left\{ u(j,i)e^{-z_i} \left(\frac{\tau^*_{r\theta}(j,i) - \tau^*_{r\theta}(j,i-1)}{\Delta z} \right) \right.$$

$$+ v(j,i)e^{-z_i} \left(\frac{\tau^*_{r\theta}(j,i) - \tau^*_{r\theta}(j-1,i)}{\Delta\eta} \right) + \frac{\eta_j e^{-z_i}}{(1-\eta_j^2)} \tau^*_{r\theta} v(j,i)$$

$$- \alpha\tau^*_{r\theta}(j,i)\left(e_{rr}(j,i) + e_{\theta\theta}(j,i)\right) - \tau_{rr}(j,i)\left(\left(\omega^*_{r\theta} - \frac{u^*_\theta}{r}\right)(j,i)\right.$$

$$\left. + \alpha e^*_r(j,i)\right) + \tau_{\theta\theta}(j,i)\left(\left(\omega^*_{r\theta} - \frac{u^*_\theta}{r}\right)(j,i) - \alpha e^*_{r\theta}(j,i)\right)\Bigg\} = 2e^*_{r\theta}(j,i)$$

$$+ 2\varepsilon Wi \left\{ u(j,i)e^{-z_i} \left(\frac{e^*_{r\theta}(j,i) - e^*_{r\theta}(j,i-1)}{\Delta z} \right) \right.$$

$$+ v(j,i)e^{-z_i} \left(\frac{e^*_{r\theta}(j,i) - e^*_{r\theta}(j-1,i)}{\Delta\eta} \right) + \frac{\eta_j e^{-z_i}}{(1-\eta_j^2)} e^*_{r\theta} v(j,i)$$

$$\left. - 2\alpha e^*_{r\theta}(j,i)\left(e_{rr}(j,i) + e_{\theta\theta}(j,i)\right) + \left(\omega^*_{r\theta} - \frac{u^*_\theta}{r}\right)(j,i)\left(e_{\theta\theta}(j,i) - e_{rr}(j,i)\right)\right\}$$

(46)

The differencing used in these equations is basically a backward Euler scheme which, unfortunately, is only first-order accurate. The advantages

of equations (43) - (46), relative to a higher-order scheme, is that they are easy to implement and the resulting computation is stable. Stability is important here because of the stiffness of the equations when u and/or v are small. While the formulation used here is stable, it does introduce dispersion errors. Attempts to implement a second-order scheme with no dispersion error were only partially successful because of the stiffness problem which caused the computed solutions in the outflow region to have an unrealistic wave character.

The actual use of equations (43) - (46) to calculate the stress at (η_j, z_i) involves the solution of the four equations for the four unknown stress components. Since equation (45) only involves $\tau_{\phi\phi}(j,i)$, that equation is easily inverted immediately for that component. The other three components are coupled.

The resulting 3x3 system was inverted symbolically using Kramer's rule. When all of the necessary coefficients are evaluated, the resulting stress components can be calculated in a straightforward manner. We note here that the above scheme takes advantage of the fact that the constitutive equation is linear in the stress components. Now that we have a discrete form of the governing equations and methods to solve them, we shall proceed to describe the computational algorithm. Given a value for the vorticity field ζ and β_1 the "force constant", we inverted equation (28) to obtain $\hat{\psi}$. We then used $\hat{\psi}$ to calculate all of the kinematic quantities needed to solve for the stress component. We then solved for the stress components using equations (43) - (46) with equation (26) as the initial condition, and used equations (10) and (11),

to determine the pressure, p, at the sphere surface. A new value of β_1 could then be calculated using (27), and this value was under-relaxed so that the overall solution scheme is stable. We used

$$\beta_1^{(\ell+1)} = \beta_1^{(\ell)} + b\left(\beta_1^* - \beta_1^{(\ell)}\right)$$

where β_1^* is the directly calculated value of β_1, and b is the relaxation parameter which was generally assigned the value 0.05. This value was found by preliminary testing which showed that $\beta_1 = .05$ gave rapid, well behaved convergence for the Newtonian problem. We found that it was actually beneficial to have β_1 vary slowly since it exerts a large influence on the solution through the initial condition on the stress components. Finally, we determined $\underline{\underline{P}}$ from equation (18) (unless it was determined directly from the differential equation). We then updated the boundary conditions on ζ (the vorticity at the body was also under-relaxed) and then inverted the relevant equation to obtain a new value of ζ. If the value of

$$\max_{i,j} \left|\zeta^*(j,i) - \zeta^{(\ell)}(j,i)\right| \leq 0.001 ,$$

the calculation was stopped. If not, we substituted

$$\zeta^{(\ell+1)} = \left(\zeta^{(\ell)} + \zeta^*\right)/2$$

and the entire process was repeated. The solutions reported in the next section were obtained by using the Newtonian solution as the initial iterate and then increasing Wi slowly. Each succedingly larger value of Wi was computed by using the preceding solution as the initial iterate. The computations took between 5 and 20 minutes each on an IBM 370-158 for increments of approximately 0.3 in Wi.

Results

The best way to present the results of these computations is by examining detailed plots of the various kinematic and stress variables. We shall plot stress tensor components directly in order to facilitate comparison with the small Weissenberg number solutions of Leslie (1961) and Giesekus (1963). Figures 1 - 4 are the Newtonian (Stokes) solution contours of the streamfunction, vorticity, τ_{rr}, and $\tau_{r\theta}$, for the flow past a solid sphere. The fore-aft symmetry of the solutions is readily apparent. The sharp radial gradient of τ_{rr} near the surface of the sphere is produced by the no-slip condition which forces τ_{rr} to be zero on the surface. Figures 5, 6 and 7 are plots of the Newtonian values of the streamfunction, vorticity and τ_{rr} for a bubble. Once again the fore-aft symmetry of the flow is apparent. The effect of the free shear stress boundary condition is to cause the streamlines to become "flatter" and displaced slightly closer to the sphere. A second feature, which will play an important part in understanding the results for viscoelastic fluids is that the normal stress component, τ_{rr}, is approximately three times larger near the bubble than it was near the solid sphere, reflecting a similar difference in the magnitude of the corresponding diagonal component of the rate of strain (or velocity gradient) tensor. These changes, relative to the solid sphere, are consistent with the idea that the bubble boundary exerts less shear force on the fluid than a solid sphere. Indeed, the shear stress $\tau_{r\theta}$ is identically zero in the case of the bubble in a Newtonian fluid. In both of the Newtonian solutions, the plots of $\tau_{\theta\theta}$ and $\tau_{\phi\phi}$ have the same appearance as the plot of τ_{rr}, but with different numerical values, which again reflect

the presence of larger values for the $\theta\theta$ and $\phi\phi$ components of the rate of strain tensor in the case of the bubble. These first seven plots are shown here for comparison with the viscoelastic plots detailed in the remainder of this section.

In all of the solutions to follow, the viscosity ratio, ε, was assigned the value 0.2. This value was arbitrarily chosen as being larger than 1/9 and still small enough to provide a "reasonable" amount of shear thinning. One of the ways of checking the accuracy of the numerical results is to compare them, in the limit of small Wi, with available asymptotic solutions for the n^{th}-order fluid models. One comparison between the numerical and asymptotic (3^{rd}-order fluid) theories is shown in Table 1, where we list the results for the drag for all cases considered. For the smallest two values of Wi shown, namely 0.1 and 1/3, the agreement between the numerical and analytical values is extremely good. We shall return to discuss the results of Table 1 in more detail later. However, one remarkable feature which can be mentioned here is the fact that asymptotic results are very close to the numerical ones up to Wi of at least 2/3 for all cases except the spherical bubble with $\alpha = 1$ where they show significant differences at somewhat lower values. The level of agreement is especially surprising in view of the fact that the analytical results are based on only three terms of an asymptotic theory which is strictly valid for $Wi \ll 1$. There has, of course, been some previous indication in other problems of the fact that the n^{th}-order fluid approximation may provide qualitatively correct results for finite values of Wi (cf. Leal 1975, Ho and Leal 1976, Chan and Leal 1979, Rivlin 1976, Giesekus 1976), but the present results are the first which afford the possibility of a

detailed numerical comparison with 'exact' results for a fully nonlinear constitutive model. Thus, in the following discussion we examine more closely the correspondence between the numerically calculated results for the constitutive model given by equation (1) and analytical results for both the second- and third-order fluid approximations. In all of the figures to follow, the points are the values from the numerical solution and the solid lines are computed from asymptotic solutions.

Figures 8 - 13 show the numerical results for flow past a solid sphere, as well as the analytical solution for a second-order fluid, for Wi = 2/3 and $\alpha = 1$. Figures 14 - 20 show the same numerical results but with the analytical solution for the third-order fluid. It is useful to recall that the constitutive model, equation (1), for $\alpha = 1$ exhibits a positive primary (or first) normal stress difference in simple shear flow, but zero second normal stress difference and a shear-rate independent viscosity. In axisymmetric extensional flow, the apparent viscosity increases rapidly as a function of the strain rate for the uniaxial case, but decreases in absolute value and changes sign in the biaxial configuration.

Prior to any attempt to discuss the details of the various plots (8) - (20) in terms of the rheological properties of the fluid in the simple rheometric flows, a few general observations about the results can be made. First, and most surprising, is the very good agreement between the numerical results for the full constitutive model, and the analytical solutions for both the second- and third-order fluids, evaluated at the same Weissenberg (Wi) number. There are considerable qualitative changes relative to the Newtonian solution, particularly in the various stress components, and the analytic solutions represent only the first two and

three terms, respectively, in an asymptotic sequence for Wi → 0. It is apparent that the n^{th}-order fluid, retarded-motion approximation provides an excellent quantitative fit to the exact (numerical) solution over a much wider range of Wi than could have been anticipated. Furthermore, in spite of the fact that the shear-viscosity is constant for $\alpha = 1$, both in the equation (1) and its retarded-motion approximation, there is a considerable modification in the shear stress distribution. We shall discuss the results for $\tau_{r\theta}$ in somewhat more detail below. However, it is evident that the shear stress field changes significantly for flow past a sphere even though consideration of rheological data in simple shear flow and in extensional flows, the two identifiable "components" of the motion around a sphere, would have suggested that little or no change should occur for a fluid with constant shear viscosity. Thus, anticipating similar results to be presented later in this section, it may be concluded that even a well-developed understanding of the fluid's behavior in simple shear or extensional flows will not totally suffice for qualitative "a priori" predictions of fluid response in the more complicated streaming flow past a solid sphere — in spite of the fact that the latter would appear to be dominated by shear flow near the surface and by extensional flow farther out into the fluid. It is the coupling between shear and normal stress components which arises from the non-Cartesian geometry of the velocity field that leads to the predicted changes in $\tau_{r\theta}$ for flow around a sphere, and such coupling effects simply do not exist in the simpler unidirectional or Cartesian geometries of the rheological flows.

Let us now turn to a more detailed consideration of the individual figures 14 - 20. If we compare these figures with the Newtonian fields

represented by figures 1 - 4, it is evident that the most striking manifestations of viscoelastic fluid behavior are in the stress components $\tau_{\theta\theta}$ and $\tau_{r\theta}$, though easily discernible changes also occur for τ_{rr}, $\tau_{\phi\phi}$ and the vorticity ω. It is of interest to see whether at least some of these changes can be understood in terms of fluid behavior in simpler flows ($\alpha = 1$). Let us first consider $\tau_{\theta\theta}$. Near the sphere surface, the velocity components u_r, u_θ, u_ϕ are all very small and the motion is closely related to a simple shearing motion, involving $u_\theta = u_\theta(r)$, and the constitutive equations (6) - (10), reduce, for this type of flow, essentially to those for a <u>viscometric</u> flow. For such a flow, the fluid's memory, as fluid elements convect through the space, is <u>not</u> an important factor, but it is expected for $\alpha = 1$ that the primary normal stress difference, $\tau_{\theta\theta} - \tau_{rr}$, should be positive, the second normal stress difference <u>zero</u>, $\tau_{rr} - \tau_{\phi\phi} \equiv 0$, and the shear stress field unchanged from its Newtonian form. Since τ_{rr} can be shown to be <u>zero</u> on the sphere's surface for $\alpha = 1$, it follows that $\tau_{\phi\phi}$ must be zero and further that $\tau_{\theta\theta}$ must be <u>positive</u> everywhere on the sphere surface. It is clearly the surface contribution to $\tau_{\theta\theta}$, associated with the existence of a positive first normal stress difference in simple shear flow, which is responsible for the strongly skewed and altered pattern for $\tau_{\theta\theta}$ in figure 16. In simple shear flow, N_1 increases with the shear rate and in the present interpretation of the flow near the surface of the rigid sphere, this would imply that the non-Newtonian contribution to $\tau_{\theta\theta}$ should increase locally on the surface with increase in $e_{r\theta}$. The latter is, of course, equal to zero at the front and back stagnation points and increases to a maximum at the equator. Examination of the surface values for $\tau_{\theta\theta}$, which

are plotted in figure 21, shows that they do, in fact, increase also in the manner expected to a maximum in the vicinity of the equator, thus again supporting the contention that the observed changes in $\tau_{\theta\theta}$ are a result of a nonzero primary normal stress difference in the simple shear-like flow which exists near the surface. The fact that $\tau_{\theta\theta}/e_{r\theta}^2$ is not exactly constant (figure 21) for the larger values of Wi, provides an indication of the degree of departure of the full fluid model (1) from the n^{th}-order fluid limit where $\tau_{\theta\theta}$ increases as $e_{r\theta}^2$. We have already noted that the non-Newtonian contributions to the other two normal stress components, resulting from the shear-flow behavior, will be <u>zero</u> at the surface and presumably small elsewhere. Thus, any changes in the fields τ_{rr} or $\tau_{\phi\phi}$ must be associated primarily with other effects. One <u>obvious</u> candidate is the extensional nature of the fluid's motion as it moves around the sphere. In the upstream portion of the velocity field (and especially near the symmetry axis), this flow resembles a biaxial extension with $e_{\theta\theta}$ and $e_{\phi\phi}$ positive, while e_{rr} is negative. Thus, the stress components $\tau_{\theta\theta}$ and $\tau_{\phi\phi}$ would be increased by the viscoelastic nature of the fluid if the flow were, in fact, a quasi-steady biaxial extension, while τ_{rr} would be decreased in absolute value. On the other hand, behind the sphere, $e_{\theta\theta}$ and $e_{\phi\phi}$ are negative while e_{rr} is positive and the flow resembles a uniaxial extension. In this case, if the flow were quasi-steady, the stress component τ_{rr} would increase for a viscoelastic fluid, while both $\tau_{\theta\theta}$ and $\tau_{\phi\phi}$ would decrease in magnitude. When superposed on the stress fields for the Newtonian fluid these changes would appear as an increase in the magnitude of $\tau_{\theta\theta}$ and $\tau_{\phi\phi}$ upstream and a decrease in absolute values downstream thus leading to the appearance of a downstream shift in the countour plots of figures 17 and 18. The axial stress component, τ_{rr}, on the other hand

would be expected to exhibit smaller absolute (i.e. less negative) values upstream and more positive values downstream, thus appearing to shift the lines of constant τ_{rr} in the upstream direction. Examination of the plots in figures 16, 17 and 18 (or 10, 11 and 12) for τ_{rr}, $\tau_{\theta\theta}$ and $\tau_{\phi\phi}$ shows that $\tau_{\theta\theta}$ and $\tau_{\phi\phi}$ both appear to be shifted in the downstream direction, though the effect is somewhat obscured for $\tau_{\theta\theta}$ by the surface shear contribution which was described earlier. Close comparison of $\tau_{\phi\phi}$ with the corresponding plot of figure 3 for a Newtonian fluid shows clearly the existence of larger positive values for $\tau_{\phi\phi}$ upstream of the sphere, and less negative (i.e. smaller absolute) values downstream just as suggested by the qualitative discussion above. Furthermore, it is evident in figure 16 (or 10) that the stress component τ_{rr} has increased positive values downstream of the sphere, relative to the Newtonian fluid, and less negative (smaller absolute) values upstream, again in qualitative accord with the existence of a significant contribution of quasi-steady extensional flow to the stress fields around the sphere. Although the qualitative behavior of the fluid in steady shear and extensional flows thus appears to largely account for the results obtained for the normal stress components τ_{rr}, $\tau_{\theta\theta}$ and $\tau_{\phi\phi}$ in flow past a solid sphere, at least for $\alpha = 1$ and $Wi = 2/3$, it should be noted that there is at least one further mechanism available which may lead to skewness in the stress and velocity fields for a viscoelastic fluid. Indeed, a factor which we have not considered above is that the flow around the sphere is <u>unsteady</u> in a Lagrangian sense, and this would be expected to imply the existence of additional changes in the stress (or velocity) distributions due to the finite "memory" of a fluid element for past configurations. In the

constitutive equation, (1), these "memory" effects can be identified primarily with the convection term, $\underline{u}\cdot\nabla\underline{\underline{\tau}}$, since other nonlinear terms involving products of $\underline{\underline{e}}$ and $\underline{\underline{\tau}}$ or $\underline{\underline{\omega}}$ and $\underline{\underline{\tau}}$ persist even in Langrangian steady flows such as simple shear flow. The idea of "memory" in the fluid is a consequence of finite "intrinsic" relaxation and retardation times in the fluid, coupled with a Lagrangian unsteadiness in the deformation of a fluid element as it is convected around the sphere. In the region upstream of the sphere, the fluid "remembers" the lower stress level it had far upstream and the magnitude of the non-Newtonian contribution to the stresses in this region is expected to be decreased, in absolute value, relative to the values in the absence of any "memory" effects. Consequently, the contours of constant stress will be displaced inward towards the sphere in this part of the domain. Similar reasoning will lead to a downstream shift of the stress contours behind the sphere relative to their position in the absence of any memory effects. Although it may be expected that these "memory" effects are present in the results represented by figures 14 - 20 (or 8 - 13), it is difficult to determine their importance for the normal stress components, τ_{rr}, $\tau_{\theta\theta}$ and $\tau_{\phi\phi}$ due to the simultaneous presence of streamwise shifting from the presence of the strain-rate dependent extensional viscosity effect which was described above. To obtain an indication of the importance of "memory" effects we must wait until we consider the numerical results for $\alpha = 0$ where the extensional viscosity is constant. Figure 20 is a plot of the "pressure" contours (remember that the "pressure" in this case is only an isotropic term which is necessary to solve the equations of motion). The contours are shifted downstream from the corresponding Newtonian fluid contours, possibly as a

consequence of the fluid's memory. Finally, we can consider the shear stress component, $\tau_{r\theta}$. We have noted above that the shear viscosity for $\alpha = 1$ is constant. Thus, the major non-Newtonian contributions to $\tau_{r\theta}$ arise from the streamline curvature and resultant coupling between $\tau_{r\theta}$ and the normal stress components τ_{rr} and $\tau_{\theta\theta}$. We note that the countours of constant shear stress, shown in figure 13, are shifted upstream at moderate distances out from the sphere, while the contours closest to the sphere are shifted downstream (i.e. in the opposite direction). The upstream shift evident at the larger distances is caused by the interaction of τ_{rr} and $\tau_{\theta\theta}$ with u_θ/r — i.e. it is caused by the curvature terms which arise from $\underline{u}\cdot\nabla\underline{\underline{\tau}}$ when the constitutive equation is transformed from rectangular to spherical coordinates. The downstream shift nearer the sphere is brought about by a similar interaction between τ_{rr}, $\tau_{\theta\theta}$ and $\omega_{r\theta}$ in the terms which appear in the co-rotational time derivative. It should be noted, in this regard, that the upstream shift is dominant for large r because u_θ/r decreases as $1/r$, whereas $\omega_{r\theta}$ falls off as $1/r^2$. Nearer the sphere, on the other hand, $u_\theta/r \sim (r - 1)/r \to 0$, while the vorticity approaches a nonzero constant and the downstream shift is dominant. Finally, we may note that the streamfunction and vorticity are both shifted very slightly downstream relative to their contours in a Newtonian fluid. Although this shift might at first appear to be another manifestation of the fluid's memory, this is not correct since the presence of "memory" is independent of α while the downstream shift occurs for $\alpha = 1$ but not for $\alpha = 0$. It appears that the shift in the streamfunction and vorticity are more closely related to the skewed stress distributions which arise from the quasi-steady shear and extensional flows near the sphere surface.

Plots of the streamfunction, vorticity, stress components and pressure for flow past a rigid sphere with Wi = 2/3 and α = 0 are shown in figures 22 - 28. In addition, more detailed plots for τ_{rr} and $\tau_{\theta\theta}$ are given, in figures 29 and 30, for the region immediately adjacent to the sphere. The constitutive model, with α = 0, exhibits a shear-thinning viscosity, and nonzero first and second normal stress differences (with $N_2 = -\frac{1}{2} N_1$) in simple shear flow, but has a constant apparent viscosity in axisymmetric extensional flows. As in the case, α = 1 and Wi = 2/3, there is excellent agreement between the analytical results — here, for a third-order fluid — and the numerical results based on the full constitutive model, equation (1). The present discussion will focus on a comparison of the results for the two limiting cases, α = 0 and α = 1, and specifically on the manner in which the predicted changes in rheological behavior for simple shear flow and uniaxial/biaxial extension (indicated above) are reflected in changes in the solutions for flow past a sphere. The two most obvious differences between the solutions for α = 0, and those discussed above for α = 1, are that the normal stress component τ_{rr} is dramatically changed near the sphere surface to a form which is at least superficially similar to $\tau_{\theta\theta}$, and that the streamlines, constant vorticity contours and shear stress contours are all shifted significantly inward toward the sphere surface. More subtle, but also evident, is the fact that the normal stress components $\tau_{\theta\theta}$ and $\tau_{\phi\phi}$ are more nearly symmetric, i.e. <u>less</u> shifted in the downstream direction. Let us consider the physical reasons for these changes, beginning with the dramatic changes in τ_{rr}. As in the case, α = 1, the flow field very near the sphere surface is dominantly shear in nature and this suggests that

the explanation for changes in the stress fields near the surface should lie in changes in the behavior of the model fluid, equation (1), for simple shear flow as α is changed from 1 to 0. Indeed, two new rheological features do appear for $\alpha = 0$, as noted above. The shear viscosity now decreases as the shear rate increases, while the second normal stress difference, N_2, is nonzero and equal to $-\frac{1}{2} N_1$ (where N_1 is the magnitude of the primary normal stress difference). Thus, since $N_1 > 0$ and increasing with shear rate in simple shear flow, we should expect $\tau_{\theta\theta} - \tau_{rr} > 0$ in the flow near the sphere surface, while $\tau_{rr} - \tau_{\phi\phi}$ $(= N_2) < 0$, with both increasing in magnitude near the equator where $e_{r\theta}$ is maximum. Since $\tau_{\phi\phi} \equiv 0$ at the sphere surface (cf. equation 9), it follows that $\tau_{rr} < 0$ at the sphere surface and the contours of constant τ_{rr} are changed in the same qualitative manner as was described for $\tau_{\theta\theta}$ in the case $\alpha = 1$ (where τ_{rr} was identically zero at the surface since $N_2 = 0$ for $\alpha = 1$). The contours of constant $\tau_{\theta\theta}$ are similar to those found for $\alpha = 1$, and the reason for their modification relative to the Newtonian fluid solution is unchanged. It should be noted, however, that since $\tau_{rr} < 0$, the magnitude of $\tau_{\theta\theta}$ at the sphere surface is smaller than for the case $\alpha = 1$, and this contributes to a smaller apparent upstream skewing of the $\tau_{\theta\theta}$ contours in the case $\alpha = 0$. Indeed, since $N_2 = -\frac{1}{2} N_1$ in the simple shear flow, the magnitude of the surface values of $\tau_{\theta\theta}$ and τ_{rr}, i.e. $|\tau_{\theta\theta}|$ and $|\tau_{rr}|$, should be expected to be identical in flow past the sphere for $\alpha = 0$. Comparison of the contours of constant τ_{rr} and constant $\tau_{\theta\theta}$ in the latter case shows that they are, in fact, virtually identical in form near the sphere with only a change in sign differentiating one from the other. The presence of a shear-thinning viscosity for the case $\alpha = 0$ in a simple shear

flow is also clearly reflected in the solutions for flow past a sphere. In particular, the contours of constant ψ, ω and $\tau_{r\theta}$ are all shifted inward toward the sphere and this is highly reminiscent of the contour shifts obtained for purely viscous, shear thinning liquids. Changing the value of α also changes the fluid response in regions of quasi-steady extensional flow, such as exists upstream and downstream of the sphere near the axis of symmetry. The presence of the strong (shear flow) induced normal stress effects near the sphere surface largely obscures the effect of this change for τ_{rr} and $\tau_{\theta\theta}$. However, the third normal stress component, $\tau_{\phi\phi}$, is not directly affected by the shear flow behavior of the fluid. In the case $\alpha = 1$, we suggested earlier that there were two contributions tending to shift $\tau_{\phi\phi}$ contours downstream: one associated with the finite memory of the fluid and the other with the strain-rate dependence of the apparent viscosity in quasi-steady extensional flows. For $\alpha = 0$, however, the extensional viscosity is constant and $\tau_{\phi\phi}$ would be unchanged from its Newtonian value in either steady biaxial or uniaxial extensional flow. Thus, if our explanation for the changes in $\tau_{\phi\phi}$ for $\alpha = 1$ were correct, the $\tau_{\phi\phi}$ contours for $\alpha = 0$ should be less shifted downstream, showing only the effect of the fluid's memory. Comparison of figures 18 and 26 shows that this is indeed the case. Furthermore, comparison of figure 26 with the normal stress contours for a Newtonian fluid provides an indication of the relative strength of the memory effect. Finally, we may note that the pressure, streamfunction and vorticity contours are all shifted upstream slightly in the solution for $\alpha = 0$, whereas the same quantities were shifted very slightly downstream for $\alpha = 1$. It may be noted that experimental evidence obtained by Zana, Tiefenbruck and Leal

(1975) showed the existence of a small upstream shift in the streamlines. However, it is not evident to us how this shift may be explained on physical grounds.

Let us now turn our attention to the case of flow past a spherical bubble. This problem differs from that for flow past a solid sphere primarily due to the fact that the no-slip boundary condition is replaced by the zero shear stress condition ($e_{r\theta} = 0$) at the sphere surface so that the flow near the surface no longer has a strong shear flow component. Thus, the rheological behavior of the model material (equation 1) in shear flow should be much less important than for the solid sphere, while the extensional flow behavior and/or memory related effects should be relatively more important. This is especially true in view of the fact that the normal strain-rate components, e_{rr}, $e_{\theta\theta}$ and $e_{\phi\phi}$ are larger in the bubble problem than for the solid sphere.

Numerical results for streaming flow past a spherical bubble, as well as the analytic solution for third-order fluid, are shown in figures 31 - 37 for the case Wi = 2/3 and $\alpha = 0$. For most of the variables (ω and $\tau_{r\theta}$ being the notable exceptions) the analytical and numerical solutions show excellent agreement. The departures between these solutions, and the only significant deviations from fore-aft symmetry of the normal stress components, all occur in the downstream wake region immediately adjacent to the sphere. Since the fluid motion is dominantly extensional in character near the sphere, and because the model fluid (1) exhibits a constant extensional viscosity for $\alpha = 0$, it would appear that the fluid behavior responsible for these changes must represent an effect of the fluid's memory in a strongly transient elongational flow. Specifically, in the downstream

region, e_{rr} starts with a value near to zero at the equatorial plane and increases to a maximum at the downstream axis of symmetry. The consequences of this kinematic pattern are that the stress, τ_{rr}, is initially small near the equatorial plane and is kept lower than the Newtonian values over the whole rear of the sphere, as a consequence of the fluid's memory. As the fluid approaches the rear stagnation point, the rate of strain tensor approaches a maximum while the velocity goes to zero. The combined effect of these two phenomena is to cause the gradient of the stress component, τ_{rr}, to become very large in the vicinity of the rear stagnation point. This large gradient then exerts an effect on the vorticity as observed in figure 32. This explanation is supported by the work of Denn, Petrie and Avenas (1975). Figure 36 is a plot of $\tau_{r\theta}$ for the case Wi = 2/3, α = 0 for the bubble. Since $\tau_{r\theta}$ is identically zero throughout the flow domain for a Newtonian fluid, the points and contours in figure 36 arise solely because of the non-Newtonian nature of the constitutive equation. In contrast to the normal stresses which are well described by the third-order fluid solution, $\tau_{r\theta}$ shows a considerable difference from the asymptotic result. This plot indicates that we are outside the range of strict applicability of the asymptotic solution, though it is also evident that we can have a marked change in a stress component and still have relatively little impact on the kinematic variables. The pressure field is plotted in figure 37. The differences in the pressure field from the asymptotic results must be laid primarily to the $\tau_{r\theta}$ field, since the other stress components were accurately reproduced by the asymptotic results. The numerically calculated pressure can be shown to be influenced strongly by the shear stress distribution.

Since extensional flow effects appeared to play a significant role for the case of a bubble with $\alpha = 0$, we can expect much greater departures from the Newtonian solutions for the case of $\alpha = 1$. Figures 38 through 44 are the plots of the kinematic and stress quantities for the case of Wi = 2/3, $\alpha = 1$ for a spherical bubble. The streamfunction, vorticity, τ_{rr} and $\tau_{r\theta}$ all show appreciable differences from the asymptotic results. The cause of these striking changes appears to be the high levels of stress which are generated at the rear of the spherical bubble. To understand the source of these high levels of stress, we can examine equation (43) at the rear stagnation point. We find that $\tau_{rr}(31,1) = 2\varepsilon_{rr}(31,1)\left(1 - 2\varepsilon Wi\, e_{rr}(31,1)\right) / \left(1 - 2Wi\, e_{rr}(31,1)\right)$. For the Newtonian liquid, $e_{rr}(31,1) = 1.0$. Therefore as the Weissenberg number approaches 0.500, we can expect changes in the velocity gradients so as to reduce τ_{rr} in the rear wake region. Naturally, this high value of the stress also gives rise to a large stress gradient, which is the direct source of the changes in the velocity field. In essence, the much larger values of τ_{rr} in the downstream region result from the same strain-rate dependence of the extensional viscosity which caused the downstream shift in τ_{rr} for the rigid sphere with $\alpha = 1$. However, the effect is more pronounced for the bubble because the values of the strain rate e_{rr} are larger. The existence of fluid memory causes the high stress levels to persist for a considerable downstream distance, thereby extending the region influenced by the strain-rate dependent extensional viscosity. This effect on the contours of τ_{rr} is quite evident in figure 40, especially when compared to figure 33 for Wi = 2/3, $\alpha = 0$ and figure 7 for a Newtonian fluid. Note the extended region between the computed contours and the downstream axis of symmetry as compared to the third-order fluid

contours. The vorticity and $\tau_{r\theta}$ show also the effects of changing velocity gradients in this region. Clearly, the sharp change in the vorticity, τ_{rr}, and $\tau_{r\theta}$ contours at the back of the sphere is not "real". This apparent sharp change is due to the limited resolution of the grid in this region, thus making a linear interpolation, of the type used to draw the figures, inaccurate. To investigate whether the limited resolution in this region might effect the gross features of the solution (rather than simply appearing as a plotting 'error'), we have obtained a solution for the bubble with Wi = 2/3 and α = 1 in which the mesh size was halved in the η coordinate. We found that all of the stress and kinematic values remained unchanged on mesh points which were common with the larger grid. The representation of all of the quantities in the plots was improved between the second last and last rows before the downstream axis of symmetry, but there still remains a sharp change (in the plots) between the last row and the axis of symmetry. Figure 45 is a plot of the contours of vorticity for this fine mesh solution.

One additional feature of the solution for Wi = 2/3 and α = 1 is worth mentioning here. This is the skewing of the stress contours for $\tau_{\theta\theta}$ and $\tau_{\phi\phi}$. In the case α = 0, shown in figures 34 and 35, these components are only slightly skewed with respect to streamwise symmetry. Here, however, where α = 1, the extensional viscosity is strain-rate dependent and the influence of the relatively large magnitudes of $e_{\theta\theta}$ and $e_{\phi\phi}$ in flow past the bubble is to produce a strong skew in the contours of $\tau_{\theta\theta}$ and $\tau_{\phi\phi}$. The stress levels upstream of the sphere, where $e_{\phi\phi}$ and $e_{\phi\phi}$ are positive, are considerably enhanced relative to the values for either α = 0 or for a Newtonian fluid. Downstream, on the other hand, where $e_{\theta\theta}$ and $e_{\phi\phi}$ are

negative, the magnitude of the stresses is decreased.

For Weissenberg number equal to one, the solutions qualitatively exhibit the same type of behavior as shown above. The kinematic variables (particularly the streamfunction) show very little change from the asymptotic values, while the stress components show an increasing deviation from the third-order fluid solutions. Figures 46 - 53 are contours of various quantities for the solid sphere at Wi = 1 and α = 0,1. Solutions for the bubble with Wi = 1 and α = 1 are shown in figures 54 - 56. Solutions were also attempted for Weissenberg number greater than one. Using the algorithm detailed earlier, it was possible to systematically reduce the error (or residuals) in the vorticity, but the rate of convergence deteriorated rapidly and the solutions were not carried to complete convergence. The results of these partially converged solutions are not unreasonable, but their accuracy is in doubt, and we shall not report them here.

Perhaps the most important quantity that can be calculated from the solutions outlined in this section is the force that the fluid exerts on the sphere or bubble. For the case of a solid sphere, the results of Giesekus (1963) for a third-order fluid may be expressed in the form

$$\frac{\text{Drag}}{2\pi\eta_o U_\infty a} = 3\left[1 - \frac{Wi^2(1-\varepsilon)}{25025}(5439 - 143\varepsilon\alpha^2 - 5038\alpha^2)\right] \qquad (47)$$

For the case of a spherical bubble, the corresponding result has been derived by Tiefenbruck (1980)

$$\frac{\text{Drag}}{2\pi\eta_o U_\infty a} = 2\left[1 - \frac{Wi^2(1-\varepsilon)}{75}(18 - 25\alpha^2 - 2\alpha^2\varepsilon)\right] \qquad (48)$$

The results from the numerical solutions for the model fluid (1) are compared with equations (47) and (48) in Table 1. It is not surprising, in

view of the preceeding detailed comparisons between the analytical and numerical solutions, that the numerically calculated results for the drag are in good agreement with the asymptotic results, except for the case of the bubble when $\alpha = 1$. A point of particular interest in Table 1 is that the drag for the corotational model ($\alpha = 0$) is smaller than predicted by equations (47) and (48) and that the difference increases as the Weissenberg number increases.

In summary, we have developed an algorithm for the numerical solution of the motion of a viscoelastic liquid past a spherical obstacle. We have found that the results are reasonably well described by third-order fluid solutions up to Wi = 1 in most cases. The algorithm mimicks the usual Newtonian method of solution, and the convergence difficulties found for Wi > 1 are undoubtedly associated with the fact that elastic terms become increasingly important for Wi > 1 as the Weissenberg number is increased.

APPENDIX: Far Field Boundary Conditions

The derivation of the far-field boundary conditions is much simpler if we employ several assumptions. The first assumption is that we are far enough away from the sphere that its effect on the fluid may be described by a point force. The second assumption is that

$$\underline{u} = \underline{i} + \underline{u}'; \quad \underline{\underline{e}} = \underline{\underline{e}}'; \quad \underline{\underline{w}} = \underline{\underline{w}}'; \quad \underline{\underline{\tau}} = \underline{\underline{\tau}}' \text{ and } p = p' \tag{A1}$$

where $\underline{i}$ is the unit vector in the direction $\theta = 0$ and all of the primed quantities tend to zero as $r \to \infty$. When we substitute (A1) into the constitutive equation and neglect any term which is quadratic in the primed variables we obtain

$$\underline{\underline{\tau}}' + Wi \frac{\partial \underline{\underline{\tau}}'}{\partial x} = 2\underline{\underline{e}}' + 2\varepsilon Wi \frac{\partial \underline{\underline{e}}'}{\partial x} \tag{A2}$$

We now use the first assumption to write the equation of motion as

$$\nabla p' = \nabla \cdot \underline{\underline{\tau}}' + 8\pi \underline{\beta} \delta(\underline{x}) \tag{A3}$$

where $\underline{\beta}$ is a constant vector which characterizes the magnitude and direction of the point force which represents the sphere and $\delta(\underline{x})$ is the three-dimensional delta function. Recall from potential flow theory that

$$\underline{\beta}\delta(\underline{x}) = -\frac{1}{4\pi} \nabla^2 (\underline{\beta}/r) \tag{A4}$$

Now substituting (A4) into (A3) and combining the result with (A2), we obtain

$$(1 + Wi \frac{\partial}{\partial x}) \nabla p' = (1 + \varepsilon Wi \frac{\partial}{\partial x}) \nabla^2 \underline{u}' - 2(1 + Wi \frac{\partial}{\partial x}) \nabla^2 (\underline{\beta}/r) \qquad (A5)$$

Now we take the divergence of equation (A5) and solve the resulting equation for p' to obtain

$$p' = 2(\underline{\beta} \cdot \underline{x})/r^3 \qquad (A6)$$

If we now take the curl of equation (A5) and solve for the vorticity, we obtain

$$(1 + \varepsilon Wi \frac{\partial}{\partial x}) \underline{\omega}' = (1 + Wi \frac{\partial}{\partial x}) \frac{2\underline{\beta} \otimes \underline{x}}{r^3} \qquad (A7)$$

which can be further simplified to

$$\omega_x' = 2 \frac{(\beta_2 z - \beta_3 y)}{r^3} - 6Wi(1 - \varepsilon) \frac{(\beta_2 xz - \beta_3 xy)}{r^5} + 0\left(\frac{\varepsilon Wi^2}{r^4}\right) \qquad (A8a)$$

$$\omega_y' = 2 \frac{(\beta_3 x - \beta_1 z)}{r^3} - 6Wi(1 - \varepsilon) \frac{(\beta_3 x^2 - \beta_1 xz)}{r^5} + \frac{2\beta_3 Wi(1 - \varepsilon)}{r^3} + 0\left(\frac{\varepsilon Wi^2}{r^4}\right) \qquad (A8b)$$

$$\omega_z' = 2 \frac{(\beta_1 y - \beta_2 x)}{r^3} - 6Wi(1 - \varepsilon) \frac{(\beta_1 xy - \beta_2 x^2)}{r^5} - \frac{2\beta_2 Wi(1 - \varepsilon)}{r^3} + 0\left(\frac{\varepsilon Wi^2}{r^4}\right) \qquad (A8c)$$

Using the usual method of obtaining a velocity field from a known vorticity field [see Batchelor (1967)], we obtain

$$u_x' = \frac{\beta_1}{r} + \frac{x(\underline{\beta} \cdot \underline{x})}{r^3} - Wi(1 - \varepsilon)\left(\frac{3x^2(\underline{\beta} \cdot \underline{x})}{r^5} - \frac{\beta_1 x}{r^3}\right) \qquad (A9a)$$

$$u'_y = \frac{\beta_2}{r} + \frac{y(\underline{\beta}\cdot\underline{x})}{r^3} - Wi(1-\varepsilon)\left(\frac{3xy(\underline{\beta}\cdot\underline{x})}{r^5} - \frac{\beta_1 y}{r^3}\right) \tag{A9b}$$

$$u'_z = \frac{\beta_3}{r} + \frac{z(\underline{\beta}\cdot\underline{x})}{r^3} - Wi(1-\varepsilon)\left(\frac{3xy(\underline{\beta}\cdot\underline{x})}{r^5} - \frac{\beta_1 z}{r^3}\right) \tag{A9c}$$

For an <u>axisymmetric</u> problem like the one under consideration here, $\beta_2 = \beta_3 = 0$. Employing this simplification and expressing the velocities in spherical coordinates, we obtain

$$u'_r = \frac{2\beta_1\cos\theta}{r} - \frac{Wi(1-\varepsilon)\beta_1(3\cos^2\theta - 1)}{r^2} \tag{A10a}$$

$$u'_\theta = -\frac{\beta_1\sin\theta}{r} \tag{A10b}$$

These velocities correspond to a streamfunction given by

$$\psi = \beta_1[r - Wi(1-\varepsilon)\cos\theta]\sin^2\theta \tag{A11}$$

Calculation of the far field stresses is now easily carried out and the results are given in equation (26) in the body of this work.

References

Akay and Kaye, Proc. VII Int. Congress on Rheology, 554 (1976).

Batchelor, "Introduction to Fluid Dynamics", Cambridge University Press, Cambridge, England, 84-87 (1967).

Caswell and Schwarz, J. Fluid Mechanics 13, 417 (1962).

Caswell and Tanner, Polymer Eng. Sci. 18, 416 (1978).

Chan and Leal, J. Fluid Mechanics , to appear in (1979)

Crochet and Pilate, Computers and Fluids 3, 283 (1975).

Crochet and Pilate, I.U.T.A.M. Congress, Delft, paper no. 598 (1976).

Denn, Petrie and Avenas, AIChEJ 21, 791 (1975).

Dorr, SIAMJ 12, 248 (1970).

Gatski and Lumley, J. Comp. Phys. 27, 42 (1978).

Giesekus, Rheologica Acta 3, 59 (1963).

Gilligan and Jones, Z. Angew. Math. Phys. 21, 786 (1970).

Hamielec, Hoffman and Ross, AIChEJ. 13, 212 (1967).

Isaacson and Keller, "Analysis of Numerical Methods", John Wiley and Sons, Inc., New York (1966).

Jenson, Proc. Roy. Soc. A249, 346 (1959).

Kawaguti, Rep. Inst. Sci. Tokyo 4, 154 (1950).

Kawahara and Takeuchi, Computers and Fluids 5, 33 (1977).

Lamb, H., "Hydrodynamics", Dover Publications, New York, 123 (1945).

Leal, Skoog and Acrivos, Can. J. Ch. E. 49, 569 (1971).

Leslie, Quart. J. Appl. Math. and Mech. 14, 36 (1961).

Oldroyd, Proc. Roy. Soc., A245, 278 (1958).

Orzag and Israeli, Ann. Rev. of Fl. Mech. 6, (1974).

Osee, Ark. f. Mat. Astr. og Fys. 6, 29 (1910).

Perera and Walters, J. Non-Newt. Fl. Mech. 2, 49 (1977a).

Perera and Walters, J. Non-Newt. Fl. Mech. 2, 191 (1977b).

Pilate and Crochet, J. Non-Newt. Fl. Mech. 2, 323 (1977).

Proudman and Pearson, J. Fluid Mech. 2, 237 (1957).

Rao and Rao, J. Eng. Math. 4, 209 (1970).

Robertson, Seinfeld and Leal, AIChEJ 19, 998 (1973).

Stokes, Camb. Phil. Trans. 9, 8 (1851).

Tanner, Nickell and Bilger, Comp. Meth. Appl. Mech. and Eng. 6, 155 (1975).

Taylor and Hood, Computers and Fluids 1, 73 (1973).

Tiefenbruck, PhD Thesis, Calif. Inst. of Technology (1980).

Tiefenbruck and Leal, J. Non-Newt. Fl. Mech., to appear (1979).

Towsend, Rheologica Acta 12, 13 (1973).

Ultman and Denn, Chem. Eng. J. 2, 81 (1971).

Wasserman and Slattery, AIChEJ 10, 383 (1964).

Yoshioka, Adachi and Ishimura, Kogaku Kogaku 35, 1147 (1971).

Zana and Leal, Int. J. Multiphase Flow 4, 237 (1978).

Zana, Tiefenbruck and Leal, Rheologica Acta 14, 891 (1975).

Table 1. Drag[†] on Rigid Spheres and Spherical Bubbles

	Solid Sphere				Spherical Bubble			
Wi	$\alpha = 0$		$\alpha = 1$		$\alpha = 0$		$\alpha = 1$	
	Eqn. (47)	Numerical	Eqn. (47)	Numerical	Eqn. (48)	Numerical	Eqn. (49)	Numerical
0.1	2.995	2.983	2.9997	2.999	1.996	1.994	2.002	2.003
1/3	2.942	2.93	2.997	2.997	1.957	1.93	2.020	2.026
2/3	2.768	2.71	2.984	2.985	1.829	1.76	2.085	2.37
1	2.478	2.35	2.964	2.98	1.616	1.53	2.192	2.98

[†]The values listed represent the actual drag divided by $2\pi\mu aU$.

Figure Captions

Figure 1. Streamlines for the flow of a Newtonian fluid past a sphere. The streamline values are A = 0.05, B = 0.20, C = 0.50, D = 1.0, E = 2.0, F = 3.0, G = 4.0, # = 5.0.

Figure 2. Lines of constant vorticity in a Newtonian fluid for flow past a sphere. A = -1.01, B = -0.50, C = -0.25, D = -0.125, E. = -0.0625.

Figure 3. Lines of constant τ_{rr} for the flow of a Newtonian fluid past a sphere. A = -0.45, B = -0.30, C = -0.15, D = +0.15, E = +0.30, F = +0.45.

Figure 4. Lines of constant $\tau_{r\theta}$ for the flow of a Newtonian fluid past a sphere. A = -1.0, B = -0.25, C = -0.0625, D = -0.015625, E = -0.00390625.

Figure 5. Streamlines for the flow of a Newtonian fluid past a bubble. A = 0.05, B = 0.20, C = 0.50, D = 1.0, E = 2.0, F = 3.0, G. - 4.0, H = 5.0.

Figure 6. Lines of constant vorticity for the flow of a Newtonian fluid past a bubble. A = -0.75, B = -0.375, C = -0.1875, D = -0.09375, E = -0.046875.

Figure 7. Lines of constant τ_{rr} for the flow of a Newtonian fluid past a bubble. A = -1.25, B = -0.45, C = -0.15, D = -.15, E - 0.45, F = 1.25.

Figure 8. Lines of constant ψ for a sphere. Wi = 2/3, α = 1. Asymptotic results are for a second-order fluid. A = 0.05, B = 0.20, C = 0.50, D = 1.0, E = 2.0, F = 3.0, G = 4.0, H - 5.0.

Figure 9. Lines of constant ω for a sphere, Wi = 2/3, α = 1. Asymptotic results are for a second-order fluid. ○ = -1.00, Δ = -0.500, t = -0.25, x = -0.125, ◇ = -0.0625.

Figure 10. Lines of constant τ_{rr} for a sphere, Wi = 2/3, α = 1. Asymptotic results are for a second-order fluid. A = -0.45, B = -0.30, C = -0.15, D = 0.15, E = 0.30, F = 0.45.

Figure 11. Lines of constant $\tau_{\theta\theta}$ for a sphere, Wi = 2/3, α = 1. Asymptotic results are for a second-order fluid. A = -0.225, B = -0.150, C = -0.075, D = 0.075, E = 0.150, F = 0.225.

Figure 12. Lines of constant $\tau_{\phi\phi}$ for a sphere, Wi = 2/3, α = 1. Asymptotic results are for a second-order fluid. A = -0.225, B = -0.150, C = -0.075, D = 0.075, E = 0.150, F = 0.225.

Figure 13. Figure 13. Lines of constant $\tau_{r\theta}$ for a sphere, Wi = 2/3, α = 1. Asymptotic results are for a second-order fluid. ○ = -1.00, Δ = -0.250, t = -0.0625, x = -0.015625.

Figure 14. Lines of constant ψ for a sphere, Wi = 2/3, α = 1. Asymptotic results are for a third-order fluid. A = 0.05, B = 0.20, C = 0.5, D = 1.0, E = 2.0, F = 3.0, G = 4.0, H = 5.0.

Figure 15. Lines of constant ω for a sphere, Wi = 2/3, α = 1. Asymptotic results are for a third-order fluid. ○ = -1.00, Δ = -0.500, t = -0.25, x = -0.125, ◇ = -0.0625.

Figure 16. Lines of constant τ_{rr} for a sphere, Wi = 2/3, α = 1. Asymptotic results are for a third-order fluid. A = -0.45, B = -0.30, C = -0.15, D = 0.15, E = 0.30, F = 0.45.

Figure 17. Lines of constant $\tau_{\theta\theta}$ for a sphere, Wi = 2/3, α = 1. Asymptotic results are for a third-order fluid. A = -0.225, B = -0.15, C = -0.075, D = 0.075, E = 0.15, F = 0.225.

Figure 18. Lines of constant $\tau_{\phi\phi}$ for a sphere, Wi = 2/3, α = 1. Asymptotic results are for a third-order fluid. A = -0.225, B = -0.150, C = -0.075, D = 0.075, E = 0.150, F = 0.225.

Figure 19. Lines of constant $\tau_{r\theta}$ for a sphere, Wi = 2/3, α = 1. Asymptotic results are for a third-order fluid. ○ = -1.00, Δ = -0.250, + = 0.0625, x = -0.015625.

Figure 20. Lines of constant p for a sphere, Wi = 2/3, α = 1. Asymptotic results are for a third-order fluid. A = 0.90, B = 0.30, C = 0.10, D = -0.10, E = -0.30, F = -0.90.

Figure 21. Ratio of $\tau_{\theta\theta}/e_{r\theta}^2$ for various values of Wi, α = 0. ○ = 0.1, Δ = 0.33, + = 0.667.

Figure 22. Lines of constant ψ for a sphere, Wi = 2/3, α = 0. A = 0.05, B = 0.20, C = 0.50, D = 1.0, E = 2.0, F = 3.0, G = 4.0, H = 5.0.

Figure 23. Lines of constant ω for a sphere, Wi = 2/3, α = 0. ○ = -1.0, Δ = -0.50, + = -0.25, x = -0.125, ◇ = -0.0625.

Figure 24. Lines of constant τ_{rr} for a sphere, Wi = 2/3, α = 0. A = -0.45, B = -0.30, C = -0.15, D = 0.15, E = 0.30, F = 0.45.

Figure 25. Lines of constant $\tau_{\theta\theta}$ for a sphere, Wi = 2/3, α = 0. A = -0.225, B = -0.150, C = -0.075, D = 0.075, E = 0.150, F = 0.225.

Figure 26. Lines of constant $\tau_{\phi\phi}$ for a sphere, Wi = 2/3, α = 0. A = -0.225, B = -0.150, C = 0.075, D = 0.075, E = 0.150, F = 0.225.

Figure 27. Lines of constant $\tau_{r\theta}$ for a sphere, Wi = 2/3, α = 0. ○ = -1.00, Δ = -0.250, + = -0.0625, x = -0.015625, ◇ = -0.00390625.

Figure 28. Lines of constant p for a sphere, Wi = 2/3, α = 0. A = 0.90, B = 0.30, C = 0.10, D = -0.10, E = -0.30, F = -0.90.

Figure 29. Lines of constant τ_{rr} near the sphere, Wi = 2/3, α = 0. A = -0.45, B = -0.30, C = -0.15, D = 0.15, E = 0.30, F = 0.45.

Figure 30. Lines of constant $\tau_{\theta\theta}$ near the sphere, Wi = 2/3, α = 0. A = -0.225, B = -0.150, C = -0.075, D = 0.075, E = 0.150, F = 0.225.

Figure 31. Lines of constant ψ for a bubble, Wi = 2/3, α = 0. A = 0.05, B = 0.20, C = 0.50, D = 1.0, E = 2.0, F = 3.0, G = 4.0, H = 5.0.

Figure 32. Lines of constant ω for a bubble, Wi = 2/3, α = 0. ○ = -0.75, Δ = -0.375, + = -0.1875, x = -0.09375, ◇ = -0.046875.

Figure 33. Lines of constant τ_{rr} for a bubble, Wi = 2/3, α = 0. A = -1.25, B = -0.45, C = -0.15, D = 0.15, E = 0.45, F = 1.25.

Figure 34. Lines of constant $\tau_{\theta\theta}$ for a bubble, Wi = 2/3, α = 0. A = -0.625, B = -0.225, C = -0.075, D = 0.075, E = 0.225, F = 0.625.

Figure 35. Lines of constant $\tau_{\phi\phi}$ for a bubble, Wi = 2/3, α = 0. A = -0.625, B = -0.225, C = -0.075, D = 0.075, E = 0.225, F = 0.625.

Figure 36. Lines of constant $\tau_{r\theta}$ for a bubble, Wi = 2/3, α = 0. ○ = 0.05, Δ = 0.025, + = 0.0125, x = -0.0125, ◇ = -0.025, ⍋ = -0.05.

Figure 37. Lines of constant p for a bubble, Wi = 2/3, α = 0. Δ = 0.15, + = 0.05, x = -0.05, ◇ = -0.15, ⍋ = -0.45.

Figure 38. Lines of constant ψ for a bubble, Wi = 2/3, α = 1. ○ = 0.05, Δ = 0.20, + = 0.50, x = 1.0, ◇ = 2.0, ⍋ = 3.0, X̄ = 4.0, Z = 5.0.

Figure 39. Lines of constant ω for a bubble, Wi = 2/3, α = 1. ○ = -0.75, Δ =-0.375, + = -0.1875, x = -0.09375, ◇ = -0.046875.

Figure 40. Lines of constant τ_{rr} for a bubble, Wi = 2/3, α = 1. Δ = -0.45, + = -0.15, x = 0.15, ◇ = 0.45, ⍋ = 1.25.

Figure 41. Lines of constant $\tau_{\theta\theta}$ for a bubble, Wi = 2/3, α = 1.
Δ = -0.225, + = -0.075, x = 0.075, $\diamond$ = 0.225, Φ = 0.625.

Figure 42. Lines of constant $\tau_{\phi\phi}$ for a bubble, Wi = 2/3, α = 1.
Δ = -0.225, + = -0.075, x = 0.075, $\diamond$ = 0.225, Φ = 0.625.

Figure 43. Lines of constant $\tau_{r\theta}$ for a bubble, Wi = 2/3, α = 1.
$\bigcirc$ = 0.005, Δ = 0.025, + = 0.0125, x = -0.0125, $\diamond$ = -0.025,
Φ = -0.05.

Figure 44. Lines of constant p for a bubble, Wi = 2/3, α = 1. Δ = -0.225,
+ = -0.075, x = 0.075, $\diamond$ = 0.225, Φ = 0.675.

Figure 45. Lines of constant ω for a refined mesh for a bubble, Wi = 2/3,
α = 1. $\bigcirc$ = -0.75, Δ = -0.375, + =-0.1875, x = -0.09375,
$\diamond$ = -0.46875.

Figure 46. Lines of constant ψ for a sphere. Wi = 1, α = 1. A = 0.05,
B = 0.20, C = 0.50, D = 1.0, E = 2.0, F = 3.0, G = 4.0, H = 5.0.

Figure 47. Lines of constant ω for a sphere. Wi = 1, α = 1. $\bigcirc$ = -1.00,
Δ = -0.500, + = -0.25, x = 00.125, $\diamond$ = -0.0625.

Figure 48. Lines of constant τ_{rr} for a sphere. Wi = 1, α = 1.
A = -0.45, B = -0.30, C = -0.15, D = 0.15, E = 0.30, F = 0.45.

Figure 49. Lines of constant $\tau_{r\theta}$ for a sphere. Wi = 1, α = 1.
$\bigcirc$ = -1.00, Δ = -0.250, + = -0.0625, x = 0.015625.

Figure 50. Lines of constant ψ for a sphere. Wi = 1, α = 0. A = 0.05,
B = 0.20, C = 0.50, D = 1.0, E = 2.0, F = 3.0, G = 4.0,
H = 5.0.

Figure 51. Lines of constant ω for a sphere. Wi = 1, α = 0. $\bigcirc$ = -1.00,
Δ = -0.500, + = -0.25, x = -0.125, $\diamond$ = -0.0625.

Figure 52. Lines of constant τ_{rr} for a sphere. Wi = 1, a = -0.45, b = -0.030, c = -0.15, d = 0.15, e = 0.30, f = 0.45.

Figure 53. Lines of constant $\tau_{r\theta}$ for a sphere. Wi = 1, α = 0. Δ = -0.250, + = -0.0625, x = -0.015625.

Figure 54. Lines of constant ψ for a bubble, Wi = 1.00, α = 1. ⬡ = 0.05, Δ = 0.20, + = 0.50, x = 1.0, ◇ = 2.0, ⏃ = 3.0, ⧖ = 4.0, z = 5.0.

Figure 55. Lines of constant ω for a bubble, Wi = 1.00, α = 1. ⬡ = -0.75, Δ = -0.375, + = -0.1875, x = -0.09375, ◇ = -0.046875.

Figure 56. Lines of constant τ_{rr} for a bubble, Wi = 1.00, α = 1. Δ = -0.45, + = -0.15, x = 0.15, ◇ = 0.45, ⏃ = 1.35.

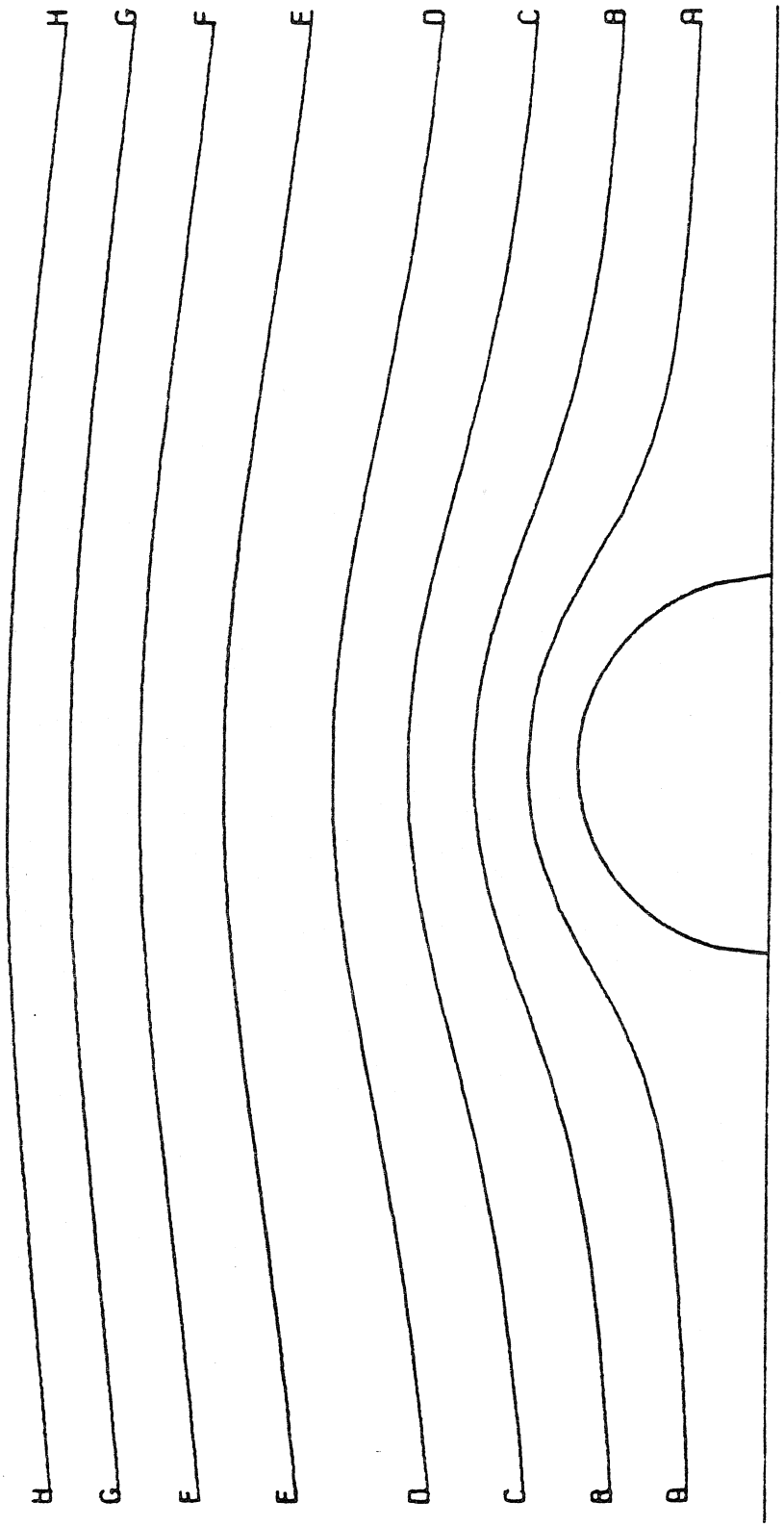

Figure 1

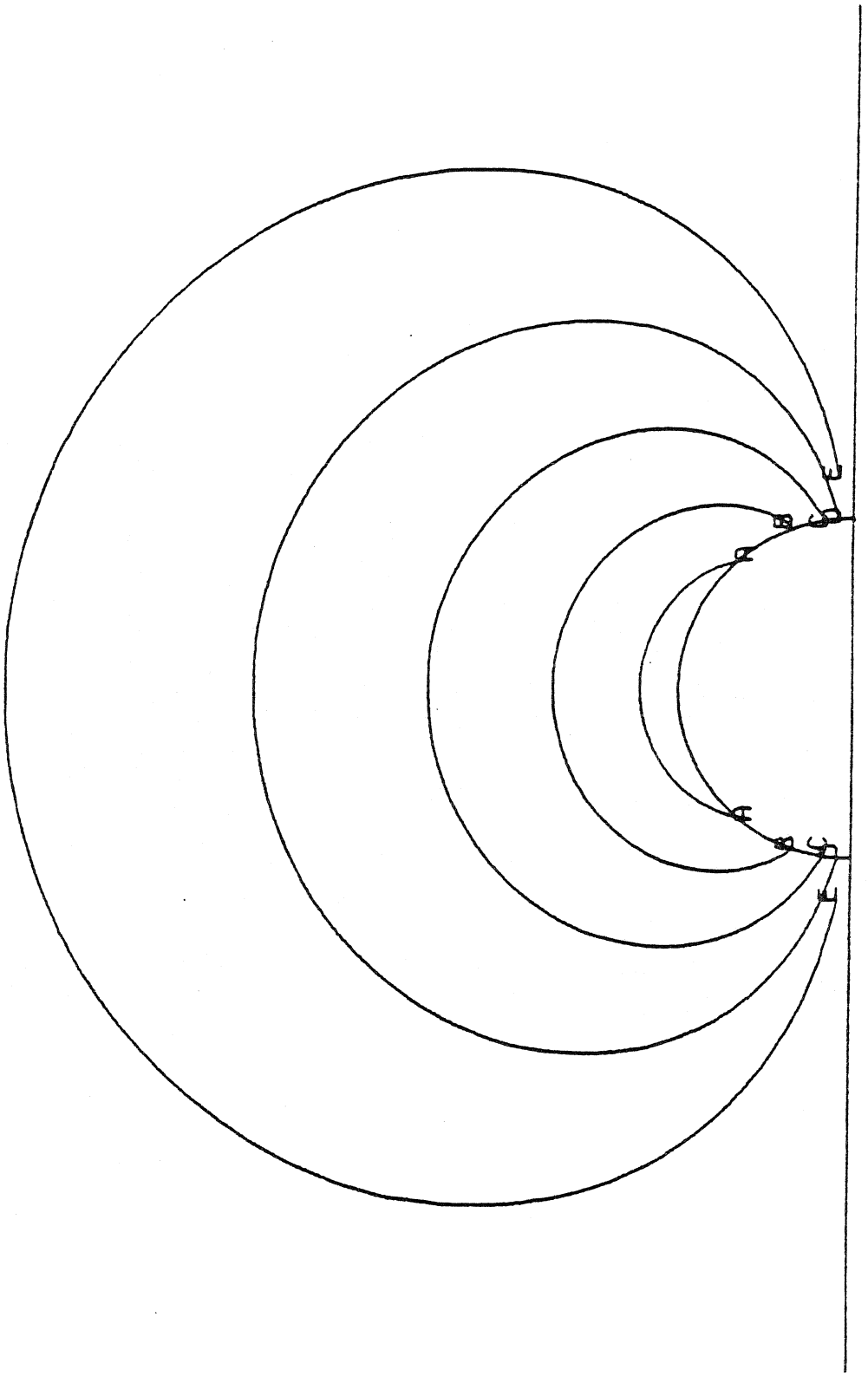

Figure 2

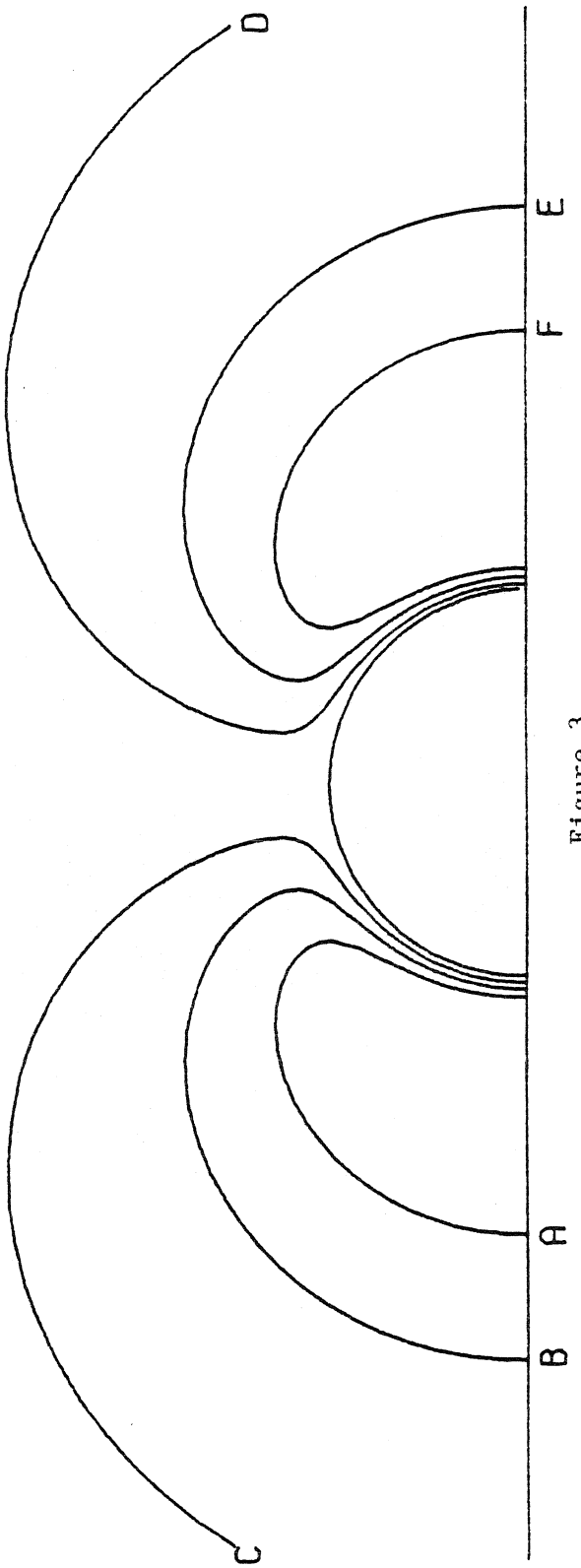

Figure 3

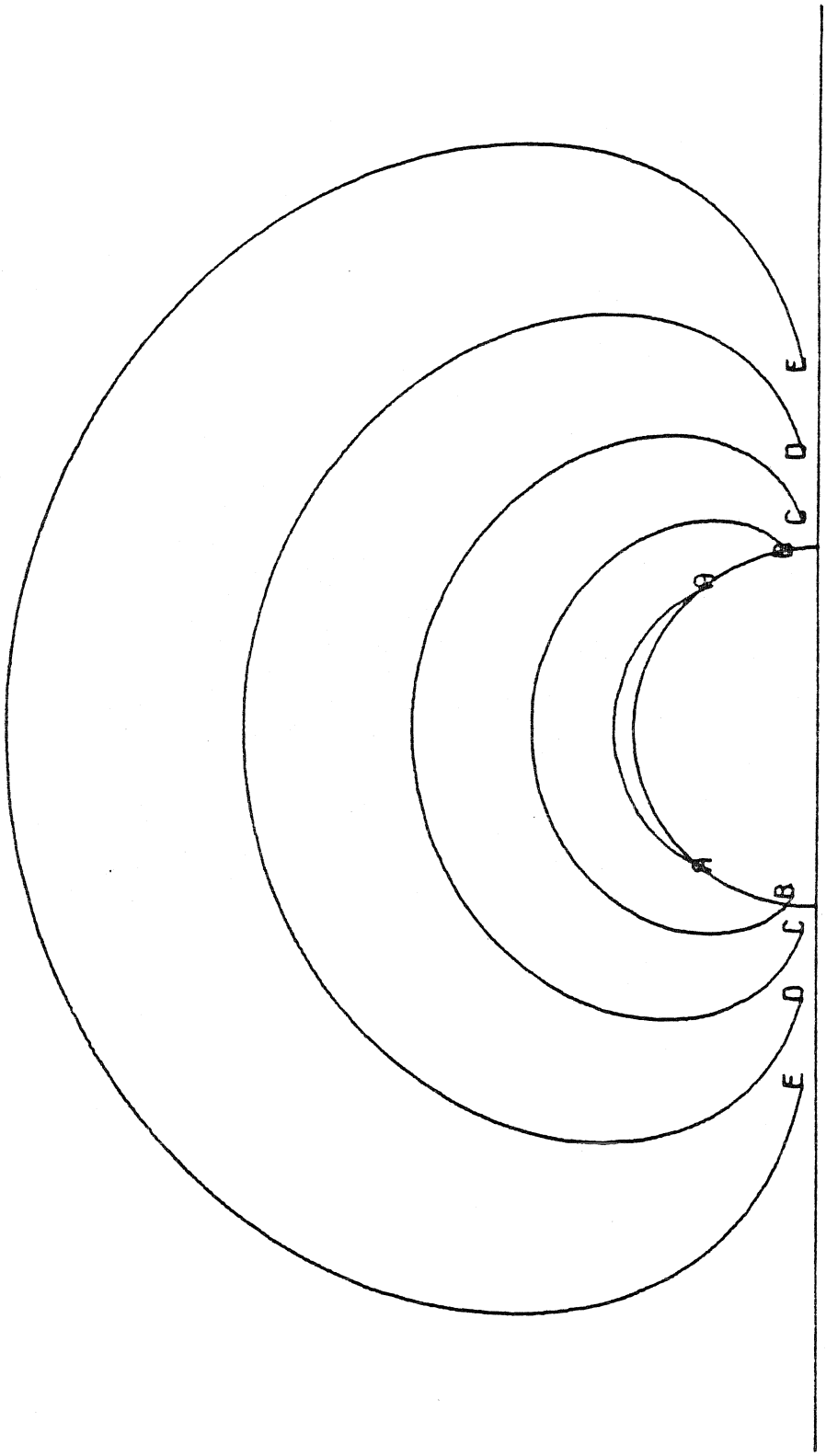

Figure 4

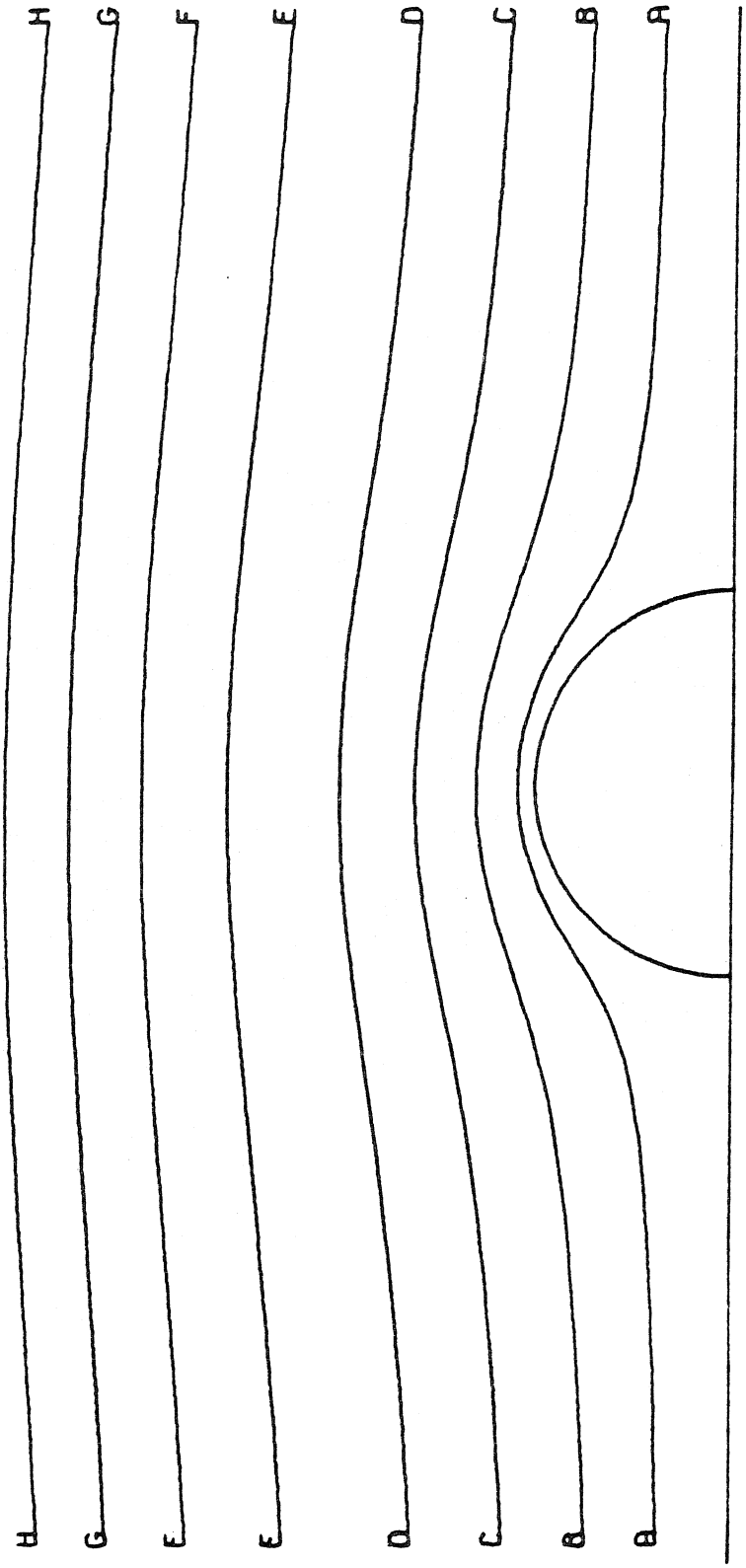

Figure 5

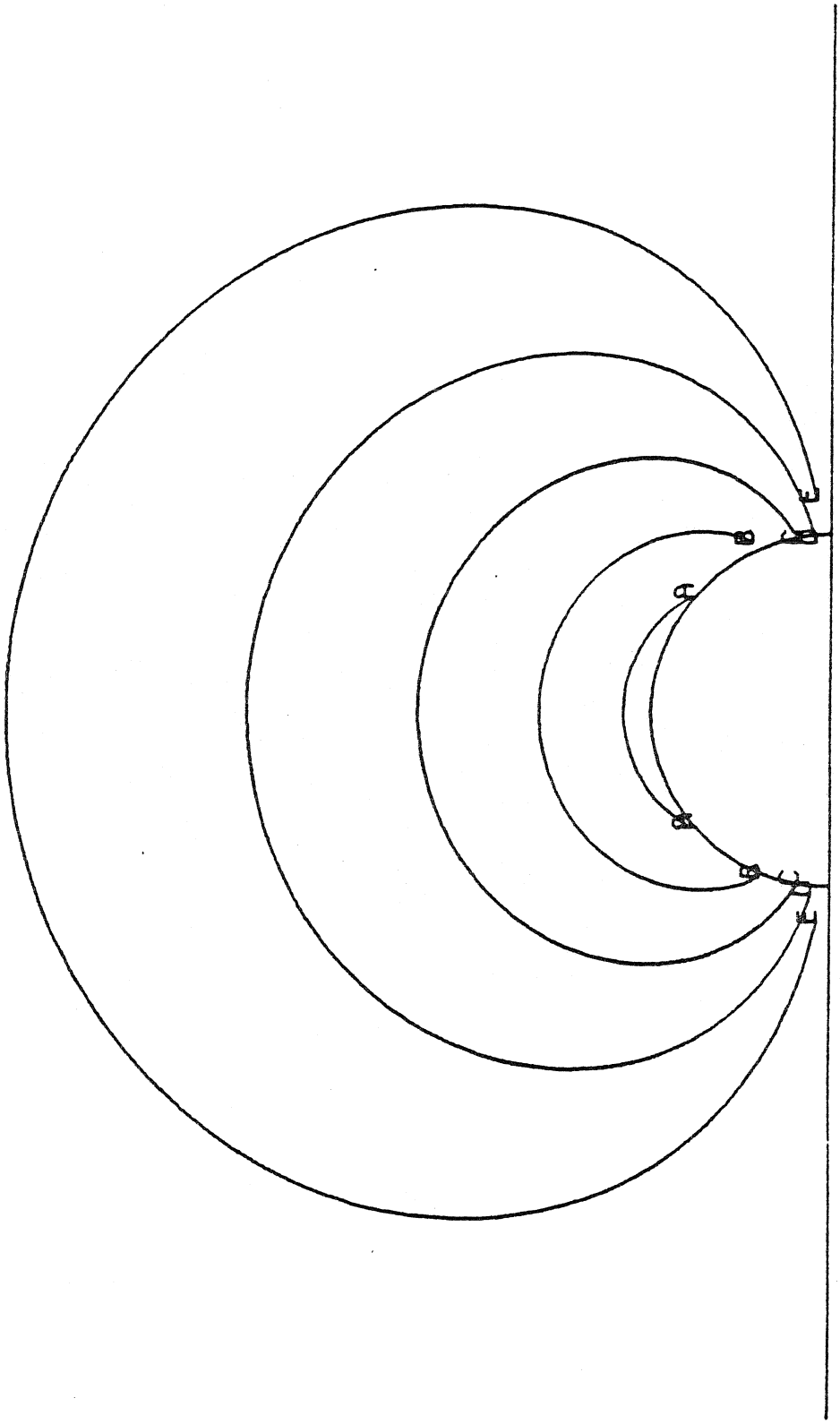

Figure 6

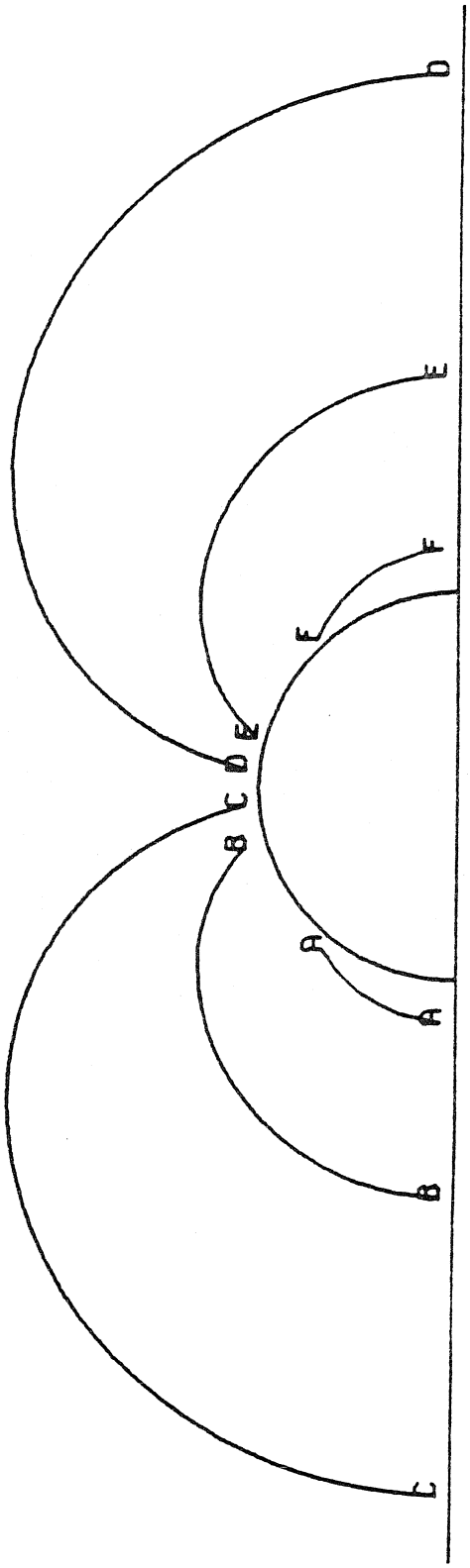

Figure 7

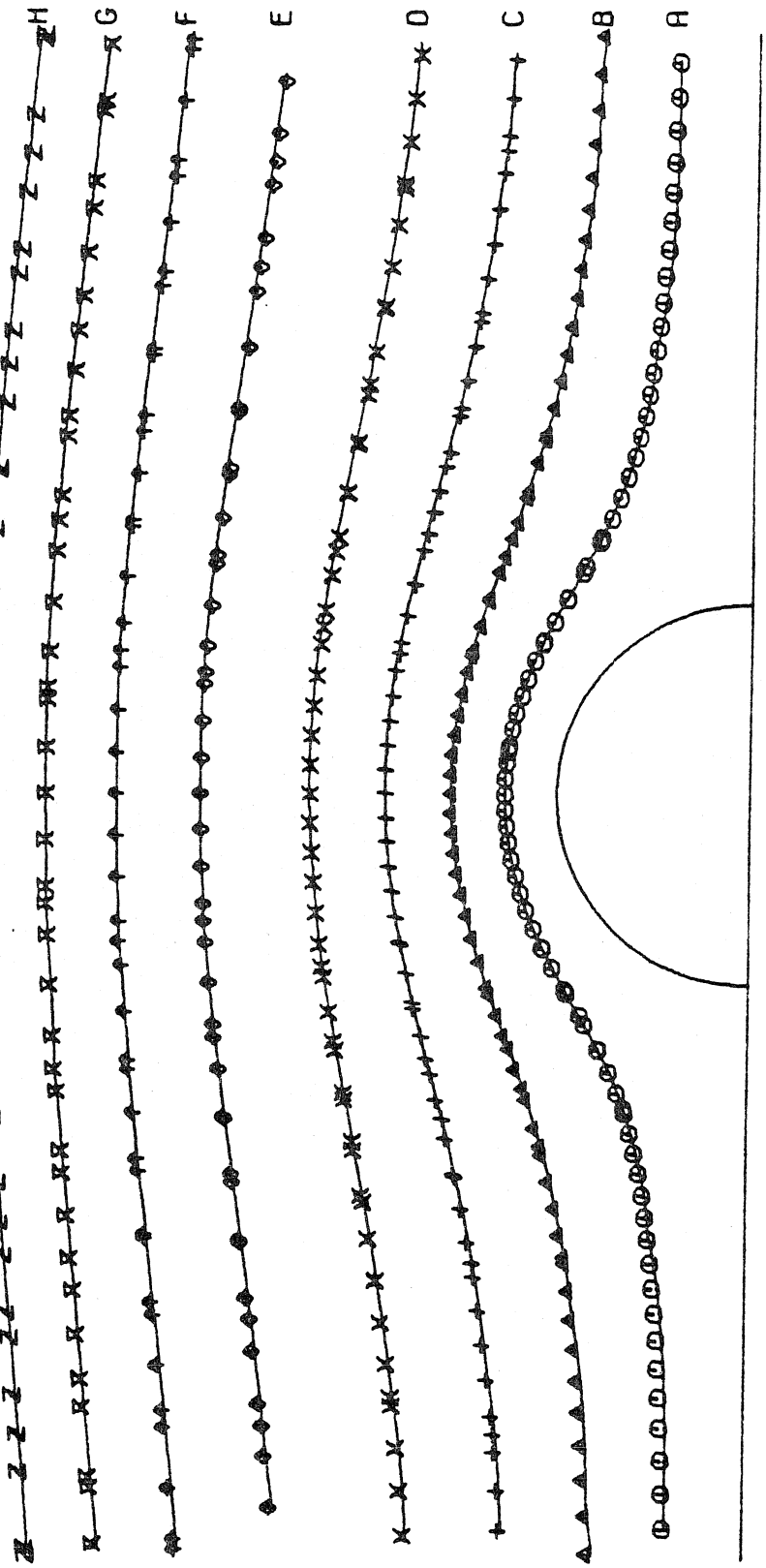

Figure 8

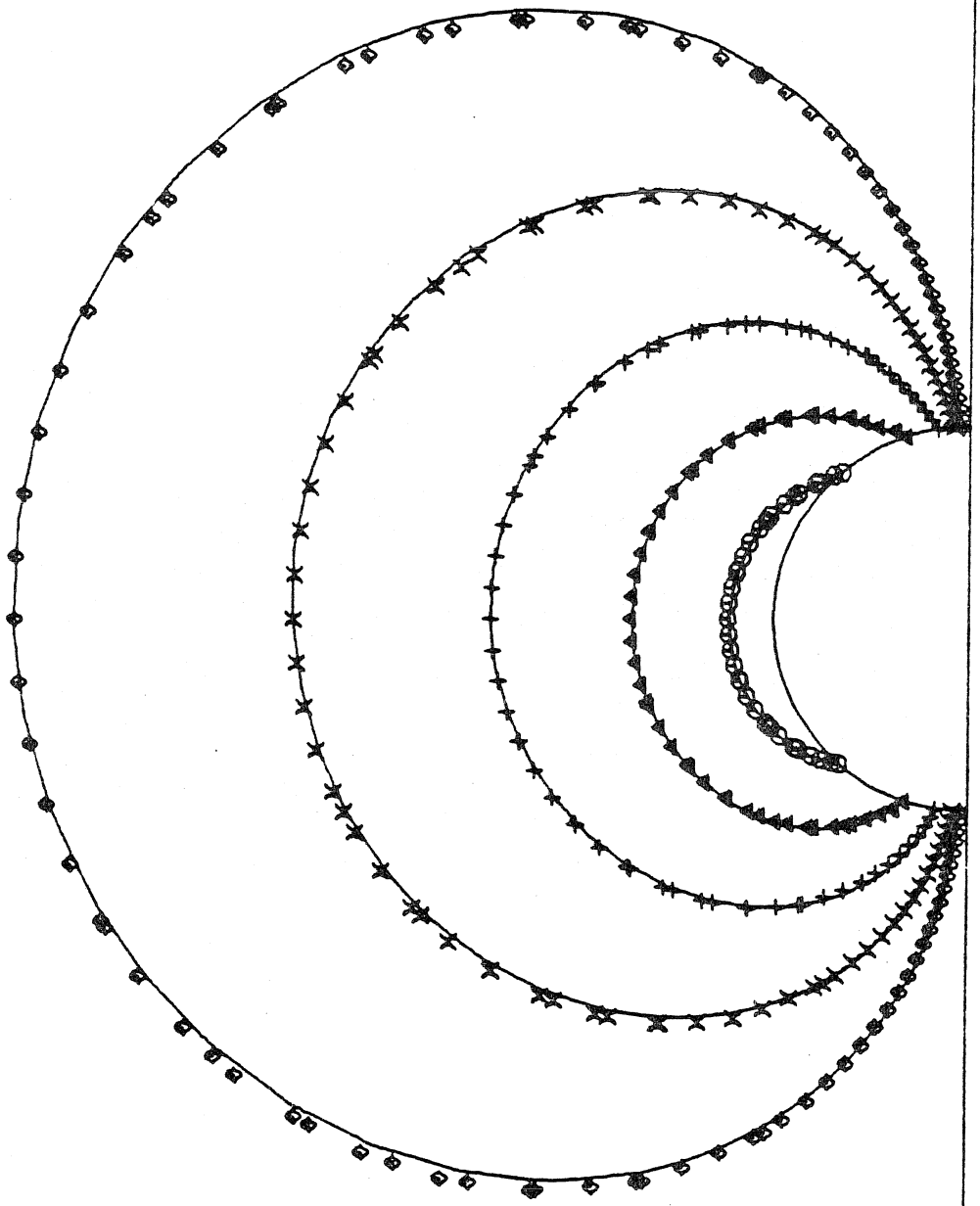

Figure 9

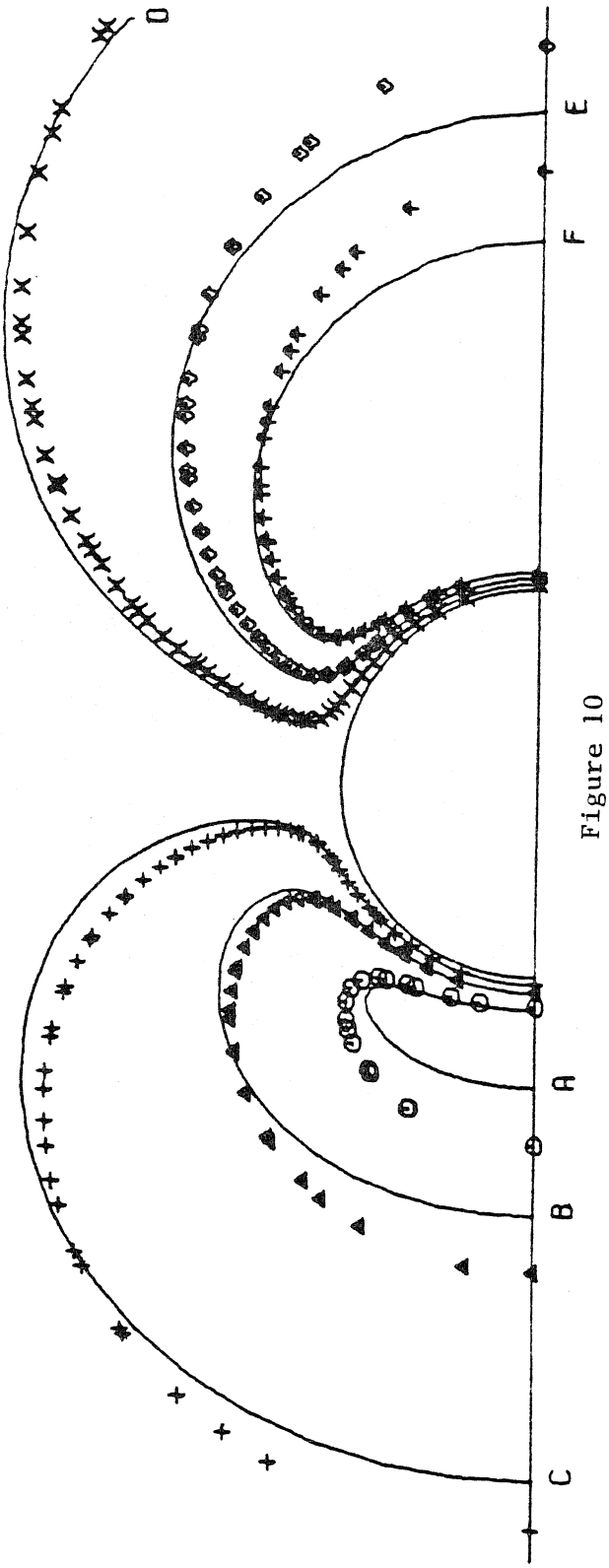

Figure 10

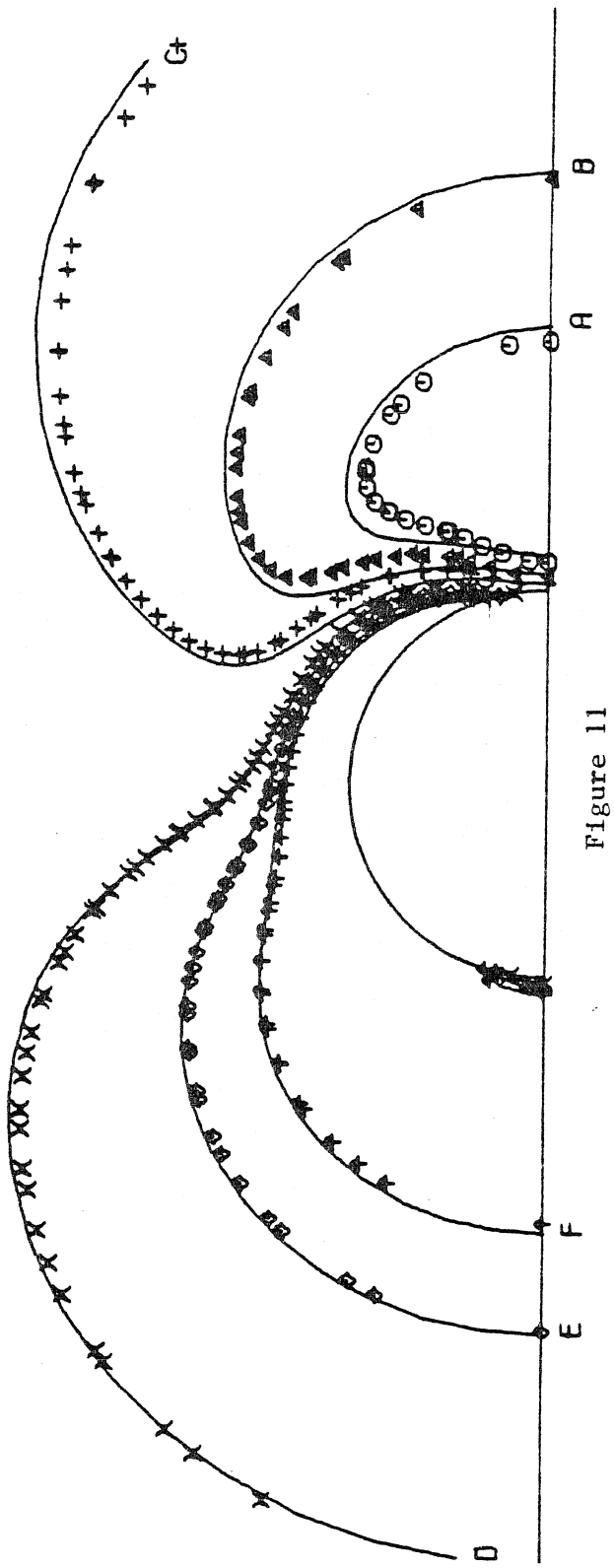

Figure 11

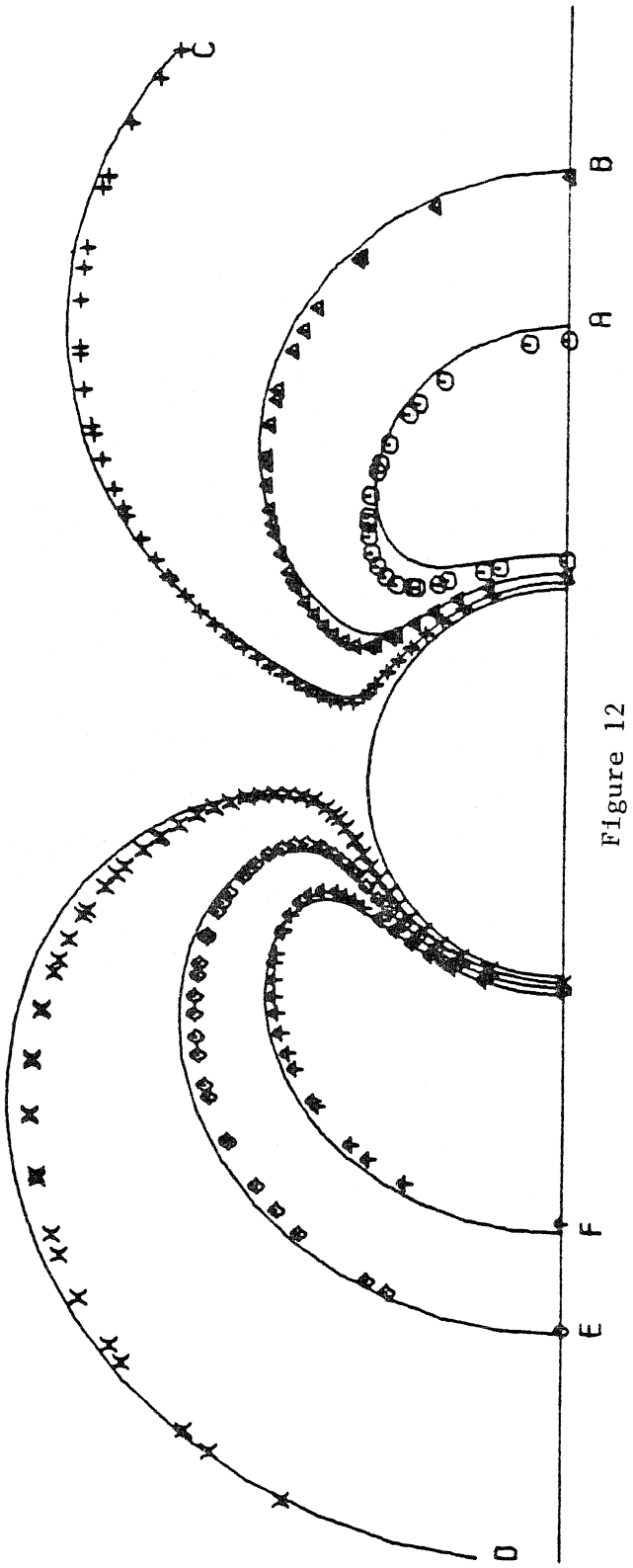

Figure 12

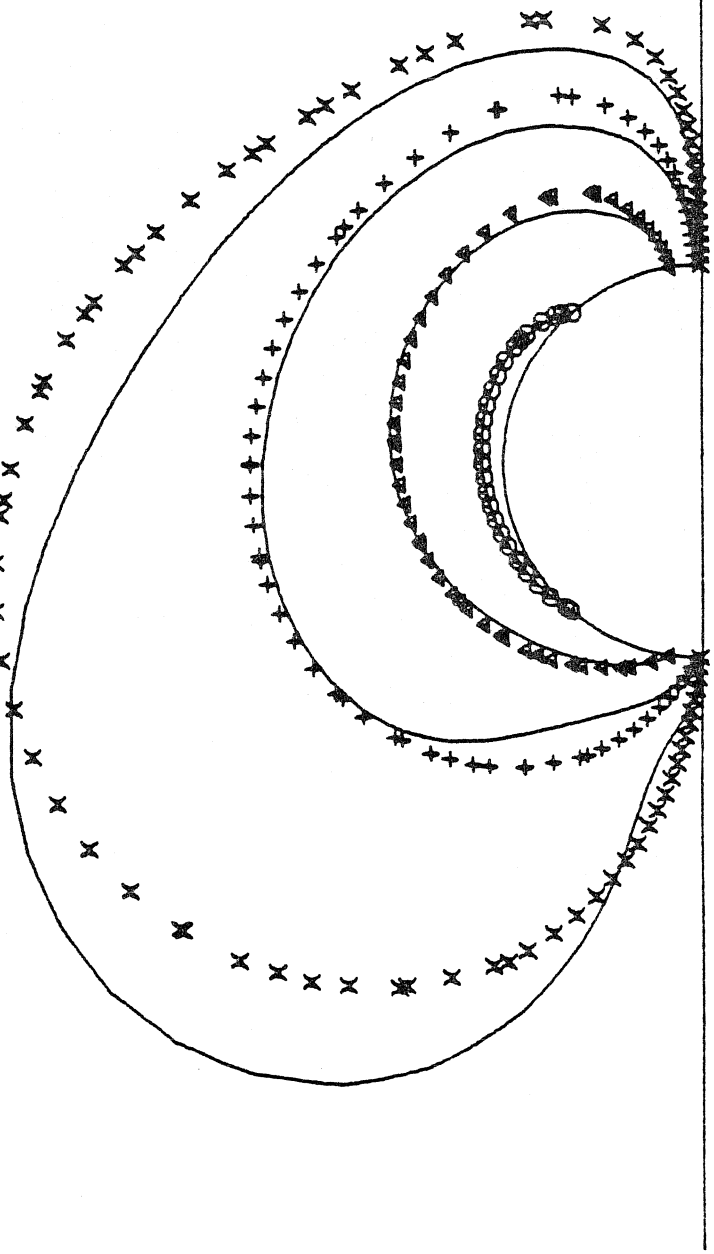

Figure 13

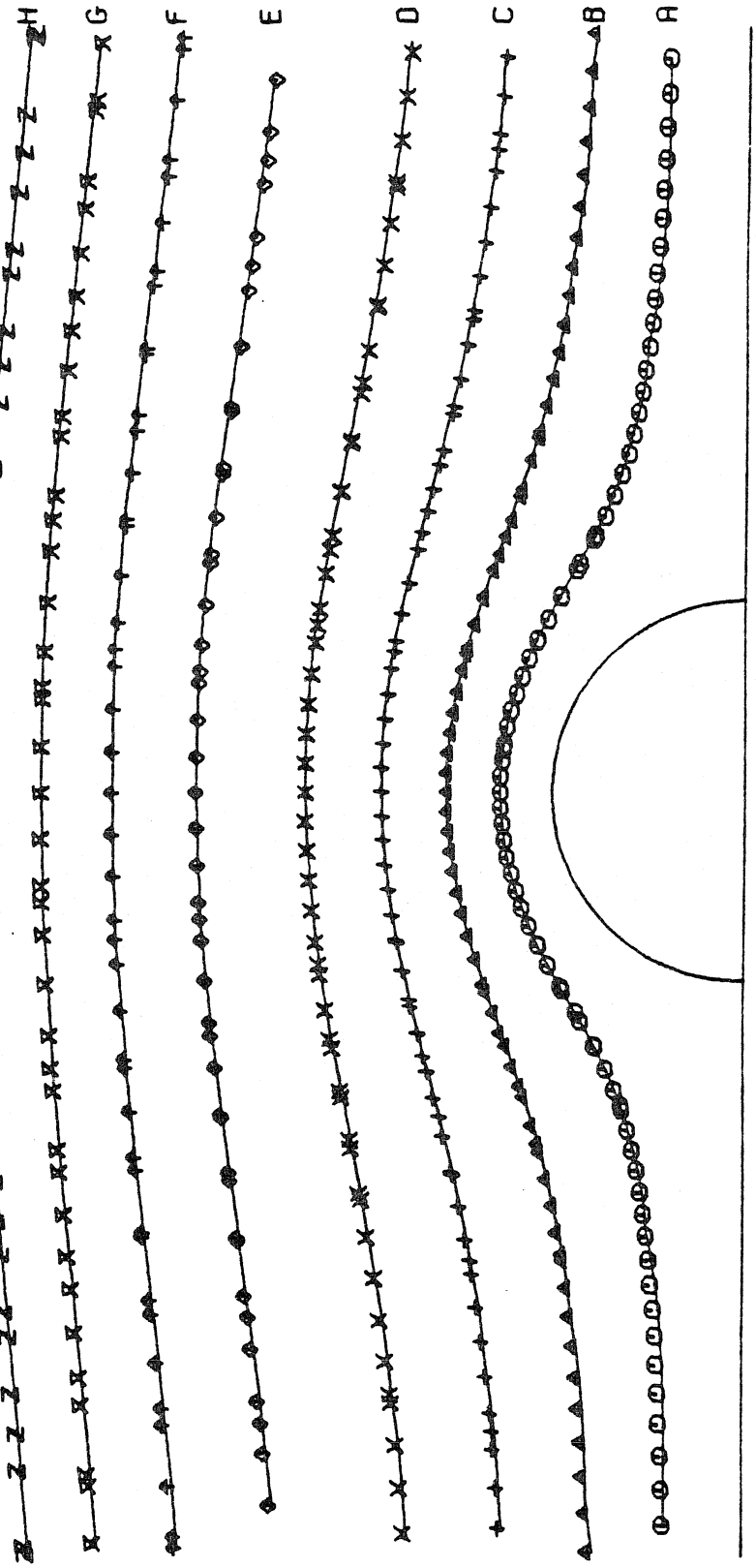

Figure 14

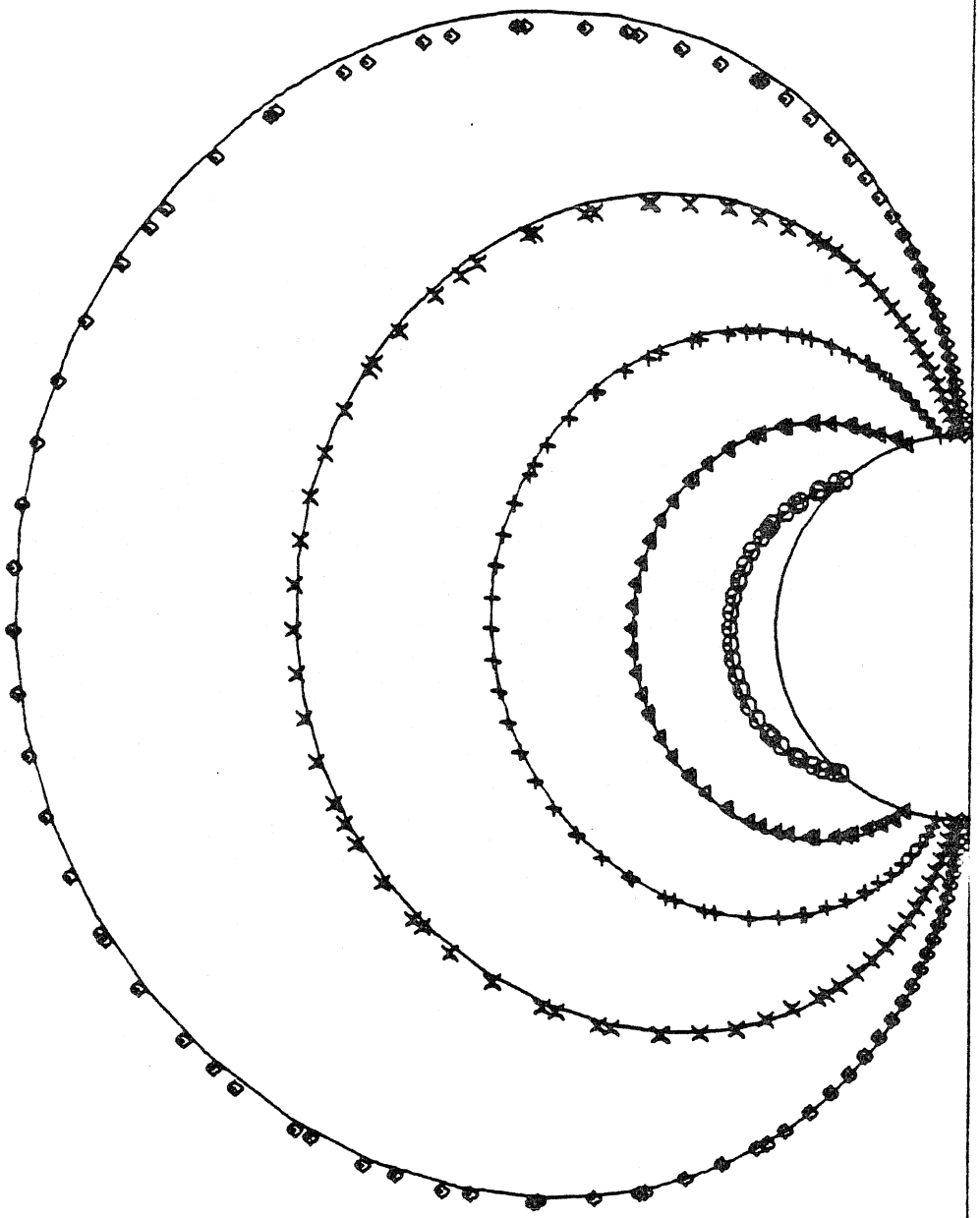

Figure 15

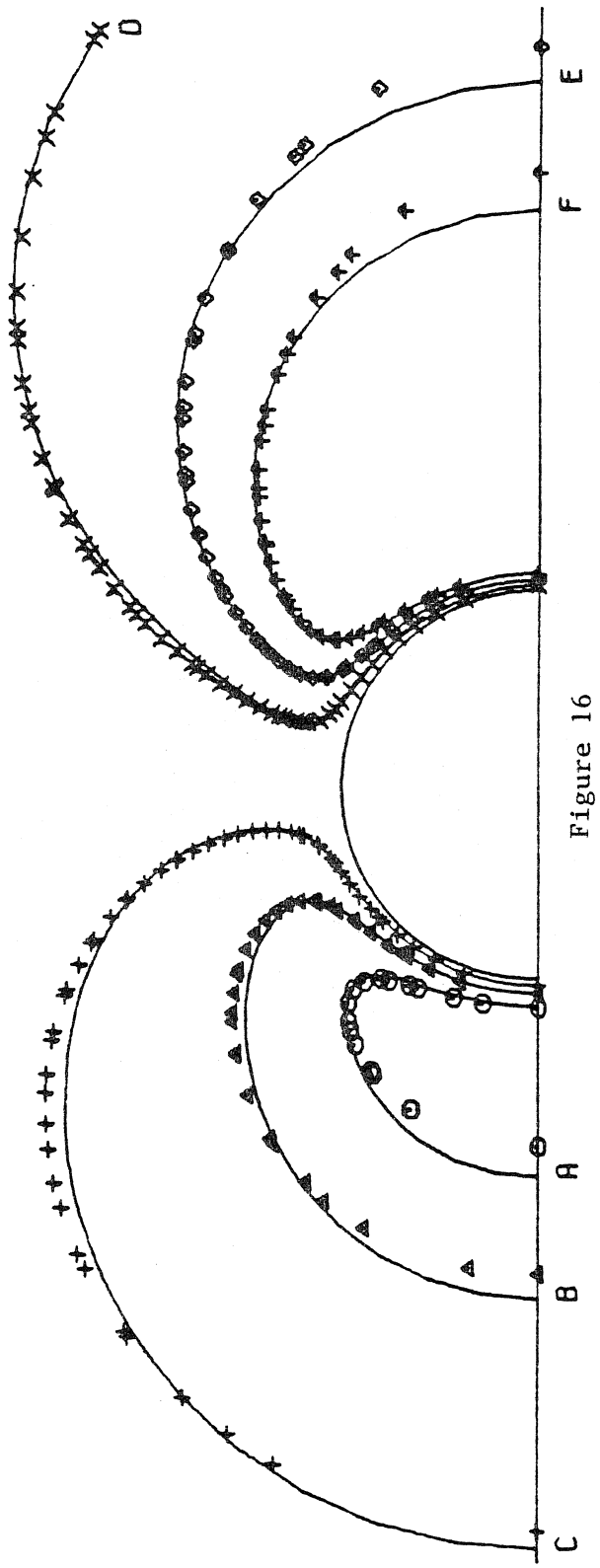

Figure 16

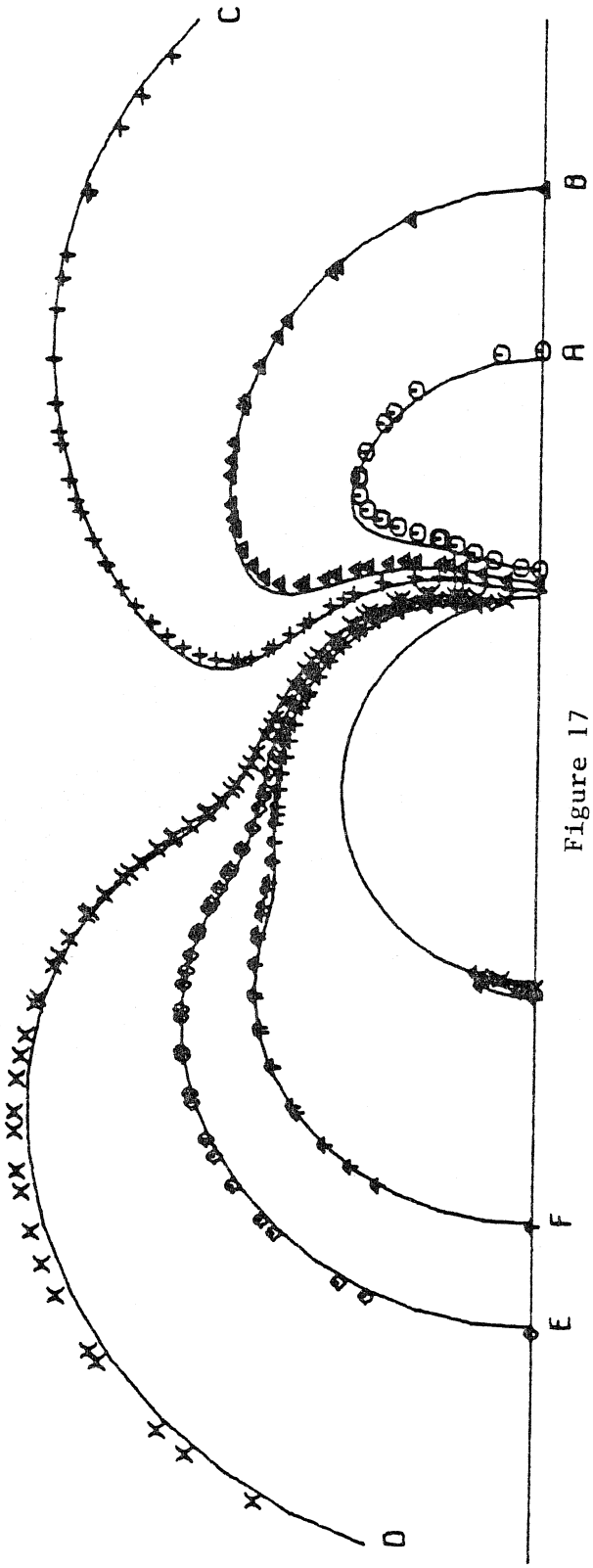

Figure 17

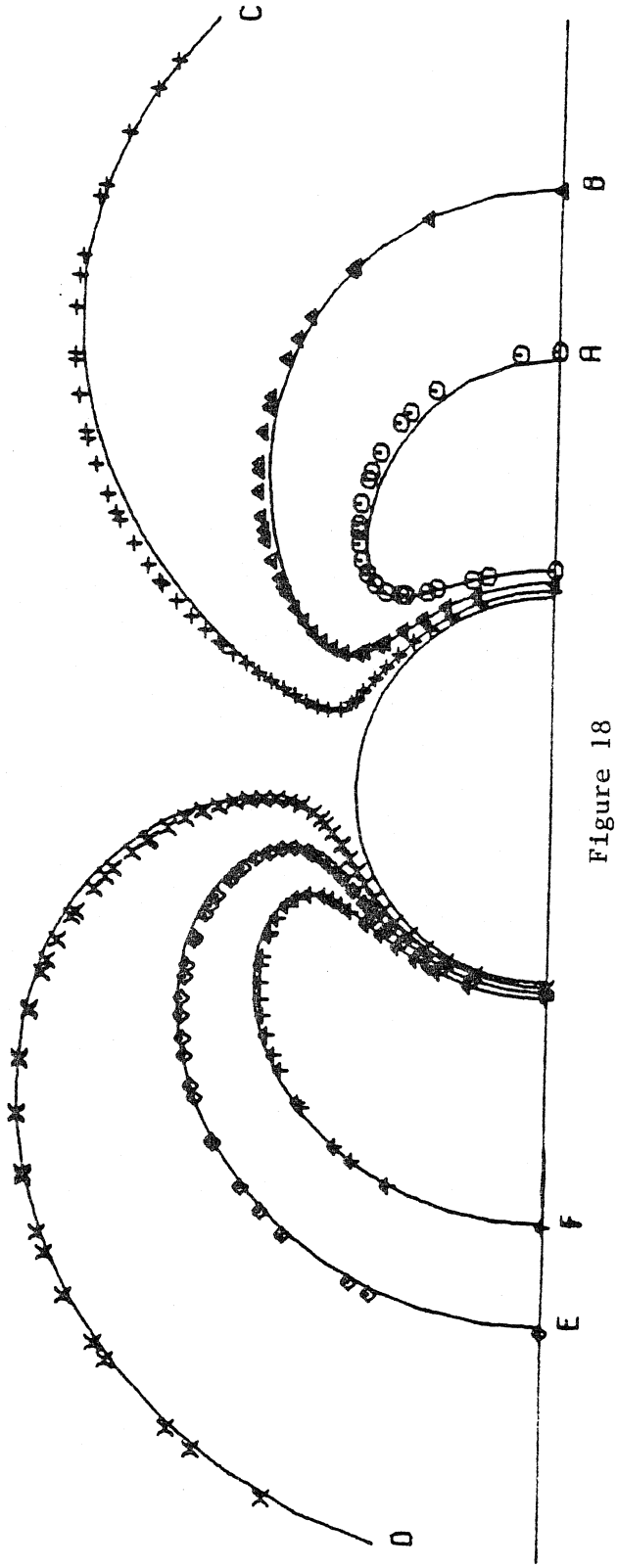

Figure 18

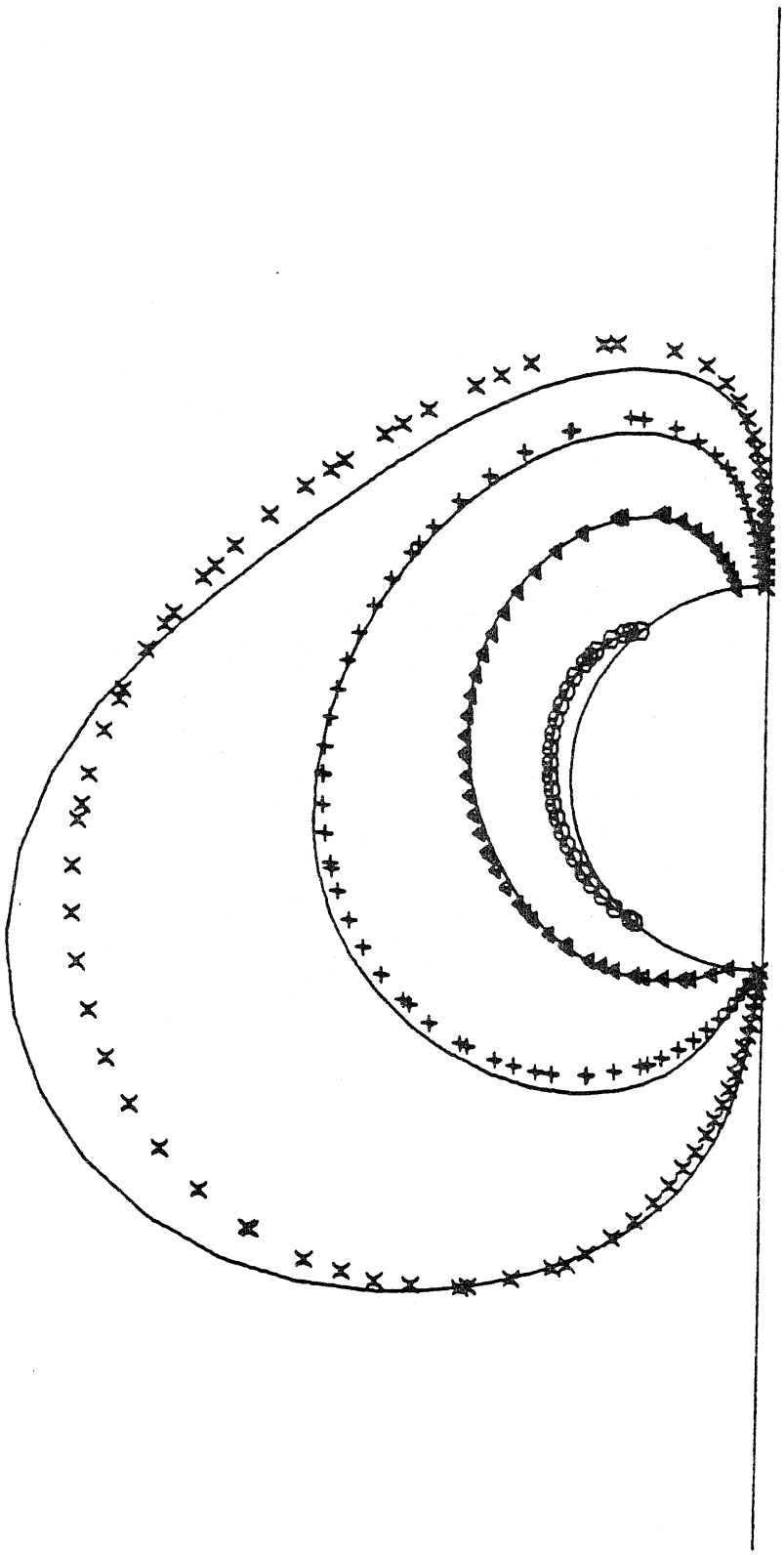

Figure 19

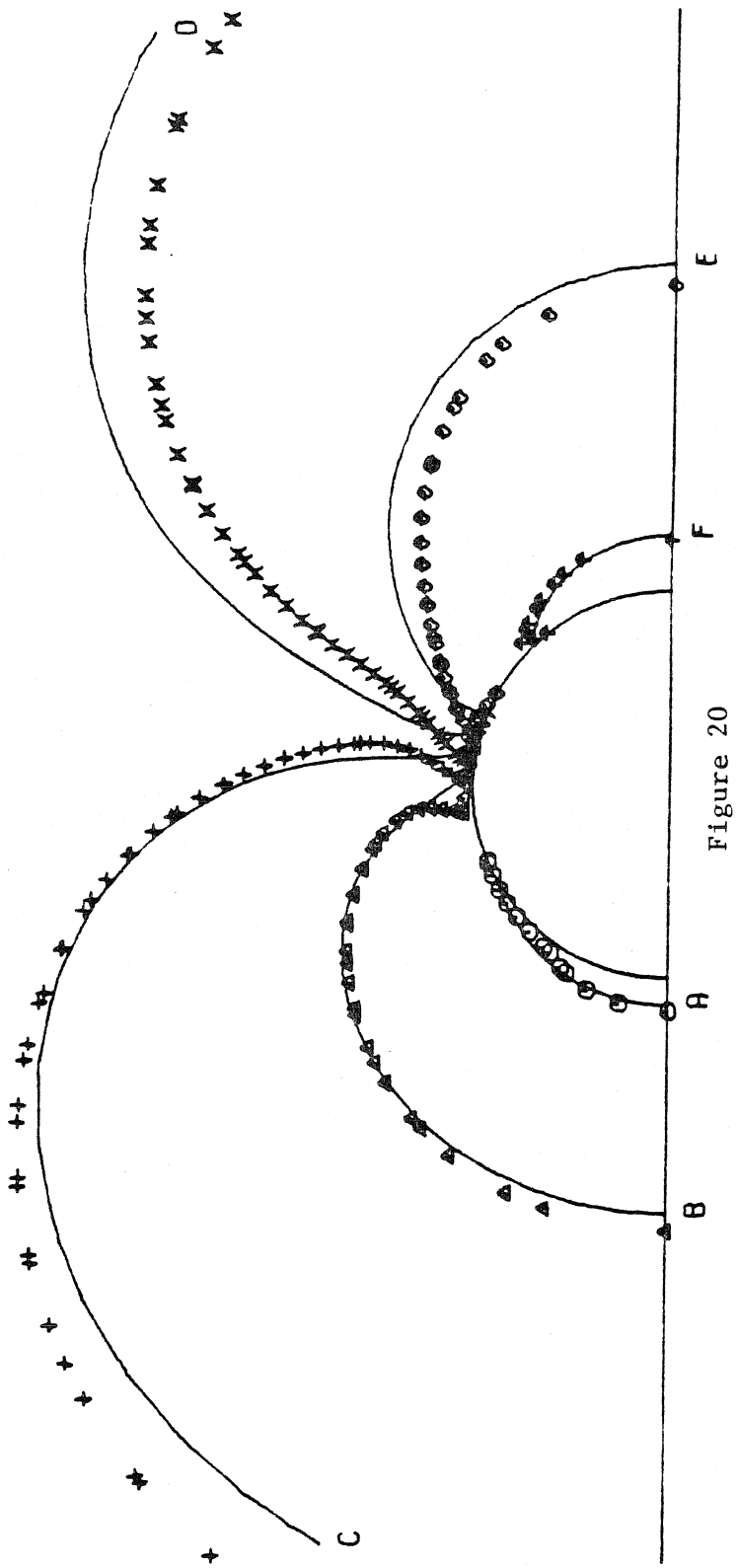

Figure 20

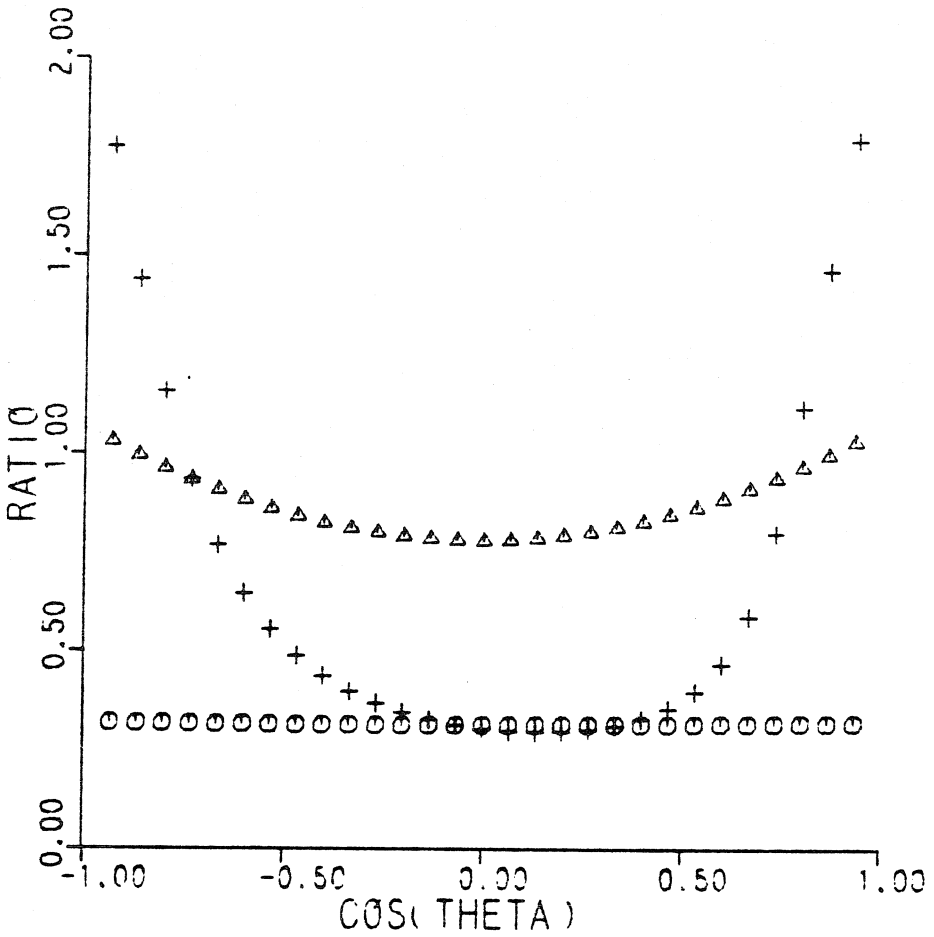

Figure 21

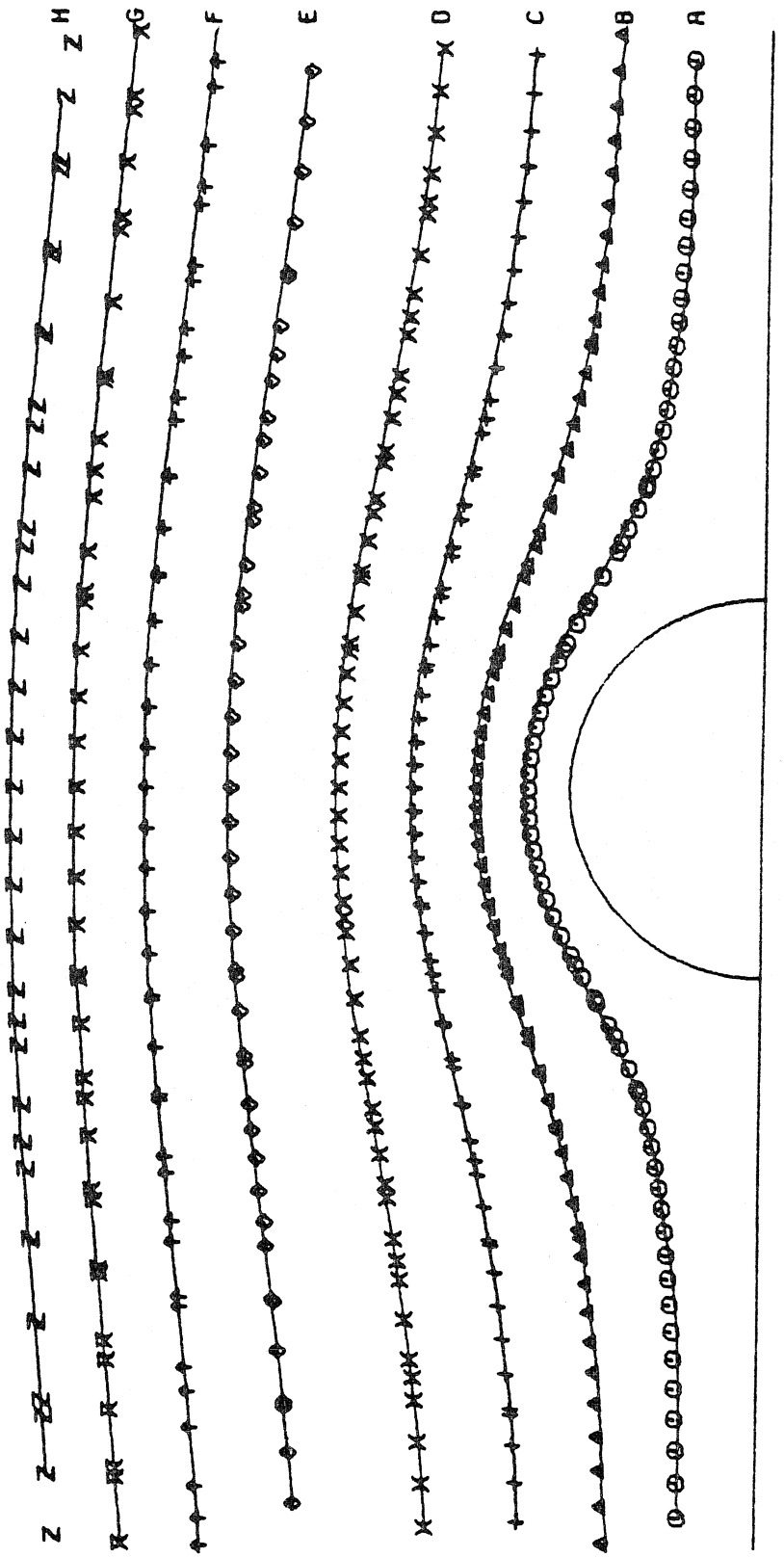

Figure 22

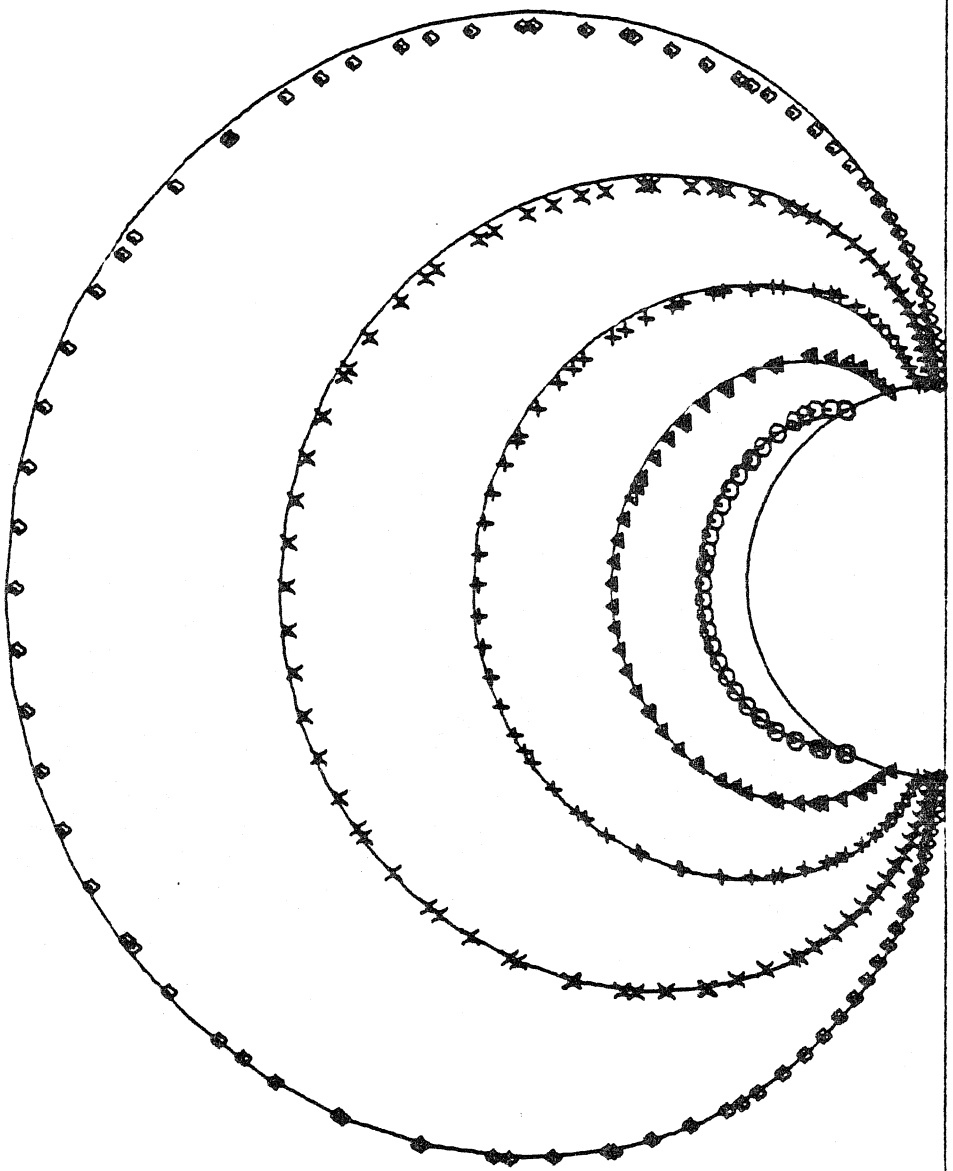

Figure 23

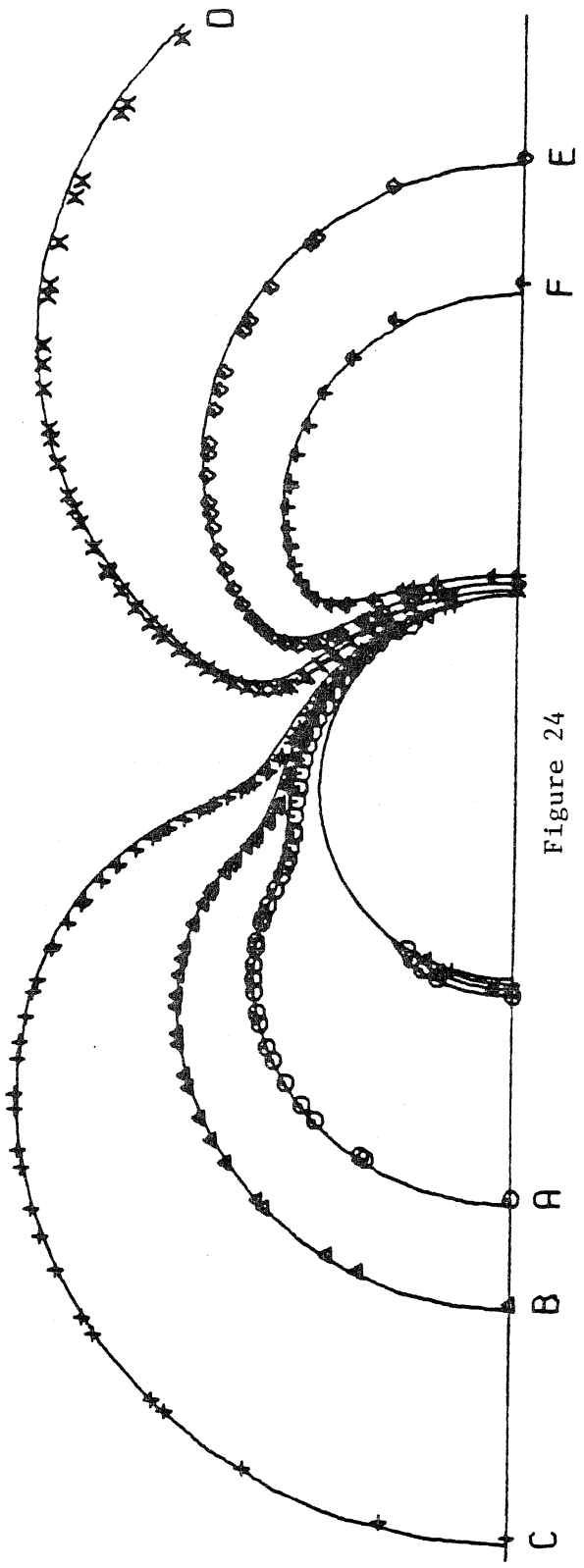

Figure 24

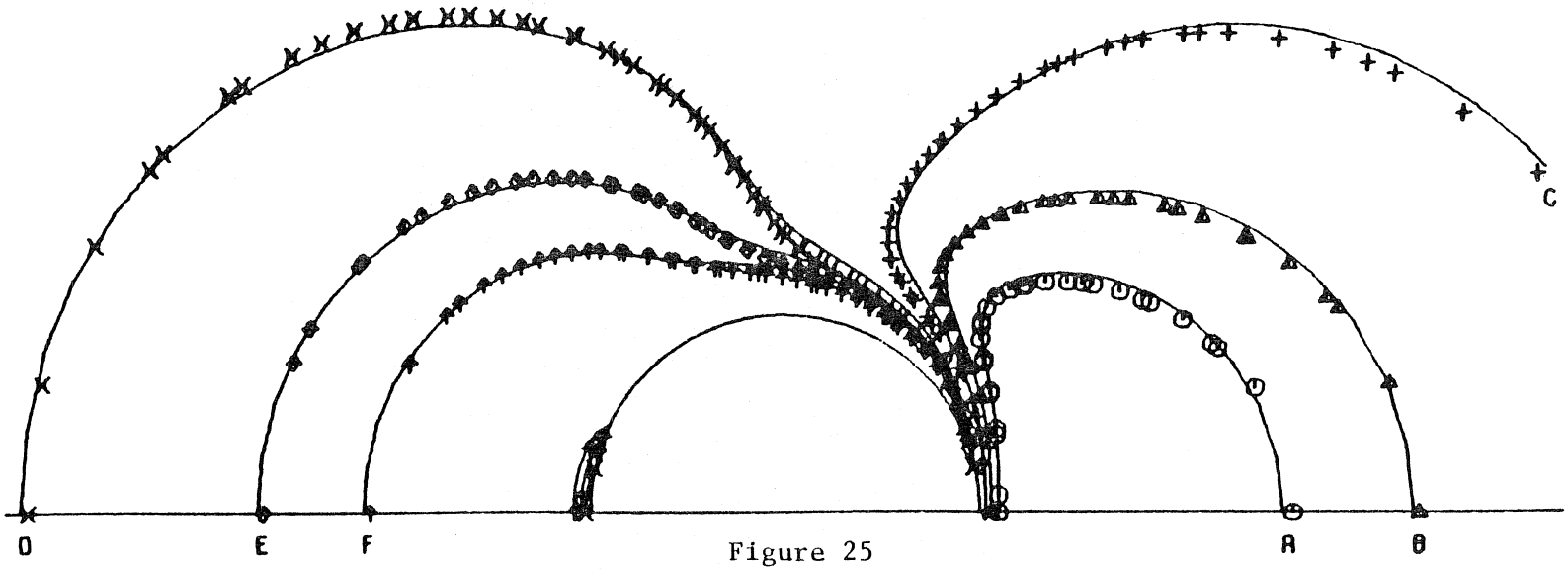

Figure 25

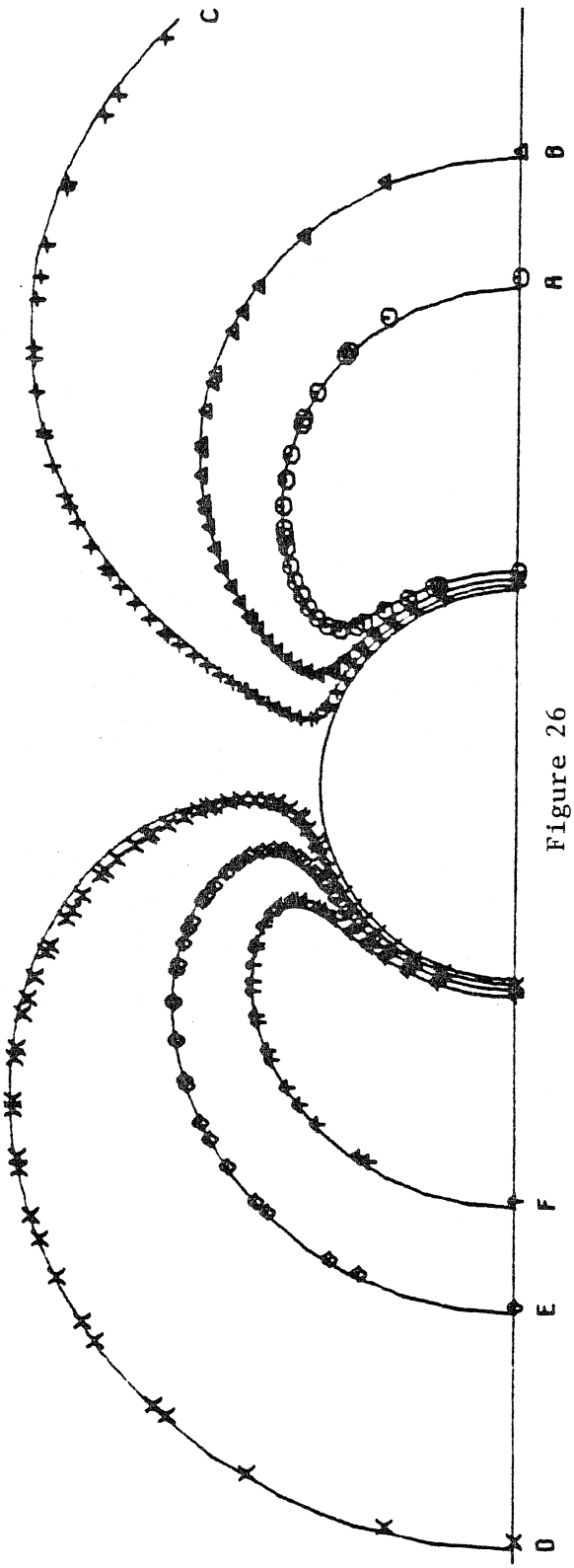

Figure 26

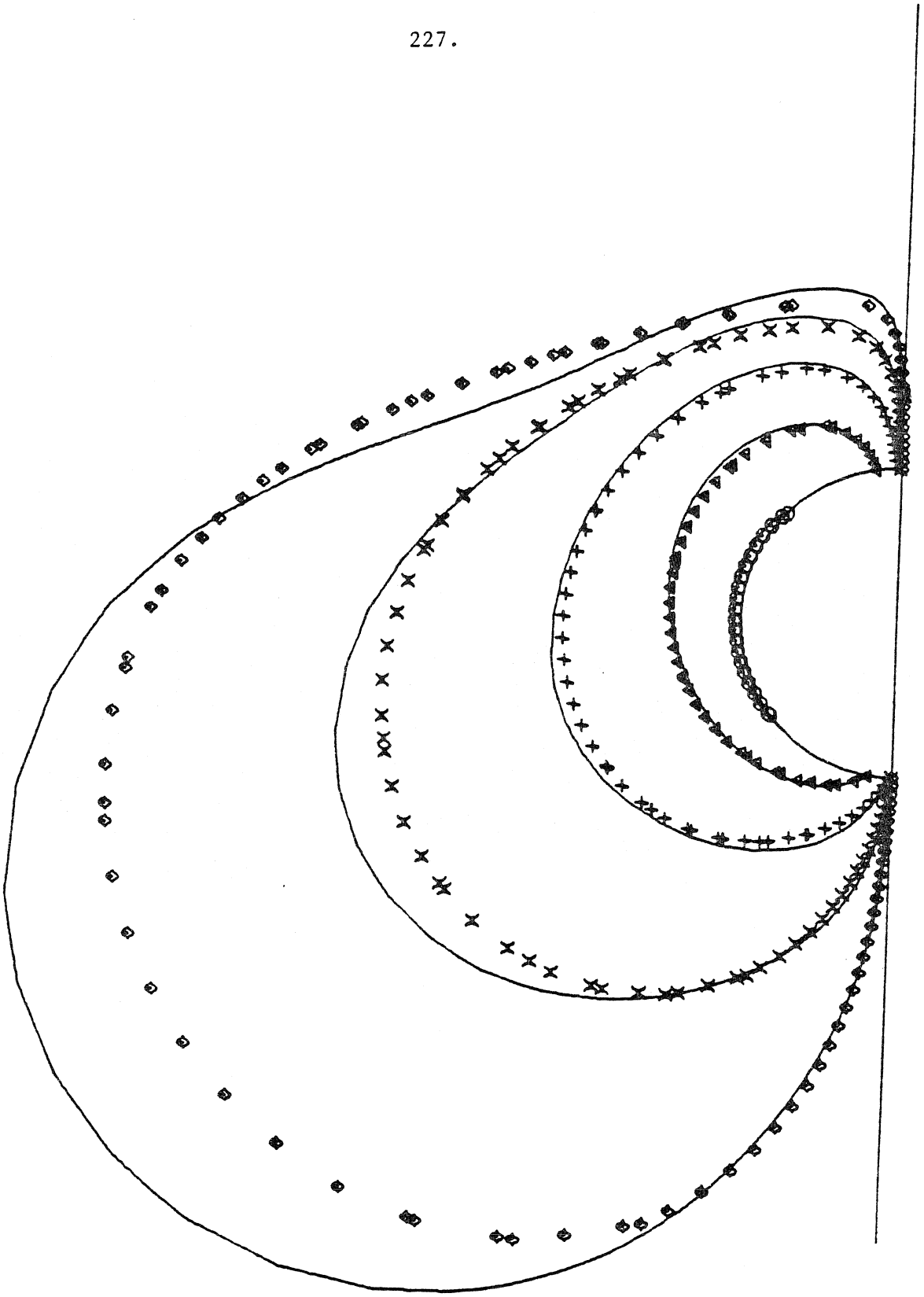

Figure 27

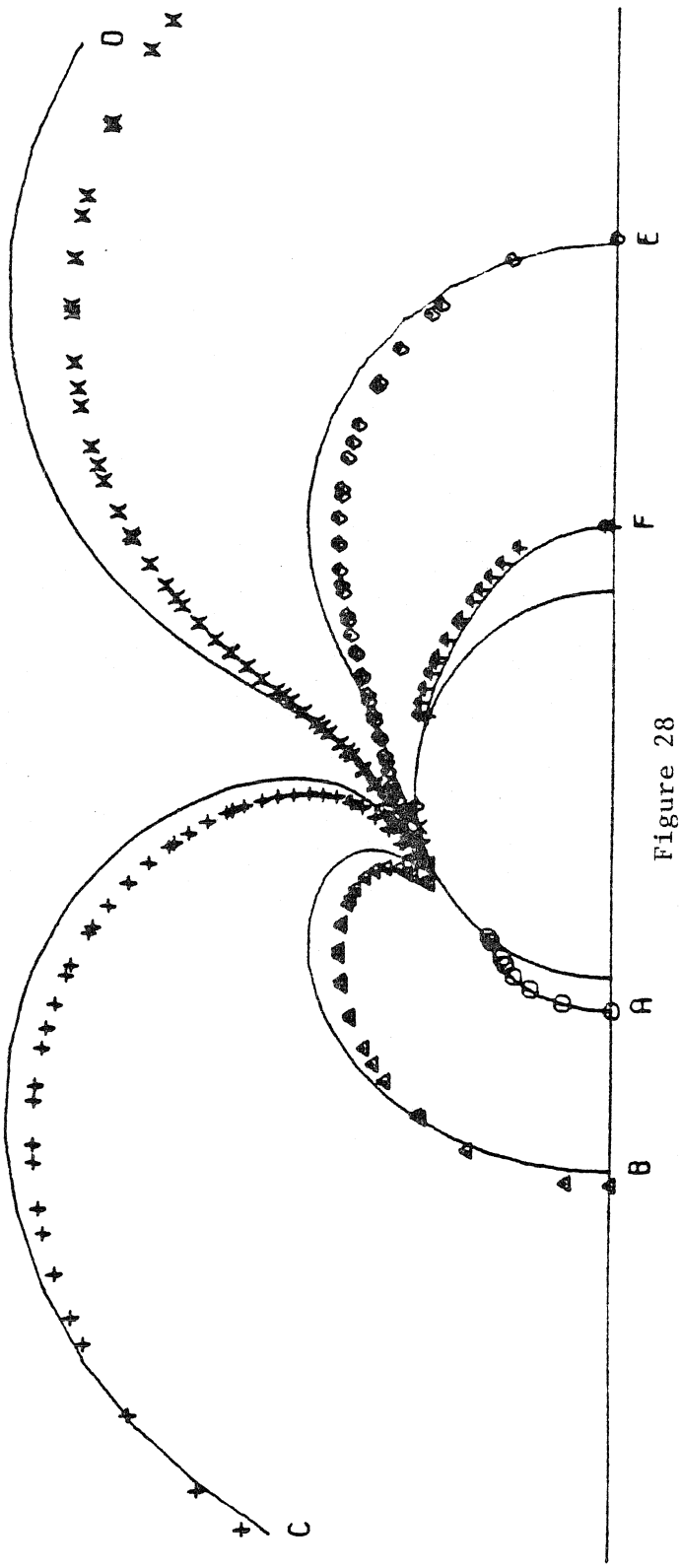

Figure 28

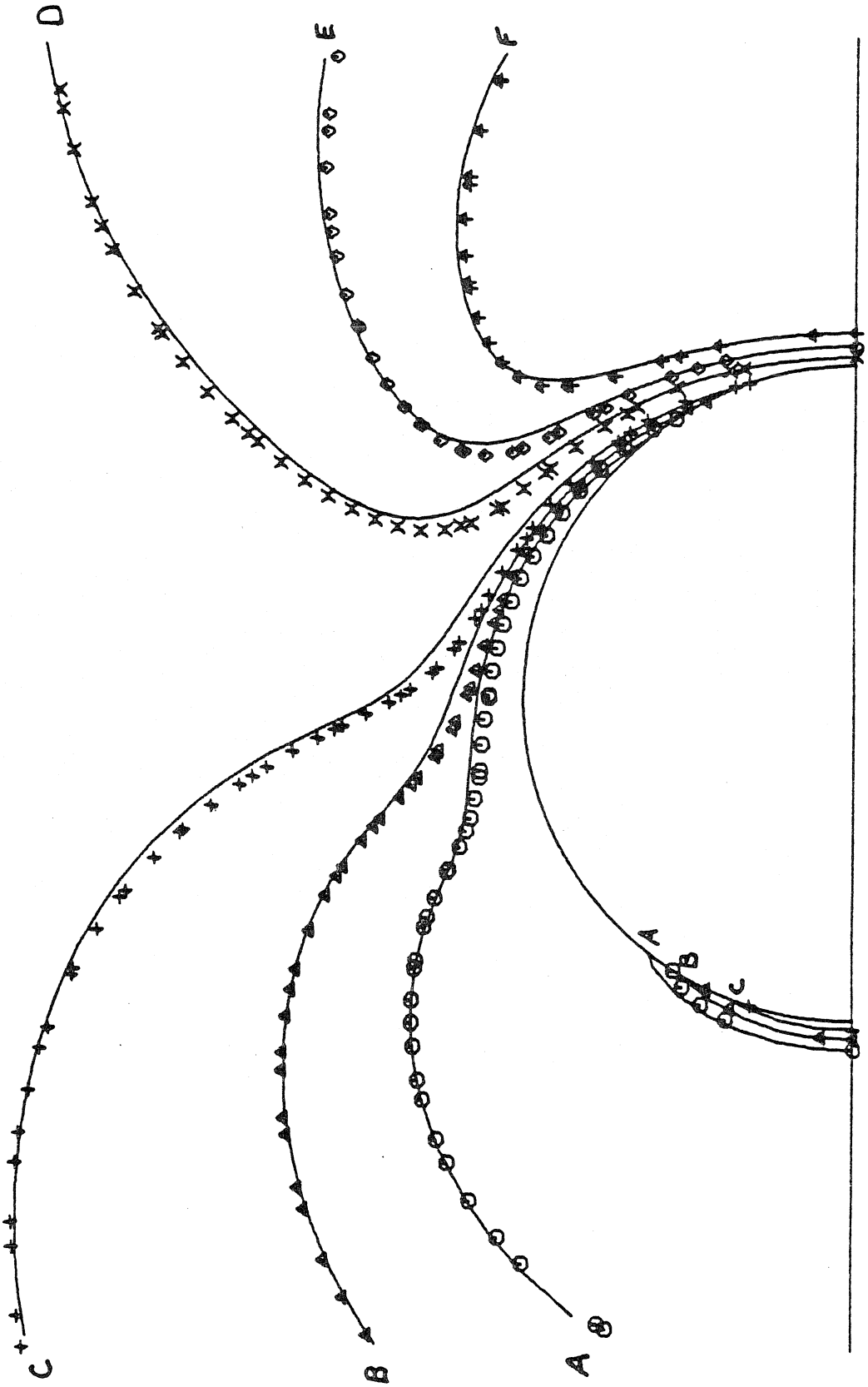

Figure 29

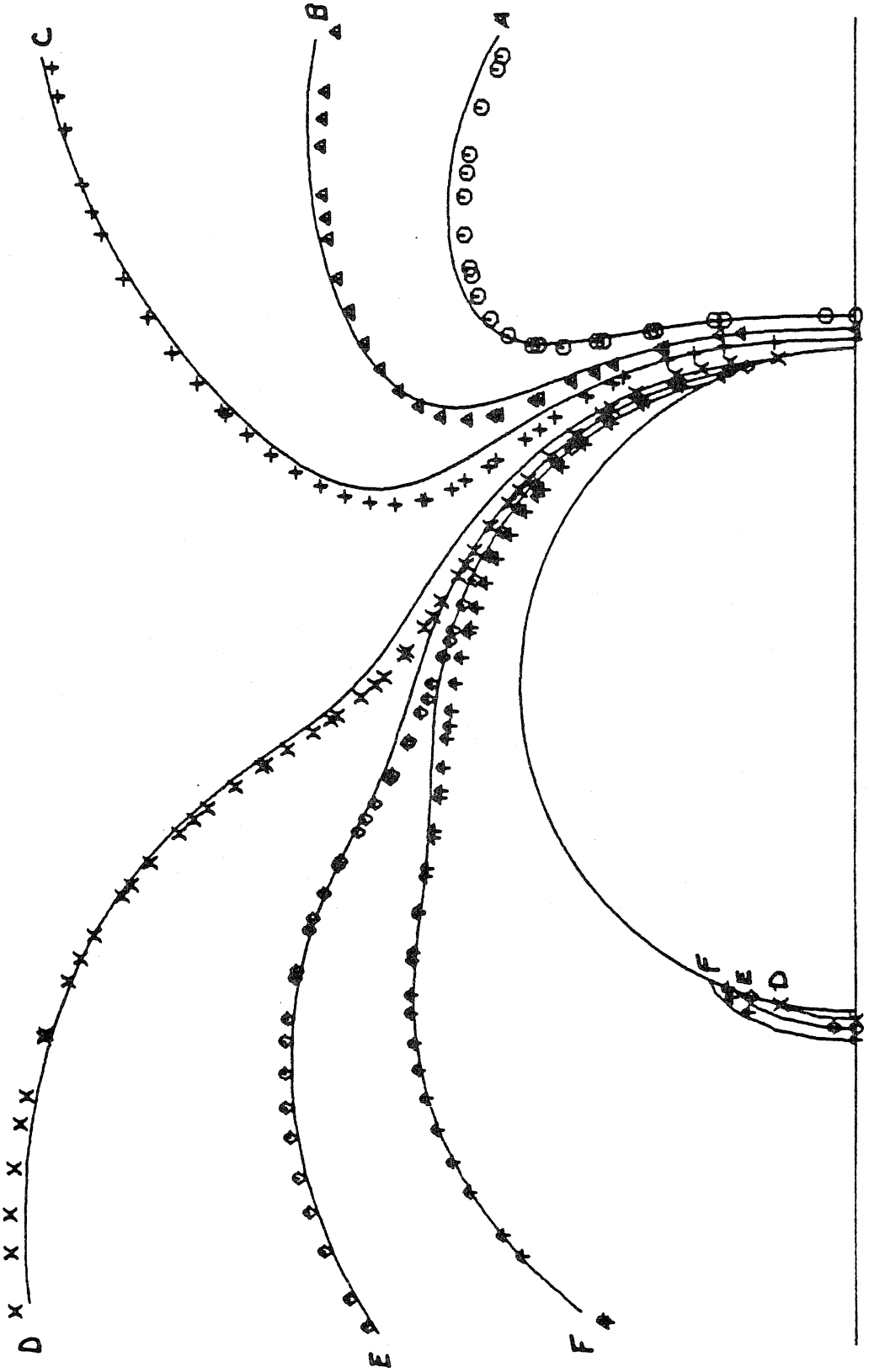

Figure 30

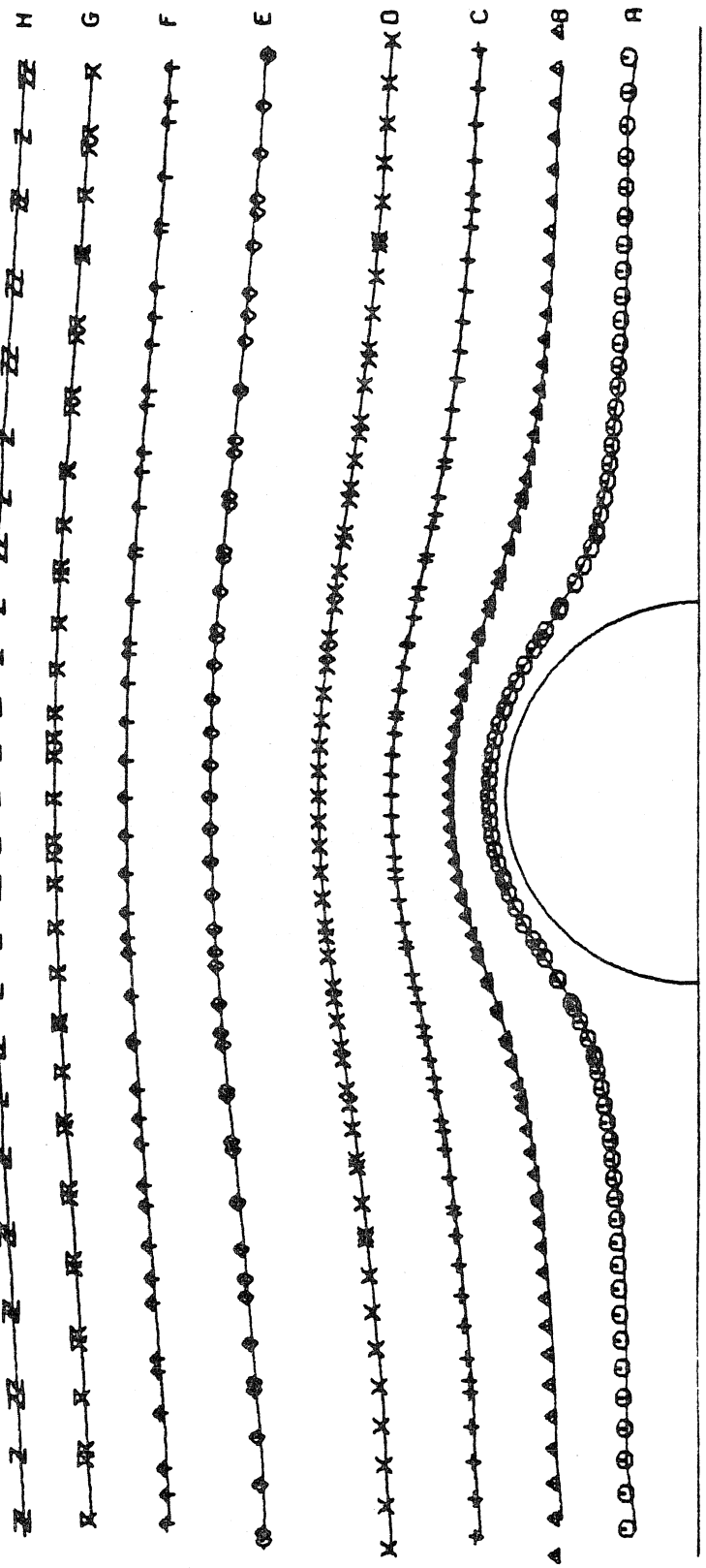

Figure 31

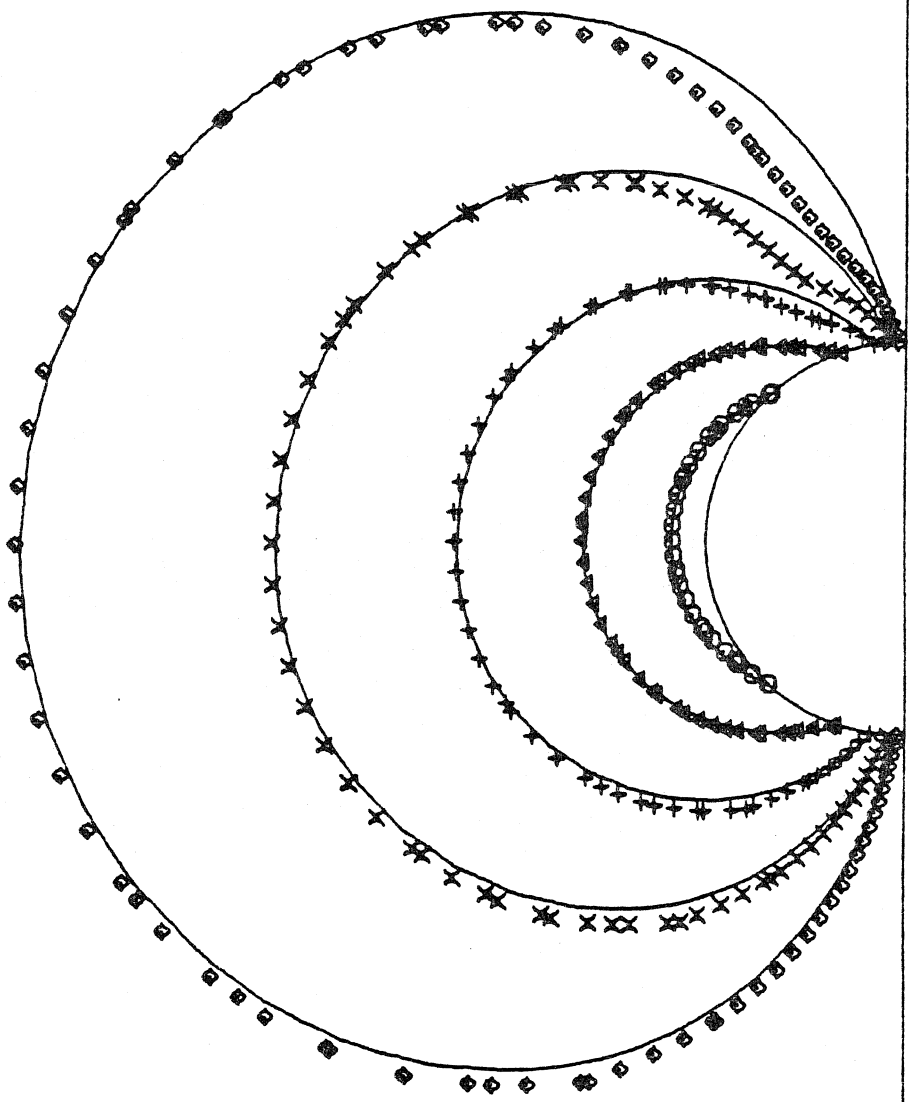

Figure 32

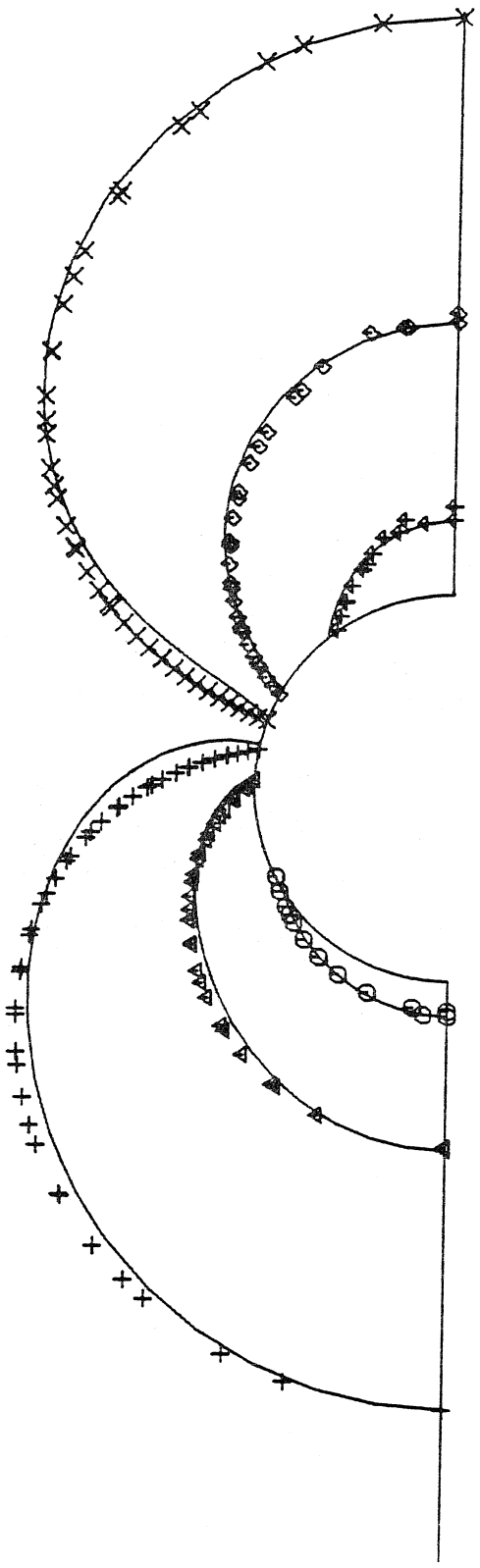

Figure 33

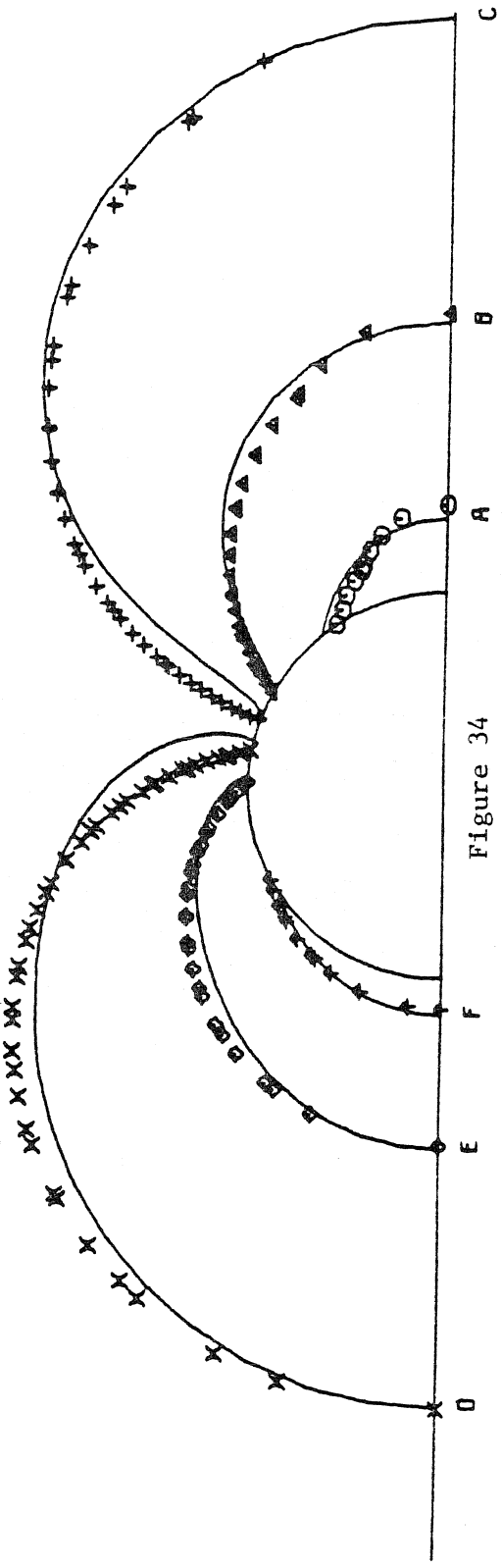

Figure 34

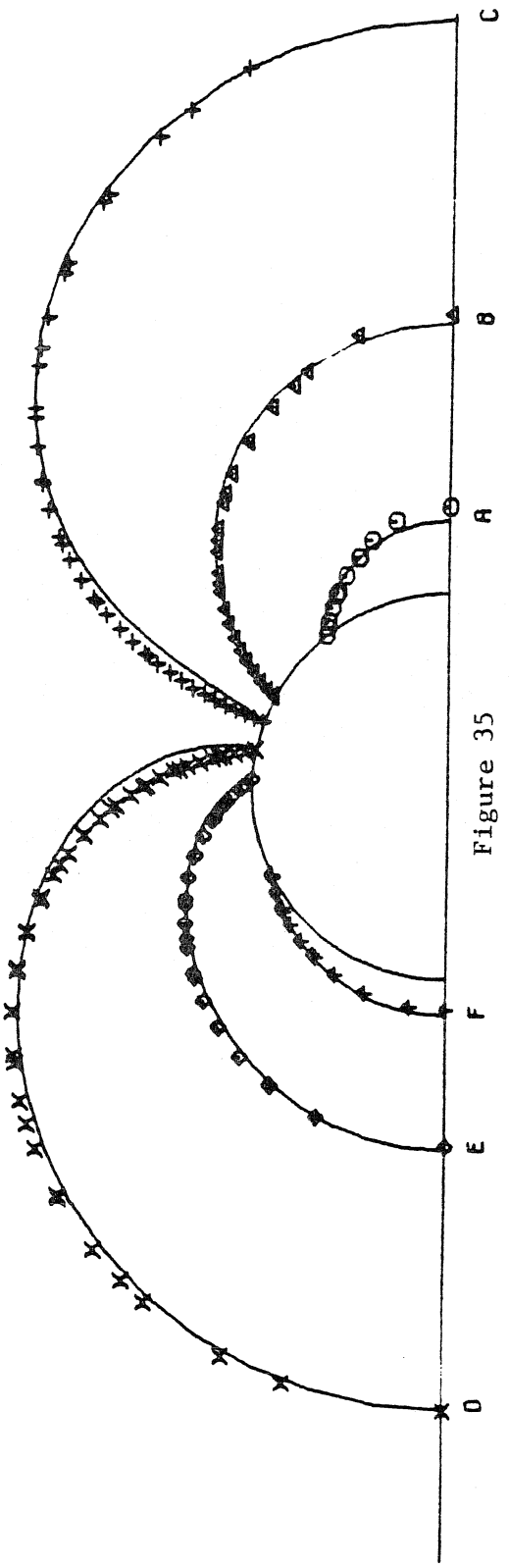

Figure 35

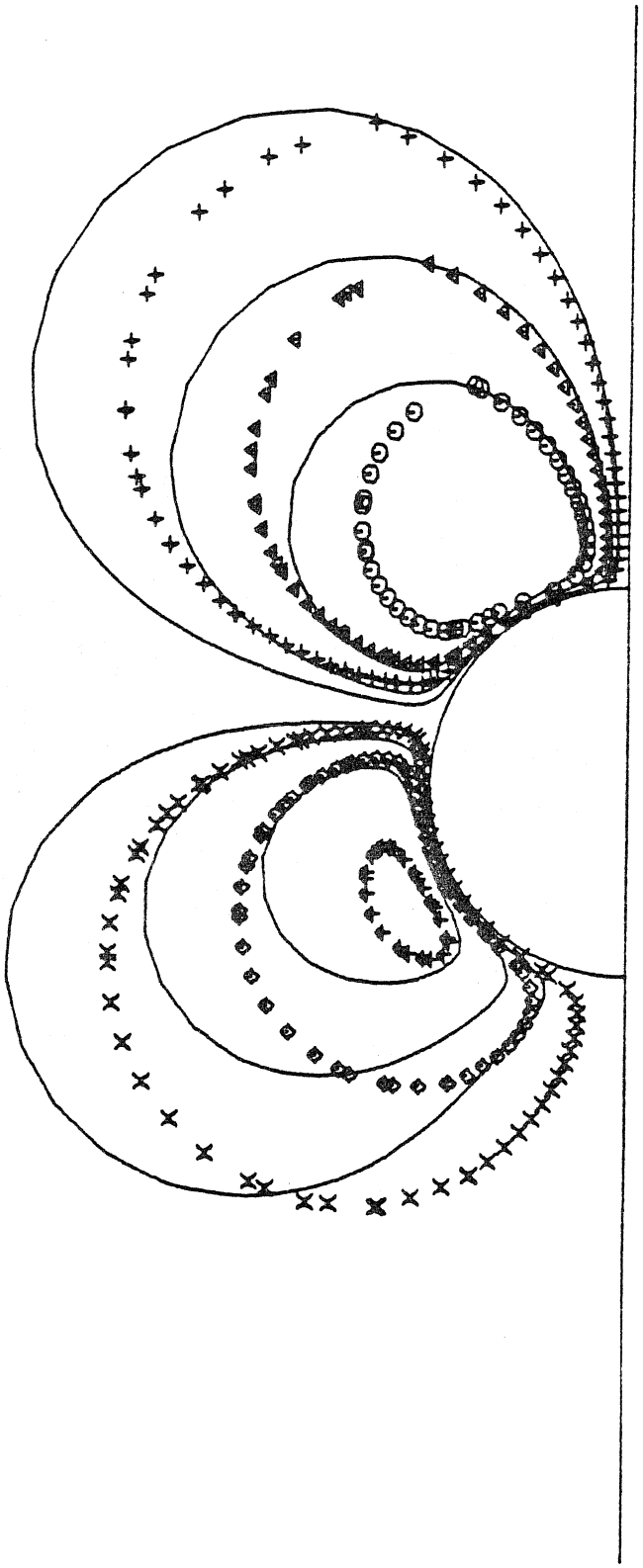

Figure 36

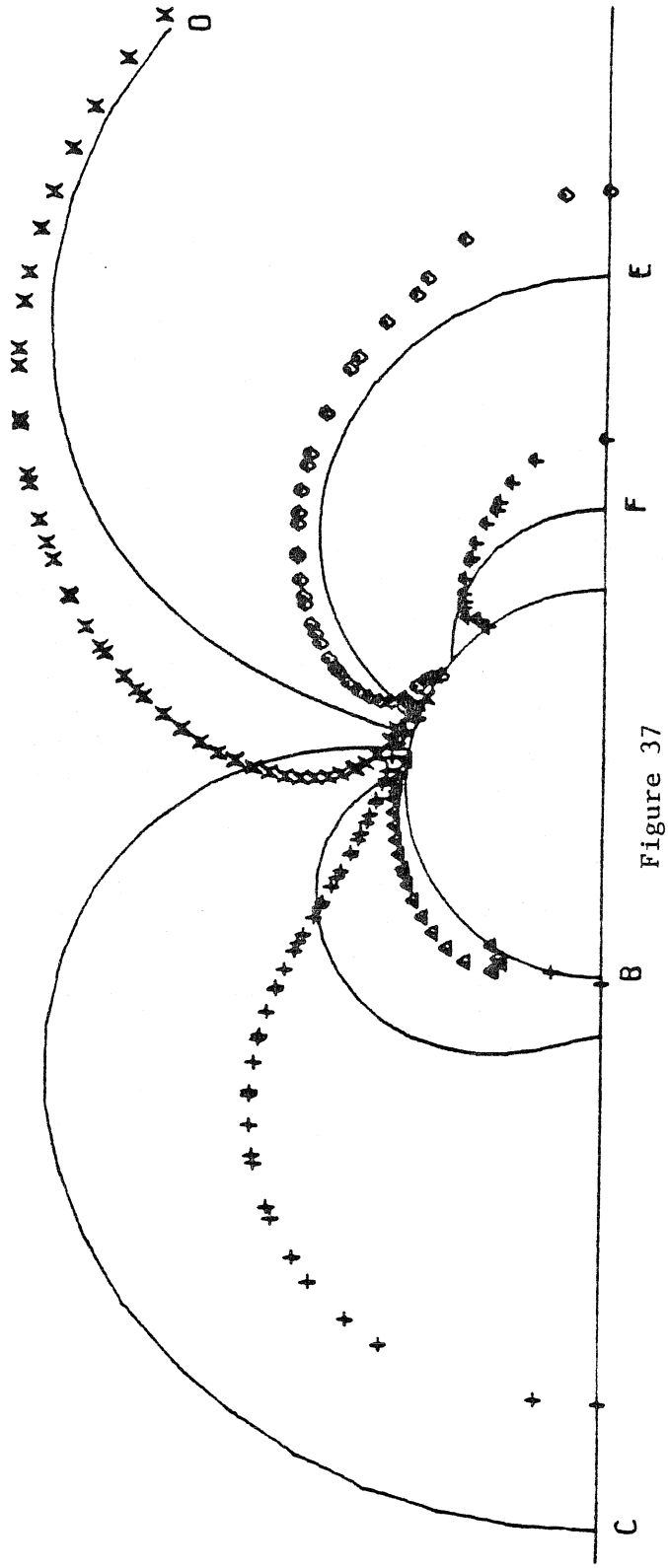

Figure 37

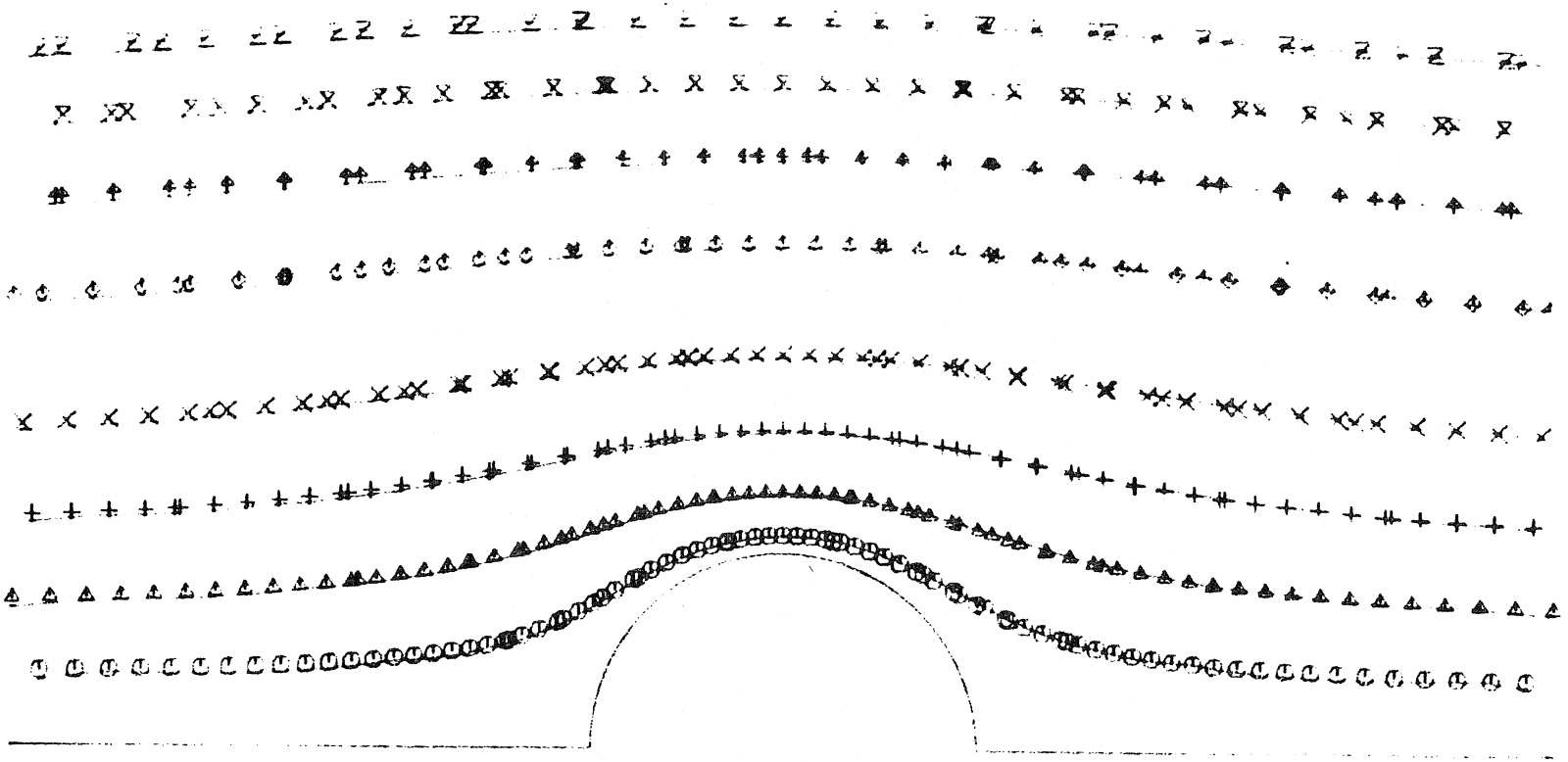

Figure 38

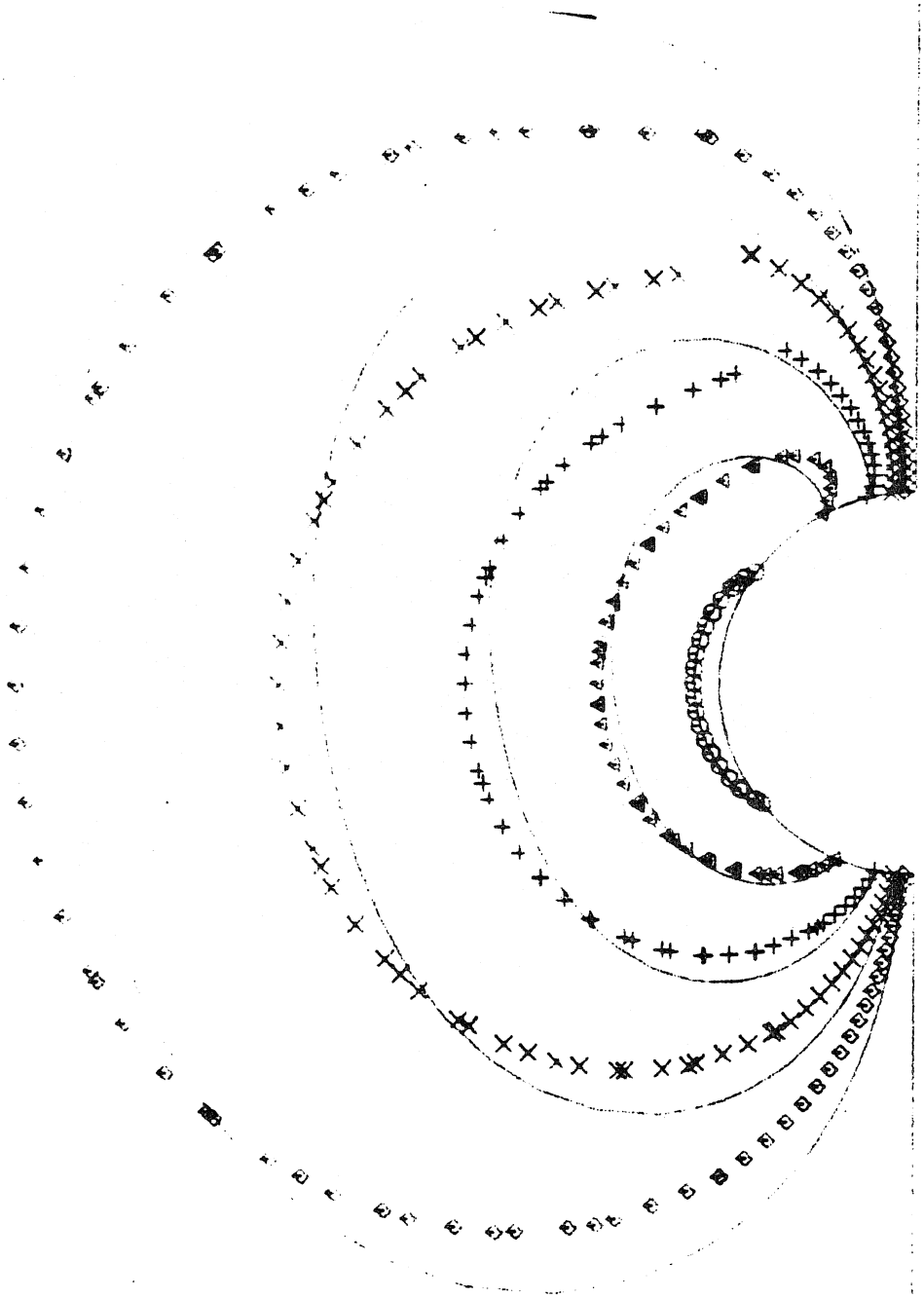

Figure 39

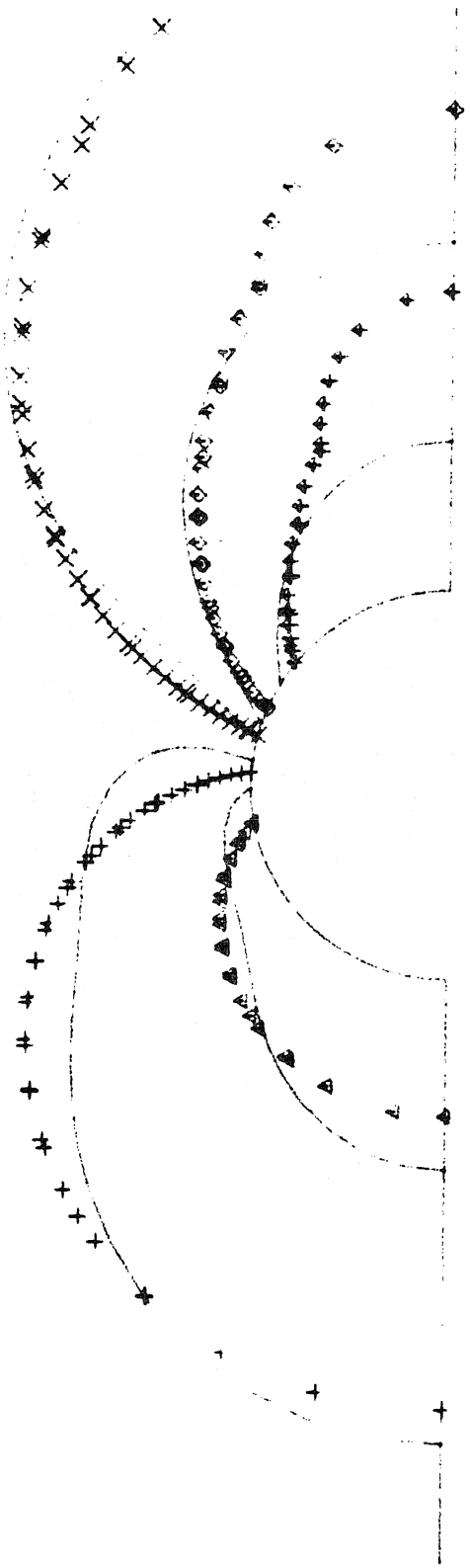

Figure 40

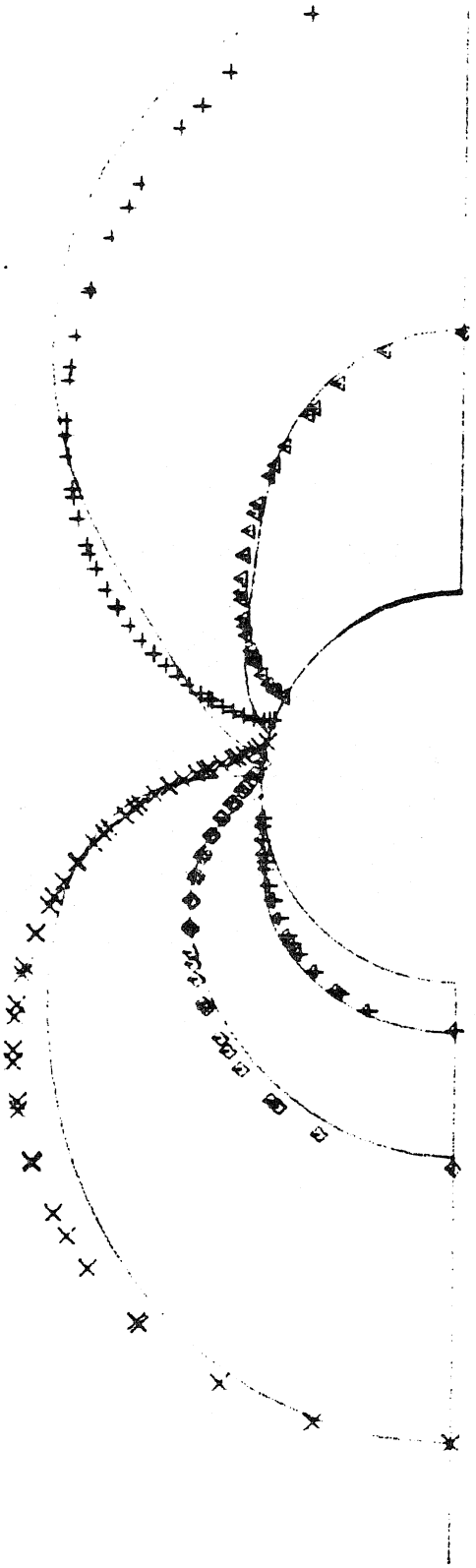

Figure 41

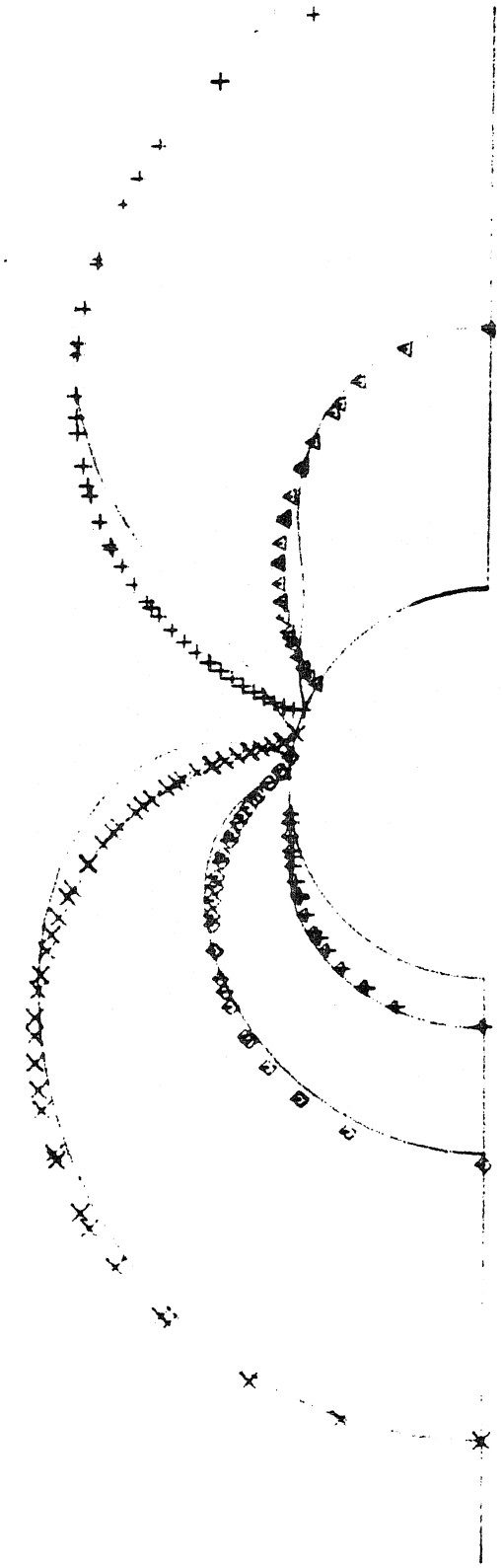

Figure 42

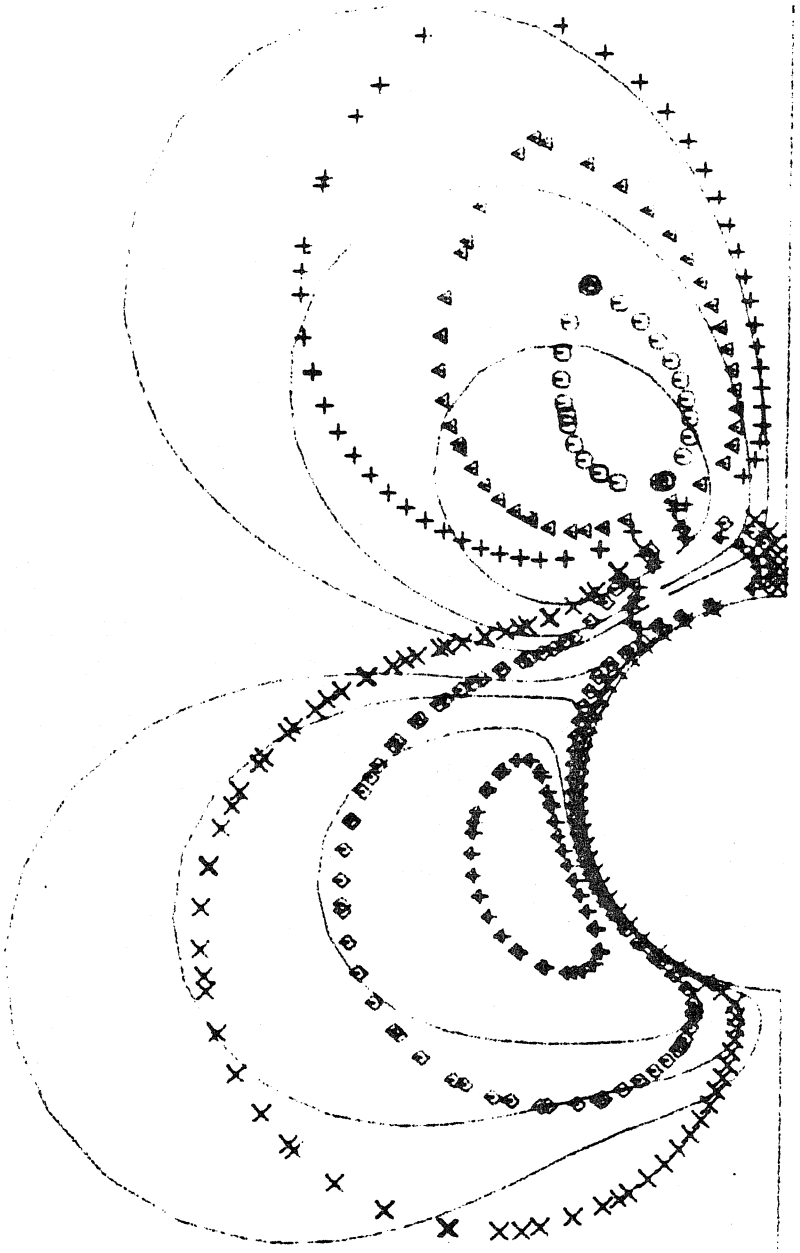

Figure 43

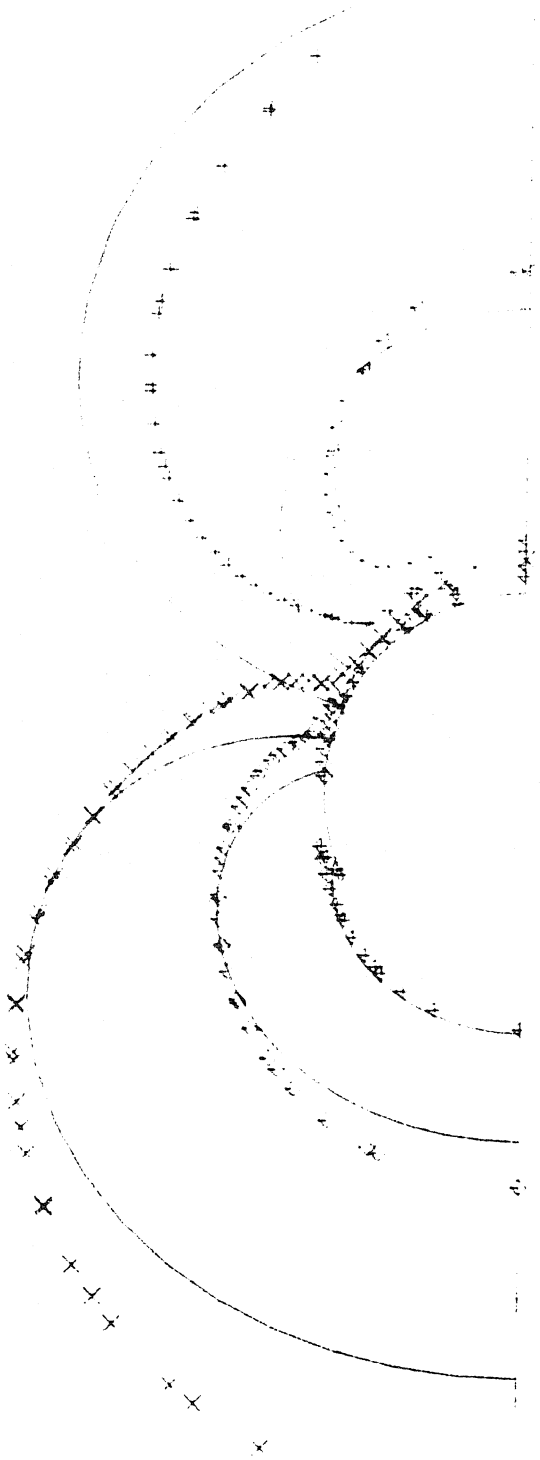

Figure 44

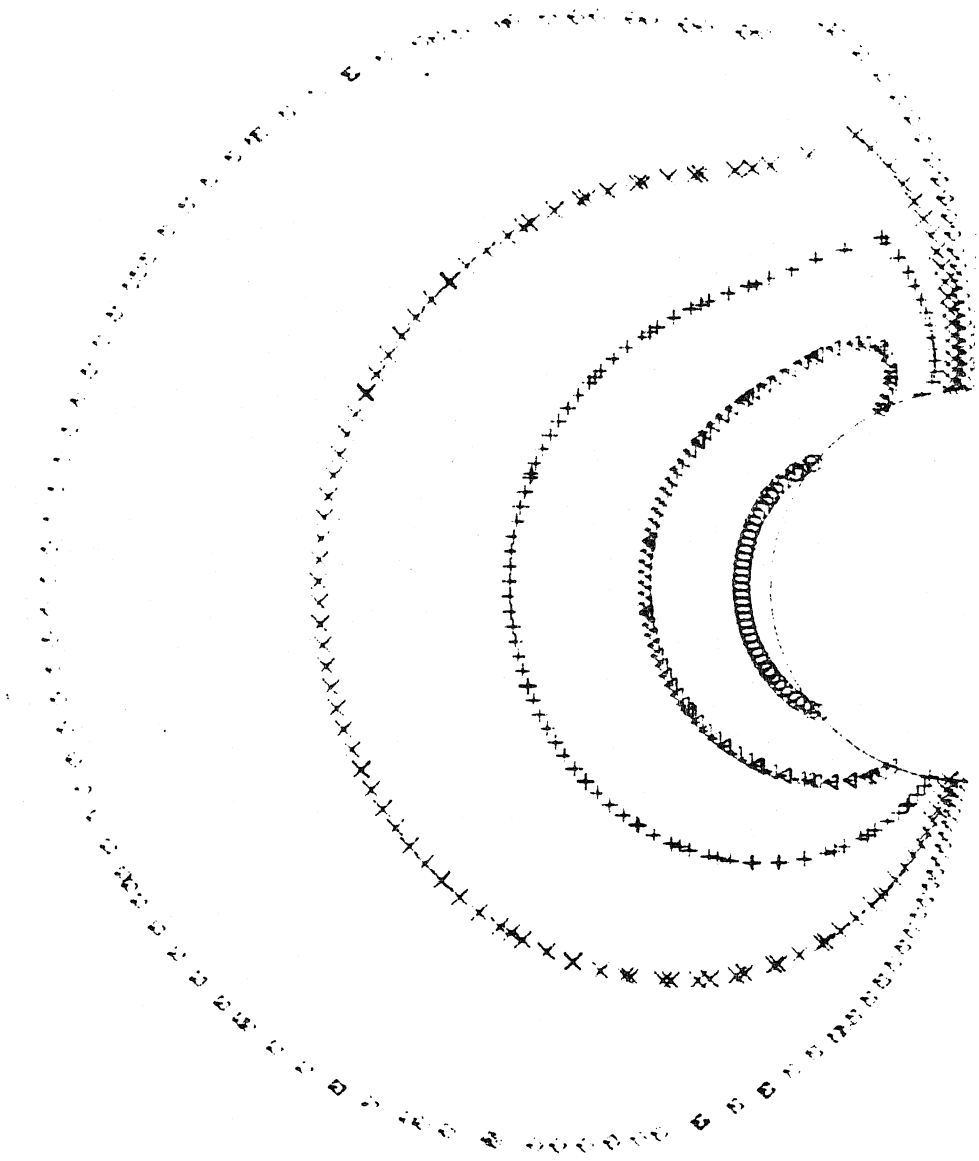

Figure 45

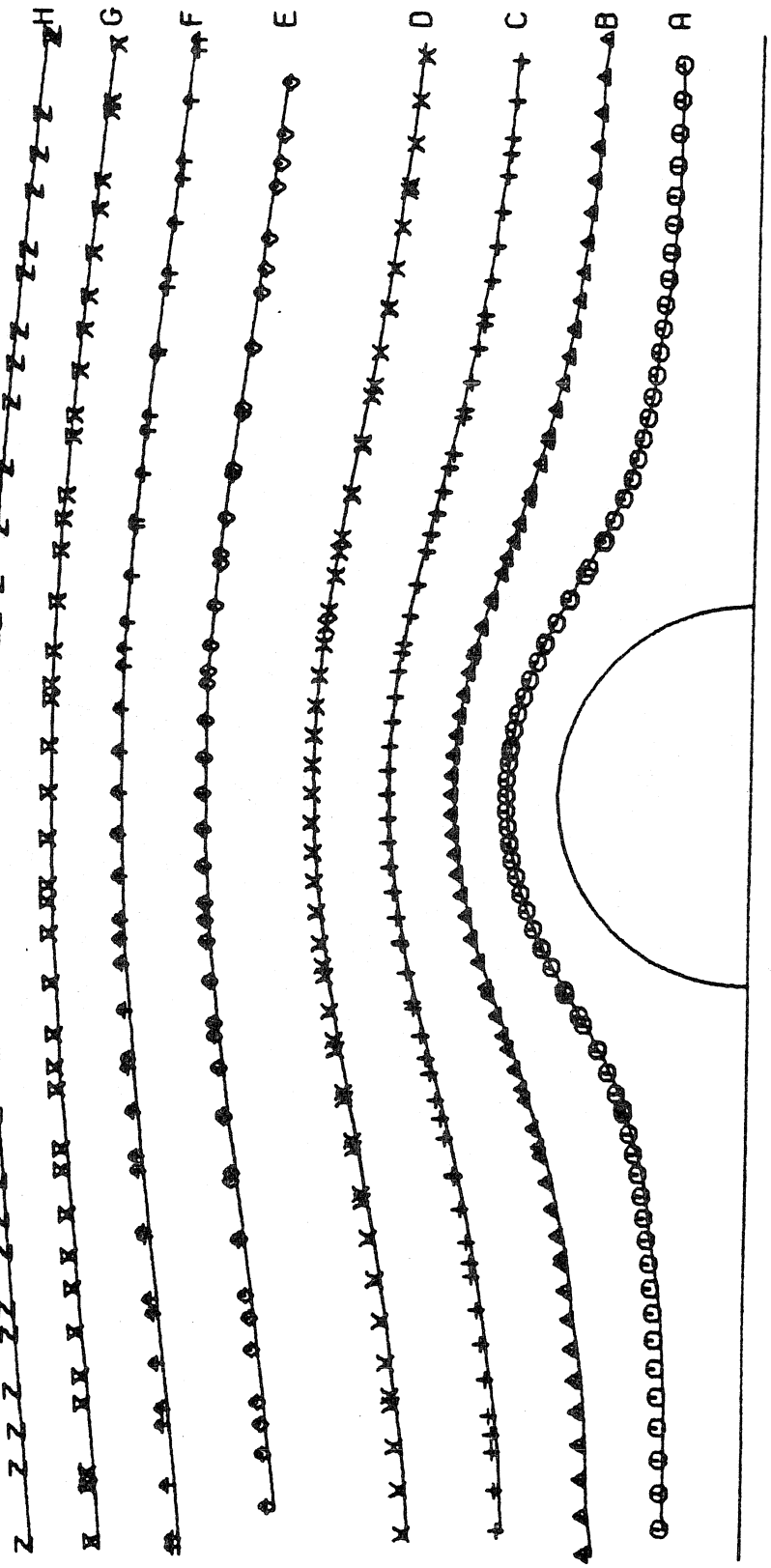

Figure 46

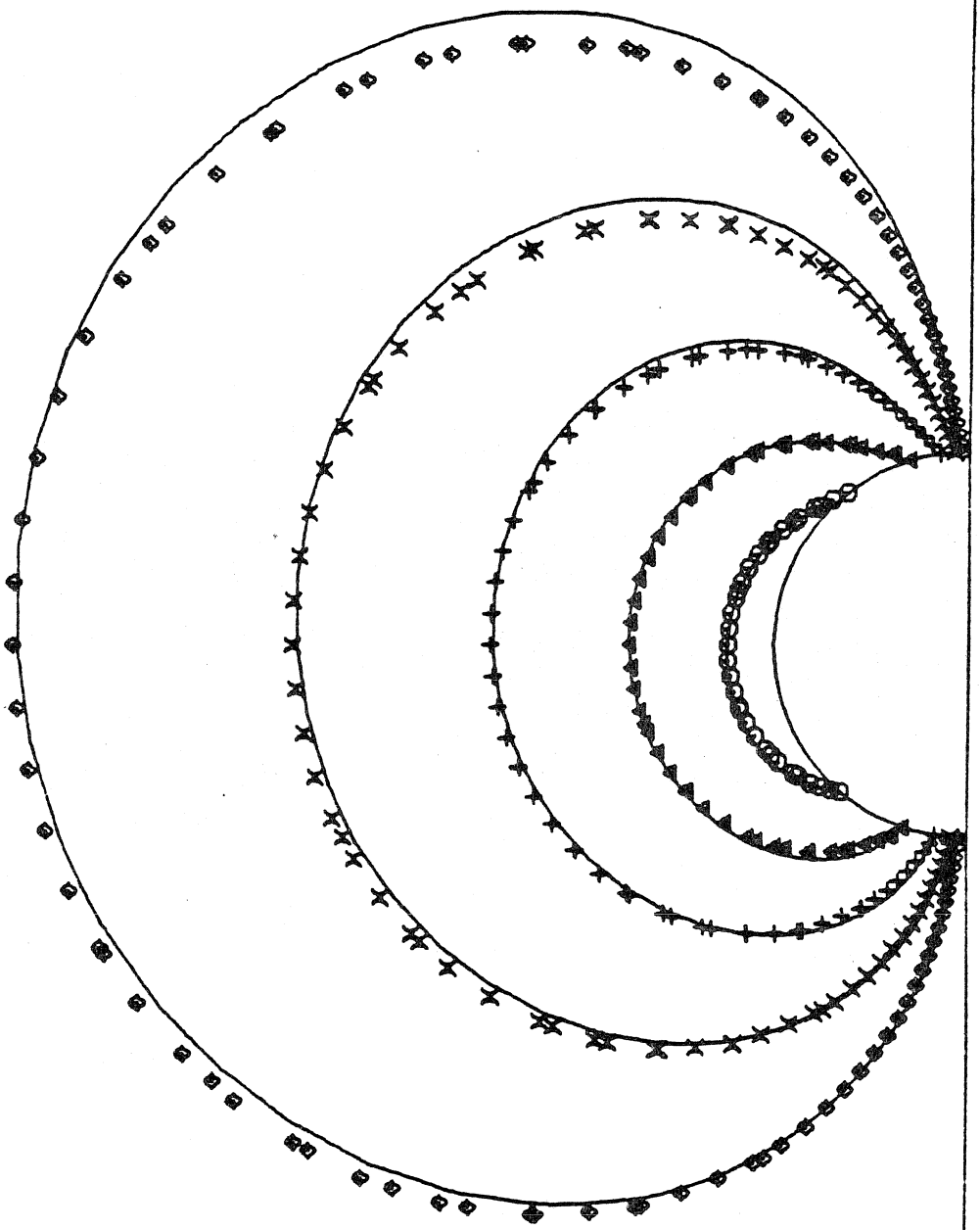

Figure 47

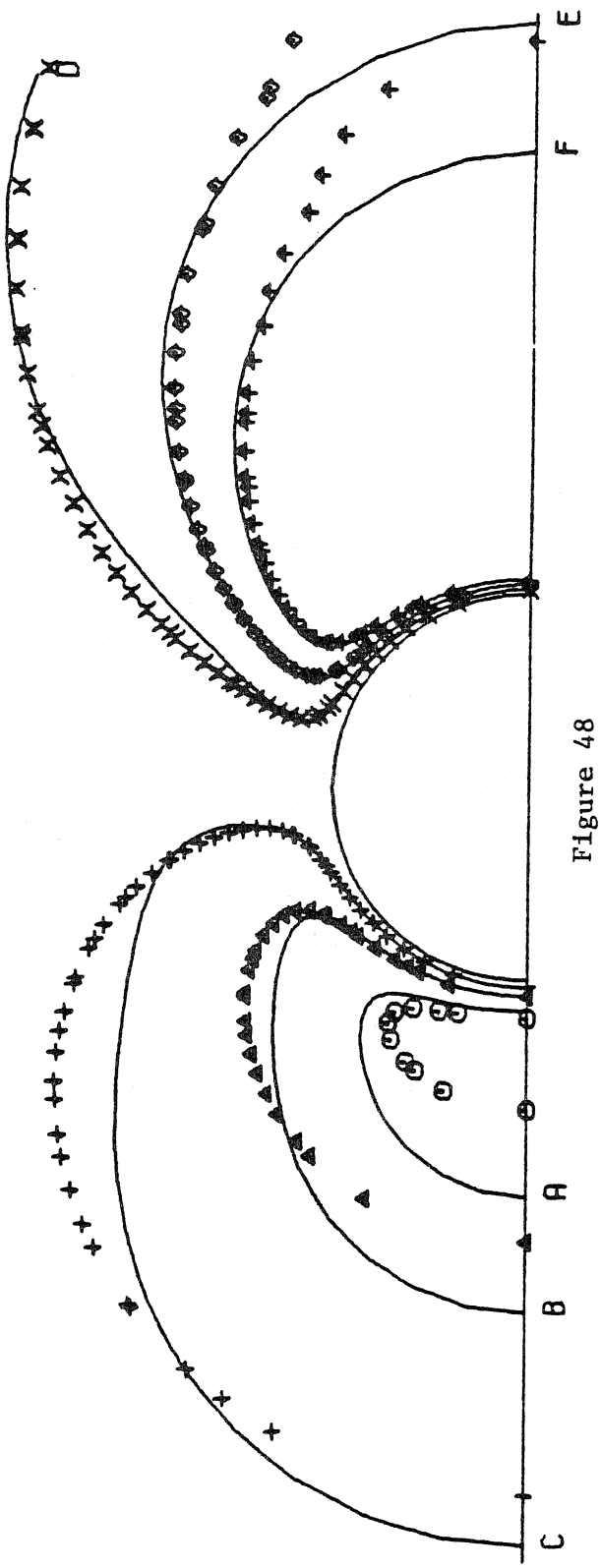

Figure 48

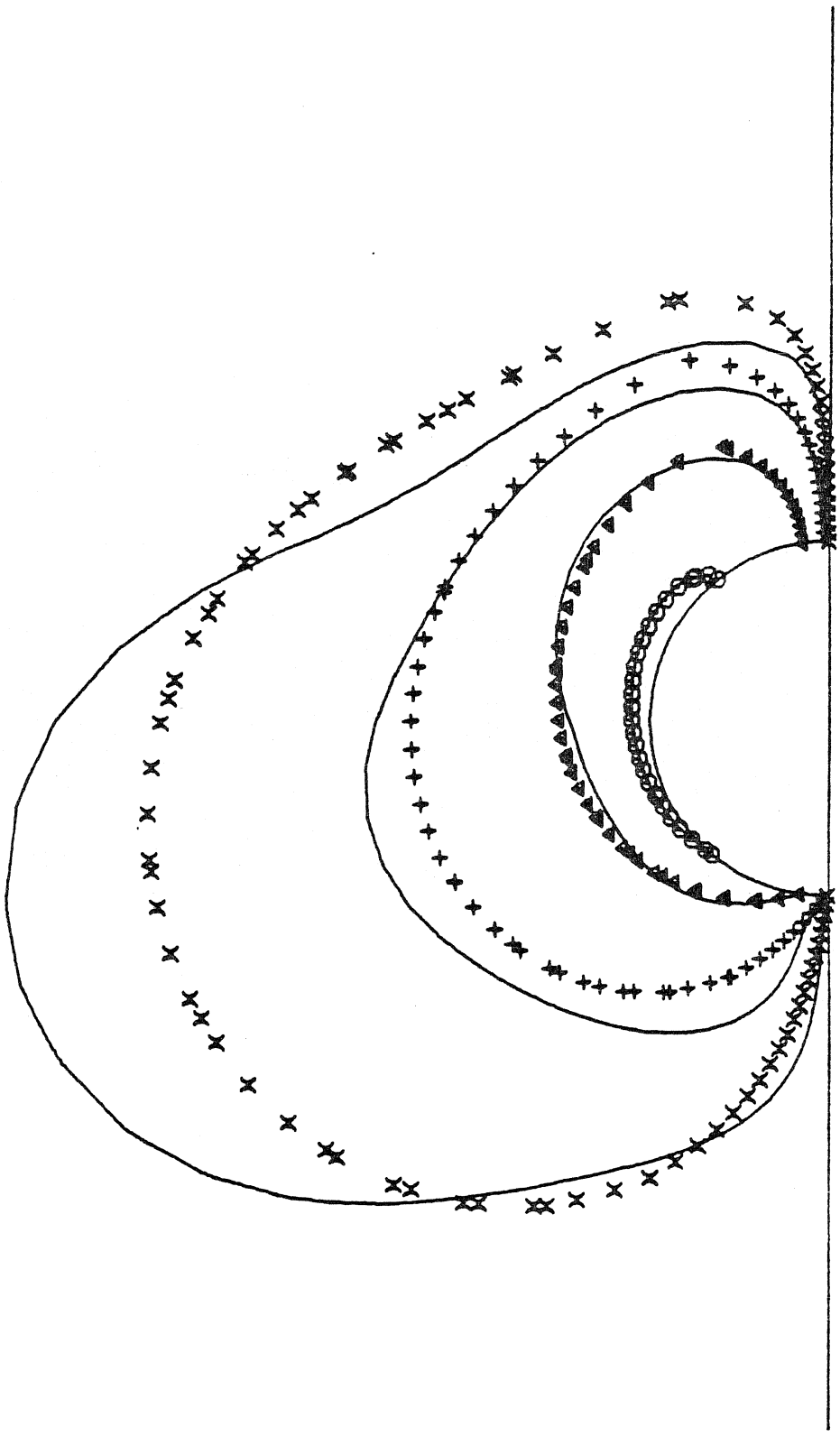

Figure 49

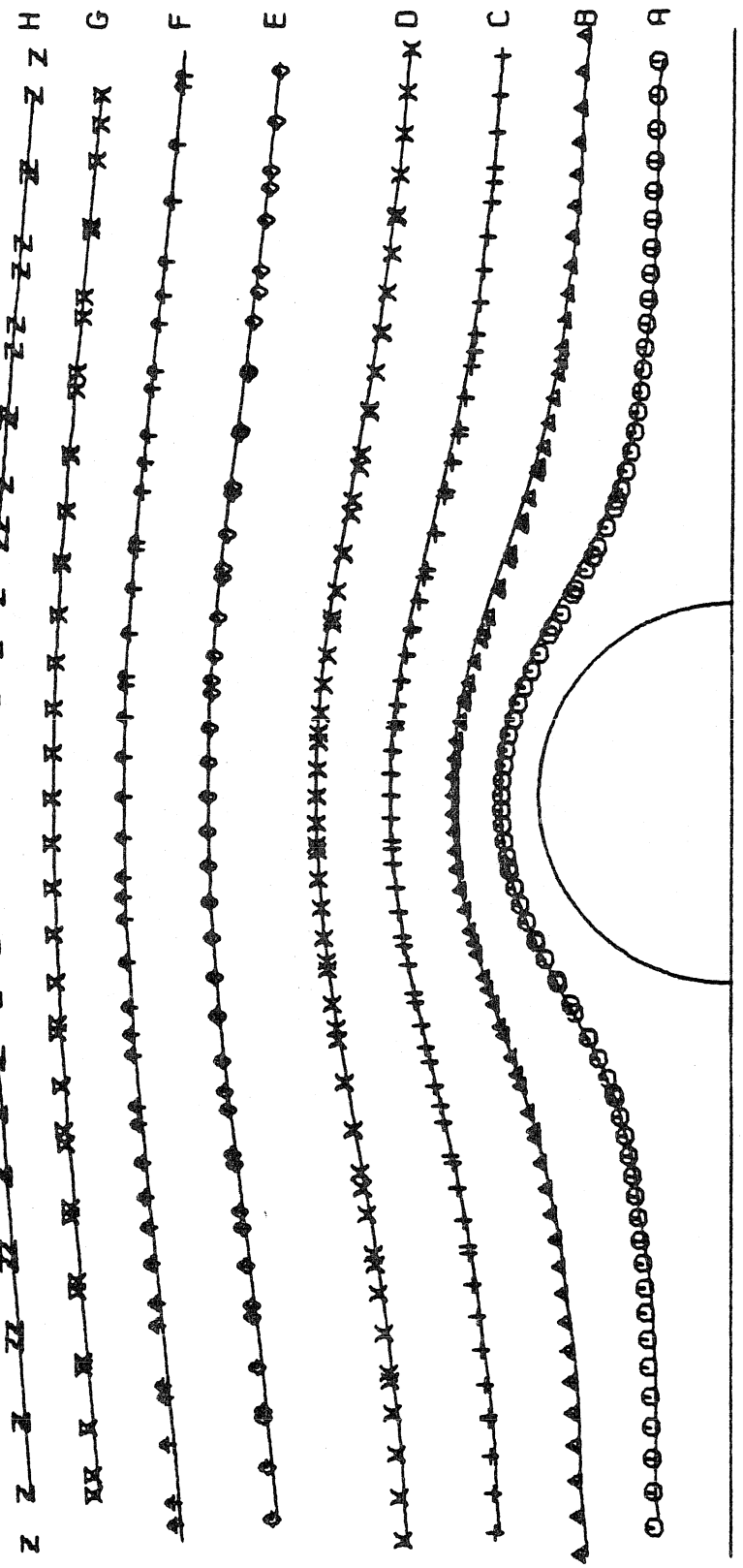

Figure 50

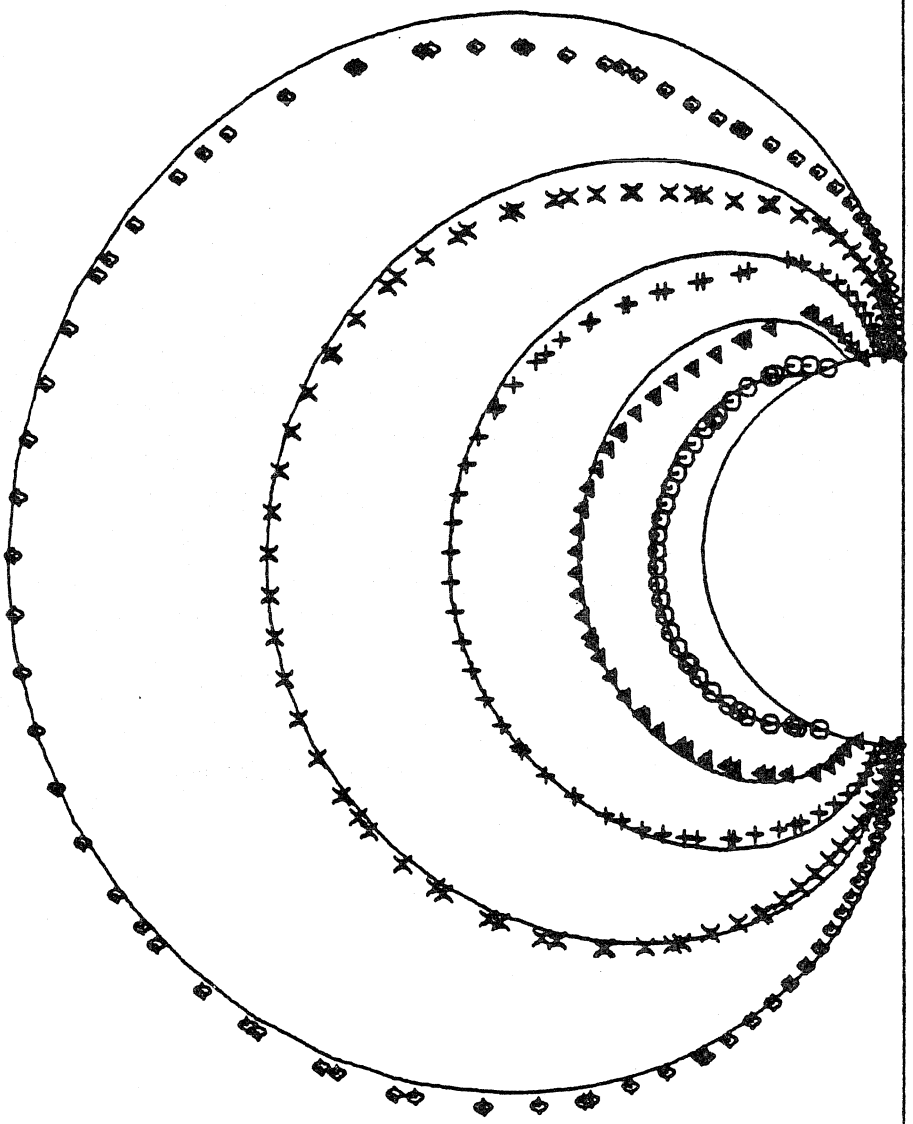

Figure 51

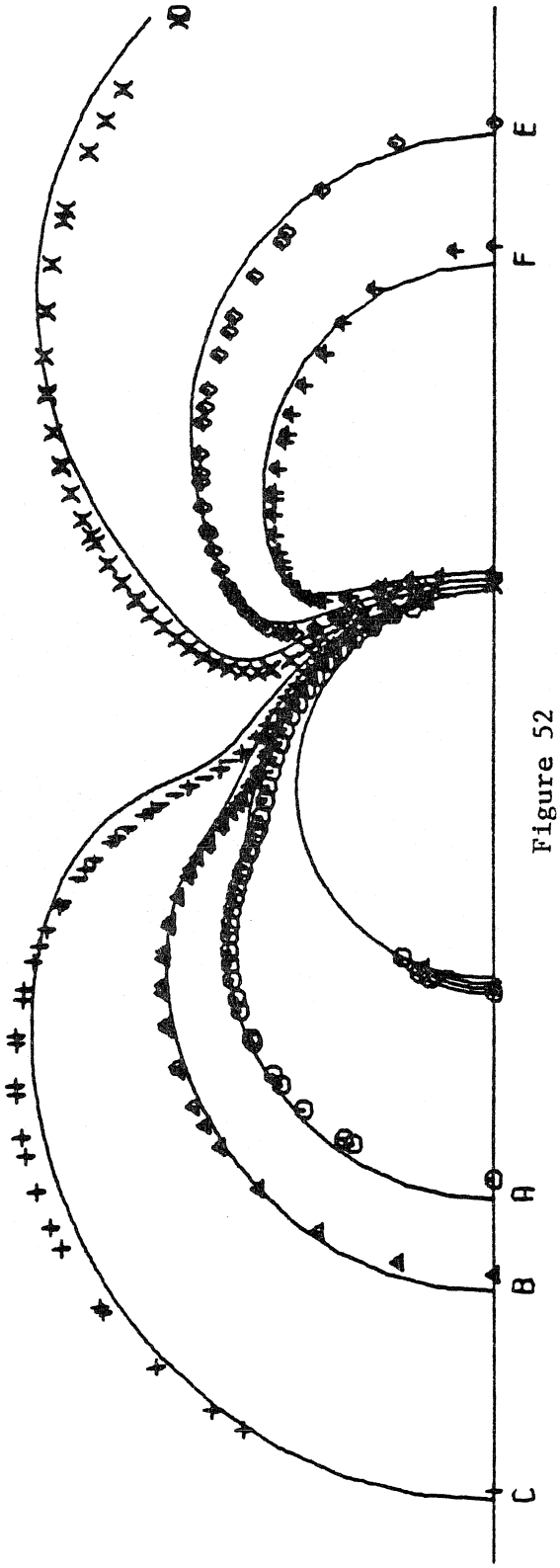

Figure 52

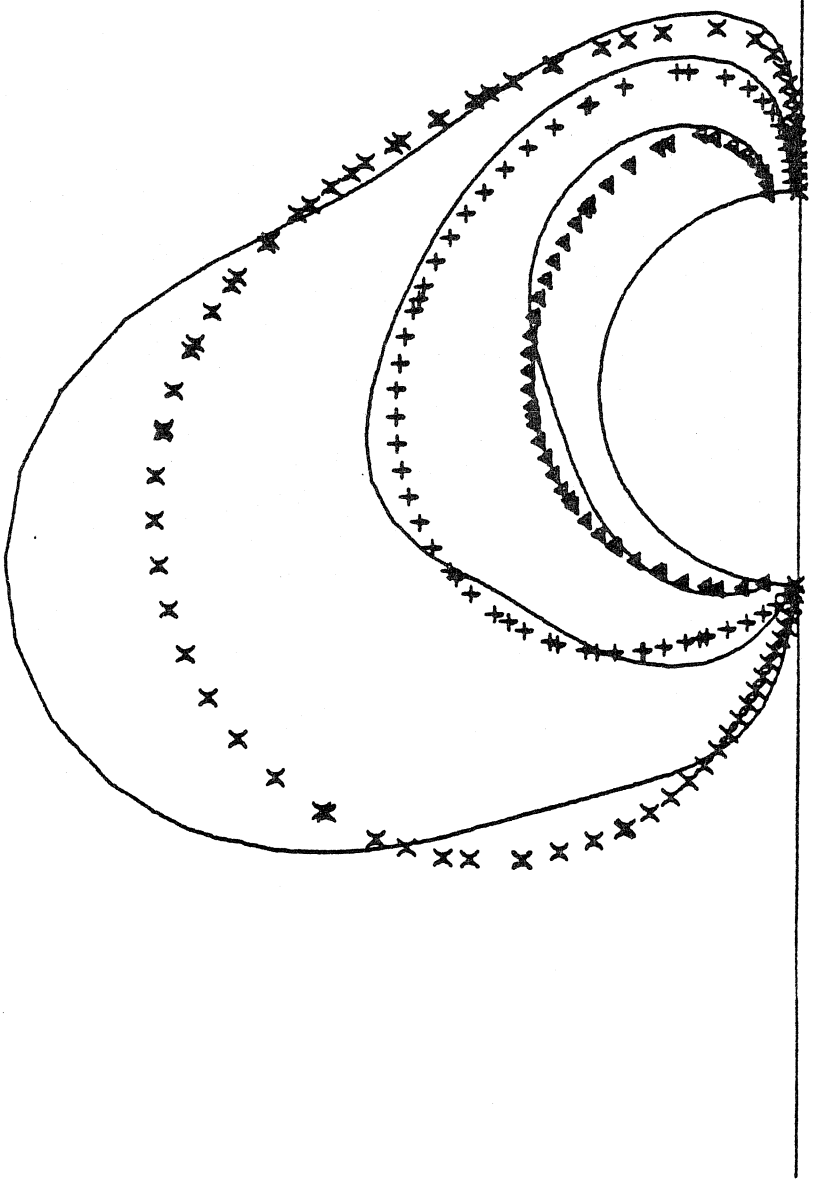

Figure 53

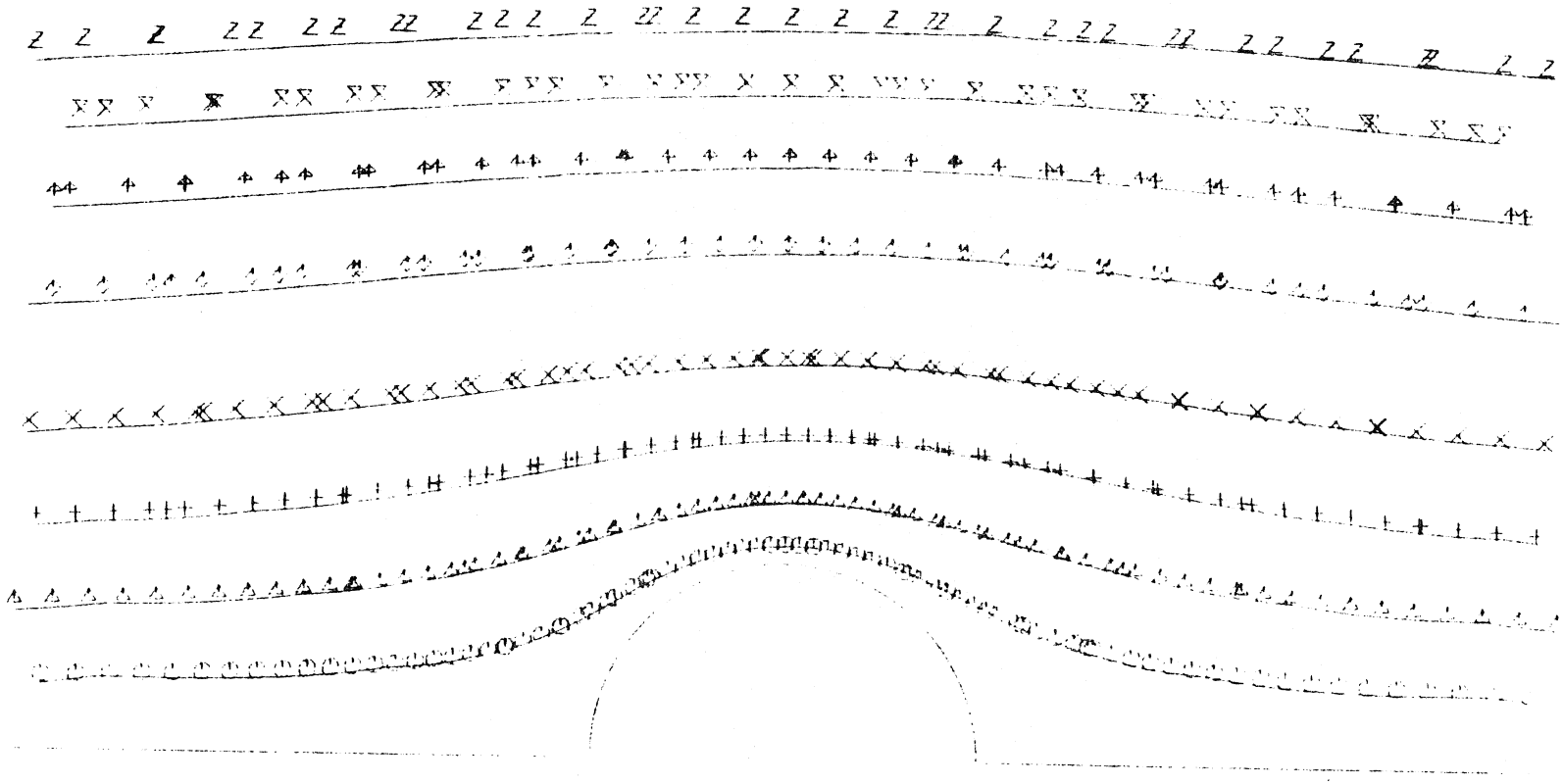

Figure 54

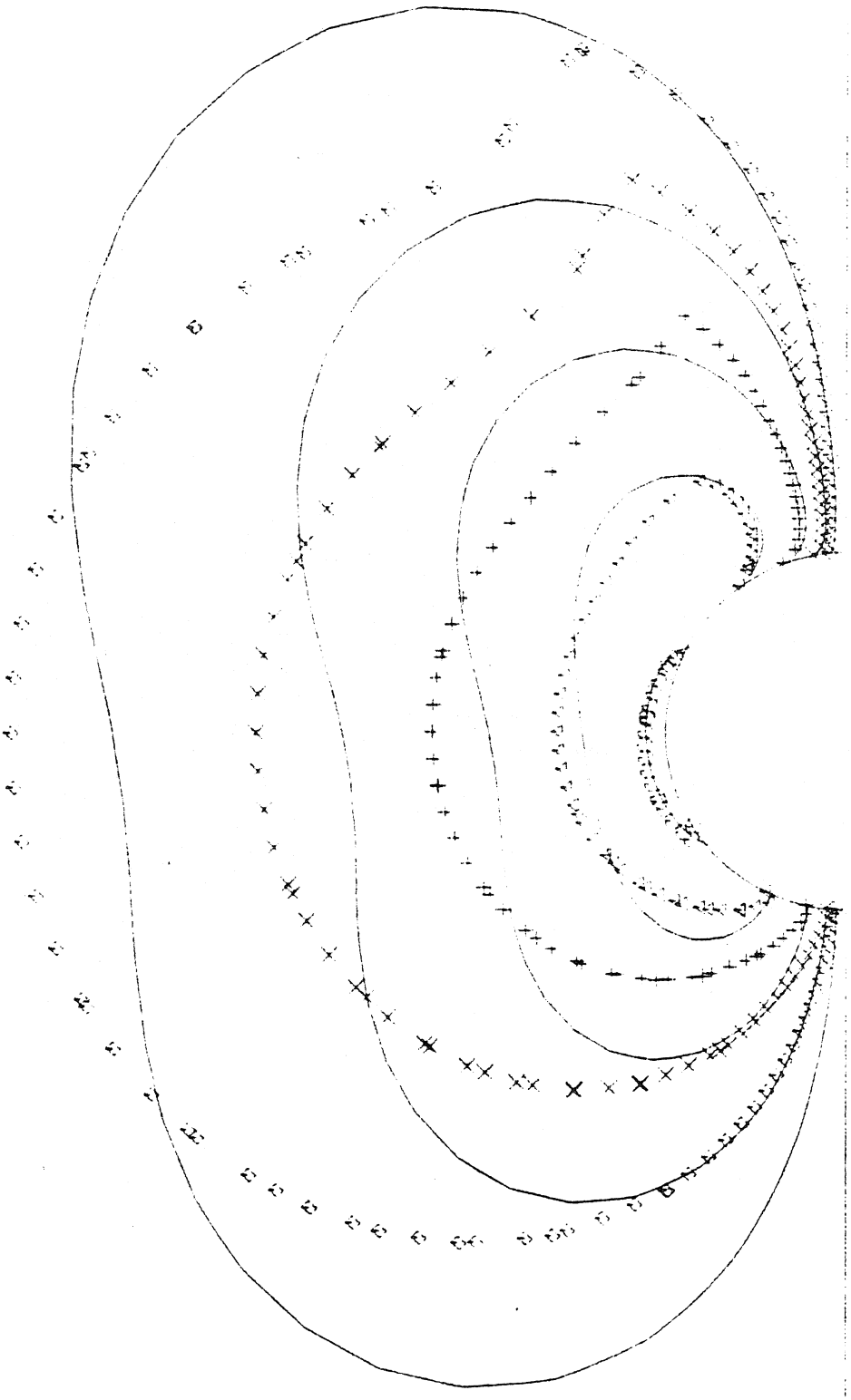

Figure 55

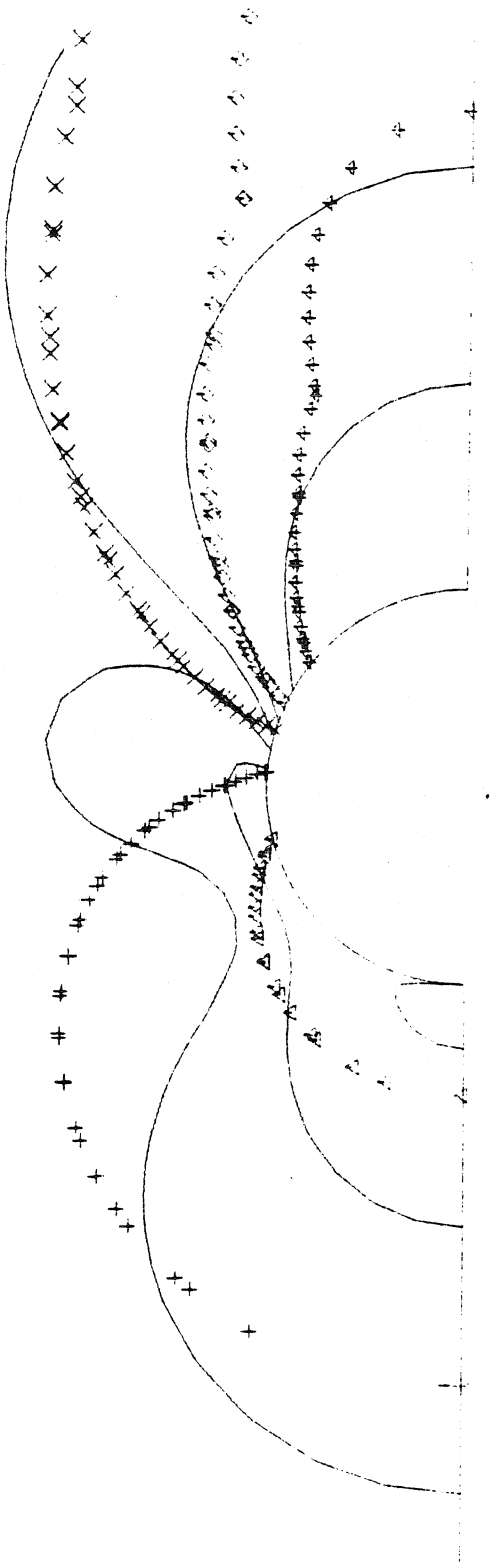

Figure 56